The Relationship Between Photosynthesis and Hybrid Vigour in Arabidopsis

Pei-Chuan Liu

A thesis summited for the Doctor of Philosophy

July 2017

CERTIFICATE OF ORIGINAL AUTHORSHIP

I certify that the work in this thesis has not previously been submitted for a degree nor has it been submitted as part of requirements for a degree except as fully acknowledged within the text.

I also certify that the thesis has been written by me. Any help that I have received in my research work and the preparation of the thesis itself has been acknowledged. In addition, I certify that all information sources and literature used are indicated in the thesis.

Signature of Student:

Date:

Acknowledgements

This research project was undertaken at CSIRO Plant Industry, Black Mountain.

First and foremost, I would like to thank my supervisors Prof. Elizabeth Dennis, Prof. Jim Peacock, Prof. Robert Furbank (ANU), Adjunct Prof. Tony Larkum and Prof. Peter Ralph for the support and guidance that they have given me throughout my PhD years. I would like to thank Jim and Liz for their passion in research that has inspired me greatly. I would like to thank Jim and Liz, whom I worked closely with on a daily basis, for their support and guidance whenever I come across a problem during my study. And I thank them for giving me opportunities to present my work to domestic and international collaborators and colleagues so that I can practise my presentation skills. They also show me that one of the many merits of being a successful scientist is the ability to communicate and work with others. I would like to thank Bob for his suggestions on experimental design, for his comments on my thesis, and for his connections to facilities that possess critical instruments for my studies. I would like to thank Tony and Peter for their discussion on the project and their valuable suggestions and comments on the draft of this thesis. I am grateful for all my supervisors, whose selfless time and care were sometimes all that kept me going.

I would like to thank Prof. Susanne von Caemmerer (ANU) for her comments on the analyses on the gas exchange results. I would also like to thank Dr Ming-Bo Wang

(CSIRO), Prof. Fred Chow (ANU), Assoc. Prof. Ryo Fujimoto (Kobe University), Dr Milan Sabo, Dr Anna Flis (ANU), Dr Zhongyi Li (CSIRO) and Prof. Barry Pogson (ANU) for their comments and inspiring discussion on this project. I would like to thank Dr Alex Whan (CSIRO) for the consultant and suggestions on statistical analysis.

My thanks also go to the Heterosis group, especially Limin Wu and Dr Anyu Zhu for the assistance and discussion on the technical aspects of this project, and Dr Ian Greaves for the assistance and discussion on statistical analysis. To all present and former members in the laboratory – Dr Li Wang, Dr Aihua Wang, Shuan Liang, You Zhang, Yifei Sheng, Ms Bjorg Sherman, Dr Michael Groszmann, Dr Rebeca Gonzalez-Bayon, Dr Maria M. Alonso-Peral and Dr Marina Trigueros, I thank you for all the help and suggestions over these years. It is my pleasure to work with you.

I am grateful for all the help and suggestions regarding the technical aspects of this project. I would like to thank the current and former staff in the High Resolution Plant Phonemics Facility at CSIRO for their technical assistance with IRGA and PAM: Scott Kwasny, Peter Kuffner, Lauren Venugoban, Peter Ansell, Dr Xavier Sirault, the late Dac Nguyen and Helen Daily; and staff from the Research School of Biology at ANU: Peter Groeneveld, Dr Florian Busch and Pruden Kell, for all your help. I would like to thank Dr Rosemary White and Dr Mark Talbot from the Microscopic Centre at CSIRO for their suggestions and discussion on the protocols for the microscopic works. I would also like to thank photographers Carl Davies and Amy Wilson from the former Creative Services at CSIRO for their assistance in taking great photos of my plants.

I would also like to thank my fellow students, Dr Joanne Lee, Dr Katherine Meacham, Dr Fang Huang, Jimmy Tung, Qiong Wu and Dr Viridiana Silva Perez, and all the colleagues in Building 2/79, especially Dr Ming Luo, Dr Xiaoba Wu and Tanya Phonkham for your friendship.

I would like to thank my parents for supporting my decision in pursuing PhD in Australia. Finally, I would like to thank my husband, Anyu, for your love, encouragement and support.

Table of Contents

List of illustrations and tables

Abbreviations

A	—	the CO_2 assimilation rate
a/b ratio	—	the ratio of chlorophyll a to b
Ca	—	the ambient CO_2 partial pressure
CCA1	—	circadian clock associated 1
Chl a	—	chlorophyll a
Chl b	—	chlorophyll b
C_i	—	the intercellular CO_2 partial pressure
Ci/Ca	—	the ratio of intercellular to atmospheric CO_2 partial pressure
CNR	—	cell number regulator
Col	—	Columbia-0
cyo1	—	shi-yo-u 1; the Japanese word for “cotyledon”
Cyt b_6f	—	cytochrome b_6f complex
DAS	—	days after sowing
DIC	—	differential interference contrast
ED	—	end-of-the-day
EN	—	end-of-the-night
FNR	—	ferredoxin NADP oxidoreductase
F, F’	—	fluorescence emission from dark- or light-adapted leaf, respectively
Fd	—	ferredoxin
F_m'	—	maximal fluorescence from dark- and light-adapted leaf

F_o, F_o' — minimal fluorescence from dark- and light-adapted leaf, respectively

F_q' — difference in fluorescence between F_m' and F'

F_q'/F_m' — PSII operating efficiency

FW — fresh weight

g_s — the stomatal conductance of water vapour

GUN — genomes uncoupled

L*er* — Landsberg *erecta*

LHC — light harvesting complexes

LHCI — light harvesting complex I

LHCII — light harvesting complex II

LHY — late elongated hypocotyl

J — chloroplast electron transport rate

J_{max} — the estimated maximum electron transport rate

µE — micro Einstein; µmol photons m^{-2} s^{-1}

MPV — mid-parent value

MS — Murashige and Skoog medium

mv — midvein

PAM — pulse amplitude modulated

PAR — photosynthetically active radiation

PC — plastocyanin

Φ_{PSII} — operating quantum yield of PSII

PLB — prolamellar bodies

PM — palisade mesophyll

PQ — plastoquinone

PS — photosystems

PSI — photosystem I

PSII — photosystem II

Q_A — plastoquinone A

Q_B — plastoquinone B

R: FR ratio — the ratio of red light to far-red lights

Rubisco — ribulose-1,5-bisphosphate carboxylase/oxygenase

RuBP — ribulose-1,5-bisphosphate

sco1 — snowy cotyledon 1

sco2 — snowy cotyledon 2

SE — standard error

TOC1 — timing of CAB expression 1

V_{cmax} — the maximum velocity of carboxylation in Rubisco

VDE — violaxanthin de-epoxylase

VPD — water vapour pressure deficit

Ws — Wassilewskija

ZE — zeaxanthin

ZT — Zeitgeber time

Abstract

Heterosis, or hybrid vigour, is the phenomenon where a F1 hybrid exceeds the parents in biomass and seed production. Hybrids are used in production in rice, maize and other crops. In *Arabidopsis*, biomass heterosis occurs in hybrids at an early developmental stage and throughout development. Previous findings suggest that heterosis is associated with altered gene expression, especially for the genes involved in the photosynthesis pathway, but the relationship between photosynthesis and the generation of biomass heterosis is not clear. The aims of this project were to analyse *Arabidopsis* hybrids for their photosynthetic parameters and growth patterns and compare them to the corresponding parents to elucidate the relationship between heterosis and photosynthesis.

To investigate whether photosynthetic properties in hybrids were different from the parents, the chlorophyll fluorescence and the CO_2 gas-exchange on a per leaf area basis were measured as indicators of the capacity of the light and dark reactions, respectively; the content of chlorophyll and the number of chloroplasts per mesophyll cell were analysed as indicators of the density of photosynthetic machinery in leaves; and leaf parameters that might affect gas-exchange in the leaf, including leaf thickness and the number of mesophyll cell layers, were examined. In all hybrids these photosynthetic parameters were at levels either between the two parents or similar to the better parent, showing that photosynthetic processes were highly conserved in hybrids and parents. Increasing photosynthesis via increasing the growth irradiance conditions did not enhance

the heterosis level of hybrids compared to the parents. These results indicate that the biomass heterosis was not due to changes in photosynthetic processes.

The growth patterns of the leaves of the heterotic C24/L*er* hybrids, showed that biomass heterosis was due largely to the newly developed leaves in the hybrid being larger than those of the parents at any point in time during development. The heterosis in leaf growth was due to greater cell size and increased cell number. Although the unit leaf area photosynthetic rate in the hybrids was not greater than the parents, the hybrids had a greater total leaf area to intercept more light to sustain the increased demands of energy and building blocks for the fast-growing new leaves. The growth heterosis in early leaf development might be a prerequisite for biomass heterosis throughout development.

A critical role for photosynthesis in cotyledons in the generation of biomass heterosis was demonstrated by a mutant, *snowy cotyledon2*, which had impaired chloroplast biogenesis, specifically in the cotyledons. Whereas Ws/L*er* hybrids had a considerable biomass heterosis compared to the parents, mutant Ws/L*er* hybrids that were unable to carry out photosynthesis in cotyledons showed no heterosis relative to the homozygous mutant parents. This result indicates that the generation of biomass heterosis in early seedling development depends on photosynthesis in the cotyledons and that this is important for the biomass heterosis in subsequent stages.

1 Chapter I Introduction

1.1 Heterosis in plants

Hybrids are the progeny of cross-fertilisation between two strains or species of organisms. A common feature of hybrids is the ability to exceed their parents in growth, survival and fitness; this phenomenon is termed heterosis or hybrid vigour (Shull, 1948). Hybrids are commonly used in livestock and pet animal breeding (Cassady et al., 2002). This breeding technique was first applied in agriculture. Hybrid plants are favoured by the agricultural industry because they generally have increased vigour in vegetative growth and fitness, and also in reproductive traits like seed size and grain yield. A well-known example is maize which has had a six fold increase in yield since the first use of hybrid back in the 1930s (Crow, 1998). Hybrids are also used in other crops like rice, canola and sorghum (Fischer et al., 2014). More than 85% of the canola grown in Canada is hybrid, which gives ~20% increase in yield (Fischer et al., 2014). Breeding of hybrid rice has also increased the yield by nearly two-fold between 1976 and 1995 in China (Yuan, 1998). Despite the extensive use of hybrids, the molecular mechanism(s) of heterosis is still largely unknown.

Many of the recent studies on heterosis have been carried out using the model plant, *Arabidopsis thaliana*. *Arabidopsis thaliana* is a flowering vascular plant that is widely used as a model organism in plant biology studies for its short life cycle, small plant size for the ease of laboratory work, a small genome that is fully sequenced and well annotated

(Arabidopsis Genome, 2000). In addition, a large number of ecotypes are available with genomic diversity and distinct phenotypes that make *Arabidopsis* a perfect system for heterosis studies. Crosses of different ecotypes give hybrids that show heterosis in many physiological traits, especially in vegetative growth (Meyer et al., 2004). The crosses between ecotypes C24 and Landsberg *erecta* (L*er*), and between C24 and Columbia-0 (Col) showed substantial heterosis in biomass (**Figure 1.1**). Heterosis in vegetative growth is also a common feature of hybrids across different crop species like maize and rice (**Figure 1.1**).

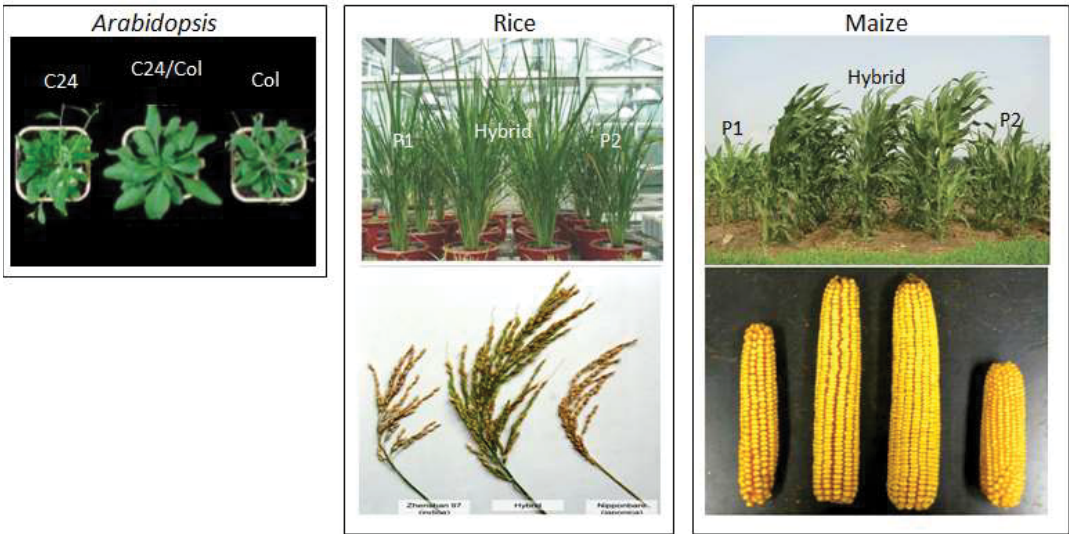

Figure 1.1. Heterosis in vegetative biomass and reproductive trait in different species. Images (from left to right) are hybrids of *Arabidopsis thaliana*, rice and maize taken from (Groszmann et al. (2014), He et al. (2010)) and Springer and Stupar (2007) respectively.

1.2 Mechanisms of heterosis

Over the last century, numerous efforts have been made to elucidate the mechanisms underlying heterosis. Thanks to the development of molecular technologies in the past decade, recent studies show that heterosis might be a consequence of genome-wide changes in epigenetic, genetic and biochemical alterations as well as a complex regulatory network appear to be involved (Greaves et al., 2012, Chen, 2013).

1.2.1 Genetic models

During hybrid formation, two genomes are brought together in the nuclei resulting in genome-wide changes in gene expression. It is reasonable to suspect that heterosis is attributable to these alterations in the patterns of gene expression. Three historical models, dominance, overdominance and epistasis of gene action, have been advanced to explain heterosis from the genetic perspective, but any one has failed to obtain a universal consensus (Crow, 1948, Birchler et al., 2003). In the dominance model, it is proposed that heterosis is due to the compensation of deleterious, recessive alleles from one parent by the more beneficial, dominant alleles from the other parent (Bruce, 1910, Xiao et al., 1995). The overdominance model, on the other hand, postulates that heterosis is due to the interactions between the heterozygous alleles in hybrids to give a superior locus (Crow, 1948, Semel et al., 2006). Finally, the epistasis model suggests heterosis is due to the interactions between two or more non-allelic loci of different parental origins (Yu et al., 1997, Kusterer et al., 2007). Although evidence for each model has been reported, none of them have accounted for all aspects of the changes in hybrid gene expression. Recent

genome-wide analysis of *Arabidopsis* hybrids found the co-occurrence of all three mechanisms (Meyer et al., 2010). It was once thought that the more genetically distinct the parents, the greater the heterosis of their hybrids (East, 1936). While this might be true for some inter-specific hybrids, such as the cross between radish and cabbage (Karpechenko, 1928), this suggestion could not explain heterosis in intra-specific hybrids like most of the cases in crops and in *Arabidopsis*, in which the genetic distance between the two parental lines is usually small and the majority of the genome is identical (Meyer et al., 2004, Chen, 2013).

1.2.2 Epigenetic regulation

For intraspecific hybrids where the parental genomes are nearly identical, epigenetic regulation might play a role in heterosis (Shen et al., 2012, Groszmann et al., 2013). Epigenetic modifications influence gene expression without changing the DNA sequence via mechanisms such as DNA methylation, histone modification, histone variants and non-coding RNA. Epigenetic regulation has been associated with the expression of genes involved in many pathways, such as cell differentiation (Reik, 2007) and how plants respond to environmental cues (Chinnusamy and Zhu, 2009). Investigation of DNA methylation profiles in *Arabidopsis* C24/*Ler* hybrids shows that the epigenetic information from the parents is mostly inherited faithfully, but distinct interactions between epigenetic modifications of different parental origins have been observed in hybrids (Shen et al., 2012, Greaves et al., 2012).

1.2.3 Other methods of gene regulation

The circadian clock regulates the expression of downstream target genes involved in many cell activities, including photosynthesis, by synchronising plant growth with the day/night cycle. In *Arabidopsis* C24/Col hybrids, some circadian clock oscillators showed altered oscillation patterns compared with the parents, including *CIRCADIAN CLOCK ASSOCIATED1* (*CCA1*), *LATE ELONGATED HYPOCOTYL* (*LHY*) and *TIMING OF CAB EXPRESSION1* (*TOC1*) (Ni et al., 2009b). *CCA1* and *LHY* are negative regulators of *TOC1* and are normally down-regulated during the day (Alabadi et al., 2001). The expression of *CCA1* and *LHY* is lower in C24/Col hybrids compared to the parents, resulting in the increased expression of target genes involved in photosynthesis and carbohydrate metabolism (Ni et al., 2009b).

1.3 Heterosis in vegetative growth

Heterosis in vegetative growth is usually characterised by a greater leaf size, as observed in maize and *Arabidopsis* hybrids. Leaf size is mainly determined by two variables: cell number and cell size (Donnelly et al., 1999, Kalve et al., 2014). In maize hybrids, heterosis in leaf size is mainly due to a greater number of cells (Pavlikova and Rood, 1987, Guo et al., 2010). The increased cell number in maize hybrid leaves has been correlated with the lower expression of a negative regulator of cell number, *Cell Number Regulator1* (*CNR1*) (Guo et al., 2010). Down-regulation of *CNR1* in an inbred line leads to an increased vegetative biomass, larger ears with a greater number of kernels per ear (Guo et al., 2010).

In *Arabidopsis* hybrids, heterosis in leaf size is associated with a greater number of cells per leaf, and increased cell size is also found in some hybrids (Groszmann et al., 2014). Alterations in the transcriptome patterns in *Arabidopsis* C24/*Ler*, C24/Col and Col/*Ler* hybrids indicate auxin synthesis is up-regulated and salicylic acid synthesis is down-regulated, compared with the average levels of the parents (Groszmann et al., 2015). Increased auxin and decreased salicylic acid has been shown to associate with increased cell number and cell size, respectively (Vicente and Plasencia, 2011, Wang and Ruan, 2013). Transgenic plants carrying the bacterial *NahG* gene which encodes a salicylic degrading enzyme phenocopy the heterosis phenotype, suggesting salicylic acid might play a role in heterosis in leaf size (Groszmann et al., 2015).

1.4 Photosynthesis and heterosis

Photosynthesis is the only carbon source for plant growth. In *Arabidopsis*, an up-regulation of photosynthetic genes has been reported in C24/*Ler* and C24/Col hybrids during early seedling development, especially during 3-7 days after sowing (DAS) (Fujimoto et al., 2012, Zhu et al., 2016). These include chloroplast-targeted genes encoding for thylakoid membrane components, photosynthesis apparatus and most of the enzymes in the tetrapyrrole and chlorophyll biosynthesis pathways. It is still unclear how and to what extent the up-regulation of photosynthesis genes at 3-7 days is affecting heterosis in vegetative growth.

Comparison of the photosynthetic properties between hybrids and parents during the vegetative stage is surprisingly scarce in the literature. The growth of the flag leaf during

the reproductive stage is associated with grain filling. Photosynthetic properties in the flag leaves of some elite hybrids in rice have been documented and showed that the unit leaf photosynthetic capacity in hybrids was not altered compared to the parents (Zhang et al., 2007, Chang et al., 2016). While the photosynthetic rates are similar to the parents, the flag leaves of hybrids stayed photosynthetic active for a longer period of time due to a delayed leaf senescence, resulted in a greater grain yield (Zhang et al., 2007, Chang et al., 2016). In *Arabidopsis*, the photosynthetic capacity of the 15 DAS C24/Col hybrids was not significantly different from the parents on a unit leaf area basis (Fujimoto et al., 2012). Further investigation in other hybrid combinations is required to verify whether hybrids have altered photosynthetic properties during the vegetative stage and how that correlates with heterosis in vegetative growth.

1.5 Photosynthesis

1.5.1 Chloroplast

Chloroplasts are the photosynthetic organelles present mainly in leaf mesophyll cells, with some in the epidermal guard cells, where photosynthesis takes place. A mesophyll cell in an *Arabidopsis* leaf could have from several dozens up to hundreds of chloroplasts, depending on the size of the cell (Pyke and Leech, 1991). Each chloroplast is surrounded by two layers of enveloping membranes. The liquid phase encompassed by the membranes is called the stroma (**Figure 1.2**). Embedding in the stroma are stacks of membranes (thylakoids) which called grana and which are connected by the un-stacked, single thylakoid called stromal lamellae. The thylakoid membrane separates the inner

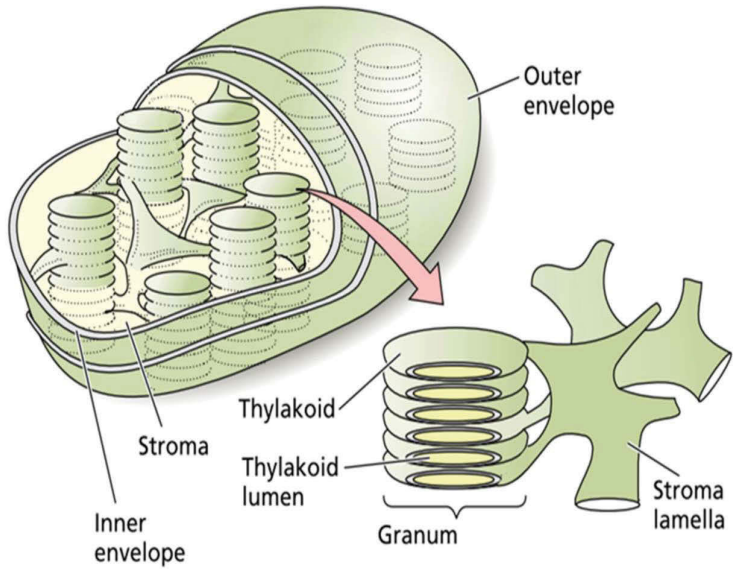

Figure 1.2. Schematic chloroplast structure. A chloroplast is comprised of two envelope membranes encompassing the stroma. The stroma lamella is a single membrane connecting grana, which are stacks of thylakoid. Adapted from Taiz and Zeiger (2010).

lumen from the stroma. The machinery of the light reaction is located in and on thylakoid membranes while the Calvin-Benson cycle occurs in the stroma.

The *Arabidopsis* chloroplast has its own genome, of about 154 kilobases, encoding the essential components for gene expression (including rRNA, tRNA, ribosomal proteins and RNA polymerase subunits), and genes for photosynthesis reactions and metabolic pathways unrelated to photosynthesis such as fatty acid biosynthesis (Wicke et al., 2011, Olejniczak et al., 2016). Although a semi-autonomous organelle with its own circular DNA, chloroplast development and gene expression are largely regulated by the nucleus. The vast majority of chloroplast proteins are encoded in the nuclear genome, synthesized in the cytosol and imported to chloroplasts by a special import machinery (Jarvis and Lopez-Juez, 2013). As a result, most of the photosynthetic apparatus is comprised of subunits encoded by both chloroplast and nucleus genomes. For instance, the ribulose-1,5-bisphosphate carboxylase/oxygenase (Rubisco) is comprised of eight large subunits encoded by a chloroplastic gene and eight small subunits that are encoded by a family of nuclear genes (Wicke et al., 2011). The coordination of gene expression in the two genomes is important for proper chloroplast protein assembly. The regulation of the nuclear-encoded chloroplast-targeted genes has been extensively studied (Leister, 2003, Jarvis and Lopez-Juez, 2013). There is evidence for chloroplast-to-nucleus signalling, also called retrograde signalling, regulating nuclear gene expression, as demonstrated by the *genomes uncoupled* (*GUN*) mutants (Mochizuki et al., 2001, Jarvis and Lopez-Juez, 2013). The mechanism of retrograde signalling has not been fully elucidated. It has been shown that perturbation in chloroplast tetrapyrrole biosynthesis is associated with the altered expression of the nuclear-encoded chloroplast-targeted genes (Mochizuki et al.,

2001). However, it is debatable whether tetrapyrrole, the precursor in chlorophyll biosynthesis, is directly involved in the retrograde signalling pathway as a mobile signaling molecule (Mochizuki et al., 2008, Leister, 2012).

1.5.2 Photosynthesis is the source of plant energy and fixed carbon dioxide

Photosynthesis is the photochemical pathway where solar energy (photons) is used to drive the assimilation of CO_2 for the synthesis of organic compounds, which in the first instance are carbohydrates, such as sucrose and starch, and in the long term the lipids, amino acids and other organic substances, that can be mobilized and used by plant tissues to sustain growth. Photosynthesis can be divided into two processes, i) the light-dependent photochemical reaction, also called the light reaction, and ii) the Calvin-Benson cycle, also known as the dark reaction. In the light reaction, the energy from photons is used to generate ATP (energy) and NADPH (reductive potential) with water molecules as the source of electrons and protons. The NAPDH and ATP are used in the subsequent Calvin-Benson cycle to drive the conversion of CO_2 into triose phosphate and the regeneration of the substrate for carboxylation, ribulose-1,5-bisphosphate (RuBP). Triose phosphate is the precursor for the synthesis of sucrose. Sucrose is the primary energy source that is mobilised and utilised by plant cells or stored as starch, which is largely remobilized in the subsequent night to sustain growth and respiration in the dark.

1.5.3 Light harvesting

In the light reaction of photosynthesis, photosystems (PS) and light harvesting complexes (LHC) are the important components. There are two light harvesting complexes, light harvesting complex I (LHCI), largely attached to photosystem I (PSI) and light harvesting complex II (LHCII), largely attached to photosystem II (PSII), which absorb light and funnel the energy in the form of photons to the PSI and PSII. A LHC monomer is comprised of a protein with three transmembrane helices that bind to several light harvesting pigments (Liu et al., 2004). Light harvesting pigments carotenoid, chlorophyll a (Chl *a*) and chlorophyll b (Chl *b*) have an excited-state energy decreasing from high to low. This makes energy transfer from carotenoid via Chl *a* to Chl *b* an irreversible and efficient process. In higher plants, Chl *a* and Chl *b* are the most abundant pigments in the chloroplasts. Chlorophyll is also present in the core of the reaction centres as the primary redox conversion system of both photosystems: special Chl *a* called P700 and P680 in PSI and PSII, respectively (P stands for pigment and the number refers to the wavelength at which the reaction centre chlorophyll shows a maximum absorption).

Changes in Chl *a* to Chl *b* ratio usually occurs in plants grown under different light environments, for instance, shaded plants usually have a lower Chl *a* to Chl *b* ratio due to an increased Chl *b* content (Tanaka et al., 2001). Other pigments, such as xanthophyll, are also found in LHC (Jahns and Holzwarth, 2012). Those pigments are not involved in the light harvesting process but serve as mediators in the photon protection mechanism that diverts excess photons away from the photosystems and dissipates the excessive energy as heat, thereby preventing the photosystems from being photo-damaged, under

excessive light, also known as the Xanthophyll cycle (**Figure 1.3d**) (Jahns and Holzwarth, 2012).

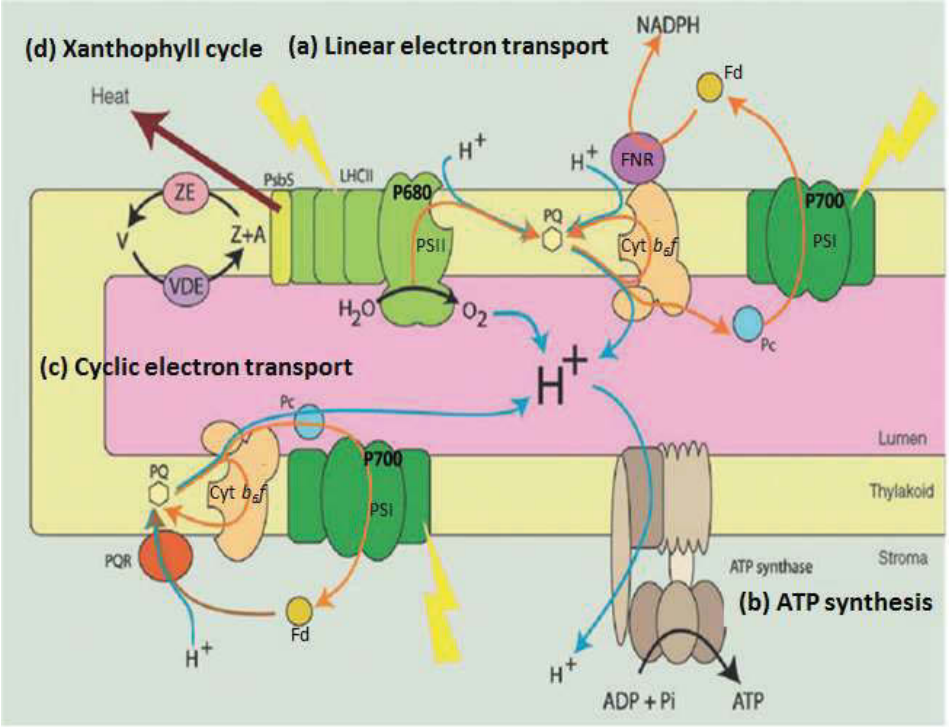

Figure 1.3. Schematic representation of the electron (orange arrows) and proton transfers, and photochemical processes that happen as a result of light absorption by the thylakoid photosystems. Under illumination, the photosystem II (PSII) and photosystem I (PSI) absorbs photons and oxidises their reaction centres, P680 and P700, respectively. (a) The linear electron transport begins from water molecules to NADPH. The first electron acceptor, plastoquinone (PQ), takes on the electrons derived from water molecules and stromal protons and generate PQH_2. From PQH_2, the electrons are transferred via the cytochrome b_6f complex (Cyt b_6f) and plastocyanin (PC) to PSI, which then transfers the electrons via a water-soluble iron sulphur protein, ferredoxin (Fd), and a ferredoxin NADP oxidoreductase (FNR) to NADP resulting in the generation of NADPH. (c) In the cyclic electron transport, the electrons from PQH_2 are returned via the Cyt b_6f to PQ.

Continued in the next page

Excitation of PSI can also result in the cyclic electron transport from PSI via ferredoxin, PQ, the cytochrome b_6f complex and plastocyanin. Reduction of plastoquinone by ferredoxin is catalysed by a plastoquinone reductase (PQR). (b) The oxidation of water molecules by PSII and PQH_2 by the cytochrome b_6f complex release protons into the thylakoid lumen generating a proton motive force across the thylakoid membrane. Movement of protons from the lumen to the stroma via the ATP synthase results in ATP synthesis. (d) During photosynthesis, as more protons accumulate in the lumen resulting in decreasing lumen pH and the PsbS protein in the PSII antenna i.e light harvesting complex II (LHCII) is protonated. PsbS then mediates the dissipation of excessive energy around PSII in the form of heat to prevent damaging of photosystems. The heat dissipation process is associated with the pH-dependent activation of violaxanthin de-epoxylase (VDE), which reduces violaxanthin (V) to zeaxanthin (ZE) and antheraxanthin (A). Adapted from Baker et al. (2007).

1.5.4 Light reaction

Photosynthesis begins from the excitation of a reaction centre after absorption of a photon and excitation energy transfer across the pigment bed from the LHC. P700 and P680 are then excited (excited states are designated as P680* and P700*, respectively). Electron transport begins with the oxidation of the reaction centre of the photosystems, and continues along the linear electron transport chain to produce NADPH (**Figure 1.3a**). The P680* transfers an electron to the primary acceptor in the electron transport chain, phaeophytin. The electron is then passed from the reduced phaeophytin to a PSII bound plastoquinone, Q_A, then to a second plastoquinone, Q_B. After accepting two electrons from Q_A, the reduced Q_B takes on two protons from the stroma, and disassociates from its protein binding site in PSII in the form of PQH_2 and binds to the cytochrome b_6f complex (Cyt b_6f) where plastocyanin is reduced. Plastocyanin is a mobile copper protein that shuttles between Cyt b_6f complex and the PSI complex. The reduced plastocyanin then binds to PSI and recovers the oxidized P700 ($P700^+$), which has been previously oxidized by donating an electron through intermidiates to ferredoxin after receiving the second photon. Ferredoxin-NADP reductase then catalyses the reduction of the final electron acceptor $NADP^+$ to NADPH. In summary, in PSI the production of one molecule of NADPH via the linear electron transport chain requires two electrons from the linear electron transport chain, which in turns requires four photons, two at each photosystem. PSII catalyses the oxidation of water molecules that generates electrons, protons and oxygen molecule. The source of electrons for the oxidized $P680^+$ and $P700^+$ is water splitting at the start of the photosynthetic electron transport system. The protons derived from water splitting are released into the thylakoid lumen, contributing to the formation of a proton concentration difference across the thylakoid membrane, also known as the

proton motive force, which drives ATP synthesis via the ATP synthase (**Figure 1.3b**). The photosynthesis apparatus can also undergo a cyclic electron transport which is a necessary source of the proton motive force. In the cyclic electron transport, the PQH_2 molecule from the stromal side diffuses to the lumen side of the thylakoid membrane to oxidize the Cyt b_6f complex, resulting in the release of two protons into the lumen (**Figure 1.3c**).

1.5.5 Dark reaction

The Calvin-Benson cycle (**Figure 1.4**) is a light-independent process where atmospheric CO_2 and water are used, initially, to produce carbohydrates that serve as precursors for many metabolic pathways. The reaction begins with the interaction between CO_2, water and RuBP to produce two molecules of 3-phosphoglycerate. This process is catalysed by the enzyme ribulose bisphosphate carboxylase/oxygenase (Rubisco). The three-carbon intermediate 3-phosphoglycerate then undergoes a ATP-dependent phosphorylation to produce 1,3-biphosphoglycerate, which is then reduced to glyceraldehyde-3-phosphate, also known as triose phosphate, using NADPH as the reductant. One triose phosphate molecule can have three different fates: (1) be used in producing sucrose as the energy currency used in cellular activities (2) be stored in the cytosol in the form of starch or (3) be used in regenerating the CO_2 acceptor RuBP to maintain the cyclic pathway. On average, the carboxylation of three RuBP molecules is required for the net synthesis of one triose phosphate molecule and the regeneration of three starting molecules, RuBP. This process requires nine molecules of ATP and six molecules of NADPH generated from the light reaction.

Rubisco also undergoes a second catalytic reaction: instead of CO_2 it can stimulate RuBP to react with a molecule of oxygen. This apparently "unwanted" reaction of RuBP is possibly the result of the fact that the evolution of Rubisco occurred in a largely anaerobic atmosphere, with high levels of atmospheric oxygen only occurring in relatively recent times. The oxygenation of one molecule of RuBP generates one molecule of 3-phosphoglycerate and one molecule of 2-phosphoglycolate. 2-phosphoglycolate is a toxic compound that inhibits the activity of triose phosphate isomerase (which is a crucial enzyme in the Calvin-Benson cycle) (Anderson, 1971), and it is recycled by the photorespiratory nitrogen cycle. In the photorespiratory nitrogen cycle, the recycling of 2-phosphoglycolate is followed by the release and re-fixation of ammonia for the production of amino acids. The whole photorespiratory nitrogen cycle is mediated by numerous enzymes and transporters in chloroplasts, peroxisomes and mitochondria (reviewed by Bauwe et al., 2010). Two molecules of 2-phosphoglycolate are required to generate one molecule of 3-phosphoglycerate and about one out of four 2-phosphoglycolate carbon atoms is released as CO_2 (Bauwe et al., 2010). This means that photorespiration operates at the expense of the CO_2 assimilated in the Calvin-Benson cycle.

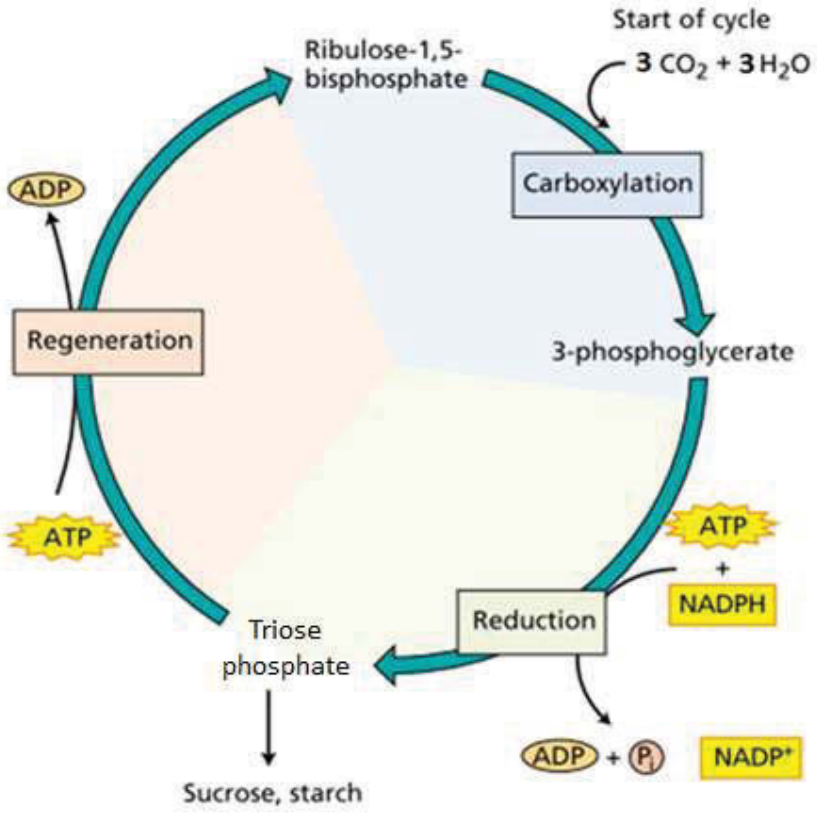

Figure 1.4. Schematic Calvin-Benson cycle. Adapted from Taiz and Zeiger (2010).

1.5.6 Determination of the biochemical capacity of photosynthesis processes

As Rubisco is a relatively large enzyme and a slow catalyst, the carboxylation process is the rate limiting reaction of photosynthesis in high irradiance and atmospheric CO_2. The parameter, the maximum velocity of carboxylation in Rubisco (V_{cmax}), is used as the indicator for the Rubisco capacity. The regeneration of RuBP depends on NADPH generated from the light reaction, where the parameter, chloroplast electron transport rate (J), is used to represent the electron transport capacity. Both V_{cmax} and J can be estimated from measurements of the net CO_2 assimilation rate (A) using an infrared gas exchange analyser. The reason why V_{cmax} and J are more robust parameters than A for studying photosynthesis in plants is mainly because A includes the photosynthetic CO_2 gain and the CO_2 loss in processes like photorespiration and mitochondrial respiration. A is also strongly affected by environmental variables, such as light, temperature, and anatomical factors such as stomatal conductance (Condon et al., 2004). The most frequently used method for determining V_{cmax} and J is by measuring A as a function of intercellular CO_2 partial pressure (C_i) under saturating light, also known as CO_2 response curves or A/Ci curves, followed by fitting to the model of C_3 photosynthesis (Farquhar et al., 1980, von Caemmerer, 2000, Sharkey et al., 2007). Alternatively, J can also be estimated from the fluorescence parameters measured from P680 of PSII using a pulse amplitude modulated fluorometer (Schreiber, 2004).

When returning to the basal energy state, the excited P680* emits fluorescence that can be quantified to describe the activity of PSII and can be used to determine photosynthesis activities (Schreiber, 2004, Baker et al., 2007). It has been shown empirically that the

quantum yield of PSII i.e. the electron flow through PSII per unit quantum flux could be calculated from chlorophyll fluorescence measurements (Genty et al., 1989), which allows the calculation of the rate of chloroplast electron transport as a function of photon flux density, also called photosynthetically active radiation (PAR; in the unit of μmol photons m^{-2} s^{-1}) (Edwards and Baker, 1993). This method is also known as the light response curve (Schreiber, 2004, Baker, 2008). The *J* estimated from the chlorophyll fluorescence assay has been shown to correlate closely with that obtained by measuring gas-exchange (Genty et al., 1989, Edwards and Baker, 1993).

1.6 Heterosis in early developmental stages

Heterosis in biomass appears early in seedling development, as early as in the cotyledon stage (Meyer et al., 2004, Groszmann et al., 2014). Some findings have shown that heterosis in early developmental stages is critical for hybrid growth in the later stages. 21 DAS *Arabidopsis* C24/Col hybrids that were bleached with the herbicide norflurazon, an inhibitor of phytoene desaturase in carotenoid biosynthesis (Breitenbach et al., 2001), from the cotyledon stage showed no heterosis in biomass compared with the parents (Fujimoto et al., 2012). Biomass heterosis in vegetative growth in early vegetative stage has been reported in hybrid crops such as *Brassica rapa* (Chinese cabbage) hybrids (Saeki et al., 2016). In *Brassica rapa* hybrids, plants with norflurazon-treated cotyledons showed no heterosis in the subsequent leaves, even though chlorophyll biosynthesis in those leaves was restored (Saeki et al., 2016). The opposite treatment, when hybrids have green cotyledons but are bleached in the first true leaves, hybrids retained heterosis in growth relative to the parents (Saeki et al., 2016). A recent study showed that photosynthesis-

related genes in 3 DAS *Arabidopsis* C24/L*er* hybrids were differentially up-regulated relative to the parents (Zhu et al., 2016). 3 DAS was when the cotyledons just emerged from the seed coat and started turning green, which marks the transition from seed to seedling development (Chaiwanon et al., 2016). It is still not clear when and how the heterosis in biomass is first set, and how photosynthesis in the early stage could have such a great impact on hybrid growth at later stages.

1.7 Research aims

Increasing population and the concomitant demand for more food is a global issue that has prompted researchers to investigate ways to increase food production. Studying the mechanism of heterosis could benefit global food production by giving potential traits for screening for hybrids with better performance, and could provide candidate molecular pathways for engineering to improve crop yield.

Biomass heterosis is a common trait in the F1 generation of many crop species. Alterations in photosynthetic properties might contribute to the biomass heterosis. Transcriptome analyses have shown that genes encoding the proteins in photosynthesis pathway are up-regulated earlier in hybrids than in the parents, but little has been shown regarding the photosynthetic properties of hybrids compared with the parents. Biomass heterosis might be determined by photosynthesis in the early seedling developmental stages. Characterisation of photosynthetic properties in different hybrids at different seedling developmental stages is important for understanding the relationship between photosynthesis and heterosis in vegetative growth.

The aims of this project were:

- To investigate the growth patterns of hybrids compared to their parents and to define the basis of heterosis in leaf size during development. In order to compare the growth patterns in hybrids and parents, the leaves of hybrids were analysed at different stages of leaf development for average cell size and total number of cells per leaf compared with that of the corresponding parent leaves. Rosette leaves are the photosynthetic tissues and source of photosynthate. To investigate whether the structure of hybrid leaves is different from the parents, the cross sectional thickness of hybrid leaves was determined and compared with that of the parent leaves.

- To analyse photosynthetic characteristics of *Arabidopsis thaliana* hybrids compared to the parents. Various photosynthetic parameters were analysed, including the CO_2 uptake rate per unit leaf area for the estimation of the maximum velocity of carboxylation in Rubisco and the electron transport rate per unit leaf area, chlorophyll fluorescence parameters for the estimation of electron transport rate per unit leaf area, chlorophyll content per unit leaf biomass, chlorophyll *a* to *b* ratio and chloroplast number per unit mesophyll cell area. Alterations in photosynthesis could contribute to the mechanism of heterosis in vegetative growth.

- To investigate whether the heterosis in vegetative growth can be further enhanced by elevated photosynthesis, hybrids were grown under high irradiance and assessed for changes in heterosis in biomass compared to that under standard irradiance.

- To investigate the impact of reduced photosynthesis in young seedlings on the generation of heterosis in subsequent vegetative growth by employing one of the *snowy cotyledon* mutants that has a white-cotyledon phenotype due to impaired chloroplast biogenesis in cotyledons. Mutant hybrids that have white, not photosynthetically competent cotyledons were assessed for alterations in heterosis in growth relative to the homozygous mutant parents, and compared to the wildtype hybrids.

2 Chapter II Methods and Materials

2.1 Plant cultivation

Arabidopsis thaliana seeds were sterilized with bleach: ethanol solution (2:1). The sterilized seeds were germinated on sterile agar medium containing Murashige and Skoog (MS) salts supplemented with 3.0% (w/v) sucrose (pH 5.7). The seeds were then cold-treated at 4°C in the dark for three days before sowing in controlled environment chambers (Conviron ATC40 growth chamber, Winnipeg, Canada) under an irradiance of 120 μmol photons m^{-2} s^{-1} (Master TL5 HO 54W/865 SLV/40, Philips Lighting), 21°C in a 16-h photoperiod. After ten days into light (hereafter defined as 10 days after sowing, or 10 DAS), the seedlings were transplanted individually into 65 mm W x 65 mm L x 100 mm H square pots containing soil (Debco Seed Raising & Superior Germinating Mix, Debco, Australia). Twenty pots were placed in two 5x2-cell pot holder, in a 318 mm W x 456 mm L x 57 mm H water tray. Each tray was covered with cling wraps for three days to retain moisture. In each tray, five plants of two parents and their reciprocal hybrids were allocated by columns. Each tray was rotated regularly to minimize possible position effects inside the growth cabinet. For each experiment, at least three trays were used. For short-day experiments, an 8-h photoperiod was used. For doubled-light experiments, plants were grown in a controlled cabinet set to 240 μmol photons m^{-2} s^{-1}, under the same temperature and photoperiod as listed above. As a control, the light box for half of the shelves in the growth cabinet were covered with a 50% cut-off light filter (Neutral filter 209 0.3ND, *LEE* Filters, USA) so that the irradiance was reduced to 120 μmol photons m^{-2} s^{-1} without changing the light quality.

2.2 Manual hybridization

Hybrid seeds were produced by manually crossing between ecotypes Columbia-0 (Col), C24, Landsberg erecta (L*er*) and Wassilewskija (Ws). When at least 5-6 inflorescences had developed on a mature plant it was selected as the recipient plant for hand-pollination. Only 3-4 buds per shoot and a maximum of 3 shoots per plant were pollinated. All lateral shoots, siliques (fruits), excessive buds and meristems were trimmed and removed. The buds were emasculated by removing all stamen under a microscope using a pair of fine-tip forceps. The removed anthers were examined under a dissecting microscope to make sure no pollen had developed. The stigma of the recipient plant was then pollinated with mature anthers taken from the donor plant. The stigma that have been successfully pollinated would turn dark within the following 2-3 days. Inbred parents were produced from self-pollination. To ensure the seed quality was comparable to the hand-pollinated hybrids (Meyer et al., 2004), the same silique-restricting procedure (as described above) was applied for generating F1 parental seeds. Each of the branches were wrapped with coloured paper tapes with the parental origins clearly stated on it (e.g. “maternal parent x paternal parent” for F1 hybrids or “self” as the F1 parents). Mature siliques were collected in 1.5 mL micro-centrifuge tubes and labeled with the parental origins and the month/year collected. The collected siliques were air-dried in the laboratory for two weeks before isolating the mature dry seeds from the siliques using a nylon mesh. The isolated seeds were stored in 1.5 mL micro-centrifuge tubes with pin holes drilled on the lids using a needle (25 G x 5/8”, TERUMO Hypodermic Needles, TERUMO, Japan). The newly collected seeds that had broken dormancy (> 2 months after maturation) were tested for germination rate before being used in experiments.

2.3 Determination of size, biomass and growth parameters

Fresh weights of rosettes or leaves were determined immediately after harvest using an electronic semi-microbalance (Type 1872, Sartorius Research, Germany). Leaf or rosette areas were determined from the photos taken upon harvesting using an image analytic software ImageJ (National Institute of Health, USA).

For leaf mass per area measurements, the largest leaves of 28 DAS plants were sampled at 2 pm (7 hours in light). A photo of the leaf was taken upon sampling for leaf area determination as described above. The fresh weight of the leaf was determined before wrapping in aluminium foil and weighed again as the total fresh weight. The packs of leaves in foil were then placed in a 75˚C oven and dried overnight until a constant weight was obtained. The leaf dry weight was determined as below:

$$\text{Leaf dry weight (mg)} = \text{leaf fresh weight} - (\text{total weight of fresh leaf in foil} - \text{total weight of dry leaf in foil})$$

2.4 CO_2 assimilation

The most frequently used method for understanding photosynthetic capacity is by measuring the net CO_2 assimilation rate (A) as a function of intercellular CO_2 partial pressure (C_i) under a saturating light, also known as CO_2 response curves or A/Ci curves. This method enables the estimation of the maximum velocity of Rubisco carboxylation

(V_{cmax}) and the electron transport rate (J). V_{cmax} and J are more robust parameters than A for studying photosynthetic capacity in plants.

2.4.1 Protocol for A/Ci curves

The measurement was carried out in a controlled growth room (light cycle 16 hr/ 8 hr, 21 ºC, 120 µmol photons m^{-2} s^{-1}). To avoid possible effects of time of day on photosynthetic rates the analyses were carried out between 2 to 8 hr after lights on. Plants to be analysed were moved out from the Conviron growth cabinets into the growth room the night before the measurement. The desiccants were replaced every time before starting the LiCOR (6400XT, LICOR). The LiCOR head (standard 2 cm × 3 cm) was mounted on a tripod and placed on the floor close to the shelf where the plants were located. After turning on the device, both the soda lime and desiccant were put to full scrub with the measurement chamber closed. The LiCOR was set to an air flow rate of 300 µmol s^{-1}, leaf temperature to 21 ºC, actinic light to 120 µmol photons m^{-2} s^{-1} (or 240 µmol photons m^{-2} s^{-1} for the doubled light-grown plants) and the leaf fan to full speed. During warm up, the CO_2 and H_2O concentrations in the measurement chamber were monitored to make sure the measurement chamber was free from leakage or malfunction. After the CO_2 and H_2O in the chamber reached to a basal concentration of 0 ± 5 µmol mol^{-1} (normally takes 15 minutes), the mixer was switched on and the reference [CO_2] was set to 400 ppm. Once the reference and sample [CO_2] (displayed as “CO2R” and “CO2S, respectively) had stabilised, the leaf of analyses was placed into the chamber (touching the thermocouple) by adjusting the positions of the pot, the height of the tripod and the angle of the device. The latch was loosen before closing to prevent damaging the leaf. After closing the

chamber, the latch was adjusted so that the sealing gasket was just touching the leaf. To test for leaks, I blew air around the chamber and changes in the [CO_2] was monitored. If the [CO_2] in the chamber (displayed as "CO2S" on the screen) increased dramatically, the latch was tighten further to ensure the airlock of the chamber. The humidity (displayed as "RH_S_%", which stands for the relative humidity in the sample cell) was monitored and controlled within a range between 60-70% by adjusting the desiccant to scrub excessive moisture.

The measurement of the A/Ci curve was carried out using the automatic logging program set as below, unless stated otherwise:

PAR: 1000 μmol m^{-2} s^{-1}

[CO_2]: 400, 50, 100, 200, 400, 600, 800, 1000, 1500, 400 μmol mol^{-1}

Stability wait: minimum 180 seconds; maximum 240 seconds

Match before log: always

Post-match recovery: minimum 10 seconds; maximum 20 seconds

After the measurement, the chamber was open carefully so that the leaf analysed was in place. Before taking out the leaf, the outline of the leaf area inside the measurement chamber was traced using a marker pen. The photo of each leaf analysed was taken and the leaf area was determined using the image analyser software ImageJ (National Institutes of Health, USA). After retrieving the result, the leaf area (cm^2) was put into the

"Area" column in the Excel sheet that contains the raw data of the corresponding leaf for further analysis.

2.4.2 Modelling for A/Ci curves

According to the Farquhar-von Caemmerer-Berry model of C_3 photosynthesis (Farquhar et al., 1980), the biochemical reactions of photosynthesis can be described by the enzymatic properties of ribulose bisphosphate carboxylase/oxygenase (Rubisco), which catalyses the first reaction in the Calvin-Benson cycle. When [CO_2] is low and the supply of the Rubisco substrate, ribulose 1,5-bisphosphate (RuBP), is abundant, the rate of photosynthesis is limited by the activity of Rubisco. This state is called Rubisco-limited photosynthesis. Under higher [CO_2], photosynthesis is limited by the regeneration of RuBP; this is called RuBP-regeneration-limited photosynthesis. Factors that could affect this process are, but not limited to, the catalytic activity of the enzymes in the Calvin cycle, and the supply of ATP and NADPH from the light reaction. Increasing [CO_2] increases A because that CO_2 is the substrate for carboxylation; increasing [CO_2] increases RuBP carboxylation at the expense of oxygenation, reducing the release of CO_2 in photorespiration; and increasing the light use efficiency of photosynthesis. When [CO_2] is high, sometimes A is insensitive to further increase of [CO_2] (Sharkey, 1985). In this condition, the rate of photosynthesis is limited by the rate at which triose phosphate is used in the synthesis of sucrose or starch, this is called triose phosphate use limitation. Other exports of carbon from the Calvin cycle can also contribute to this state, including direct use of the photorespiration end products glycine and serine (Bauwe et al., 2010).

2.4.3 Equations for curve-fitting

To estimate V_{cmax} and J, the A/C_i curves were fitted to the C_3 photosynthesis model using the fitting method developed by Sharkey et al. (2007). When A is Rubisco limiting, photosynthesis rate can be described by the following equations:

$$A = V_{cmax}\left[\frac{C_c - \Gamma^*}{C_c + K_C(1 + O/K_O)}\right] - R_d$$

where V_{cmax} is the maximum velocity of Rubisco for carboxylation, C_C is the partial pressure at Rubisco active sites, K_c is the Michaelis constant of Rubisco for carbon dioxide, O is the partial pressure of oxygen at Rubisco active sites, K_O is the inhibition constant of Rubisco for oxygen, R_d is the day respiration and Γ* is the [CO2] at which the CO_2 uptake in the carboxylation is equivalent to the CO_2 releases from the oxygenation i.e. the compensation point of CO_2.

When A is RuBP regeneration limiting, photosynthesis rate can be described by the following equation:

$$A = J\frac{C_c - \Gamma^*}{4C_c + 8\Gamma^*} - R_d$$

where J is the rate of electron transport required to support NADPH synthesis for RuBP regeneration at the measurement light intensity.

When A is triose phosphate use limiting, photosynthesis rate can be simply described as:

$$A = 3TPU - R_d$$

where *TPU* is the rate of use of triose phosphates.

C_c can be descirbed as

$$C_c = C_i - A / g_m$$

where g_m is the mesophyll conductance estimated from the RuBP regeneration-limited data.

Data points with C_i <200 ppm were considered as the Rubisco-limited photosynthesis (designated as "1"); the data point with C_i between 200-300 ppm was excluded from the fitting (designated as "0"); data points with Ci >300 ppm were considered as RuBP regeneration-limited (designated as "2"); and the data points located at the plateau region of the curve that had a consistent or reduced A were considered as the triose phosphate use-limited (designated as "3").

2.5 Chlorophyll fluorescence assay

The chlorophyll fluorescence of the PSII reaction centres of photosystem II (PSII) has been empirically proven a good tool for the investigation of photon fluxes around PSII, such as the distribution of energy dissipation pathways, photochemistry efficiency (reviewed by Schreiber (2004)). The photon-use efficiency of PSII electron transport was

as described by Genty et al. (1989) and Schreiber (2004) using a pulse amplitude modulated (PAM) fluorometer (Closed FluorCam FC 800-C, Photon Systems Instruments, Czech Republic). The PAM fluorometer is fitted with light-emitted diode panels to induce PSII photosynthesis, and charge-coupled device that can record the fluorescence profiles emitted from the excited PSII. To obtain the fluorescence parameters for estimating photon use in PSII photosynthesis, three different light beams were used: (1) blue light (447 nm) was used to induce PSII photochemistry, termed as photosynthetically active radiation (PAR) or actinic light; (2) weak far-red light (~740 nm, 30 μmol photon m^{-2} s^{-1}) was used to induce photosynthesis at PSI, which removes the electrons from the PSII electron transport chain; (3) saturating pulse (cool white light with a colour temperature 6500K; ~6,000 μmol photon m^{-2} s^{-1}) was used to simultaneously saturate all the PSII reaction centres. To avoid possible effects of time of day on photosynthetic rates the analyses were carried out between 2 to 8 hr after lights on.

2.5.1 Saturation pulse method

First a weak red actinic light (0.1 μmol photon m^{-2} s^{-1}) was switched on. This weak light intensity was insufficient to induce photochemistry in PSII, but elicited some basal fluorescence. After 5 seconds, the fluorescence was recorded as the baseline fluorescence, designated as F_o. Next, the actinic light (447 nm) was switched on to induce photosynthesis. In order to obtain fluorescence of steady-state photosynthesis, the actinic light was on for 5 minutes before the fluorescence was recorded, designated as F'. The duration for the actinic light incubation was chosen according to a trail measurement

carried out on C24 from 3 up to 30 minutes showed that F' became a constant within 5 minutes. Right before the actinic light was switched off, a flash (800 millisecond duration) of saturating light was applied and the fluorescence was recoded, designated as F_m' (where m stands for "maximum", as all the P680 reaction centre were excited in the saturating pulse, resulting in a relative maximum fluorescence). The fluorescence measurement was finished by applying the far-red light for 1 second and the relative minimum fluorescence, F_o', was recorded. The prime notation (') used after a fluorescence parameter indicates that the fluorescence parameters are recorded under a continuous actinic light exposure, also known as the light-adapted parameters. For light response curves the illumination cycle described above was repeated with an increasing intensity of actinic light: 30, 200, 330, 440, 550, 640, 720 and 850 µmol photons m^{-2} s^{-1}. These light intensities were selected based on a trial light response curve carried out on the seedlings of C24 and Ler ecotypes using several intensities from 40 up to 2000 µmol photons m^{-2} s^{-1} showed that the light response curve reaches the plateau phase at around 600 µmol photons m^{-2} s^{-1}.

2.5.2 Calculations of efficient quantum yield of PSII and electron transport rate

The effective quantum yield of PSII (Φ_{PSII}) can be calculated from the light-adapted fluorescence parameters as illustrated below:

$$Effective\ quantum\ yield\ of\ PSII\ (\emptyset_{PSII}) = F_q'/F_m' = [F_m' - F']/F_m'$$

Quantum yield means the quanta (photons) used in a reaction i.e. photosynthesis in this case. It is assumed that all the photons absorbed by P680 are used to generate electrons.

The differences between F' and F'_m is defined as the quenched fluorescence (F'_q). The term "quenched" is used to describe the energy fluxes around PSII to energy-dissipating processes like photosynthesis, light-regulated heat-loss and spontaneous, non-regulated decay (Baker, 2008). F'_q is the fluorescence emitted from the excited P680* under a given photon flux density. The ratio of F'_q to F'_m represents the proportion the P680 presenting on the surface of a sample being excited, which reflects the fraction of an incident light being used in PSII photosynthesis.

$\emptyset_{PSII}$ fluctuates with the illumination intensity and reflects the part photosynthesis efficiency shortly before the measurement. Under low light, $\emptyset_{PSII}$ is proportional to the light intensity. As the illumination increases, $\emptyset_{PSII}$ decreases. It is because as the proton gradient continues to accumulate and the pH in thylakoid lumen decreases, the photon protection mechanism is activated and redirects photons from the PSII-LHC to be dissipated as heat. Despite the decreasing $\emptyset_{PSII}$, the total photons being used by PSII under high light are still greater than that under lower light. In order to reflect the actual photon utilisation in PSII, $\emptyset_{PSII}$ was used to calculate the rate of electron transport, as illustrated below:

$$Electron\ transport\ rate\ (ETR\ or\ J) = PAR \times abs \times \beta \times \emptyset_{PSII}$$

where PAR is the incident photosynthetically active radiation and *abs* is the leaf absorptance. On average, a healthy leaf of higher plants absorbs about 84% of the incident PAR (Demmig and Bjorkman, 1987). β represents the fraction of the absorbed photons that are subsequently absorbed by PSII. It is generally assumed that the absorbed photons

are equally distributed between the two photosystems, PSII and PSI, and a value of β = 0.5 is used. The equation for electron transport rate can be illustrated as:

$$ETR\ (or\ J) = PAR \times 0.84 \times 0.5 \times [F_m' - F']/Fm'$$

2.5.3 Curve-fitting

By plotting ETR against an increasing PAR generates a light-response curve. When light intensity is low, the photosynthesis rate is limited by the light thus the rise of the curve is proportional to the irradiance given. Under high irradiance, ETR is limited by the size of reductant/oxidant pool in the electron transport chain and the ETR reaches a plateau. The light response curve can be described as the function illustrated below:

$$ETR\ = \frac{\alpha + ETR_{max} - \sqrt{(\alpha + ETR_{max})^2 - 4\theta\alpha ETR_{max}}}{2\theta}$$

where α is the initial slope of the curve; ETR_{max} is the estimated maximum electron transport rate; θ is an empirical curvature factor. These calculated parameters were fitted for least square deviation using a fitting sheet developed by Katherine Meacham (unpublished).

2.6 Chlorophyll quantification

Leaf (or cotyledon) tissue was weighed and extracted for chlorophylls by homogenizing in liquid nitrogen, using a pestle and motar. The tissue powder was dissolved in 95% (vol/vol) ethanol. The tissue debris was centrifuged and the supernatants were kept on ice,

in the dark for further analysis. The chlorophyll-containing supernatants were taken for absorbance determination at wavelength 664.2 and 648.6 nm as described by Porra et al. (1989). The chlorophyll a and chlorophyll b content were determined using the formulae described by (Lichtenthaler and Buschmann, 2001):

$$Chlorophyll\ a\ (\mu g/ml) = 13.36 \times A^{664} - 5.19 \times A^{648}$$

$$Chlorophyll\ b\ (\mu g/ml) = 27.43 \times A^{648} - 8.12 \times A^{664}$$

2.7 Chloroplast content

The number of chloroplasts per mesophyll cells was determined following the protocol described by Okazaki et al. (2009). Briefly, cotyledons or leaves were fixed with 3.5% glutaraldehyde for 2 hrs and de-calcificated with 0.1 M Na_2-EDTA (pH 9.0) at 50 ^{o}C for 15 min. Single mesophyll cells were isolated by gently pressing the fixed tissue between a glass slide and a cover slip using the eraser end of a pencil. The microscopic images of the isolated, intact mesophyll cells were taken under Differential Interference Contrast (DIC) optics using an optical microscope (Axio Imager, ZEISS, USA) and the number of chloroplast per cell were counted. The number of chloroplast per cell was then divided by the cell area determined by the image analytical software ImageJ (National Institutes of Health, USA).

2.8 Palisade mesophyll cell size and cell number determination

Cotyledons or leaves were fixed with acetic acid: ethanol (3:1) for one week. The buffer was replaced every two days until all pigments were removed. Buffer was at least ten times the volume of the specimen. Specimens were stored in the fixative buffer until the day before examination. The specimen was cleared with chloral hydrate: water: glycerol (8:2:1) overnight. Specimen were mounted on glass slides and the edges of glass cover slides were sealed with nail polish. The specimen was examined under DIC optics (Axio Imager, ZEISS, USA) using the 20X objective. For each leaf examined, the microscopic images of the palisade mesophyll (PM) cell layer were taken at a total of 6 positions: 3 positions from the tip to bottom of the leaf blade on either side of the midvein. The number of palisade mesophyll cells at each position was counted. For cells touching the margins, only those on the left and bottom margins were counted. The average size of PM cells was determined by dividing the average PM cell number by the field area (600 μm x 528 μm). The area of the leaf lamina was determined by ImageJ. The total number of PM cell per leaf was determined by dividing the leaf area by the average PM cell size. Leaf area was determined by ImageJ.

2.9 Determination of leaf cross-section thickness

The thickness of a leaf varies greatly at different positions e.g. it is thicker in the middle of the leaf and thinner towards the leaf margins. The measurements of leaf thickness were carried out using cross-sections prepared from the centre of the leaf lamina (as illustrated in **Figure 2.1a**). The microscopic images of leaf sections were taken at the regions near the midvein as illustrated in **Figure 2.1b**; the distance between the adaxial and abaxial

epidermal layers was determined as the representative leaf thickness. All measurements of leaf thickness were carried out at positions without trichomes.

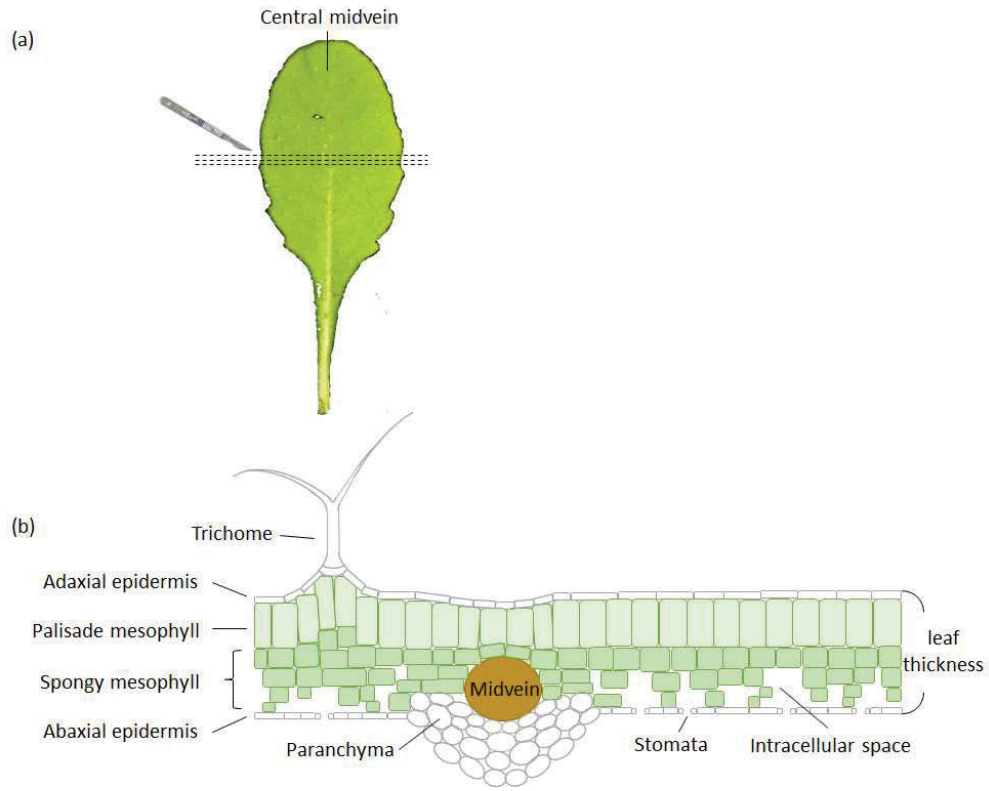

Figure 2.1. Determination of the thickness of leaf lamina. (a) Preparation of leaf cross-sections from the middle part of a leaf blade, across the central midvein, by free-hand sectioning using a fine shaving blade or scalpel. The dashed lines indicate the direction of sectioning. **(b)** Schematic illustration of the cross-section of midvein and the flanking lamina tissue. The thickness of the leaf was defined by the distance between the upper (adaxial) and lower (abaxial) epidermis.

2.10 Iodine staining for starch granules

Whole rosettes were harvested at the end of the day and the end of the night respectively at 19 DAS. Rosettes were cleared with ethanol to remove pigments before staining with Lugol's solution (0.1% I_2 dissolved in 1% KI) overnight. The stained rosettes were then rinsed three times with water to remove the excessive Lugol's solution. The rosettes were then transfer to a petri dish with water and displayed for photographing.

2.11 Starch quantification

Starch were extracted as described by Ni et al. (2009a). Pools of 2-3 rosettes were harvested at the end of the night i.e. one hour before lights on (ZT15 for long-day; ZT7 for short-day) and the end of the day i.e. one hour before lights off (ZT-1) respectively at the end of the vegetative phase (19 DAS under long-day plants; 5 weeks under short-day). ZT stands for Zeitgeber time; a zeitgeber means any environmental cue that entrains an organism e.g. the light for growth. The rosettes were weighed and snap-frozen in liquid nitrogen to stop metabolism. Frozen tissue was ground in liquid nitrogen using a mortar and the homogenate was washed three times with 80% (vol/ vol) ethanol to remove pigments. The starch-containing pellets were collected by centrifugation and re-suspended with absolute ethanol (100 mg fresh weight in 5 mL). The starch suspension were heated in a boiling water bath for 10 minutes and vortexed at 2 minutes-intervals to extract starch. One hundred µl of the homogenate was transferred to 2 mL Eppendorf® Safe-Lock microcentrifuge tubes (Sigma-Aldrich). To reduce the volume of the starch samples, the tubes were placed in a vacuum concentrator (Savant SpeedVac Concentrator,

Thermo Scientific) for 3-4 hours and the starch slurry were used for further analyses. For each sample analysed, four duplicates of starch slurry were used.

For enzymatic quantification, the Total Starch Assay Kit (Amyloglucosidase/α-Amylase method, Megazyme, Ireland) was used and the manufacturer's protocol was followed. Two hundred µL of MOPS buffer (50 mM MOPS, 5 mM $CaCl_2$, 0.002% sodium azide, pH 7.0) was added to all four replicates. One of the four duplicates was used as the blank for free D-glucose. Ten µL of thermostable α-amylase (3,000 U/mL, dissolved in 100 mM sodium acetate buffer, pH 5.0) was added to the other three replicates and heated in boiling water bath for 10 minutes and vortexed every 2-minutes. Subsequently, 300 µL of sodium acetate buffer (200 mM, 0.002% sodium azide, pH 4.5) and 10 µL amyloglucosidase (3,300 U/mL) was added. The same procedures were applied to the glucose blanks, except for that the enzyme solution was replaced with the same volume of water. A starch control was also included, using the maize starch standard provided by the manufacturer. Four duplicates of 2 mg maize starch were treated as described above. The samples and starch controls were then incubated at 50°C in a Hybaid oven (Shake 'n' Stack Hybridisation Ovens, Thermo Fisher Scientific) for 1 hour then centrifuged at full speed for 10 minutes. Twenty µL of the supernatants and 180 µL of GOPOD reagent buffer (20X GOPOD stock diluted in distilled water) were transferred into 96-well plates (flat bottom). For each 96-well plate analysed, glucose controls consist of 2.5, 5, 7.5 and 10 µL of D-glucose standard solution (1 µg/µL) and 180 µL GOPOD reagent and a reagent blank solutions consist of 10 µL water and 180 µL GOPOD reagent were included. The plate was sealed with affix adhesive plate cover (Platemax axyseal sealing film, AXYGEN, USA) before incubating at 50°C in a Hybaid oven for 20 minutes. The

absorbance of each sample and the glucose control at 510 nm were read against the reagent blank using a plate reader (FLUOstar Omega Filter-based multi-mode microplate reader, BMG LABTECH, Germany). The starch content of each sample was presented as the amount of glucose equivalent per unit fresh weight. The calculation is as illustrated below:

$$\mu g\ glu^{equ}\ per\ mg\ fresh\ weight = \frac{\Delta A \div a \times D1 \times D2 \times \frac{162}{180}}{FW}$$

where ΔA is the average absorbance read from three replicates against the reagent blank subtracted by the absorbance read from the background free D-glucose; α is the slope of the glucose standard curve, which was generated by plotting the absorbance of the glucose controls against the concentrations; D1 is the dilution factor of the GOPOD mixture (= total volume/ sample volume = 520 ul/ 20ul = 26); D2 is the dilution factor of the sample solution on incubation with amyloglucosidase/α-amylase (= total starch suspension/ 100 µL); 162/180 stands for the adjustment of molecular weight from free-D-glucose to anhydro D-glucose as occurs in starch; FW is the fresh weight of the leaf samples.

2.12 Validation of *snowy cotyledon2* mutation

The genomic DNA were extracted using DNeasy Plant Mini Kit (Qiagen). To extract genomic DNA from *sco2* mutant and wildtype Ler, the true leaves of five 15 DAS seedlings were harvested and ground in liquid nitrogen with a pestle and mortar. Four µL Buffer AP1 was added to the tissue powder. The tissue suspension was transferred to a 1.5 mL microcentrifuge tube. Four µL RNase A was added to the tissue suspension and

vortexed to mix. After 10 minutes of incubation at 65 ˚C (the tube was inverted 2-3 times during incubation), 130 µL Buffer P3 was added. After incubated for 5 minutes on ice, the lysate was centrifuged at 14,000 rpm for 5 minutes (5424 Microcentrifuge, Eppendorf). The supernatants were transferred into a QIAshedder spin column placed in a 2 mL collection tube. The column was centrifuged at 14, 000 rpm for 2 minutes. Three hundred µL of the flow through was transferred into a 1.5 mL microcentrifuge tube. 450 µL (1.5 volumes) of Buffer AW1 was added to the lysate and mixed by pipetting. 650 µL of the mixture was transferred to a DNeasy Mini spin column placed in a 2 mL collection tube. The column was centrifuged at 8,000 rpm for 1 minute. The spin column was removed from the collection tube and the flow through was discarded. The centrifugation was repeated with the remaining sample. The spin column was placed into a new 2 mL collection tube. Five hundred µL Buffer AW2 was added to the column and centrifuged at 8,000 rpm. The flow through was discarded. Another 500 µL Buffer AW2 was added to the column and centrifuged at 8,000 rpm for 2 minutes. The spin column was placed to a new 1.5 mL microcentrifuge tube and 100 µL Buffer AE was added to the membrane of the column for elution. After incubated for 5 minutes, the spin column and the microcentrifuge tube was centrifuged at 8,000 rpm for 1 minute. The DNA concentration was determined using a Nanodrop (Thermo Fisher Scientific).

To amplify the *SCO2* and *sco2* gene, polymerase chain reaction (PCR) was carried out on the extracted genomic DNA using iProof High-Fidelity DNA polymerase (BIO-RAD). 250 ng of the extracted genomic DNA was aliquoted into a 200 µL PCR tube along with 10 µL iProof 5X buffer, 2 µL 5 mM dNTPs, 2.5 µL 20 µM primer mix (forward primer: TCGCACTCAGGGTTATCGTTT; reverse primer: TACTCCTCCAGAGAAAGGGC)

and 0.5 µL iProof polymerase. The mixture was topped with distilled water to a total volume of 50 µL. The PCR reaction was carried out using a Thermocycler (C1000 Touch Thermal Cycler, BIO-RAD) and the PCR program is described in **Table 2.1**.

Table 2.1. Thermal cycling protocol

Temperature	Time	Number of cycles
98˚C	30 sec	1
98˚C	5 sec	35
58˚C	10 sec	
72˚C	38 sec	
72˚C	300 sec	1

The PCR product (predicted size: 2507 bp) was validated by electrophoresis (PowerPac Basic Power Supply 300, BIO-RAD) at 100 V for 40 minutes on a 1% agarose gel pre-stained with DNA stain (RedSafe Nucleic Acid Staining Solution DNA stain, iNtRON Biotechnology) against a 1 Kb DNA ladder (Gold Biotechnology). The PCR product was diluted 5X in distilled water. To sequence the *SCO2* and *sco2* gene, the BigDye Direct Sanger Sequencing Kit (Thermo Fisher Scientific) was used. One µL of the 5X diluted PCR product was transferred into a 200 µL PCR tube with 1 µL BigDye, 3.5 µL 5X buffer, 10 µM sequencing primer (primer 1: ccagagctccgcttttgacc, primer 2: TATCCCTTGGCAGGGTATGC, primer 3: CACCCCAGTTTTGGGTGTGT and primer 4: ttgttgtagGGCGTCTCCTG) and 14 µL distilled water. The second PCR reaction was was carried out using a thermocycler (C1000 Touch Thermal Cycler, BIO-RAD) and the PCR program is described in **Table 2.2**.

To prepare the sample for sequencing, the PCR products was precipitated by ethanol and sodium acetate. Twenty µL of sequencing reaction into a 1.5 mL microcentrifuge tube

with 50 µL (2.5 volumes) absolute ethanol and 2 µL (1/10 volumes) 3 M sodium acetate. After precipitation at room temperature for 15 minutes, the mixture was centrifuged at full speed for 20 minutes. The DNA pellet was then washed with 250 µL ice-cold 70% ethanol solution and then centrifuged again at full speed for 5 minutes. The DNA pellet was dried in a vacuum concentrator (Savant SpeedVac Concentrator, Thermo Fisher Scientific) for 2 minutes. The samples were sequenced using Sanger sequencing technology by the ACRF Biomolecular Resource Facility at The John Curtin School of Medical Research (ANU, Canberra, Australia). The sequencing result of *sco2* samples were aligned against the wildtype sample using a *in silico* assembly software (VectorNTI, Thermo Fisher Scientific).

Table 2.2. Thermal cycling protocol

Temperature	Time	Number of cycles
94˚C	300 sec	1
96˚C	10 sec	35
50˚C	5 sec	
60˚C	240 sec	
10˚C	∞	1

2.13 Statistical analysis

Statistical comparisons between hybrids and the parents (or the average level of the parents) as well as all other comparisons were carried out using the Fit An Analysis Of Variance Model function (function “aov”, R Stats Package “stats v3.4.1”) in conjunction with the compute Tukey Honest Significant Differences (function “TukeyHSD”, R Stats Package “stats v3.4.1”). All the data used for the comparisons are in Appendices. The numbers of the appendices refer to the figure in the thesis.

3 Chapter III Analyses of heterosis in *Arabidopsis thaliana* hybrids

3.1 Introduction

Increased vegetative growth is one of the common traits found in hybrids including *Arabidopsis* and crop species (Meyer et al., 2004, He et al., 2010, Springer and Stupar, 2007). It is not clear whether the increased growth of hybrid plants is due to a more efficient photosynthetic process on a per unit leaf area basis or whether it is due to an increased photosynthetic capacity per plant as a result of larger leaves and more chloroplasts. C24/L*er* reciprocal hybrids were chosen for investigation for their strong heterosis in vegetative growth (Meyer et al., 2004, Groszmann et al., 2014). To see if hybrid vigour in vegetative growth is attributable to accelerated seedling development the germination time, leaf emergence and flowering time of hybrids were recorded and compared to the parents. Seedling growth (determined by rosette area) was measured on hybrid seedlings during early seedling development (1 week-old) and at later stages of vegetative phase (19 and 30 days after sowing; DAS). The level of heterosis (hybrid vigour) was defined as the percentage increase from the average of the parents referred to as the mid-parent value (MPV).

To investigate the anatomical basis for the larger hybrid leaves, hybrid leaves were analysed for palisade mesophyll cell size, estimated palisade mesophyll cell number per leaf, leaf thickness, and leaf mass per area (dry weight per leaf area), and compared to the

parents. Leaf size is defined by two processes: cell expansion and cell division (Donnelly et al., 1999, Gonzalez et al., 2012). The former can be measured by the size of leaf palisade mesophyll cells and the latter by the total number of palisade mesophyll cells per leaf (Kalve et al., 2014). There are two types of mesophyll cells, palisade mesophyll cells and spongy mesophyll cells. Palisade mesophyll cells are chosen because of their homogenous shape and regular arrangement due to fewer intercellular air spaces than in the spongy mesophyll.

To see whether hybrids have an increased photosynthetic capacity, the C24/L*er* hybrids were analysed for unit leaf area CO_2 assimilation rate, unit leaf area light harvesting efficiency, unit rosette biomass chlorophyll content and number of chloroplasts per mesophyll cell, and compared to the parents. In order to have a better understanding of the correlation between photosynthetic capacity and hybrid vigour, hybrids derived from different parents, such as C24/Col, Col/L*er* and Ws/L*er*, were included in some of the experiments, along with C24/L*er* hybrids.

3.2 Germination

The C24/L*er* hybrid seeds were scored for germination time and compared to the parents (**Figure 3.1**). Germinated seed was defined by the protrusion of the radicle (embryonic root) from the seed coat (**Figure 3.1a**). To be able to correlate germination time with subsequent seedling growth, this experiment was carried out under a light cycle of 16 hr/8 hr, the same conditions used for plant growth. All seeds completed germination within 72 hours of sowing (**Figure 3.1b**). Both C24/L*er* reciprocal hybrids germinated earlier than the parents, as indicated by the time when over half of the population had germinated; C24 x L*er* and its reciprocal hybrid at 39 and 37 hours after sowing, respectively; while the parents C24 and L*er* took 49 hours and 43 hours respectively (**Figure 3.1b**).

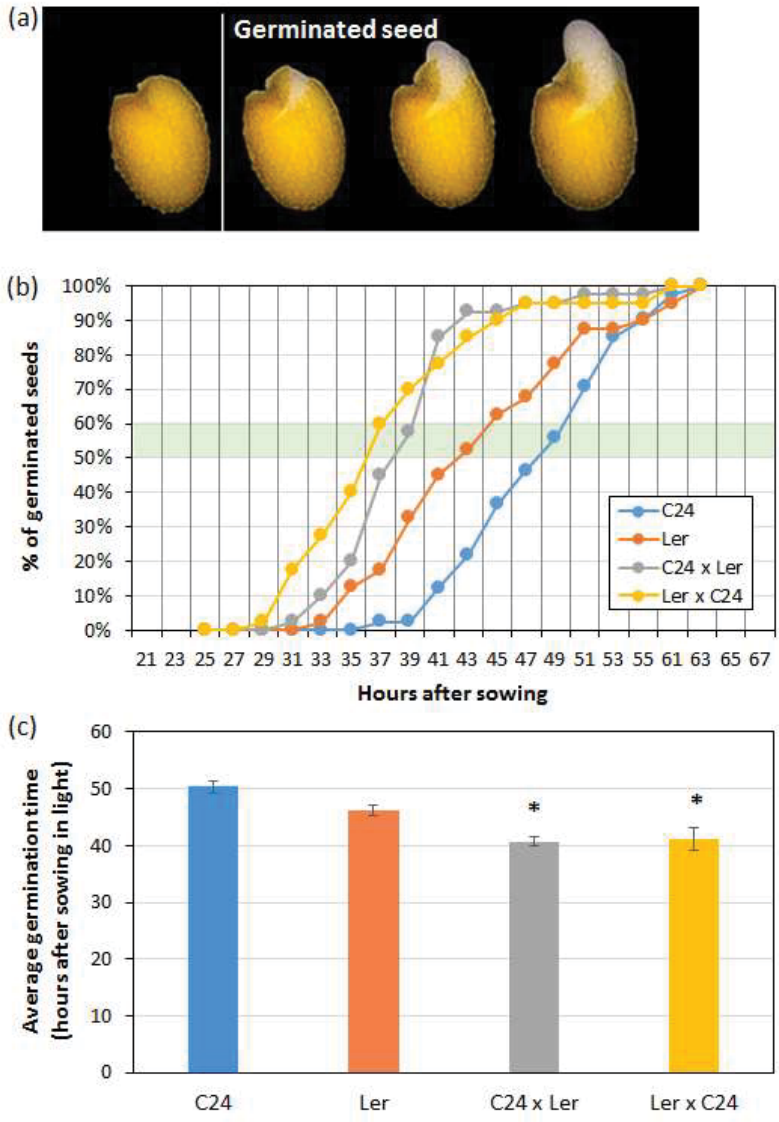

Figure 3.1. Comparison of germination time between C24/L*er* hybrid and parents. (a) Scoring of germinated seed by the protruding radicle. Photo credit: Wageningen Seed Lab (Netherland). **(b)** The percentage of germinated seeds within a population of n=20 seeds over a time course. Seeds were sown on Murashige and Skoog medium (3% sucrose). The seeds were kept at 4°C in the dark for three days before sowing in a temperature controlled culture room under a light cycle of 16hr-light/8hr-dak under a light intensity of 120 µmol photons m^{-2} s^{-1} at 21°C. All the seeds were moved into the culture room at 10:00 h (three hours after lights-on) and scored for germination every 2 hours. For statistical analysis, ANOVA was used to compare **(c)** the average germination times between hybrids with the better parent L*er* ($p < 0.001$, indicated by asterisks).

3.3 Leaf number per rosette

Changes in the number of leaves are an indication of altered seedling development. The C24/L*er* hybrids seedlings were scored for the number of leaves at 15, 18 and 21 DAS, and compared to the parents (**Figure 3.2**). For plants that had bolted, only rosette leaves were counted. Observations were carried out at the same time of day (10:00 -11:00 h).

At each time point examined, both C24/L*er* reciprocal hybrids had a greater number of leaves than the parents by at least one leaf (**Figure 3.2b**). The 15 DAS hybrid seedlings had an average of 7 leaves per rosette while the parents had 6 leaves (**Figure 3.2b**). At 18 DAS, hybrids had an average of more than 9 leaves per rosette whereas the parents had an average of just over 8 leaves per rosette (**Figure 3.2b**). Shortly after 18 DAS, the early flowering ecotype L*er* ceased to produce new leaves. The 21 DAS hybrids had 12 leaves or more per rosette while C24 had 11 leaves (**Figure 3.2b**). The differences in leaf number were attributed to the newly developed leaf located at the centre of the rosette whorl, suggesting each newly generated hybrid leaf emerges earlier than in the parents.

(a)

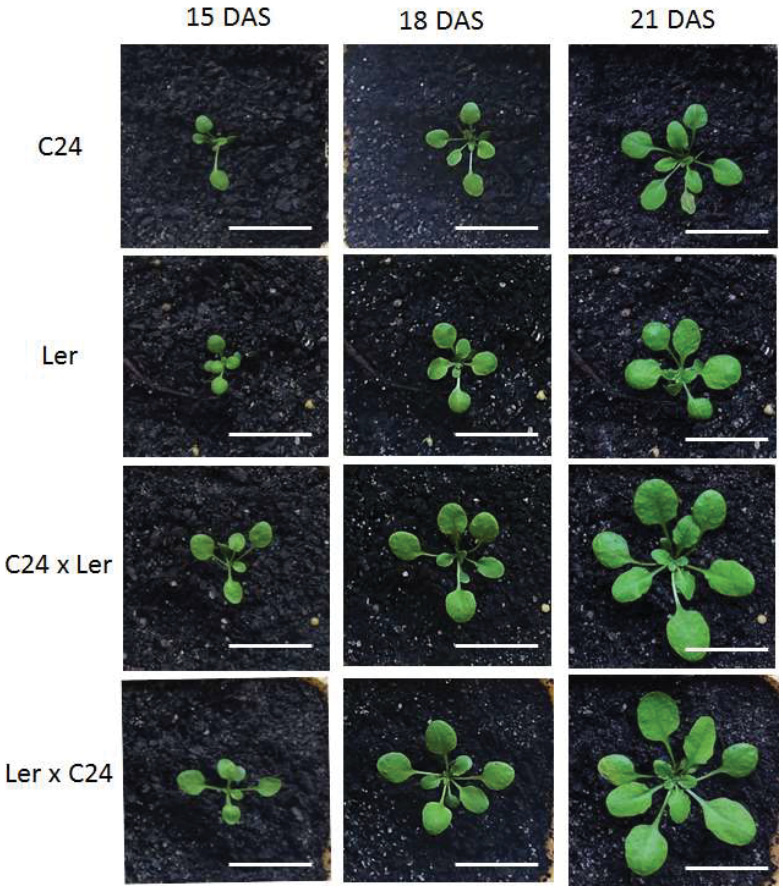

(b)

Lines	15 DAS	18 DAS	21 DAS
C24	6 ± 0.2	8 ± 0.4	11 ± 0.2
Ler	6 ± 0.2	9 ± 0.4	8 ± 0.4
C24 x Ler	7 ± 0.3 *	9 ± 0.3	13 ± 0.5 ***
Ler x C24	7 ± 0.3 *	10 ± 0.5 *	12 ± 0.4 ***

Figure 3.2. Number of leaves on C24/L*er* hybrid rosettes at 15, 18 and 21 DAS. (a) Images of seedlings at each time point stated. Scale bar: 2 cm. **(b)** Data show the average and SE of n=6-12 seedlings that were randomly selected from a population of n=30. The seedlings were sown and grown on Murashige and Skoog medium (3% sucrose) for 10 days before transplantation into soil. ANOVA was used to compare between each reciprocal hybrid to one of the parents. Significant differences to at least one of the parents (15 DAS L*er*; 18 DAS C24) are indicated by black asterisks and red asterisks indicate the hybrid is significantly different from both of the parents (*: $p < 0.05$; **: $p < 0.001$).

3.4 Hybrid vigour in young seedlings

To compare seedling growth between hybrids and parents the rosette area of the 6 DAS seedlings was determined (**Figure 3.3**). The presence or absence of sucrose did not alter hybrid growth, as indicated by a comparable rosette area under both conditions (**Figure 3.4**). Hybrids had a heterosis level over 30%, except for L*er* x C24, Col x C24 and L*er* x Ws that had a relatively lower level at around 10% (**Figure 3.4**). When no sucrose was added to the growth medium, a greater rosette area was found in the Ws x L*er* hybrid and most parental lines, except C24 (**Figure 3.4b**). In the absence of exogenous sucrose, lower levels of heterosis were found due to a slightly increased ($p < 0.01$; ANOVA) rosette area in the parental lines L*er*, Col and Ws while hybrid size remained unchanged (**Figure 3.4b**).

To investigate whether the heterosis in cotyledon size is due to the differences in germination time, C24/L*er* hybrids and the parents that have been manually selected for a matching germination time were compared (**Figure 3.5**). As measured by the area of 3 DAS cotyledons, aligning germination time did not affect the ranking of hybrid size relative to parents (**Figure 3.5**). A direct correlation between hybrid cotyledon size and embryo size i.e. seed size has been previously reported (Groszmann et al., 2014), showing that hybrid cotyledon size is greatly influenced by the initial embryo size.

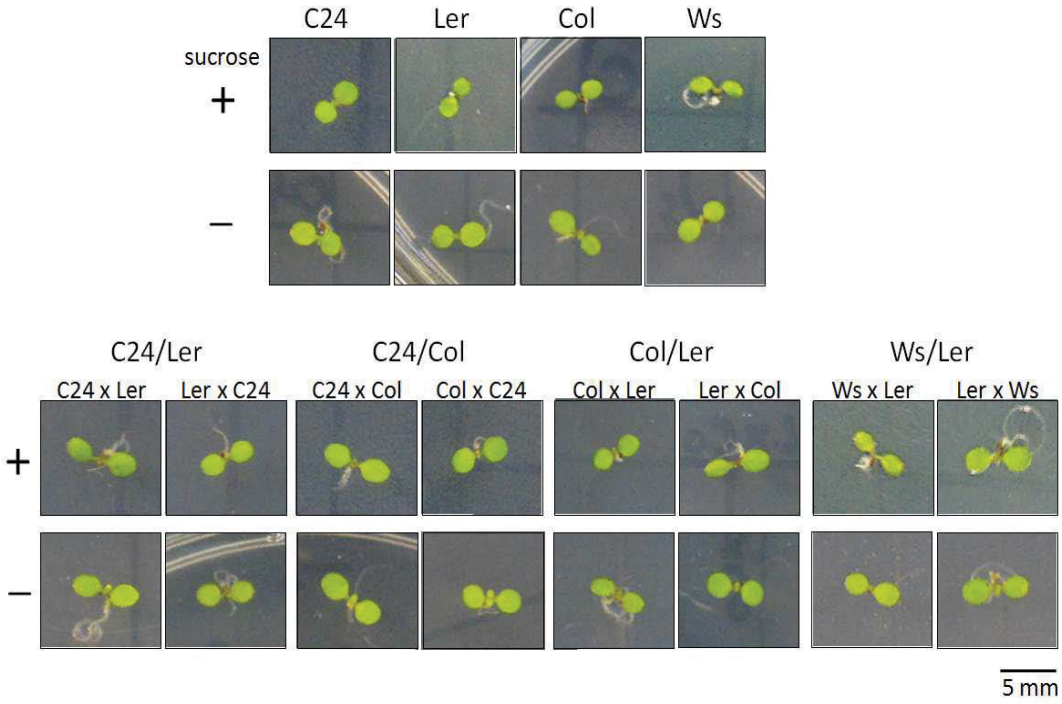

Figure 3.3. Morphology of 6 DAS *Arabidopsis thaliana* F1 hybrids derived from ecotypes C24, L*er*, Col and Ws. The seedlings were grown on Murashige and Skoog medium either with or without 3% sucrose. Images shown are the representatives of n= 10 seedlings.

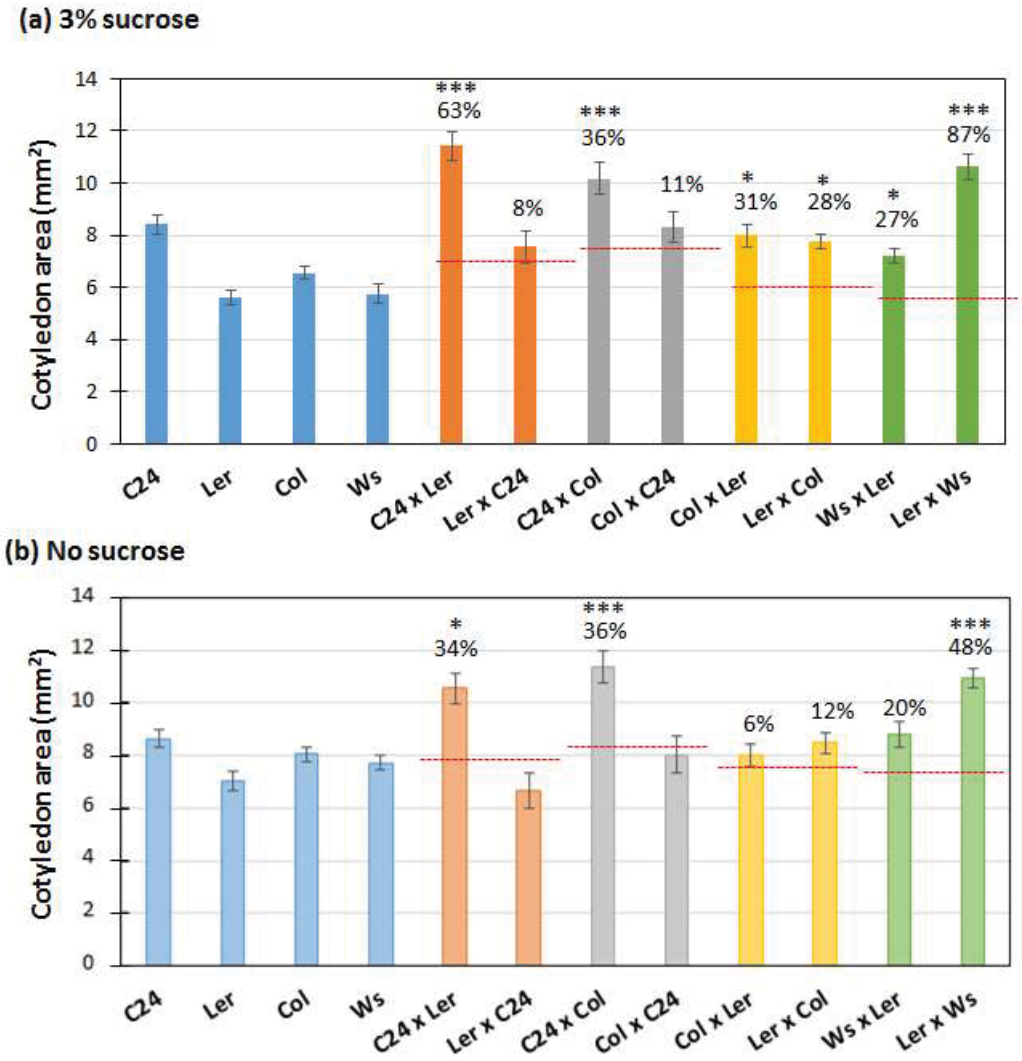

Figure 3.4. Comparisons of seedling growth between *Arabidopsis thaliana* hybrids and parents at early seedling development. The reciprocal hybrids from the same parents are shown in the same colour. 6 DAS seedlings were sown and grown on Murashige and Skoog medium either with (a) or without (b) 3% sucrose. The area of cotyledons was determined from the images shown in **Figure 3** using an image analysing software ImageJ (Rasband, W.S., ImageJ, U. S. National Institutes of Health, Bethesda, Maryland, USA). Data show the average and standard error of n ≥ 5 seedlings. The numbers shown above hybrids are the percentage increase from the average of the parents (red dashed lines). Asterisks indicate significant difference between a hybrid and the average value of its parents: *: $p < 0.05$ and ***: $p < 0.001$ (ANOVA).

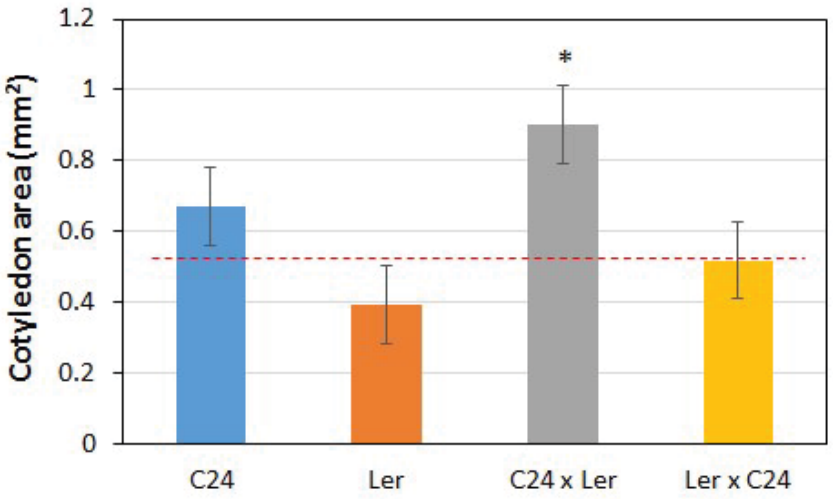

Figure 3.5. Comparison of cotyledon size between the 3 DAS C24/L*er* hybrids and parents with a matching germination time. A population of n=40 seeds were germinated on Murashige and Skoog medium (3% sucrose) under a light cycle 16hr-light/ 8hr-dark, under a growth irradiance of 120 µmol photons m^{-2} s^{-1} at 22˚C. To eliminate the effects of germination time difference on growth, seeds were examined under a microscope after 24-32 hours in light. Only the seeds that germinated within this 8-hour time window were selected and cotyledon size measured. Seedlings germinated within 32 hours after sowing were manually selected and kept growing until analysis. Images of 3 DAS cotyledons were taken under a dissecting microscope. Cotyledon area was determined from the microscopic images using ImageJ. Data represents the average and SE of n=25-38 seedlings from two repeats. Asterisk indicates significant difference (ANOVA, $p < 0.001$) between the hybrid and the average value of the parents. (Plotted from unpublished results by Naomi Miyaji)

3.5 Hybrid vigour in late seedling development

Hybrid growth at later stages of seedling development was studied. As vegetative growth ceases upon floral initiation, heterosis in vegetative biomass were determined before the transition to reproductive phase. In this experiment C24/L*er* hybrids were analysed for heterosis levels in rosette area at 19 DAS (before the early flowering L*er* started flowering; see **Chapter 3.6**) and 30 DAS (**Figure 3.6**). Each leaf of a rosette was dissected and analysed individually for leaf area (**Figure 3.6c, d; Figure 3.7**). Each hybrid leaf was compared to its corresponding parent leaf and the heterosis level was assessed (**Figure 3.8**).

Each hybrid leaf had a leaf area greater than the average size of the corresponding parent leaves (**Figure 3.7a**). Different leaves of a hybrid plant vary in the level of heterosis. In the 19 DAS C24 x L*er* hybrid seedlings leaves 1 and 2 had a heterosis level ~40%; 40-60% heterosis in the leaves 3-6; and > 60% in leaves beyond position 6 (**Figure 3.7a**). Lower levels of heterosis were found in the leaves of the reciprocal L*er* x C24 hybrid (**Figure 3.7a**). When comparing the total area of all the leaves in a rosette, the 19 DAS C24 x L*er* hybrid and the reciprocal L*er* x C24 hybrid seedlings contained a total leaf area 58% and 28% greater than the average of the parents, respectively (**Figure 3.8b**).

The 19 DAS plants of C24/L*er* hybrids and parents contained eleven to twelve leaves per rosette (**Figure 3.9a**). In the 19 DAS hybrid seedlings, the largest leaves at positions 3-6 (**Figure 3.7a**) were the primary contributors for heterosis in growth as they accounted for ~60% of the total leaf area (**Figure 3.9b**). The newly formed leaves at positions 7-12

made relatively little contribution to the heterosis at 19 DAS as they only accounted for a small fraction of the total biomass (**Figure 3.9b**). The vigour of these newly developed leaves could contribute to hybrid growth in subsequent stages.

At 30 DAS, both the C24/L*er* reciprocal hybrids showed increased heterosis in total leaf area up to 200% greater than the average of the parents (**Figure 3.9b**). The increasing difference between hybrids and parents in the total leaf area was mainly due to a greater number of new leaves produced in hybrid rosettes. The 30 DAS hybrid seedlings contained an average of twenty leaves per rosette (**Figure 3.9a**). The largest leaves were found in positions 9-13 (**Figure 3.7b**), which accounted for >50% of the total leaf area (**Figure 3.9b**). Those leaves were not present in the 30 DAS L*er* seedlings (**Figure 3.7b**). The early flowering ecotype L*er* ceased to produce new rosette leaves shortly after 19 DAS and leaves 9-12 became cauline leaves. Despite having fewer leaves per rosette, the 30 DAS L*er* plant had a leaf size equaling the hybrids in all nine leaves present (**Figure 3.7**). The heterosis levels of the C24 x L*er* leaves 1-8 became less marked at 30 DAS, compared to the previous time point ($p < 0.01$, ANOVA) (**Figure 3.8**). The 30 DAS C24 plants were not producing new leaves as actively as the hybrids and contained an average of 14 leaves per rosette (**Figure 3.9a**).

These results showed that, during seedling development, hybrid vigour is contributed by the succession of newly developed leaves which subsequently become less heterotic as the parent leaves, especially L*er*, could catch up in size when fully expanded.

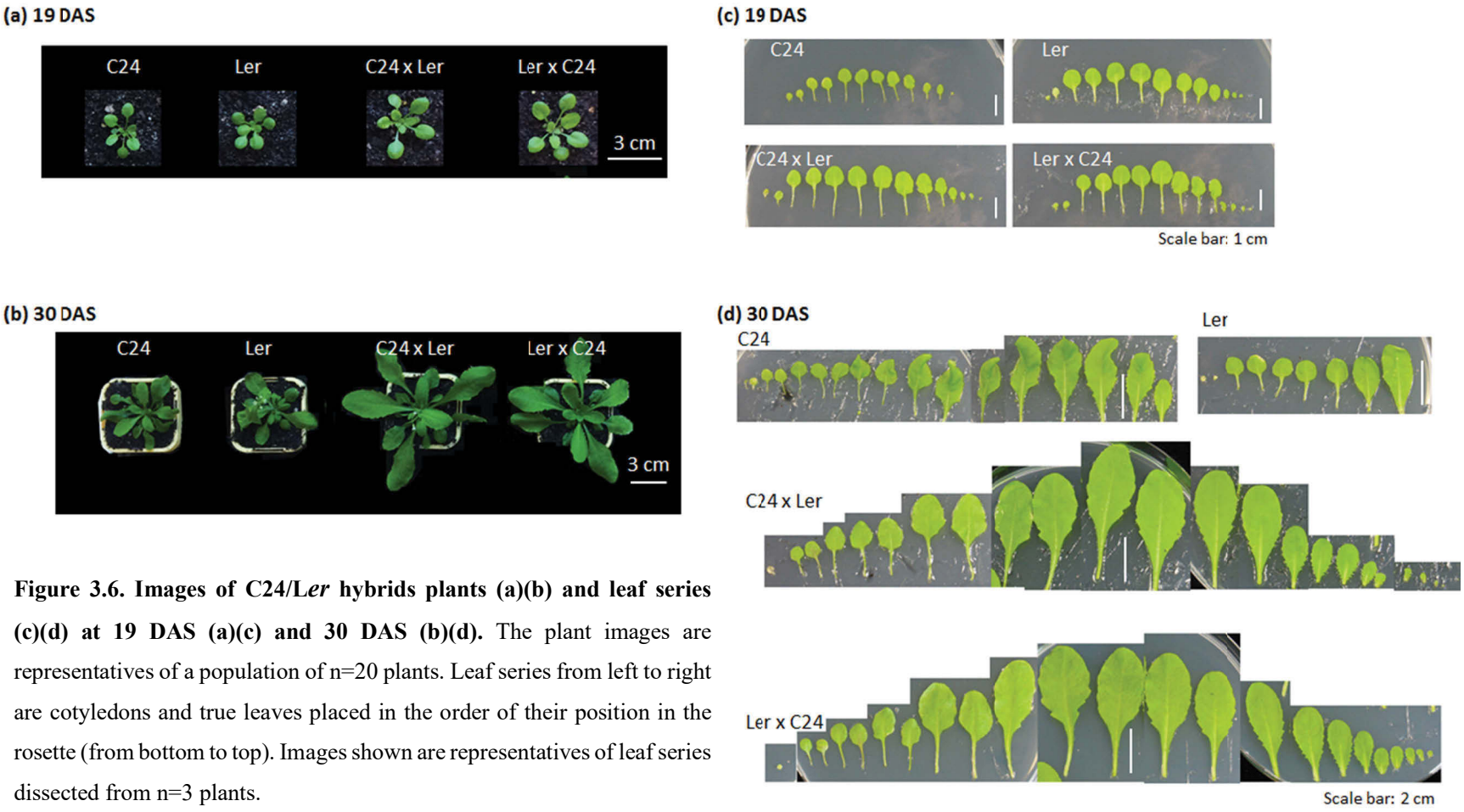

Figure 3.6. Images of C24/L*er* hybrids plants (a)(b) and leaf series (c)(d) at 19 DAS (a)(c) and 30 DAS (b)(d). The plant images are representatives of a population of n=20 plants. Leaf series from left to right are cotyledons and true leaves placed in the order of their position in the rosette (from bottom to top). Images shown are representatives of leaf series dissected from n=3 plants.

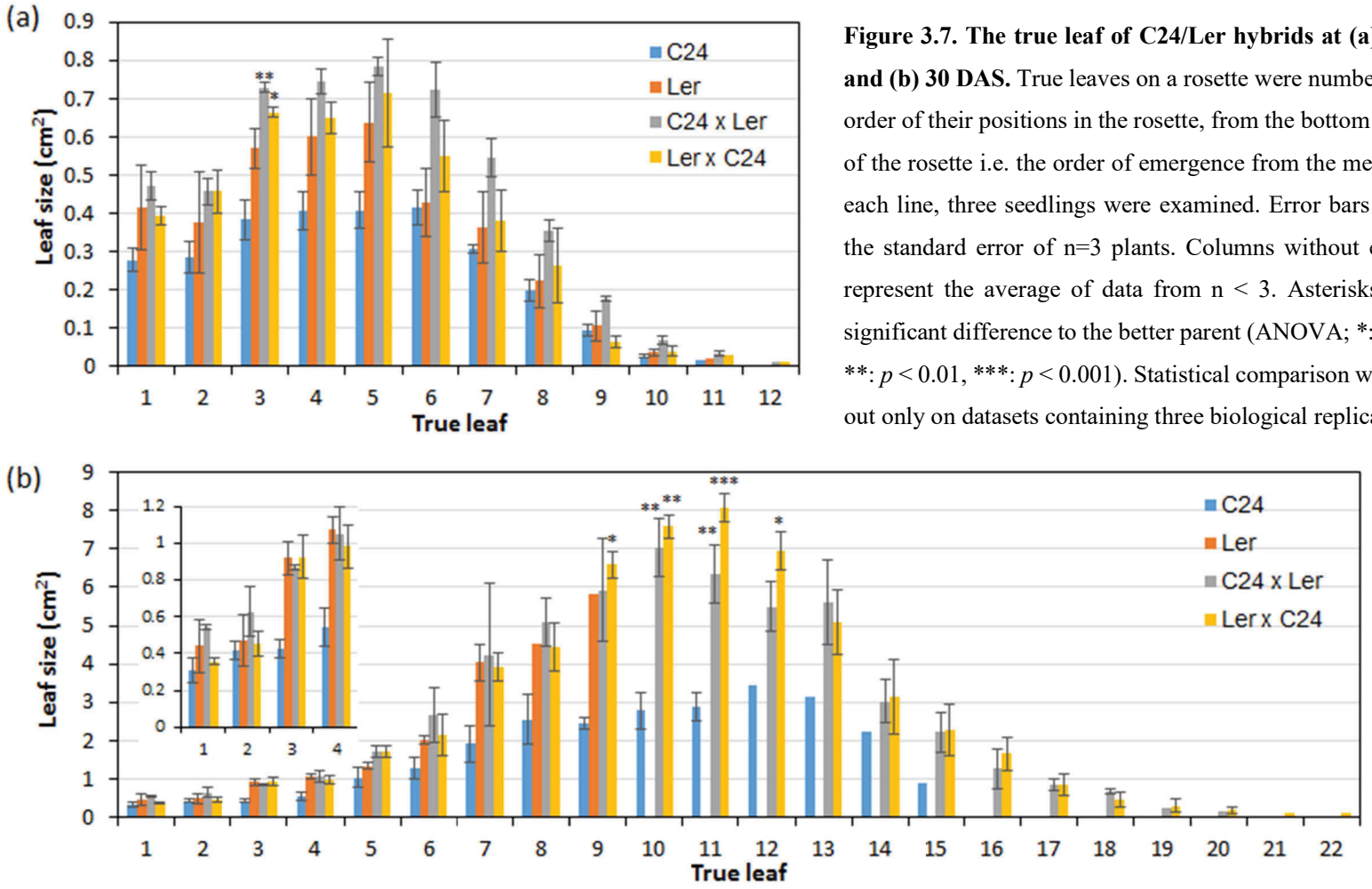

Figure 3.7. The true leaf of C24/Ler hybrids at (a) 19 DAS and (b) 30 DAS. True leaves on a rosette were numbered in the order of their positions in the rosette, from the bottom to the top of the rosette i.e. the order of emergence from the meristem. In each line, three seedlings were examined. Error bars represent the standard error of n=3 plants. Columns without error bars represent the average of data from n < 3. Asterisks indicate significant difference to the better parent (ANOVA; *: $p < 0.05$, **: $p < 0.01$, ***: $p < 0.001$). Statistical comparison was carried out only on datasets containing three biological replicates.

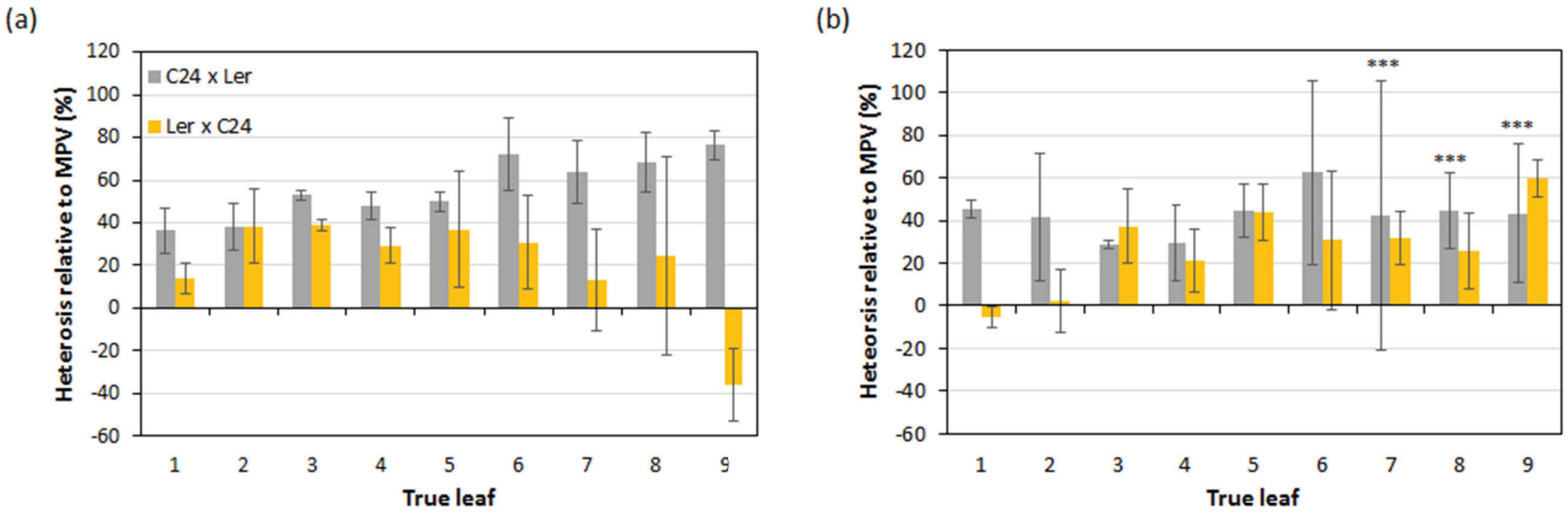

Figure 3.8. Heterosis levels of individual leaves of the C24/Ler hybrids at (a) 19 DAS and (b) 30 DAS. Data represent average and standard error of n=3 seedlings. In 30 DAS seedlings, the heterosis levels of leaves 10 and beyond were not shown as those leaves were not present in the rosette of the 30 DAS Ler seedlings. Asterisks above 30 DAS columns indicate significant difference from 19 DAS leaves (ANOVA, ***: $p < 0.001$).

(a)

Lines	19 DAS	30 DAS
C24	11 ± 0.3	14 ± 1.5
Ler	12 ± 0.3	8 ± 0.7 *
C24 x Ler	11 ± 0.3	19 ± 1.7
Ler x C24	11 ± 0.6	21 ± 0.7

(b)

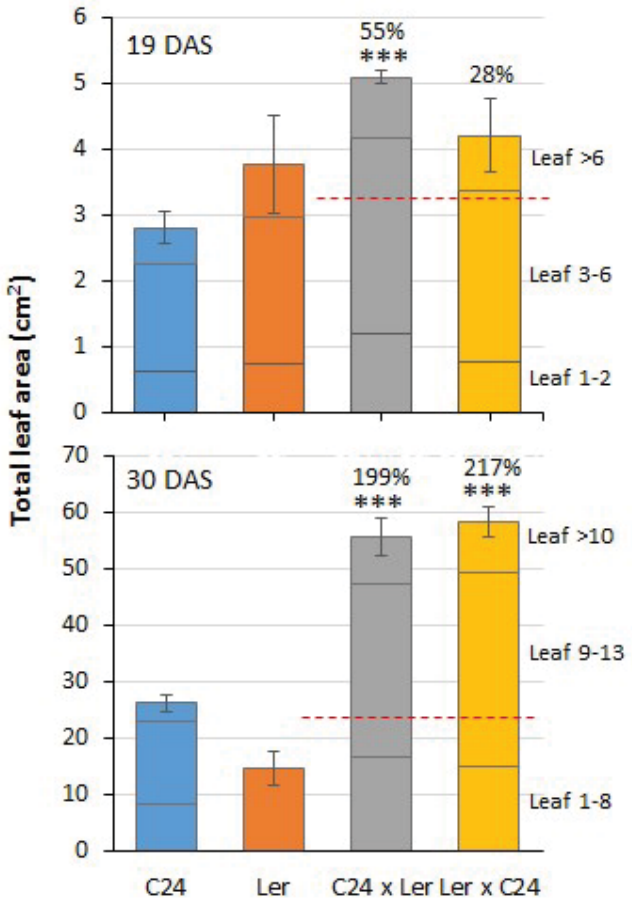

Figure 3.9. (a) Number of rosette leaves on 19 DAS and 30 DAS C24/Ler plants. Asterisk indicates significant difference from others (ANOVA, $p < 0.05$). **(b) Relative contributions of leaves to the whole rosette mass.** Datasets shown in **Figure 6** were used. Data represents the average and SE of n= 3 plants. Each total leaf area data was divided into three fractions according to the relative contributions of indicated sets of leaves and their positions in a rosette. Percentage above each hybrid column represents the heterosis level in total leaf area relative to the average of parents (red dashed lines). Asterisks indicate significant differences from the average level of the parents (ANOVA, ***: $p < 0.001$).

3.6 Flowering time

The C24/L*er* hybrids flowered later than the parents and flowering times differ significantly between the parental lines (**Figure 3.10**). L*er* showed a bolting time at around 24 DAS while the other parent, C24, bolted at 30 DAS (**Figure 3.10b**). Both C24/L*er* reciprocal hybrids bolted at around 38 DAS (**Figure 3.10b**).

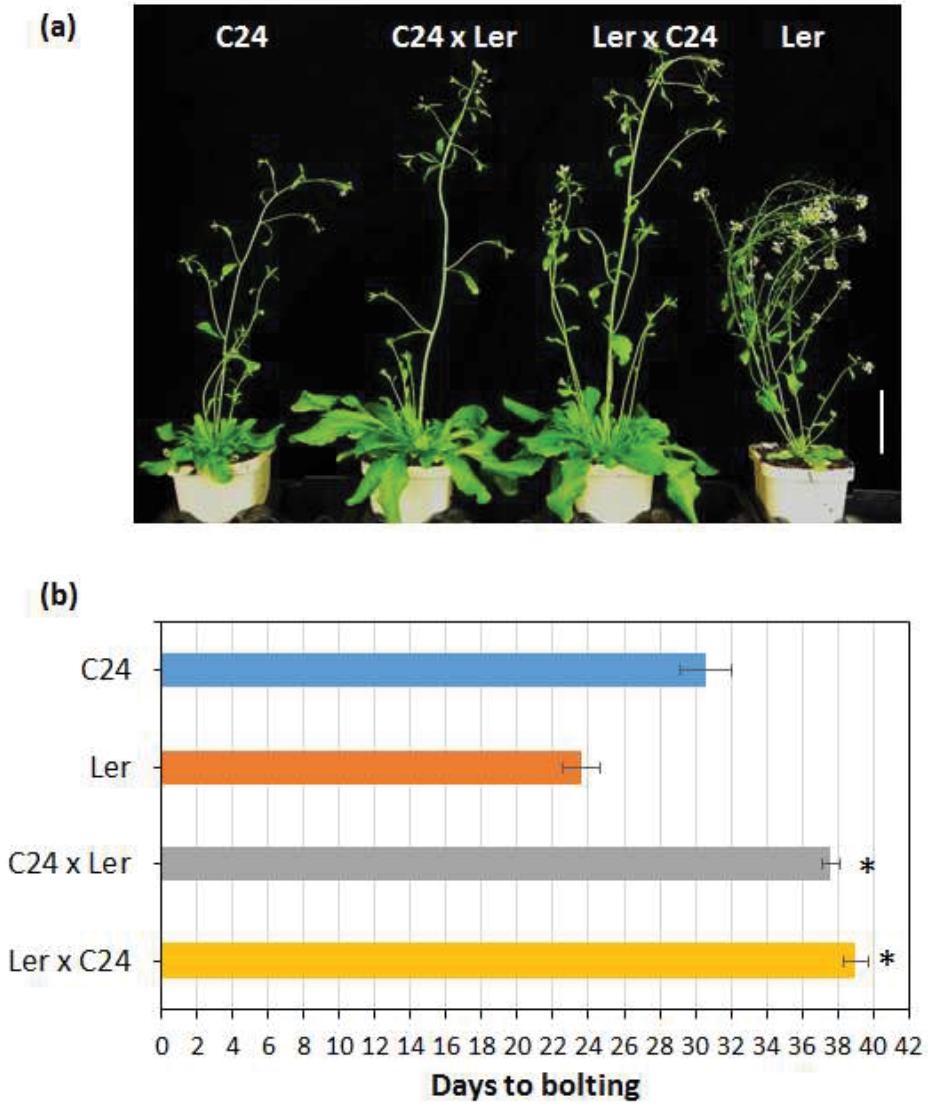

Figure 3.10. Flowering time of C24/Ler hybrids compared to parents. (a) Image of 44 DAS soil-grown C24/L*er* hybrid and parent plants. Scale bar: 5 cm. **(b)** Flowering time determined by the bolting of shoot (about 1 cm). Data represents the average and SE of n=5 plants. Asterisks indicate significant difference from the late flowering parent C24 (ANOVA, $p < 0.001$).

3.7 Palisade mesophyll cell size and cell number

Leaf development can be divided into a general cell division phase, a transition phase and a cell expansion phase (Gonzalez et al., 2012). During the transition phase, cell division first ceases at the tip of the leaf and is gradually replaced by cell expansion in a direction towards the base of the leaf (Gonzalez et al., 2012). To avoid any growth effects due to developmental differences, the comparisons of hybrid and parent leaves were carried out using fully expanded leaves. As indicated by leaf diameter, leaf 3 of both hybrid and parent reached full expansion at around 24 DAS (**Figure 3.11**). The following analyses were carried out using leaves 3 and 4 of 28 DAS plants (**Figure 3.12**).

Variations in palisade mesophyll cell size and cell number were found between the parental lines. Among all the ecotypes analysed, C24 had the smallest leaves due to fewer cells in each leaf (**Figure 3.12a, b**). The leaves of L*er* were the largest amongst all parental lines analysed, at a level that was comparable to F1 hybrids (**Figure 3.12a**). The greater area of L*er* leaves was mainly attributable to a greater area per cell compared to other ecotypes (**Figure 3.12b**). Most hybrids analysed showed a significantly greater number of palisade mesophyll cells than the average of the parents, except for the Col x L*er* and Ws/L*er* hybrids (**Figure 3.12c**). An increased cell size was found in some hybrids, especially in those with strong heterosis in leaf size, including C24 x L*er*, C24 x Col and Col x C24 (**Figure 3.12a, b**). In contrast, the least heterotic hybrid Ws/L*er* showed no vigour in the area per cell, at a level similar to the lower parent Ws (**Figure 3.12b**). These results showed different hybrids generate large leaves by means of increasing cell number and/or cell size to different extents.

As shown in **section 3.5**, a greater level of heterosis was found in the newly developing leaves of the C24/L*er* hybrid, as the parent leaves (especially L*er*) were able to catch up in size (**Figure 3.7**). To investigate the cellular basis of heterosis in young hybrid leaves, true leaves 3/4 of the 19 DAS C24/L*er* hybrid and parent plants were analysed for palisade mesophyll cell size and cell number and compared to the 28 DAS leaves (**Figure 3.13**). As a comparison, true leaves 5/6 that were developmentally younger than leaves 3/4 were also included. As indicated by leaf area, C24 x L*er* showed significant heterosis compared to both parents at an early stage of leaf development (**Figure 3.13a**). A similar pattern was observed in the measurements of cell size. A slight increase in cell size ($p = 0.57$), was found in the 19 DAS C24 x L*er* leaves compared to the better parent (**Figure 3.13b**). A similar cell number was found in the 19 DAS leaves of hybrids and L*er* while C24 showed the lowest number, which is in line with the observations in the 28 DAS leaves (**Figure 3.13c**). A similar pattern of leaf size and cell size was found in the 19 DAS leaves 5/6 (**Figure 3.13**). However, the differences between hybrids and the average levels of the parents in cell size was not statistically significant (ANOVA, $p > 0.05$). More biological replicates are required to validate this observation. Nonetheless, these results suggest C24 x L*er* hybrid might achieve vigour in early leaf growth via a faster cell expansion than the parents.

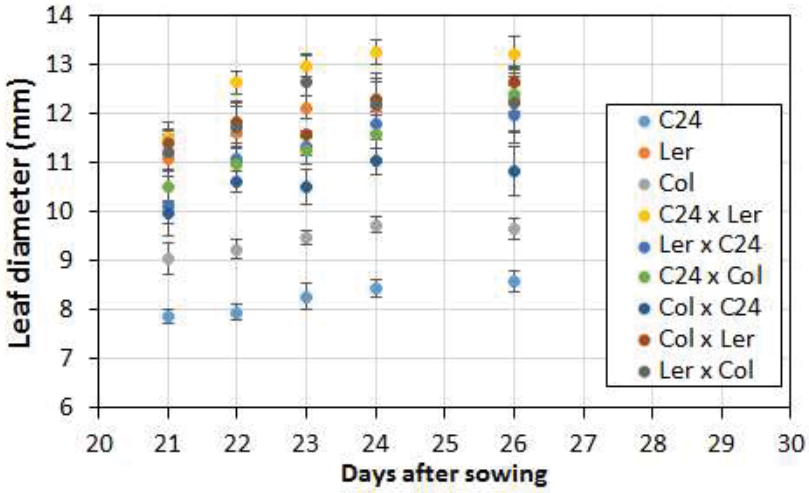

Figure 3.11. Leaf 3 of soil-grown *Arabidopsis thaliana* plants reached full expansion at around 24 DAS. Data presented were the average and SE of n=10 plants.

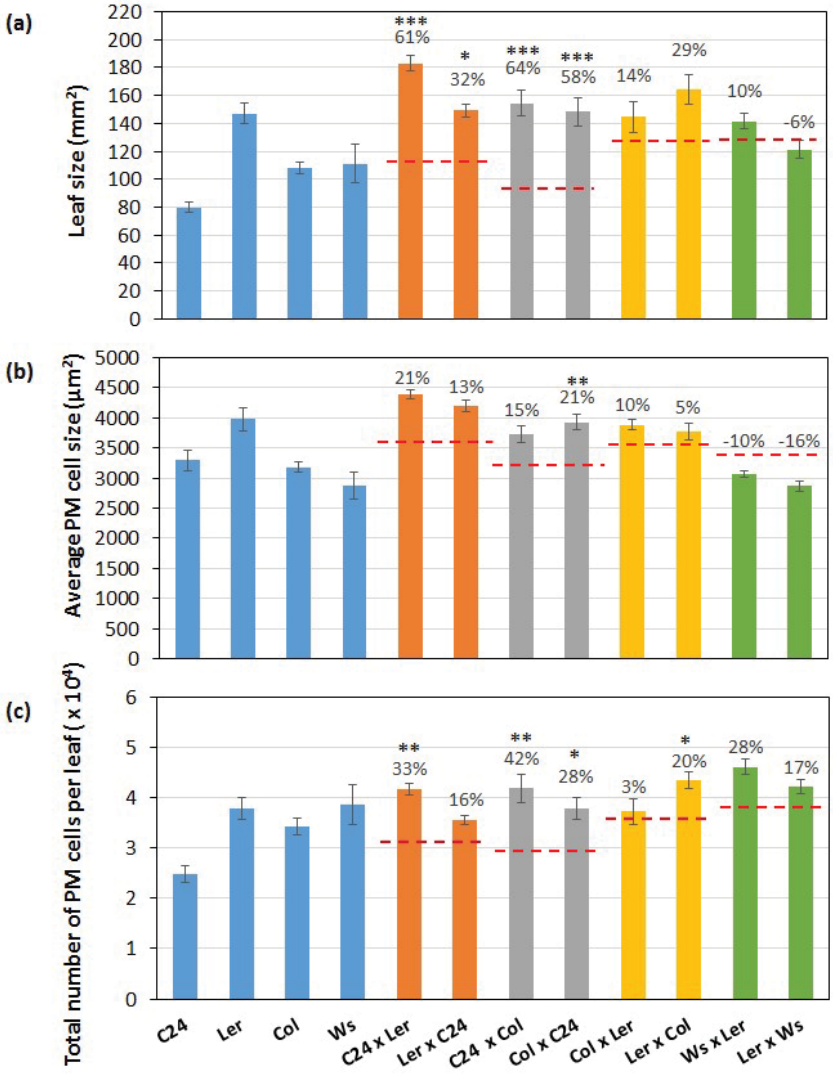

Figure 3.12. Cellular basis of leaf size differences between hybrids and parents. The fully expanded leaves 3/4 of the 28 DAS seedlings were used. For each leaf analysed, microscopic images of palisade mesophyll layer were taken at six positions and the average cell number per image was calculated. The average area of individual palisade mesophyll cell was determined by dividing the known leaf area in a microscopic image by the average cell number per image, and the estimated total number of palisade mesophyll cells per leaf was calculated by dividing the total leaf area by the average palisade mesophyll cell area. Data presented were the average and SE of n=7-12 leaves from 3-6 plants. Values above columns represent percentage increase from the average of the parents (red dashed lines). Asterisks indicate significant increase compared with the average levels of the parents (ANOVA; *: $p < 0.05$, **: $p < 0.01$, ***: $p < 0.001$). PM: palisade mesophyll.

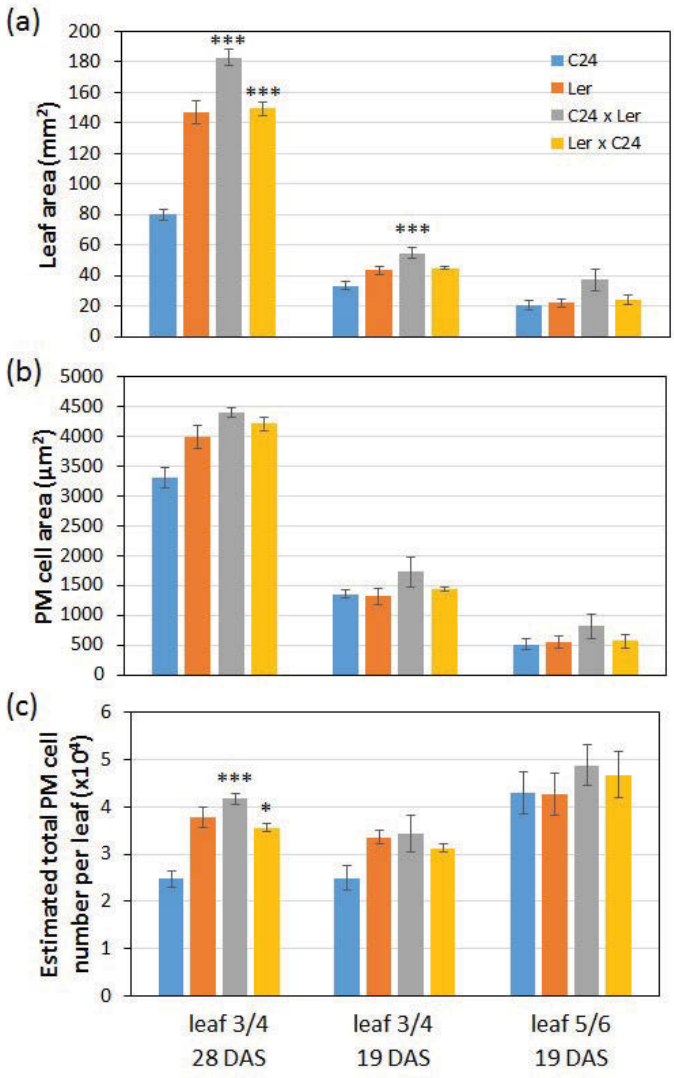

Figure 3.13. Measurements of palisade mesophyll cells of true leaves 3/4 and 5/6 of 19 DAS C24/L*er* hybrid plants compared with the parents. The datasets of the fully expanded true leaves 3/4 of 28 DAS plants (re-plotted from **Figure 12**) were also included as a comparison. Data of the 19 DAS leaves were the average and SE from n=6 leaves collected from three plants. Asterisks indicate significant increase relative to the average levels of the parents (ANOVA; *: $p < 0.05$, ***: $p < 0.001$). PM: palisade mesophyll.

3.8 Leaf mass per area

To see whether hybrid leaves retain the same biomass relative to parent leaves, hybrid leaves were analysed for leaf mass per area (dry weight per fresh leaf area) and compared to parents (**Figure 3.14**). All the hybrids examined, C24/L*er*, Col/L*er* and Ws/L*er*, showed a leaf mass per area at levels within the range of the corresponding parents.

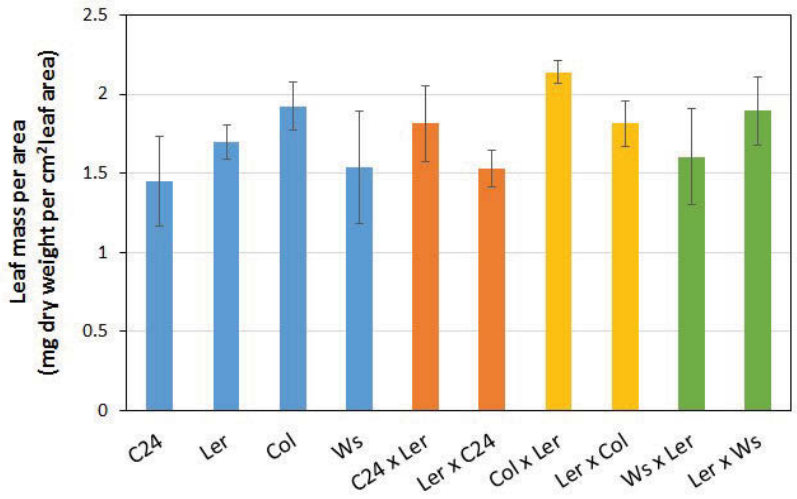

Figure 3.14. Comparisons of leaf mass per area between hybrids and parents. Data shown were calculated using data sets measured from leaves 5 or 6 of 4 week old, soil-grown plants. Each leaf sampled was oven-dried and determined for dry weight. Leaf area was determined from the leaf image taken upon harvesting using ImageJ. Each data set represents the average and standard error of n=5 plants. No significant differences were found between hybrids and the better parent (ANOVA, $p > 0.05$).

3.9 Leaf cross-section thickness

The cross-sectional thickness of C24/L*er* hybrid leaves was compared to that of the parents (**Figure 3.15**). Both C24/L*er* reciprocal hybrids showed a leaf thickness similar to L*er* at a level just below 200 μm (**Figure 3.15b**). Leaves of C24 were significantly thinner than L*er* and the F1 hybrids, with a leaf thickness just over 150 μm (**Figure 3.15b**).

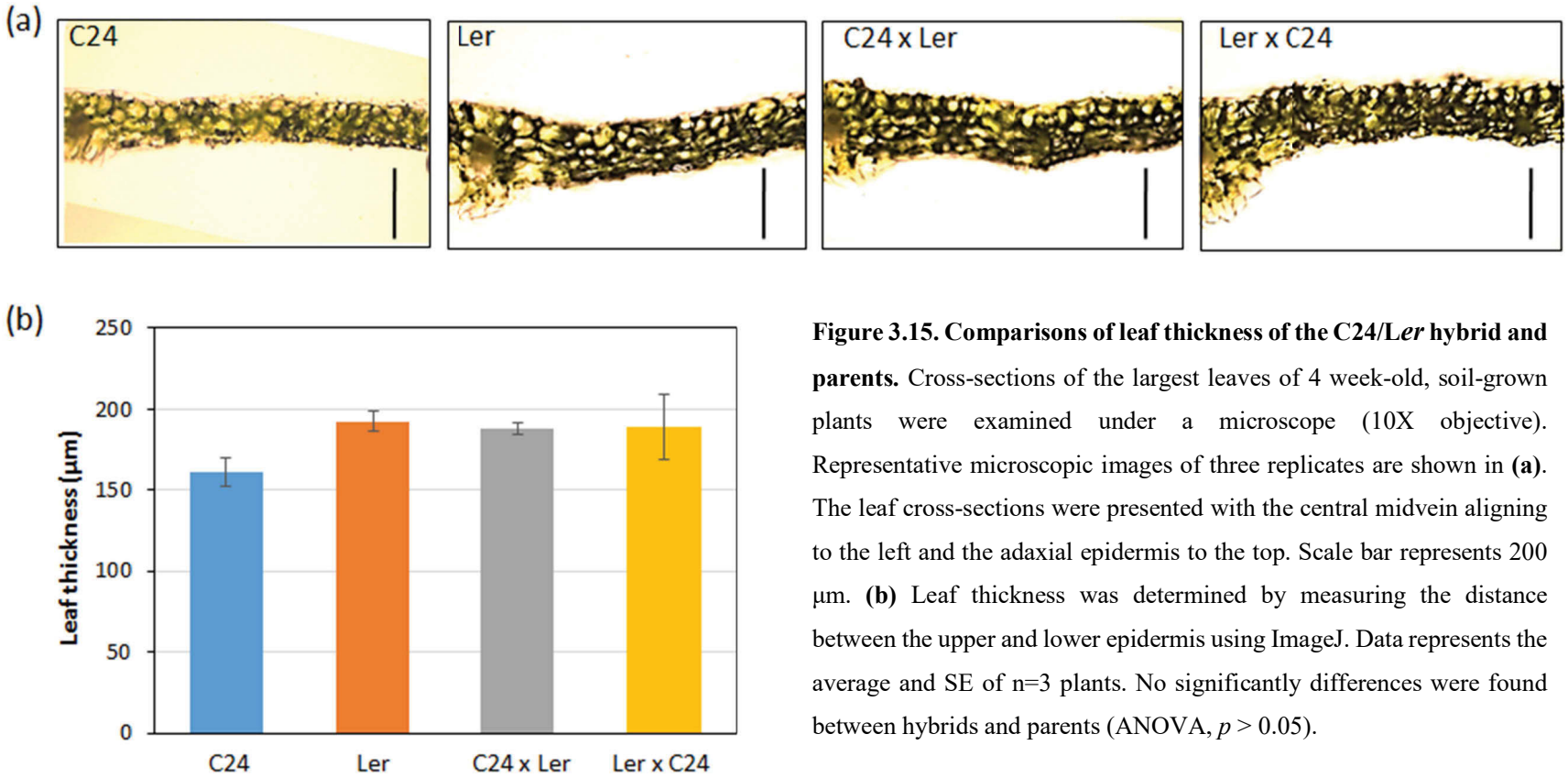

Figure 3.15. Comparisons of leaf thickness of the C24/L*er* hybrid and parents. Cross-sections of the largest leaves of 4 week-old, soil-grown plants were examined under a microscope (10X objective). Representative microscopic images of three replicates are shown in **(a)**. The leaf cross-sections were presented with the central midvein aligning to the left and the adaxial epidermis to the top. Scale bar represents 200 µm. **(b)** Leaf thickness was determined by measuring the distance between the upper and lower epidermis using ImageJ. Data represents the average and SE of n=3 plants. No significantly differences were found between hybrids and parents (ANOVA, $p > 0.05$).

3.10 Comparison of photosynthetic capacity between hybrids and parents

To investigate if hybrid vigour in seedling growth is associated with altered photosynthetic properties, the reciprocal hybrids of C24/L*er*, C24/Col, Col/L*er* and Ws/L*er* were analysed for electron transport rate (photosynthetic capacity) at 6 days and 3 weeks after sowing. The 3 week-old seedlings were analysed for CO_2 assimilation rate under an increasing CO_2 partial pressure under saturating light using an infrared gas-exchange analyser (LI-6400XT, LICOR). For young seedlings (6 DAS) that were too small for gas-exchange analysis, a chlorophyll fluorescence assay was used.

3.10.1 Electron transport rate of the 6 DAS seedlings of hybrids and parents

Young seedlings of eight hybrids derived from four ecotypes C24, L*er*, Col and Ws were analysed for relative electron transport rate under increasing light intensities using the chlorophyll fluorescence assay (**Figure 3.16**). No significant increase was found in the ETR between hybrids and the corresponding better parents (ANOVA, $p > 0.05$). To compare photosynthetic capacity between hybrids and parents, the light-response curves were fitted and the estimated maximum electron transport rate (J_{max}) compared (**Figure 3.17**). No significant increase was found in the J_{max} between hybrids and the corresponding better parents (ANOVA, $p > 0.05$).

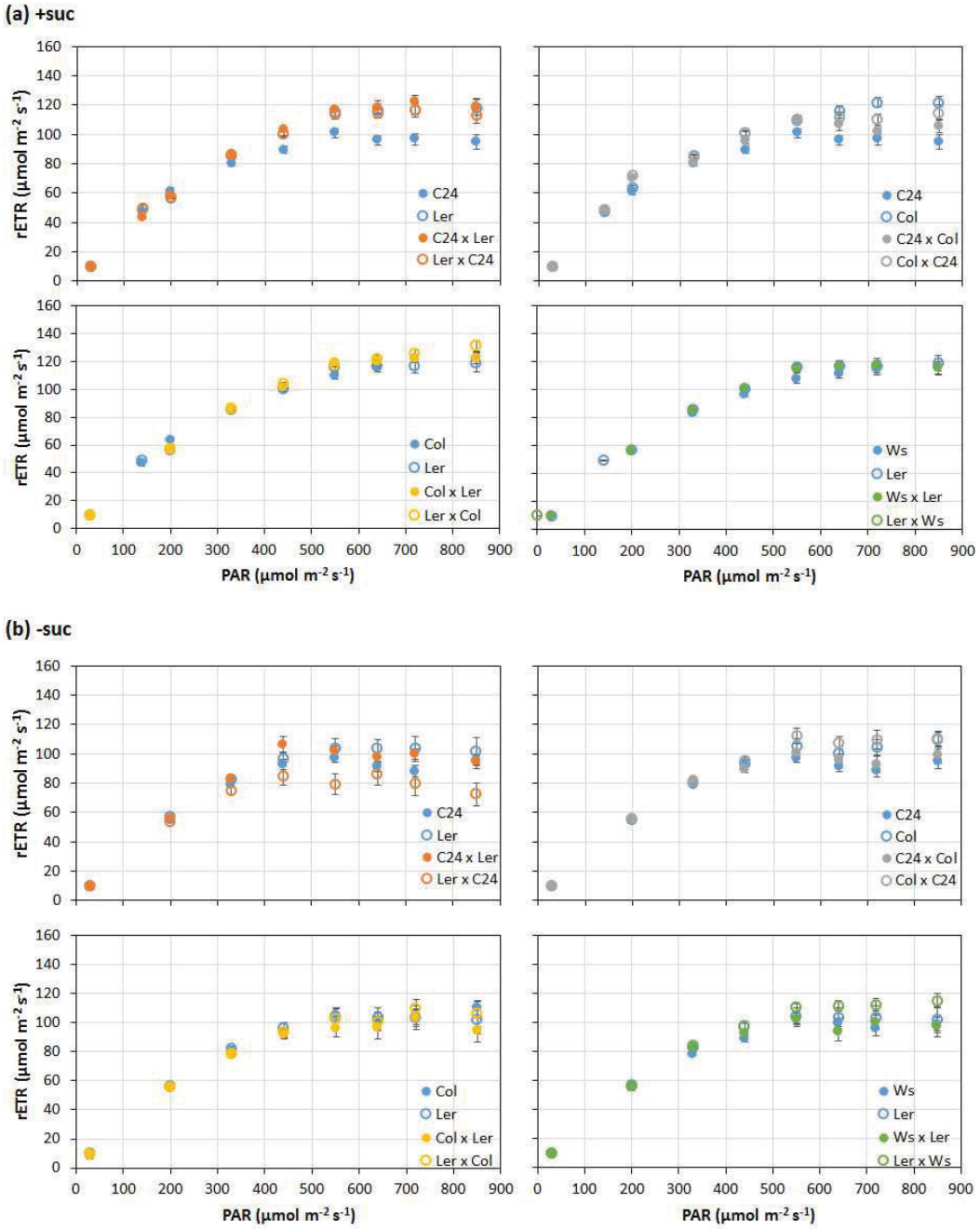

Figure 3.16. The light-response curves of the relative electron transport rate (rETR) of the 6 DAS hybrid seedlings grown on MS medium either (a) with or (b) without 3% sucrose. The chlorophyll fluorescence parameters were used to calculate the quantum yield of PSII (φ_{PSII}) as described by Genty et al. (1989) using a pulse amplitude modulated fluorometer (Closed FC 800-C, PSI). Each data point represents the average and SE of $n \geq 5$. The rETR was calculated $rETR = \varphi_{PSII} \times PAR \times 0.5 \times 0.84$, as described in Edwards and Baker (1993). φ_{PSII}: the quantum yield of PSII; PAR: photosynthetic activation radiance. All measurements were carried out between 2-9 hr after lights-on. No significant increase was found between hybrids and the better parent (ANOVA, $p > 0.05$).

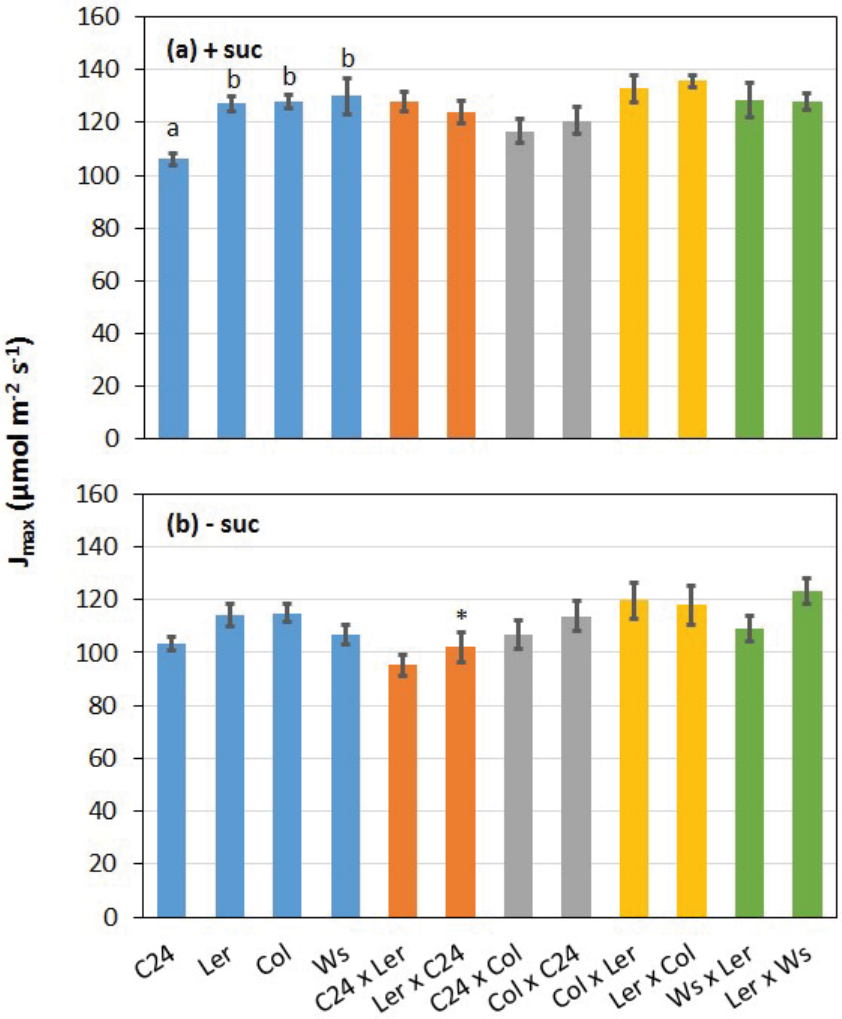

Figure 3.17. **Comparisons of the estimated maximum electron transport rate (J_{max}) between F1 hybrids and the parents.** The 6 DAS seedlings were grown on MS medium either with (a) or without (b) 3% sucrose. The four parental lines are shown in blue. The reciprocal hybrids derived from the same parents are shown in the same colour. Data represents the average and SE of n = 5-12 seedlings from two replicates. Statistical comparisons among parents are shown, datasets with different letters are significantly different from the others (ANOVA, $p < 0.05$). Asterisk indicate significant difference between hybrid and the better parent (ANOVA, $p < 0.05$).

3.10.2 The CO_2 assimilation rate of the 3 week-old hybrid and parents

In this experiment, 3 week-old soil-grown hybrids and parent were analysed for CO_2 assimilation rate per unit leaf area under an increasing CO_2 partial pressure (**Figure 3.18**). The CO_2 assimilation rate (A) was plotted against the intercellular CO_2 partial pressure (C_i) to generate the A/Ci curves. All hybrids examined had A/Ci curves that plateaued under high CO_2 at levels between the parents, except for the Ws/L*er* hybrids, which plateaued at levels slightly greater than the parents (**Figure 3.17**). To compare photosynthetic capacity between hybrids and parents, the maximum velocity of Rubisco carboxylation (V_{cmax}) of hybrids and parents was estimated by fitting the A/Ci curves to the Farquhar-von Caemmerer-Berry model for C_3 photosynthesis using the curve fitting calculator developed by Sharkey et al. (2007). All genotypes measured had a similar V_{cmax} on a unit leaf area basis, at a level of 40 μmol CO_2 m^{-2} s^{-1} (**Figure 3.19**). All eight hybrids analysed showed a V_{cmax} at levels within the range of the corresponding parents (**Figure 3.19**). These results indicate that hybrids have no increase in the photosynthetic capacity relative to the parents on a unit leaf area basis, consistent with the results obtained from young seedlings using the chlorophyll fluorescence assay.

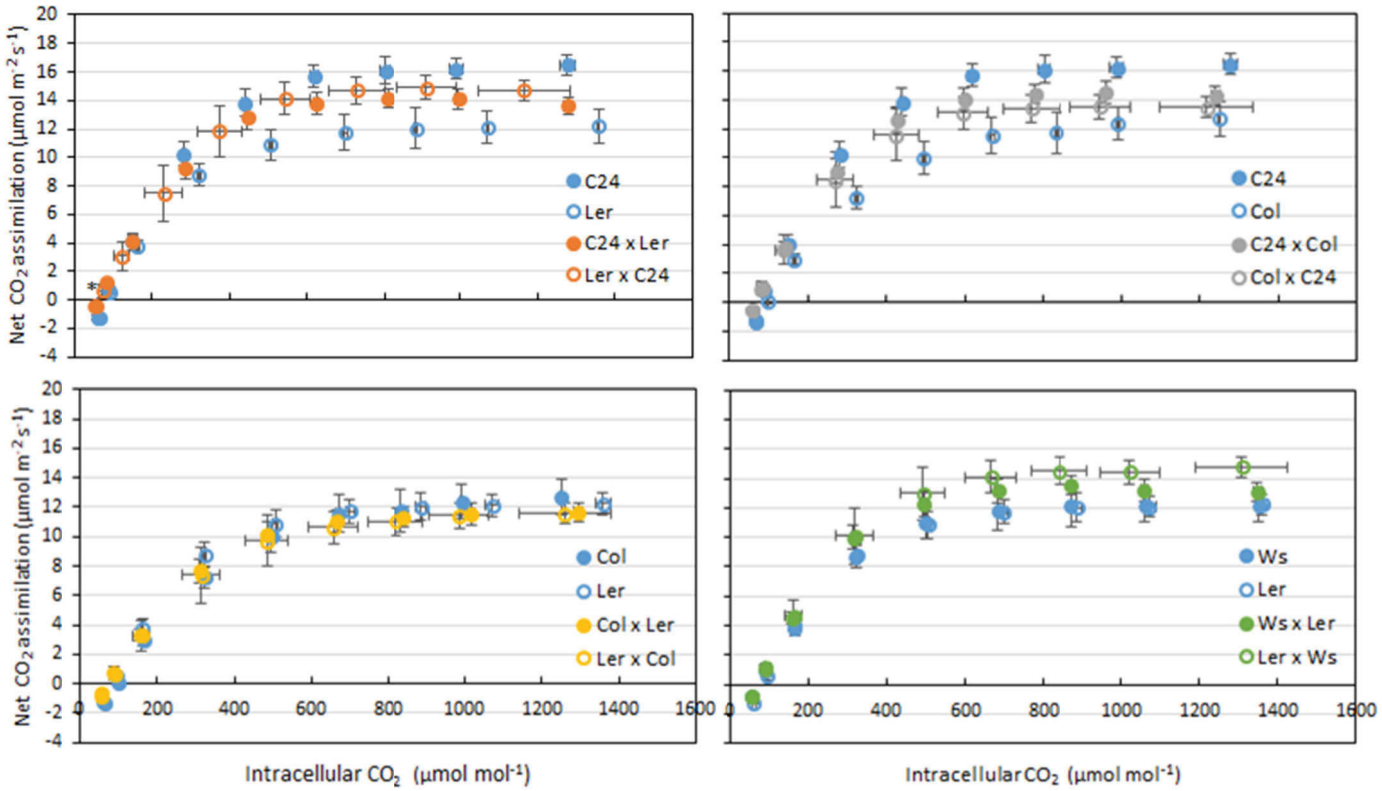

Figure 3.18. A/Ci curves of 3-week old hybrid. The net CO_2 assimilation rate (A) and the intercellular CO_2 partial pressure (C_i) of the largest leaf on hybrid rosettes were measured under an increasing partial pressure of atmospheric CO_2 under a saturating irradiance at 1000 µmol m^{-2} s^{-1} using an infra-red gas analyser (LI-6400XT, LI-COR). Each data point represents the average and SE of n≥3. All measurements were carried out between 2-9 hr after lights-on. Asterisk above the second datapoint of the C24/Ler dataset indicate significant difference between the hybrids and the better parent (ANOVA, $p < 0.01$).

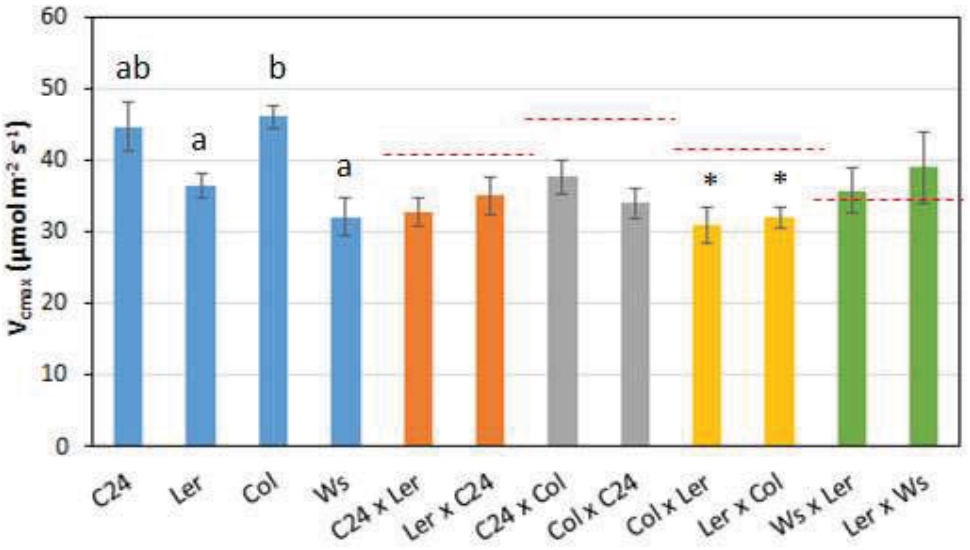

Figure 3.19. Comparison of the maximum rate of Rubisco carboxylation (V_{cmax}) between hybrids and parents. Each A/C_i curve (data sets shown in Figure 8) were fitted to the biochemical model for C_3 photosynthesis as described by Farquhar, von Caemmerer and Berry (1980) using PCE Calculator developed by Sharkey et al. 2007. For each set of reciprocal hybrids, the average level of the parents is indicated by red dashed line. Data shown were the fitting results at leaf temperature (22 ˚C). Data presented are the average and SE of n ≥ 3 plants. A: net CO_2 assimilation; C_i: intercellular CO_2 partial pressure. Rubisco: ribulose 1-5-bisphosphate carboxylase/oxygenase. Statistical comparisons were carried out between different parental lines. Different letters above columns indicate significantly different from the others (ANOVA, $p < 0.05$). Asterisks indicate significant difference from the better parent (ANOVA, $p < 0.05$). No differences were found between hybrids and the average levels of the parents (indicated by red dashed lines; ANOVA, $p > 0.05$).

3.11 Unit leaf biomass chlorophyll content

The 15 DAS C24/L*er* hybrid seedlings had an average of 1.1 µg chlorophyll per mg fresh weight, similar to that of the C24 ecotype (**Figure 3.20**). A greater amount of chlorophyll was found in the other parent, ecotype L*er*, which contained ~1.18 µg chlorophyll per mg fresh weight (**Figure 3.20**). No significant difference in the chlorophyll a to b ratio was found in hybrids compared to the parents (ANOVA, $p > 0.05$) (**Figure 3.20**).

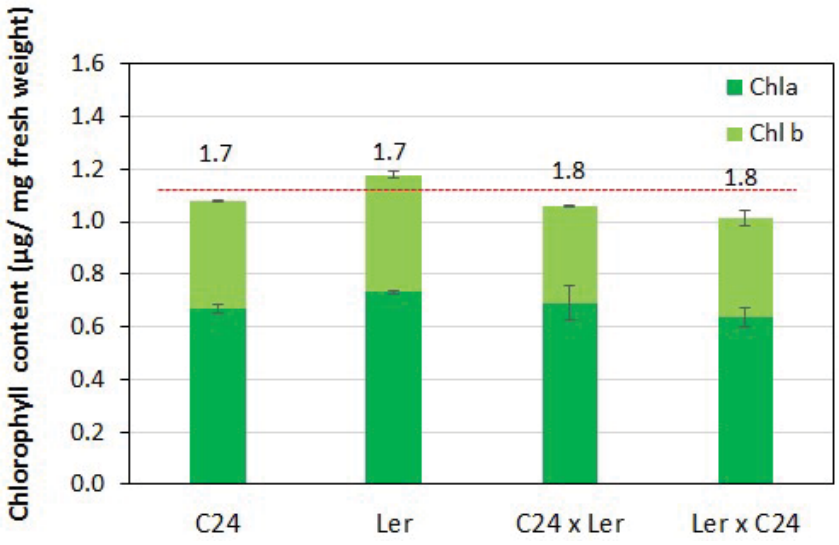

Figure 3.20. Comparison of chlorophyll content between the C24/L*er* hybrid and parent seedlings. Pools of n=3 rosettes of the 15 DAS soil-grown seedlings were used. All seedlings were sown and grown on Murashige and Skoog (MS) medium for 10 days before transplanting into soil. Data shown is the average and SE of three technical replicates. The number above each column shows the ratio of chlorophyll a to b. The average levels of the parents were indicated with red dashed lines. No significant differences were found between hybrids and the average levels of the parents (ANOVA, $p > 0.05$).

3.12 Chloroplast content per unit mesophyll cell area

Cotyledons and true leaves 1 and 2 were sampled from 10 DAS and 19 DAS seedlings respectively and examined for chloroplast number in individual mesophyll cells. Both hybrids and parents had a similar chloroplast content on a unit cell area basis (**Figure 3.21a**). No significant difference was found between the hybrids and parents (ANOVA, $p > 0.05$). A positive correlation was found between the number of chloroplasts per cell and the cell area (regression coefficient > 0.9) (**Figure 3.21b**), as previously described by Pyke and Leech (1991).

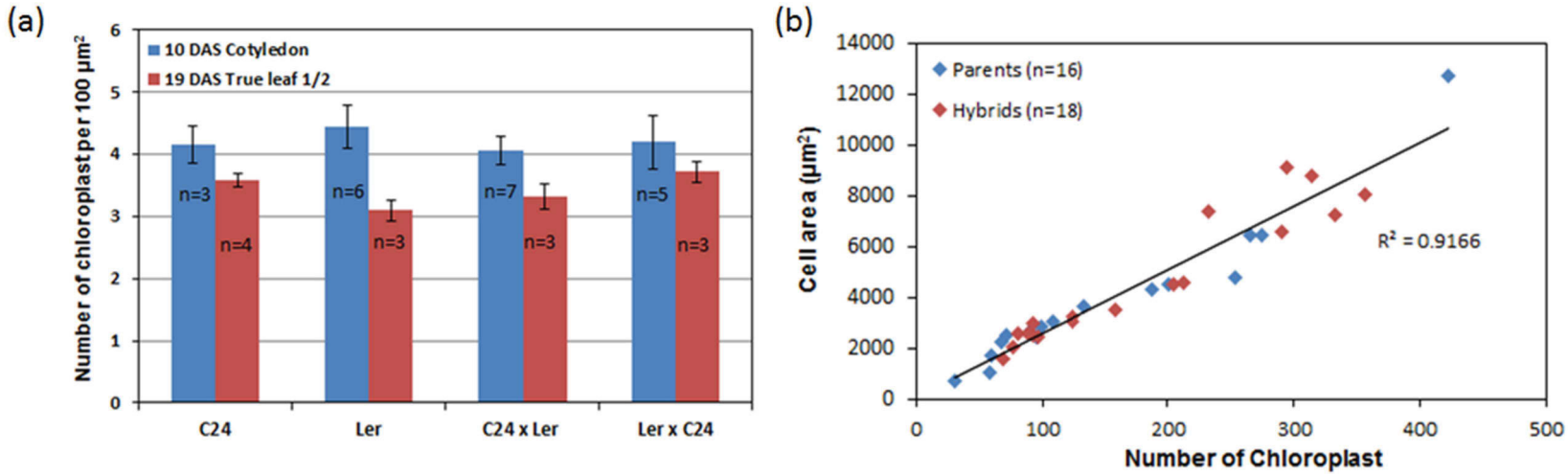

Figure 3.21. (a) Comparisons of chloroplast content between the C24/L*er* hybrids and parents. The mesophyll cells from the cotyledons and true leaf 1/2 of C24/L*er* hybrid seedlings at 10 and 19 days after sowing (DAS), respectively, were examined individually using Nomarski light microscopy and the number of chloroplasts was counted. The cell area was determined using ImageJ. Data presented are the average and SE from number of replicates as indicated. No significant differences were found between hybrids and the parents (ANOVA, $p > 0.05$). **(b) The correlations between chloroplast number per mesophyll cell and the cell area.** R^2: The coefficient of definition of the regression (black line).

3.13 Discussion

3.13.1 Hybrids have no increase in unit area photosynthetic capacity compared to parents

As determined by relative electron transport rate and CO_2 assimilation rate, a similar photosynthetic rate was found in *Arabidopsis* hybrids and parents on a unit leaf area basis (**Figure 3.17, Figure 3.19**). Measurements of chlorophyll content in unit biomass basis and chloroplast content in unit cell area basis showed a similar photosynthetic apparatus content in hybrid leaves and parent leaves (**Figure 3.20, Figure 3.21**). There is an ongoing debate whether photosynthesis parameters should be expressed on a leaf area or a leaf mass basis (Poorter et al., 2014). As suggested by a similar leaf mass per area ratio in both hybrids and parents (**Figure 3.14**), the photosynthetic parameters are presumably the same, either on a unit biomass or unit area basis. *Arabidopsis* hybrids and parents had a similar photosynthetic capacity on unit area/biomass basis. Although the unit area/biomass photosynthesis is the same, there is a greater rosette area in each hybrid plant, hence a greater photosynthetic production compared to the parents on a per-plant basis. This is in line with a previously reported study of a single hybrid in *Arabidopsis* (C24/Col) (Fujimoto et al., 2012) and the findings in other crop species such as rice (Zhang et al., 2007, Chang et al., 2016), maize (Morot-Gaudry et al., 1984, Mehta and Sarkar, 1992), wheat (Yang et al., 2007) and Chinese cabbage (Saeki et al., 2016).

3.13.2 Contributions of individual leaves to heterosis on a per plant basis

An *Arabidopsis* rosette consists of leaves that are developmentally different, including young leaves that have just emerged from the meristem, developing leaves with strong expansion, and older leaves that have reached maximum size. Previous studies on heterosis mainly focused on the difference between hybrid and parents on a per plant basis (Meyer et al., 2004, Fujimoto et al., 2012, Groszmann et al., 2014). It has not been reported whether individual hybrid leaves have equal contribution to the heterosis on a per plant basis; and whether the vigour of a hybrid leaf is maintained throughout the leaf development. The present data in C24/L*er* hybrids showed that heterosis in total rosette area was mainly contributed by newly developing leaves (**Figure 3.7)**. Heterosis in mature leaves was less marked, as parent leaves, especially L*er*, eventually caught up to a comparable hybrid leaf size.

3.13.3 Heterosis in vegetative growth might be due to altered leaf development

In *Arabidopsis thaliana*, rosette leaves were generated from the shoot meristem embedded in the centre of the rosette. The development of a leaf primordium to a mature leaf consists of temporal and spatial coordination of cell division and cell expansion that can be divided into five phases: an initiation phase, a general cell division phase, a transition phase, a cell expansion phase and a meristemoid cell division phase (Gonzalez et al., 2012). After initiation, leaf growth is mediated by cell division. Cell division first ceases at the tip of the leaf and is replaced by cell expansion. The transition region between cell division and cell expansion is known as a “cell cycle arrest front”. The cell

cycle arrest front gradually moves down towards the base of the leaf and cell division is restricted to a small region in the leaf base while the majority of the cells are expanding. During the cell expansion phase, meristemoid cells that are dispersed in the leaf epidermis carry out asymmetric cell division to form guard cells and pavement cells. Meristemoid cell division eventually ceases and leaf growth is mainly mediated by cell expansion. As demonstrated by *Arabidopsis* mutants, alterations in the duration of each developmental window or in the activities of regulatory pathways result in changes in leaf size due to altered cell size or/and cell number (Gonzalez et al., 2012). As suggested by measurements of palisade mesophyll cell size and cell number, the increased leaf size in hybrids compared to parents might be due to alterations in leaf development (illustrated in **Figure 3.22**).

3.13.3.1 Changes in hybrid cell size

As indicated by the palisade mesophyll cell area, the mature hybrid leaves showed a cell size comparable to L*er*; whereas in younger leaves, a greater cell area was found in C24 x Ler hybrids than L*er* shortly after appearing from the meristem (**Figure 3.13**). The increased cell size in young hybrid leaves may be achieved by an increased cell expansion rate; or by an accelerated leaf development. The latter was indicated by the earlier germination of hybrid seeds and the earlier leaf emergence of hybrid seedlings relative to that of the parents (**Figure 3.1, Figure 3.2**), indicating a shift in seedling development and, consequently, an earlier commencement of leaf development in hybrids than parents.

Increased final cell size was found in hybrids with strong heterosis in leaf size, such as C24/L*er* and C24/Col (**Figure 3.7**). In *Arabidopsis*, only a few regulators of cell expansion has been described (Kalve et al., 2014). Cell growth in dividing cells is mainly due to increase cytoplasmic volume whereas in expanding cells it is primarily attributable to the increasing vacuolar volume driven by turgor (Kalve et al., 2014). Cytoplasmic growth consists of the synthesis of macromolecules which is mediated by the Target of Rapamycin pathway (Kalve et al., 2014). Turgor-driven cell expansion is regulated by expansin that controls cell wall loosening while the plant hormones auxin and brassinosteroid are involved in regulating water uptake (Kalve et al., 2014). Endoreduplication is commonly observed in *Arabidopsis* leaves when cells carry out DNA replication without subsequent mitosis, resulting in triple (triploid) or quadruple (tetraploid) copies of chromosomes (Galbraith et al., 1991). Ploidy level has been reported to affect the size of cells in *Arabidopsis* leaves, although some reports showed this is not the case (Katagiri et al., 2016, Gonzalez et al., 2012). In C24/Col hybrids, there are no changes in the ploidy ratio compared to the parents, indicating the increased cell size and leaf size of hybrids were not due to increased endoreduplication (Miller et al., 2012).

3.13.3.2 Changes in hybrid cell number

Previous reports on heterosis in vegetative growth in *Arabidopsis* and other species showed a correlation with an increased cell number (Nebraska Agricultural Experiment and Kiesselbach, 1922, East, 1936, Groszmann et al., 2014, Saeki et al., 2016). In *Arabidopsis*, an increased cell number was found in almost all hybrid leaves analysed, both in the mature leaves (**Figure 3.12**) and developing leaves (Groszmann et al., 2014), suggesting hybrids have an increased cell division rate relative to the parents. During the cell division phase, cell size is generally unchanged (Donnelly et al., 1999). The earlier emergence of the newly developed leaves in C24/L*er* hybrid also supports the hypothesis that hybrids might have an increased cell division rate. In plants, cell division rate is regulated by the activities of proteins involved in cell cycle, especially those that regulate DNA replication and mitosis (Inze and De Veylder, 2006, Kalve et al., 2014). The hypothesis that hybrids have an altered rate of cell division is based on an assumption that the period for each leaf developmental phase is the same in both hybrids and parents. Without changing the cell division rate, a prolonged cell division period has also been shown to increase leaf size with an increased cell number (reviewed by (Gonzalez et al., 2012, Kalve et al., 2014). Cell division is also regulated by plant hormones including auxin, cytokinin, gibberellins and brassinosteroid (Wang and Ruan, 2013, Kalve et al., 2014). Transcriptome analysis of *Arabidopsis* hybrids showed a differentially up-regulated auxin biosynthesis pathway, suggesting the increased cell number in hybrid leaves might be due to an altered auxin level, although the auxin level in hybrid leaves has not been measured (Groszmann et al., 2015).

I have shown that the C24/L*er* hybrid might have an altered leaf development that resulting in increased cell size and cell number and, consequently, larger leaves than the

parents at a point in time (as summarised in **Figure 3.22**). A detailed kinematic analysis of hybrid leaves (a time-course measurement of leaf area, cell number and size over leaf development as described by Rymen et al. (2010) is required to verify the pathways or components that are responsible for the altered leaf development in hybrids.

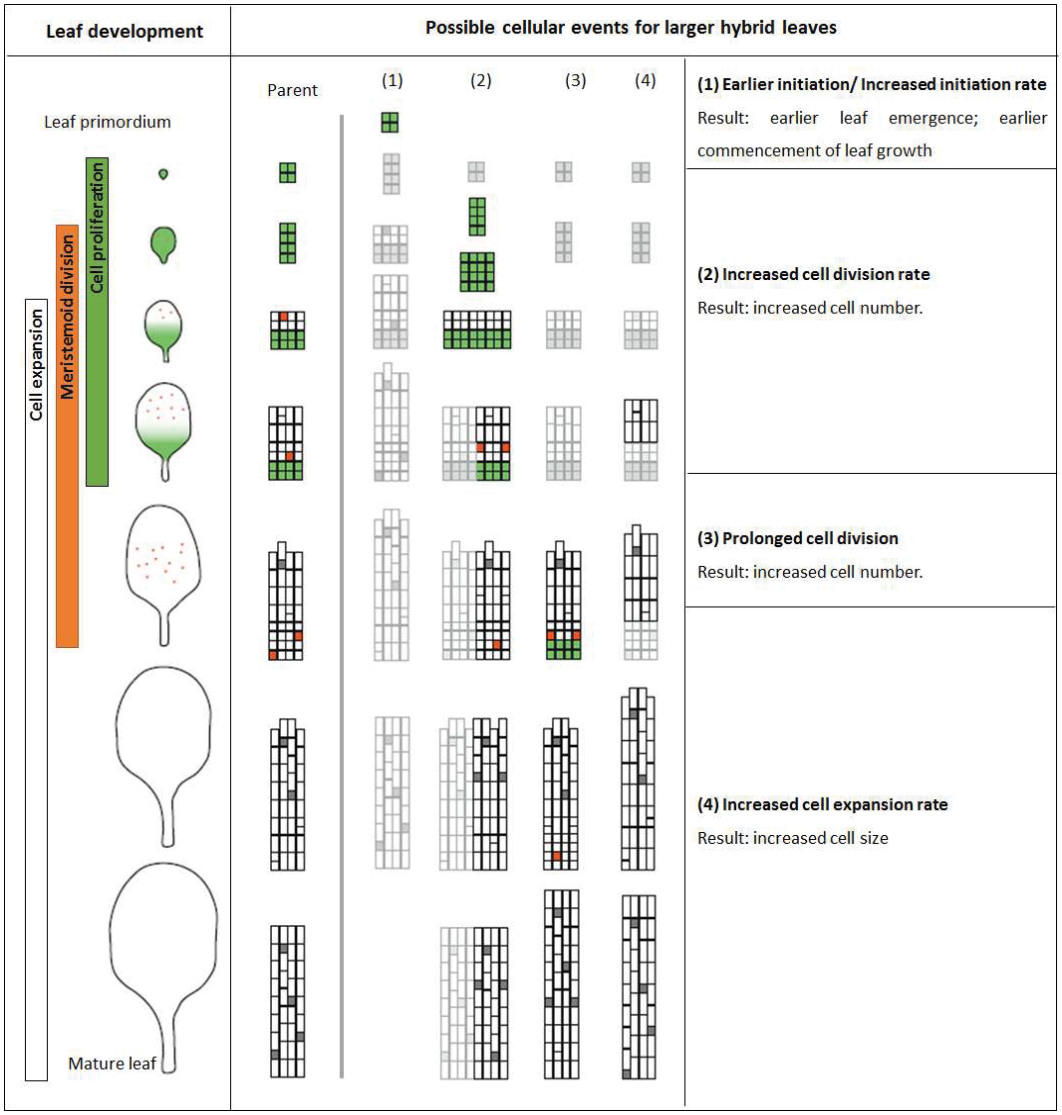

Figure 3.22. Schematic hypothesis of the cellular events leading to leaf size differences between C24 x L*er* hybrid and parents and between the parental lines. Dividing cells are shaded green and expanding cells in white; meristemoid cells in tangerine; stomatal cells in grey. For the ease of understanding, each cellular events are described separately. Under an indicated cellular event the affected regions are highlighted. Illustration adapted from Gonzalez et al. (2012).

3.14 Summary

1. Hybrid vigour in vegetative growth was not due to an increased photosynthetic capacity per unit leaf area as all photosynthetic parameters, including CO_2 assimilation rate, chlorophyll content and chloroplast content of hybrids were within the parental levels. As hybrid plants have larger leaves i.e. greater photosynthetic area the total photosynthetic amount per hybrid plant was greater than that in a parent plant.
2. In C24/L*er* hybrids, heterosis in vegetative growth was mainly contributed by a succession of newly developing leaves each being larger than the parent leaves, suggesting a more advanced seedling development.
3. The larger hybrid leaves were due to an increased cell size and/or cell number; and different hybrids showed different extents of these two factors. In the young, developing leaves of C24 x L*er* hybrid, the increased leaf area relative to parents was due to larger cells, may be due to more rapid cell expansion.
4. The C24/L*er* hybrid flowered later than the parents. Flowering time was a great influence on heterosis levels, especially at the end of hybrid seedling development. Hybrid plants continued to produce new leaves that were not present on the parent plants, resulting a greater difference in rosette biomass between hybrids and parents, compared to earlier time points.

4 Chapter IV Heterosis in response to different light regimes

4.1 Introduction

Light is the energy source for photosynthesis and is also an important environmental cue that controls various biological processes, such as developmental transitions (germination and flowering), circadian rhythm, plant movement and plant morphology (Chaiwanon et al., 2016). Doubling the growth irradiance has been reported to further increase heterosis levels for some *Arabidopsis* hybrids (Meyer et al., 2004). The mechanism of increasing heterosis under higher irradiance is not clear.

Increases in light intensity directly affect photosynthesis by changing the amount of energy available for electron transport and carbon fixation, and consequently, more carbohydrates such as sugars or starch and other organic compounds such as lipids, proteins and pigments, such as flavonoids, are produced. During the day, some assimilated carbon is converted into sucrose and translocated to growing tissues. Part of the assimilated carbon is also stored in the chloroplasts as starch to serve as the carbon source in the following night. In *Arabidopsis* leaves, the starch content peaks at the end of the day and a baseline level of starch remains at the end of the night. During the night a major fraction of this starch reserve is degraded, converted to sucrose for translocation and used as a general energy and carbon source for growth and respiration (Smith, 2012, Streb and Zeeman, 2012). This diurnal change of starch content is also called starch turnover. It has been reported that the starch contents in C24/L*er* and C24/Col hybrids

are greater than the parents at the end of the day, on a unit leaf biomass basis (Ni et al., 2009b, Ng et al., 2014). However, it is not clear whether hybrids have a greater starch turnover than the parents at night, and how that correlates with heterosis in vegetative growth. In my experiments, C24/L*er* hybrids were grown under doubled light intensity (240 µmol photons m^{-2} s^{-1}) and assessed for changes in hybrid vigour compared with those under the control light (120 µmol photons m^{-2} s^{-1}). The C24/L*er* hybrids grown under both irradiances were analysed for starch content at the end of the day and at the end of the night.

Plants acclimated to different irradiance levels develop anatomical and physiological changes in their leaves. Extensive studies in sun- and shade-grown leaves show that plants grown under higher light environments have greater photosynthetic capacity due to the production of thicker leaves that increases the diffusion of CO_2 to chloroplasts (Terashima et al., 2011) with a greater investment of nitrogen into photosynthetic apparatus (Boardman, 1977, Bjorkman, 1981, von Caemmerer and Farquhar, 1981) and a greater capacity in the metabolism of photosynthates (Oguchi et al., 2003, Athanasiou et al., 2010, Dyson et al., 2015). Thicker leaves can be achieved by increasing palisade mesophyll cell height or by forming more layers of mesophyll cells (Terashima et al., 2011). To determine whether hybrids and parents respond differently to higher irradiance, the 240 µmol photons m^{-2} s^{-1}-grown C24/L*er* hybrids and the parents were analysed for leaf parameters including leaf thickness, chlorophyll content and the biochemical parameters V_{cmax} and J as the indicators of photosynthetic capacity. To determine if the development of hybrids and parents responded differently to higher light levels, the leaf number per rosette of the 240 µmol photons m^{-2} s^{-1}-grown hybrids and parents were measured and compared to those in 120 µmol photons m^{-2} s^{-1}.

4.2 Heterosis under doubled light

To investigate whether the biomass heterosis of C24/L*er* hybrids could be increased by increasing growth irradiance the 10 DAS C24/L*er* seedlings were transferred into a high light condition (240 µmol photons m^{-2} s^{-1}) where the growth irradiance was twice the level the standard irradiance (120 µmol photons m^{-2} s^{-1}). After one week, the 18 DAS 240 µmol photons m^{-2} s^{-1}-grown plants were assessed for heterosis in vegetative biomass and compared to the 120 µmol photons m^{-2} s^{-1}-grown seedlings.

The 240 µmol photons m^{-2} s^{-1}-grown plants were characterized by shorter petioles and a more compact rosette than the 120 µmol photons m^{-2} s^{-1}-grown plants (**Figure 4.1a**). The 240 µmol photons m^{-2} s^{-1}-grown plants, both hybrids and parents, showed a biomass more than twice of the 120 µmol photons m^{-2} s^{-1}-grown plants (**Figure 4.1b**). However, the heterosis level of the 240 µmol photons m^{-2} s^{-1}-grown hybrids was not significantly different from the 120 µmol photons m^{-2} s^{-1}-grown plants ($p>0.05$). The C24/L*er* hybrids were 60-70% greater than the average biomass of the parents under both the light conditions tested (**Figure 4.1c**).

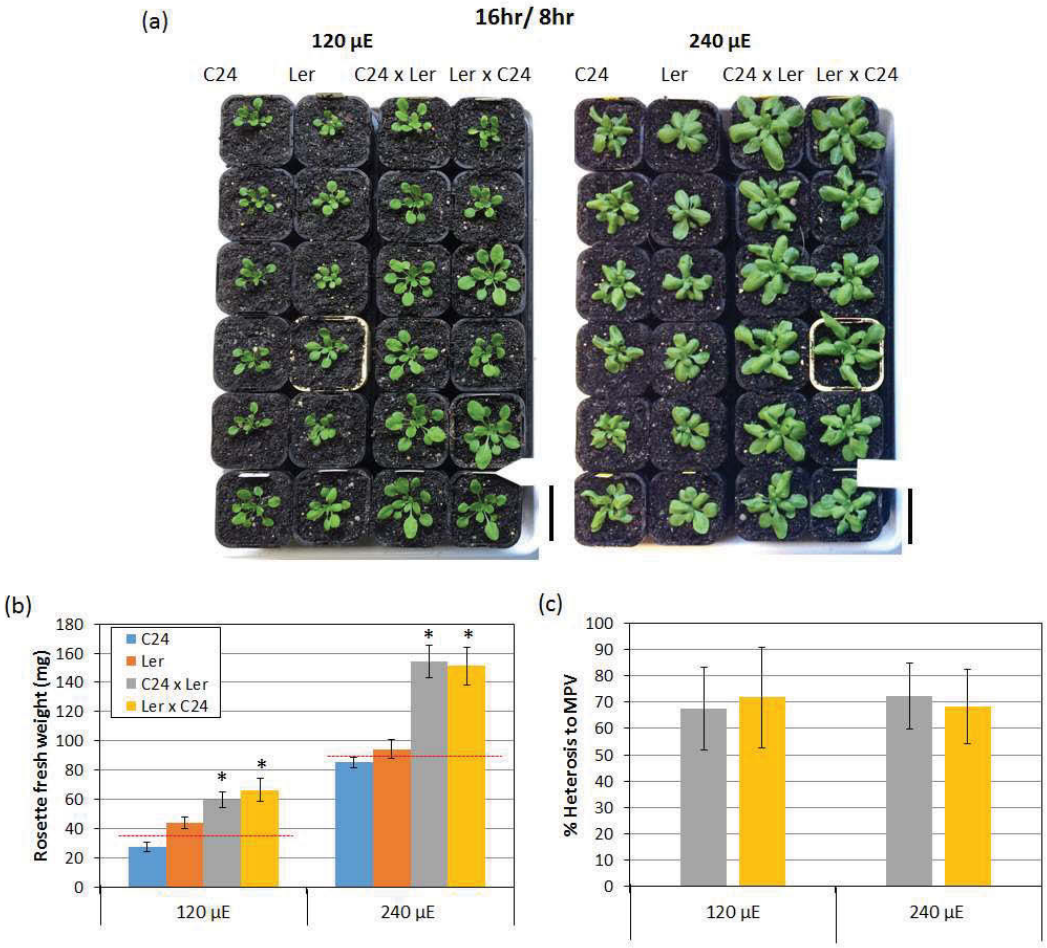

Figure 4.1. Morphology of the C24/L*er* hybrid seedlings grown under control or doubled photon flux under 16hr/ 8hr light cycle. The seedlings were sown and grown on Murashige and Skoog medium (3% sucrose) under a standard irradiance of 120 µmol photons m^{-2} s^{-1} before transplanting into soil at 10 DAS. Half of the population was randomly selected and shifted to a doubled light conditions (240 µmol photons m^{-2} s^{-1}) while the other half was kept under control conditions. **(a)** shows representative images of the 21 DAS C24/L*er* seedlings. Scale bar: 5 cm. **(b)** Comparison of rosette biomass between the 18 DAS hybrids and parents. Asterisks indicate significant differences from the average level of the parents (ANOVA, $p < 0.001$). The level of heterosis relative to the mid-parent value (red dashed line) is shown in **(c)**. Data presented are the average and SE of n=9 seedlings. No significant difference in the heterosis levels was found between the light intensities for growth (ANOVA, $p > 0.05$). µE: µmol photons m^{-2} s^{-1}. The experiment was repeated three times.

4.3 Leaf emergence under doubled-photon flux

The 240 µmol photons m^{-2} s^{-1}-grown C24/L*er* seedlings were scored for the number of leaves at 15, 18 and 21 DAS, and compared to the 120 µmol photons m^{-2} s^{-1}-grown plants. Rosette leaves of each seedling were counted, including the emerging new leaves in the centre of the rosette.

All 240 µmol photons m^{-2} s^{-1}-grown seedlings had a greater number of leaves than the 120 µmol photons m^{-2} s^{-1}-grown plants at all time points examined (**Figure 4.2**). At 15 DAS, the 120 µmol photons m^{-2} s^{-1}-grown seedlings contained, on average, six leaves (**Figure 4.2 left panel**) while the 240 µmol photons m^{-2} s^{-1}-grown seedlings contained seven leaves (**Figure 4.2 right panel**). Six days later, except for L*er*, the 21 DAS 120 µmol photons m^{-2} s^{-1}-grown seedlings had produced 5-6 new leaves while the 240 µmol photons m^{-2} s^{-1}-grown seedlings generated 8-9 new leaves over the same period of time (**Figure 4.2**). Beyond 18 DAS the early flowering ecotype, L*er*, ceased to increase rosette leaf number, due to the transition to reproductive growth. By the end of the experiment, all L*er* seedlings contained no more than ten leaves per rosette. Under both light conditions, the C24/L*er* hybrid seedlings possessed one leaf more than the parent seedlings at all time points examined (see **Appendices** for *p* values). These results indicate that the C24/L*er* seedlings have an elevated rate of leaf emergence under doubled light intensity. However, increasing growth irradiance did not further increase the leaf number difference between hybrids and parents.

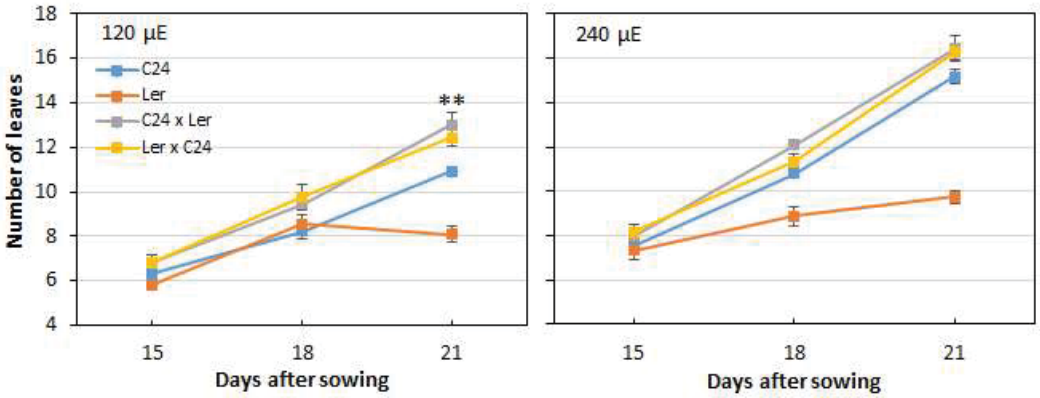

Figure 4.2. The number of leaves of C24/L*er* seedlings grown under control (left) and doubled light intensity (right) at three time points. Each data point represents the average and SE of n=5-12 randomly selected plants from a population of 30 plants. µE: µmol photons m^{-2} s^{-1}. Asterisks indicate significant difference from the better parent (ANOVA, **: $p < 0.01$).

4.4 The newly developing leaves of hybrids had increased heterosis under doubled-light

Individual leaves of the 240 µmol photons m^{-2} s^{-1}-grown hybrid seedlings were analysed for heterosis levels relative to the corresponding leaves of the parents and compared to those grown under 120 µmol photons m^{-2} s^{-1}. At 19 DAS, the total area of all the 240 µmol photons m^{-2} s^{-1}-grown leaves was greater than those grown at 120 µmol photons m^{-2} s^{-1} (**Figure 4.3a**). Each leaf area of the C24 x L*er* hybrid was ~60% greater than the average of the corresponding leaf of the parents under 120 µmol photons m^{-2} s^{-1}, while this was less marked for the L*er* x C24 hybrid (**Figure 4.3c**). Under doubled-light, a greater difference in leaf size between hybrids and parents was found in leaves 5-8 (**Figure 4.3b**), resulting in higher levels of heterosis for these leaves (~90%) (**Figure 4.3d**). Leaves 5-8 were the largest leaves at 19 DAS for the 240 µmol photons m^{-2} s^{-1}-grown rosettes (**Figure 4.3b; indicated by asterisks**). In a later stage of seedling development, at 30 DAS, a similar increase in the level of heterosis was found in both 240 µmol photons m^{-2} s^{-1}-grown reciprocal hybrids.

At 30 DAS, the greatest leaf area was found in leaves 10-13 of hybrid seedlings, under both 120 µmol photons m^{-2} s^{-1} and 240 µmol photons m^{-2} s^{-1} (**Figure 4.4a, b; Figure 4.5**). Those leaves were not present in the L*er* parent as the early flowering ecotype only produces 9-10 rosette leaves. When compared to the corresponding leaves of the C24 parent, a greater level of heterosis was found in the leaves 11-14 of the 240 µmol photons m^{-2} s^{-1}-grown hybrids (up to 150-250% greater than the average of the parents). In the 120 µmol photons m^{-2} s^{-1} growing condition heterosis was lower, around 50-150% greater

than the parents (**Figure 4.4c**). Doubling irradiance seemed to affect only the newly developing leaves, the leaves that are actively developing at the time of sampling. This effect was transient as leaves 6-9 of the 240 µmol photons m^{-2} s^{-1}-grown hybrids which had increased heterosis at 19 DAS, showed no increase in heterosis at 30 DAS compared to the level under 120 µmol photons m^{-2} s^{-1} (**Figure 4.4c, d**).

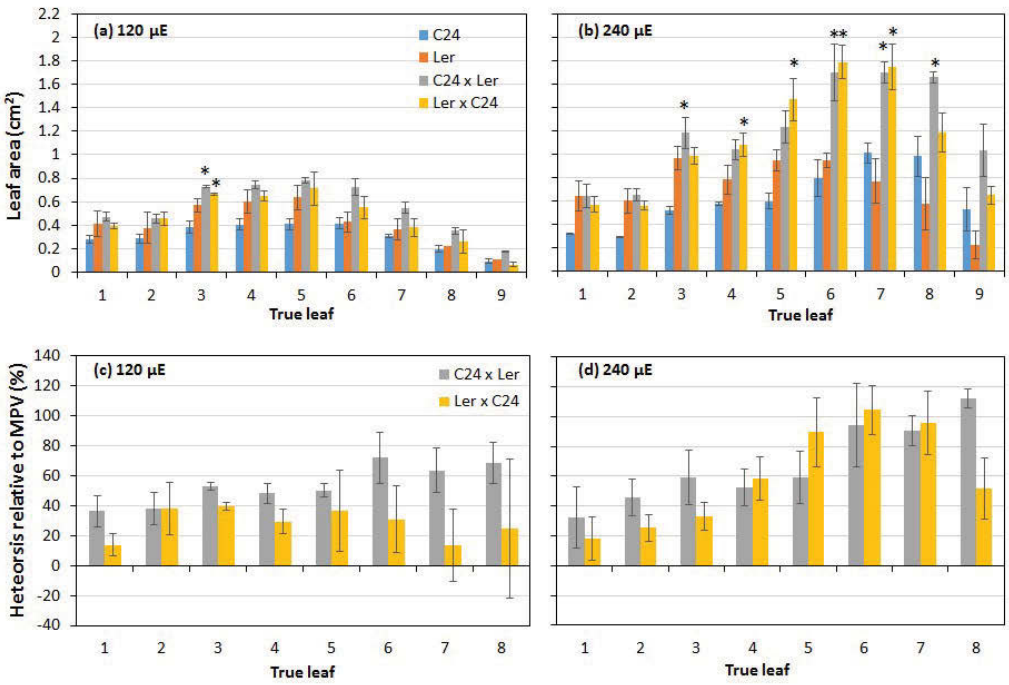

Figure 4.3. Comparison of individual leaves of the 19 DAS C24/L*er* seedlings under (a)(c) standard and (b)(d) doubled light conditions. (a)(b) Leaf size determined from the projected area. Each true leaf was numbered in the order of emergence on a plant. Asterisks indicate significant differences from the average level of the parents (ANOVA, $p < 0.05$). Columns without error bars represent data not available in at least one of the replicates (n < 3). **(c)(d) The levels of heterosis of each hybrid leaf relative to the average of the parents.** Statistical comparisons were carried out between the light conditions and amongst leaves (ANOVA, $p > 0.05$). Error bars represent the standard error of n=3 seedlings. µE: µmol photons m^{-2} s^{-1}.

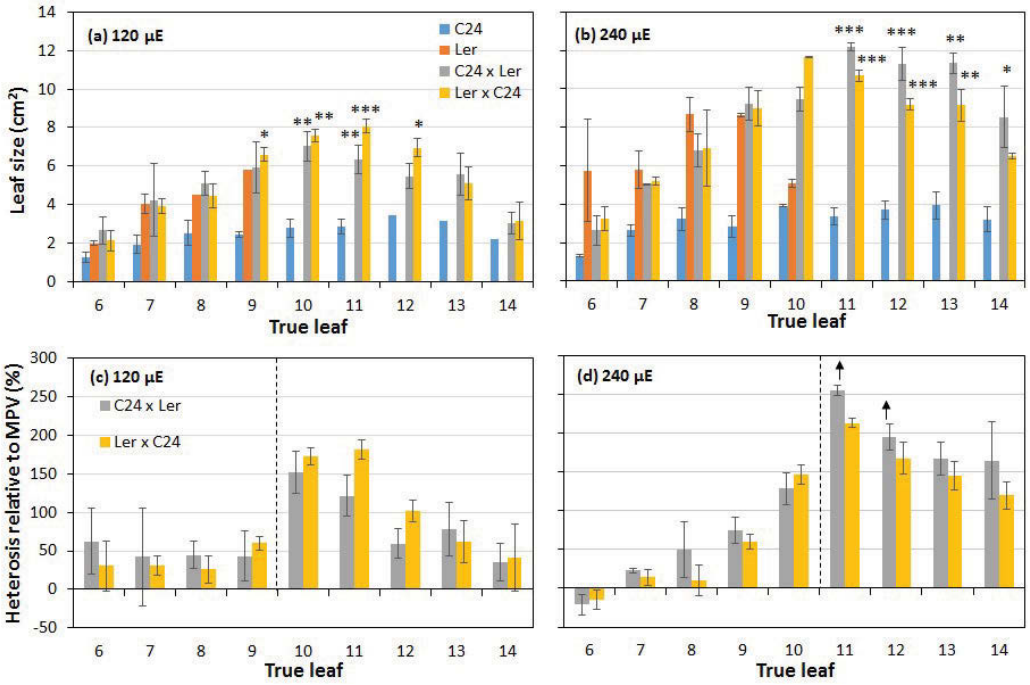

Figure 4.4. Comparison of individual leaves of the 30 DAS C24/L*er* seedlings under (a)(c) standard and (b)(d) doubled light conditions. (a)(b) Leaf size determined from the projected area; (c)(d) The levels of heterosis of each hybrid leaf relative to the average of the parents. The early flowering ecotype L*er* ceased to produce rosette leaves after leaf number 9/10 and the levels of heterosis of the subsequent leaves were calculated against the other parent, C24 (separated by dashed line). Significant differences from C24 are indicated by asterisks (ANOVA; *: $p < 0.05$, **: $p < 0.01$, ***: $p < 0.001$). Hybrid leaves with altered levels of heterosis under doubled light relative to that under normal light conditions were indicated by arrows (ANOVA, $p = 0.06$). Error bars represent the standard error of n=3 seedlings. For the measurements on all the leaves, see **Figure 4.5**. µE: µmol photons m^{-2} s^{-1}.

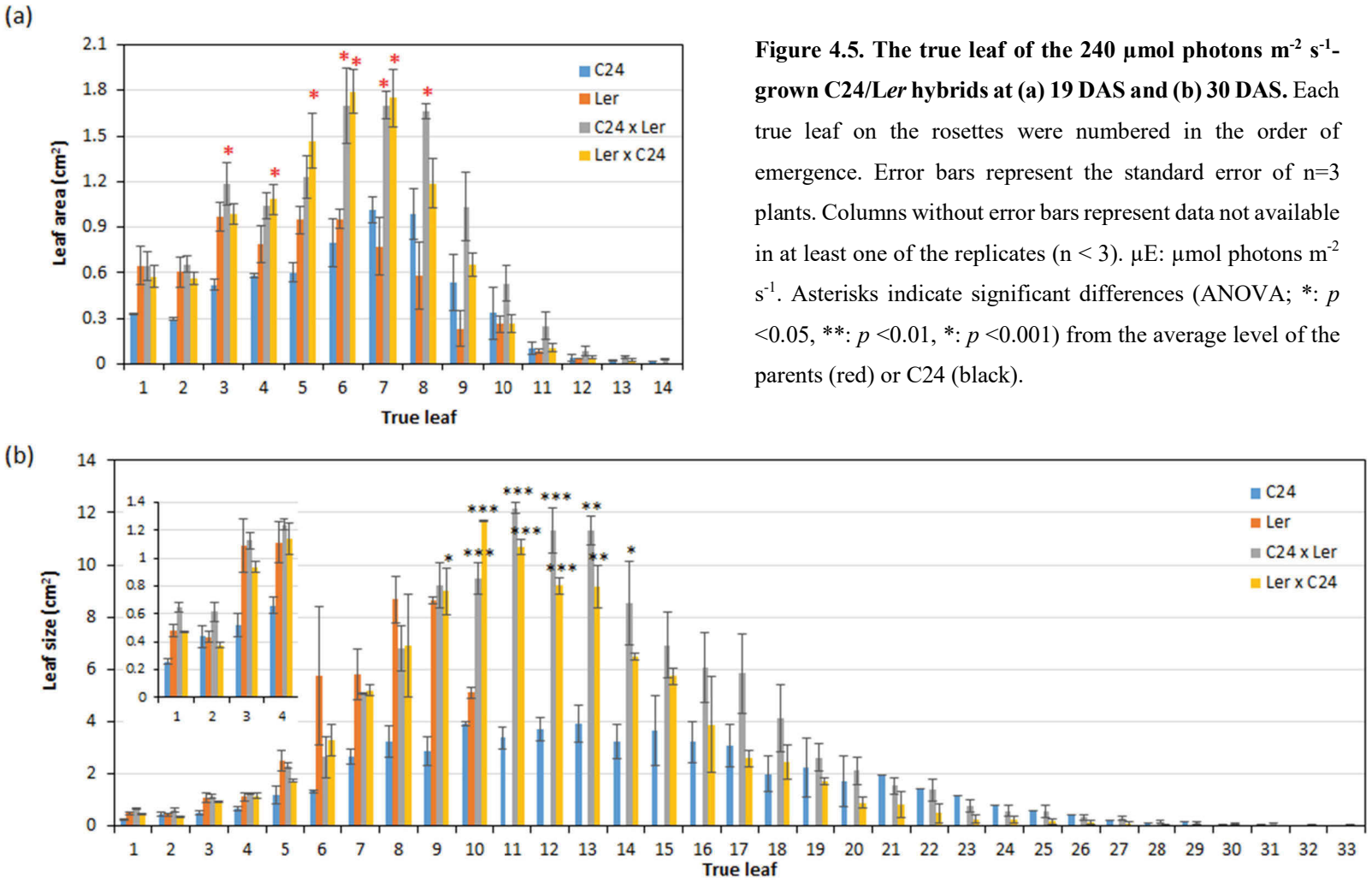

Figure 4.5. The true leaf of the 240 µmol photons m^{-2} s^{-1}-grown C24/L*er* hybrids at (a) 19 DAS and (b) 30 DAS. Each true leaf on the rosettes were numbered in the order of emergence. Error bars represent the standard error of n=3 plants. Columns without error bars represent data not available in at least one of the replicates (n < 3). µE: µmol photons m^{-2} s^{-1}. Asterisks indicate significant differences (ANOVA; *: p <0.05, **: p <0.01, *: p <0.001) from the average level of the parents (red) or C24 (black).

4.5 Increased leaf thickness under doubled light

Arabidopsis thaliana has been shown to develop thicker leaves under high light (Heyneke et al., 2013). To determine if hybrids have altered leaf thickness under doubled-light relative to the leaves of the parents, cross-sections of leaves were analysed.

Leaf thickness of the 120 µmol photons m^{-2} s^{-1}-grown C24/L*er* seedlings was on average 190 µm, except for the parent C24, which had thinner leaves (~160 µm) (**Figure 4.6**). At similar positions in the lamina, leaves of all the 240 µmol photons m^{-2} s^{-1}-grown seedlings were 30-40% thicker than those grown under 120 µmol photons m^{-2} s^{-1} (**Figure 4.6**). Leaf thickness of each of the 240 µmol photons m^{-2} s^{-1}-grown reciprocal hybrids was similar to that of the better parent, ecotype L*er* (260 µm) while leaf thickness of ecotype C24 was ~220 µm (**Figure 4.6**).

Plants acclimated to high light had thicker leaves due to increased cell volume and/or a greater number of mesophyll cell layers (Boardman, 1977, Bjorkman, 1981, Terashima et al., 2011). The volume of mesophyll cells in the 240 µmol photons m^{-2} s^{-1}-grown plants was greater than those under 120 µmol photons m^{-2} s^{-1} (**Figure 4.7**). Under both light conditions, there was one layer of palisade mesophyll cells and three to four layers of spongy mesophyll cells (**Figure 4.7**).

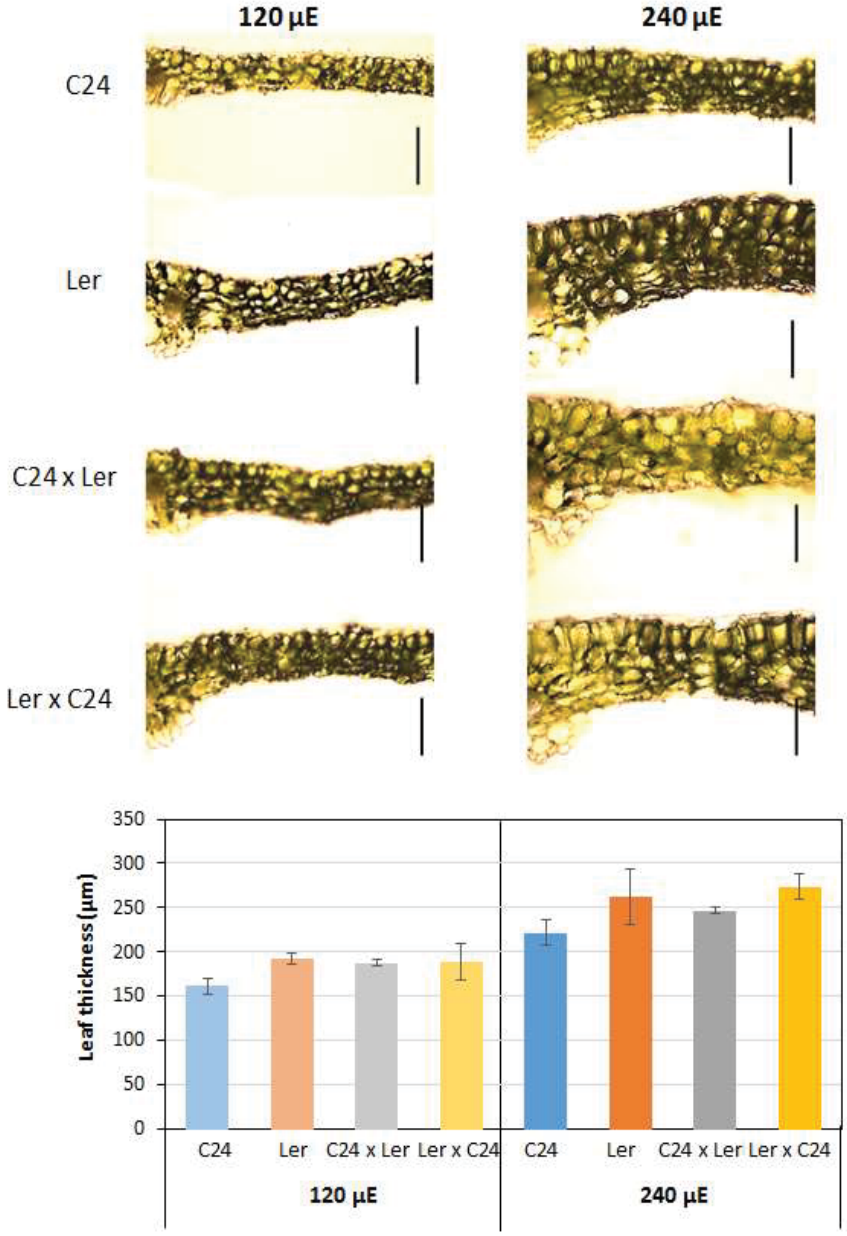

Figure 4.6. Comparisons of leaf thickness of the C24/L*er* seedlings grown under normal or doubled light intensity. Cross-sections of the largest leaves of the 4 week-old seedlings were examined under a microscope (10X objective). Top panel shows representative microscopic images of three replicates. The leaf cross-sections were presented with the central midvein (mv) aligning to the left and the adaxial epidermis to the top. Scale bar represents 200 µm. Leaf thickness was determined by measuring the distance between the upper and lower epidermis using ImageJ. Data presented were the average and SE of n=3 seedlings. Statistical comparisons between hybrids and the parents, and amongst the lines in different growing lights were carried out and no significant differences were found (ANOVA, $p > 0.05$).

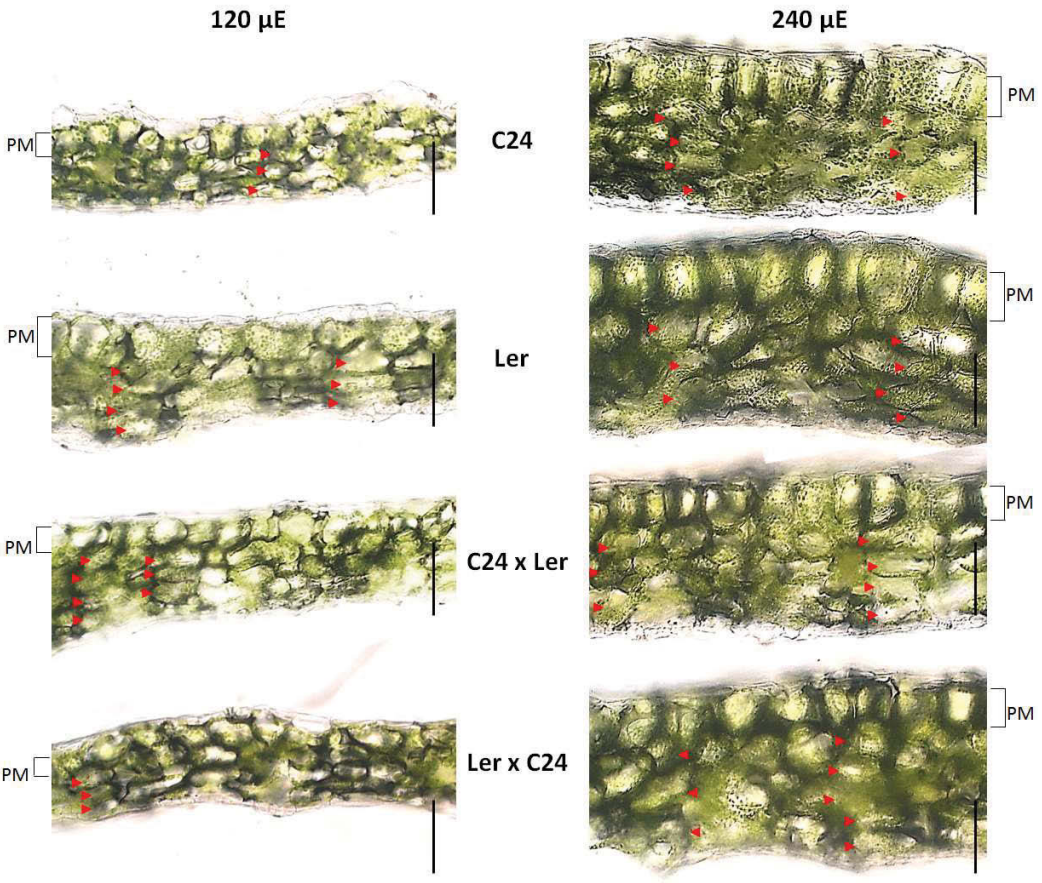

Figure 4.7. Number of mesophyll cell layers of the C24/L*er* seedlings grown under 120 µmol photons m^{-2} s^{-1} and 240 µmol photons m^{-2} s^{-1}. Each microscopic image (20X objective) shown was representative of three replicates. The palisade mesophyll (PM) cell layer was indicated by brackets. Spongy mesophyll cells were indicated by red arrows. Scale bar represents 100 µm.

4.6 The CO_2 assimilation rate under the doubled irradiance

To see whether C24/L*er* hybrids and parents have altered photosynthetic capacity under high irradiance, the 240 µmol photons m^{-2} s^{-1}-grown plants were analysed for CO_2 assimilation against increasing CO_2 partial pressure (A/C_i curves), and compared with those grown in 120 µmol photons m^{-2} s^{-1} (**Figure 4.8**). When measured at their responsive growth irradiance, the A/Ci curves of the 240 µmol photons m^{-2} s^{-1}-grown plants showed greater rates of CO_2 assimilation than the 120 µmol photons m^{-2} s^{-1} plants (**Figure 4.8a, c**). The greater rates of CO_2 assimilation in the 240 µmol photons m^{-2} s^{-1}-grown plants may be due to the irradiance under which the CO_2 assimilation was measured being greater than in the 120 µmol photons m^{-2} s^{-1}-grown plants.

To determine whether the 240 µmol photons m^{-2} s^{-1}-grown plants have altered capacity in photosynthetic processes relative to the 120 µmol photons m^{-2} s^{-1}-grown plants, measurements of CO_2 response curves were carried out at a saturating irradiance of 1000 µmol photons m^{-2} s^{-1} (**Figure 4.8b, d**). The biochemistry parameters, maximum velocity of Rubisco in carboxylation (V_{cmax}) and the rates of electron transport (J) for the 240 µmol photons m^{-2} s^{-1}-grown plants were estimated and compared to that of the 120 µmol photons m^{-2} s^{-1}- grown plants (**Figure 4.9**). No significant changes in V_{cmax} or J values were found between the 240 µmol photons m^{-2} s^{-1}-grown hybrids and parents ($p > 0.05$) (**Figure 4.9**). All the C24/L*er* seedlings, grown under either 120 µmol photons m^{-2} s^{-1} or 240 µmol photons m^{-2} s^{-1}, exhibited a similar level of V_{cmax} and J within a range of 30-40 µmol CO_2 m^{-2} $s^{-1}$and 70-90 µmol electron m^{-2} s^{-1}, respectively (**Figure 4.9**). Under both light conditions, all plants showed a J/V_{cmax} ratio at levels between 2.1-2.3 and no

significant difference was found between hybrids and parents (**Table 4.1**). This indicates that the photosynthetic processes in 240 µmol photons m^{-2} s^{-1}-grown plants were operating similarly to the 120 µmol photons m^{-2} s^{-1}-grown plants. These results indicate that the unit area photosynthetic capacity in hybrids was similar to the parents, regardless of the growth irradiance. The photosynthetic machinery in the 240 µmol photons m^{-2} s^{-1}-grown plants was operating with a photosynthetic capacity similar to that in the 120 µmol photons m^{-2} s^{-1}-grown plants.

Although no changes were found in the biochemical parameters, the light-saturated rates of CO_2 assimilation of the 240 µmol photons m^{-2} s^{-1}-grown plants were greater than the 120 µmol photons m^{-2} s^{-1}-grown plants, especially under high CO_2 (**Figure 4.8b, d; Figure 4.10a**). When the photosynthetic processes are operating similarly, greater rates of CO_2 assimilation can be achieved if more CO_2 is available in the mesophyll tissue (Terashima et al., 2006). To see whether the 240 µmol photons m^{-2} s^{-1}-grown plants have greater intracellular CO_2 than the 120 µmol photons m^{-2} s^{-1}-grown plants, the datasets of the A/C_i curves measured in the saturating light were examined for the ratio of intracellular CO_2 partial pressure to an ambient CO_2 partial pressure at 400 ppm (C_i/C_a) (**Figure 4.10**). All plants analysed have C_i/C_a ratio at comparable levels between 0.70-0.75, except for the 120 µmol photons m^{-2} s^{-1}-grown L*er* (**Figure 4.10b**). It has been reported that the *erecta* mutation influences stomata density and increases gas exchange through stomata (Masle et al., 2005). The high levels of C_i/C_a ratio in the L*er* plants may be associated with the altered stomatal patterning that affects CO_2 conductance.

Whereas stomatal conductance of water vapour (g_s) in hybrids grown under 240 µmol photons m^{-2} s^{-1} was greater than that under 120 µmol photons m^{-2} s^{-1}, the g_s in the parents

were at similar levels regardless of the growth irradiance (**Figure 4.10c**). The g_s in the 120 µmol photons m^{-2} s^{-1}-grown L*er* was the highest amongst all the 120 µmol photons m^{-2} s^{-1}-grown plants and was higher than the 240 µmol photons m^{-2} s^{-1}-grown L*er* (**Figure 4.10c**). Under strong transpiration, high readings of g_s and C_i/C_a ratio can be falsely obtained if excessive water vapour accumulates in the measurement cells of the gas exchange analyser. However, this was not the case as the average vapour pressure deficit i.e. the evaporative demands from leaf to air of the 120 µmol photons m^{-2} s^{-1}-grown L*er* was at a level comparable to other lines (**Figure 4.10d**).

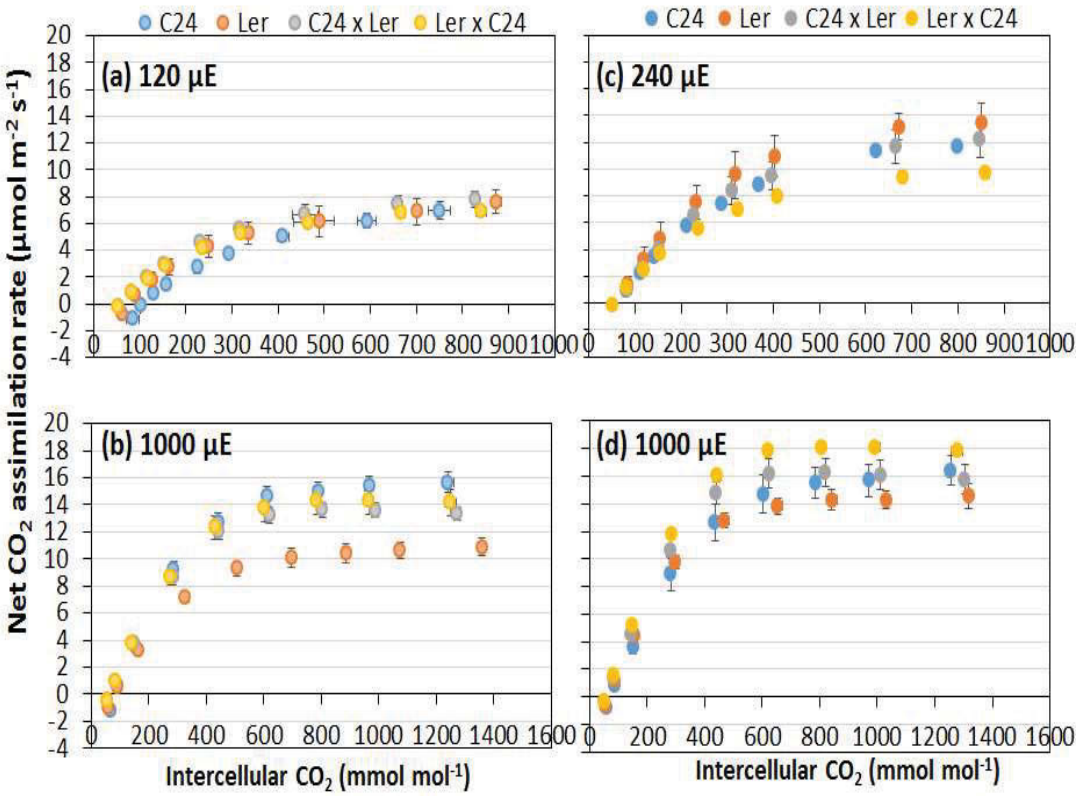

Figure 4.8. A/Ci curves of the 3 week-old C24/L*er* seedlings grown under (a)(b) 120 µmol photons m^{-2} s^{-1} or (c)(d) 240 µmol photons m^{-2} s^{-1} under a light cycle 16hr-light/ 8hr-dark. Analyses of CO_2 assimilation were carried out under (a)(c) the corresponding growth irradiance or (b)(d) a saturating light using a gas exchange analyser (LI-6400XT, LICOR). The light intensity used was indicated in the charts. Data sets of (a) and (b) were collected separately from independent experiments. Data presented were the average and SE of $n \geq 3$ replicates. Data in (b) left panel represent the average of two independent experiments (n=3 replicates each). Statistical comparisons between hybrids and parents were carried out for each data points and no significant difference was found between hybris and the better parents (ANOVA, $p > 0.05$) (see **Appendices** for ANOVA table). A: net CO_2 assimilation; C_i: Intercellular CO_2 partial pressure; PAR: photosynthetically active radiation; µE: µmol photons m^{-2} s^{-1}.

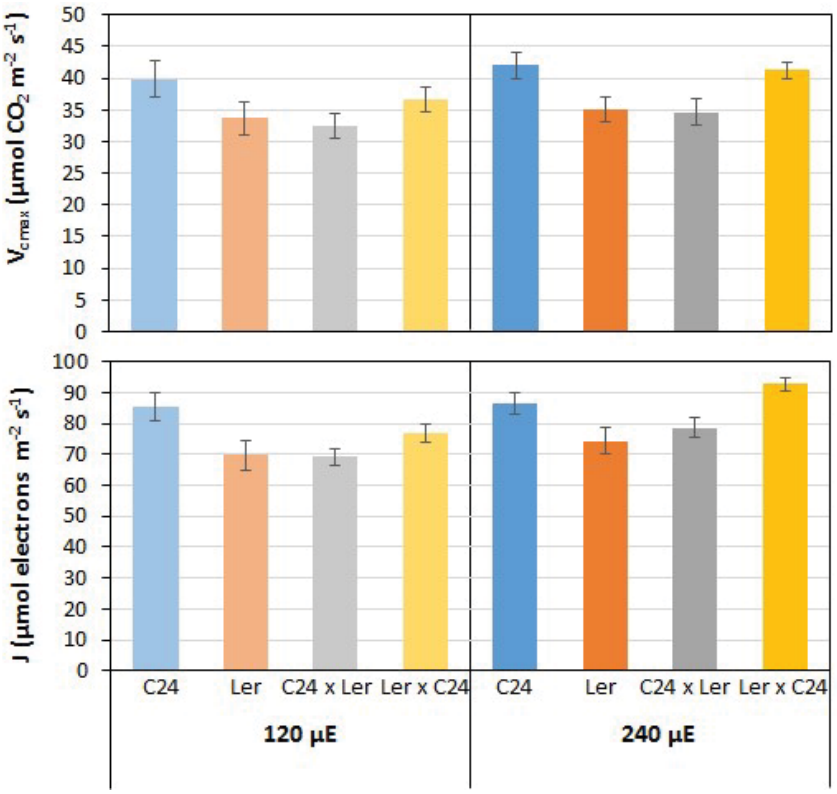

Figure 4.9. Comparisons of the photosynthetic capacity of the 4 week-old C24/L*er* hybrid seedlings grown under ambient and doubled photon flux. The datasets of the A/C_i assay shown in **Figure 5** were analysed by fitting each individual A/Ci curve to the model of C_3 photosynthesis (Farquhar et al., 1980), using the spread sheet developed by (Sharkey et al., 2007). Each curve was analysed using the same configurations. Briefly, data points at C_i between 200 and 300 ppm were not included in the curve-fitting; data points with $C_i < 200$ ppm were designated as Rubisco-limited photosynthesis; data points with $C_i > 300$ ppm were designated as electron transport-limited photosynthesis; and data points located at the plateau phase of the curve with an increasing C_i and a constant or decreasing A were designated as triose phosphate usage-limited photosynthesis (see **Methods and Materials** for details). Data represents the average and SE of maximum rate of Rubisco carboxylation (V_{cmax}) and estimated electron transport rate (J) determined from $n \geq 3$. No statistical differences were found between hybrid and parents and amongst the lines in different light intensities.(ANOVA, $p > 0.05$) µE: µmol photons m^{-2} s^{-1}.

Table 4.1. The ratio of J to V_{cmax} of the 240 µmol photons m^{-2} s^{-1}-grown plants compared to the 120 µmol photons m^{-2} s^{-1}-grown plants. Data represent average and SE of n=3-6. µE: µmol photons m^{-2} s^{-1}. No significant difference was found between hybrids and parents and within the lines in different growth light intensity (ANOVA, $p > 0.05$).

Light condition	Line	J/ V_{cmax} ratio
120 µE	C24	2.2 ± 0.08
	L*er*	2.1 ± 0.05
	C24 x L*er*	2.1 ± 0.09
	L*er* x C24	2.2 ± 0.07
240 µE	C24	2.1 ± 0.17
	L*er*	2.1 ± 0.04
	C24 x L*er*	2.3 ± 0.04
	L*er* x C24	2.3 ± 0.06

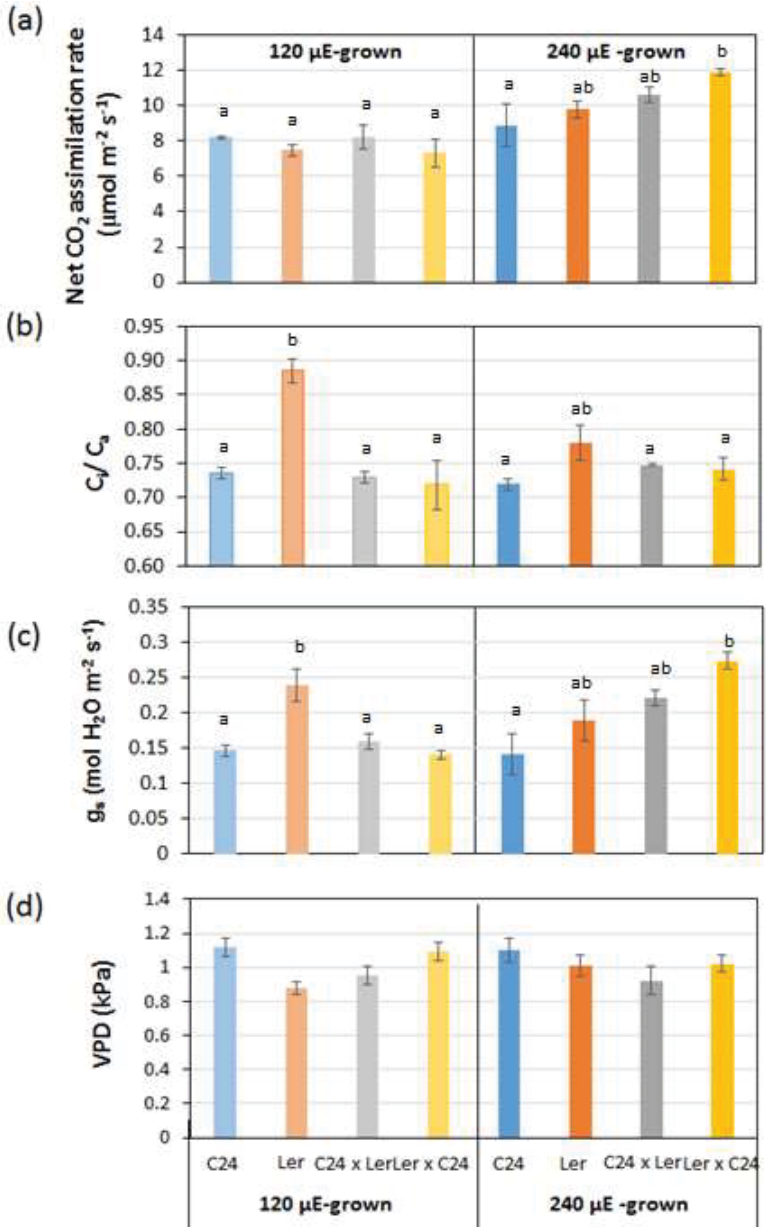

Figure 4.10. Comparisons of gas exchange variables between C24/L*er* hybrid and the parents acclimated to a standard (120 µmol photons m^{-2} s^{-1}) or doubled (240 µmol photons m^{-2} s^{-1}) irradiance. Data represents the average and SE of n ≥ 3 data points from the datasets of the A/C_i curves shown in **Figure 4.8** in a saturating light (1000 µmol m^{-2} s^{-1}) under ambient CO_2 partial pressure of 400 ppm. Different letters indicate significant difference from the others (ANOVA, $p < 0.05$). g_s: stomatal conductance of water vapour; Ci/Ca: the ratio of intercellular to atmospheric CO_2 partial pressure; VPD: water vapour pressure deficit; µE: µmol photons m^{-2} s^{-1}.

4.7 Chlorophyll content under 240 µmol photons m^{-2} s^{-1}

To examine if doubling irradiance alters the abundance of the light harvesting apparatus in the C24/L*er* seedlings, the 28 DAS C24/L*er* seedlings grown under either 120 µmol photons m^{-2} s^{-1} or 240 µmol photons m^{-2} s^{-1} were analysed for the chlorophyll content per unit rosette biomass. The chlorophyll content in the 240 µmol photons m^{-2} s^{-1}-grown plants was slightly lower than that under 120 µmol photons m^{-2} s^{-1} (**Figure 4.11**). Although chlorophyll content was slightly lower in 240 µmol photons m^{-2} s^{-1}, no significant changes were found in the composition of light harvesting pigments. All the plants analysed showed a similar chlorophyll a to b ratio at a level of ~2 (**Figure 4.11**). Under both the light conditions, a similar chlorophyll content was found in hybrids and parents (**Figure 4.11**). This indicates that hybrids and parents have a similar amount of photosynthetic machinery on a unit biomass basis.

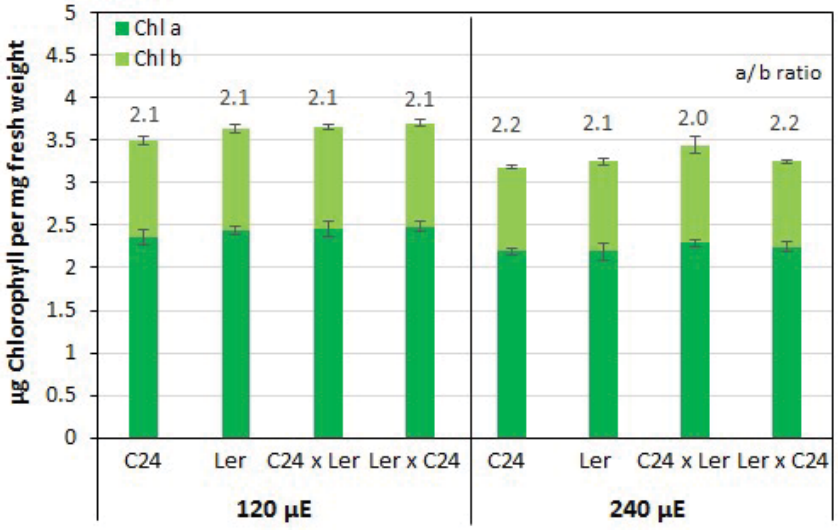

Figure 4.11. Chlorophyll content of 4 week-old C24/L*er* hybrid seedlings grown under either 120 µmol photons m^{-2} s^{-1} or 240 µmol photons m^{-2} s^{-1}. Data represent the average and SE of three replicates (pools of n=2 seedlings). The value shown above each column is the ratio of chlorophyll a to b (a/b ratio). Chl: chlorophyll; µE: µmol photons m^{-2} s^{-1}. Statistical comparisons were carried out between hybrids and parents; and amongst plants growing under different light conditions (ANOVA). No significant differences were found ($p > 0.05$).

4.8 Starch turnover under doubled light

To investigate whether the production and consumption of carbohydrates in hybrids is different from that in the parents, C24/L*er* hybrids and the parents were analysed for starch contents at the end of the day and at the end of the night (**Figure 4.12**). As indicated by the iodine staining, starch content in all plants examined was high at dusk and low at dawn (**Figure 4.12a**); this is typical of the diurnal starch turnover in *Arabidopsis* (Smith, 2012). The 120 µmol photons m^{-2} s^{-1}-grown C24/L*er* hybrid seedlings contained 6.5 µg starch per mg fresh weight at the end of the day, similar to the average of that of the parents (**Figure 4.12b**). At the end of the night the starch content was 1.5 µg/ mg FW (**Figure 4.12b**). Starch turnover per night was determined by calculating the difference in starch content at the beginning and end of the night. Starch turnover in both the C24/L*er* reciprocal hybrids was just above 5 µg/ mg FW, which was slightly greater than the average of that of the parents but not greater than the best parent C24 (**Figure 4.12c**). By the end of the night, both hybrids and parents grown under 120 µmol photons m^{-2} s^{-1}-grown metabolised >75% of the starch accumulated at the end of the day.

Doubling the light intensity substantially increased starch biosynthesis. The 240 µmol photons m^{-2} s^{-1}-grown hybrids and parents contained an average of 13.3 µg/ mg FW of starch at the end of the day (**Figure 4.12b**). This is twice the amount of that under 120 µmol photons m^{-2} s^{-1} (**Figure 4.12b**). Although starch biosynthesis was greater under doubled irradiance, the unit biomass starch turnover remained the same. The end-of-the-night starch content for the 240 µmol photons m^{-2} s^{-1}-grown plants was 5-8 µg/mg FW

(**Figure 4.12b**). As a result, the starch turnover of the 240 μmol photons m^{-2} s^{-1}-grown seedlings was comparable to that under 120 μmol photons m^{-2} s^{-1} (**Figure 4.12c**).

These results indicate that the 240 μmol photons m^{-2} s^{-1}-grown plants were not able to remobilise the increased amount of starch accumulated in the doubled irradiance. Under both light levels tested, the starch turnover of hybrids was comparable to the parents, on unit leaf biomass basis.

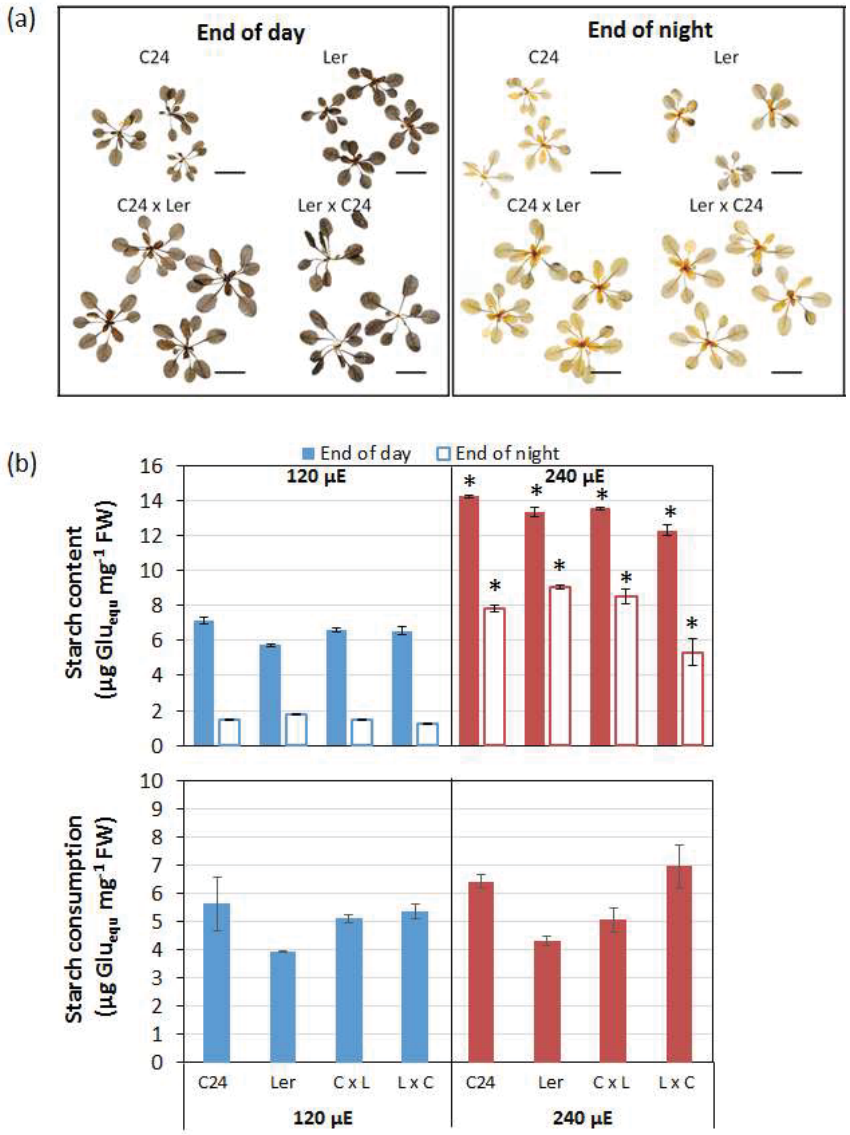

Figure 4.12. (a) Starch turnover under standard condition. Rosettes of 21 DAS seedlings were stained with Lugol's iodine solution (0.1%). Dark purple stain indicates the presence of starch granules. End of the day: one hour before lights off; end of the night: one hour before lights on. Scale bars: 2 cm. **(b) Quantitative analyses of starch content of the 21 DAS C24/L*er* seedlings grown under normal or doubled light intensity.** Starch content is presented as the equivalent amount of glucose. Data shown were the average and SE of three technical replicates from a pool of n=4-6 rosettes. **(c) The unit biomass starch turnover per night.** Each data was calculated by subtracting the average starch content at the end of the night from that at the end of the day. Asterisks indicate significant differences from the 120 µE-grown plants (ANOVA, $p < 0.001$).

4.9 Increased starch turnover under short daylength, doubled light

To see whether the unit biomass starch turnover in the 240 μmol photons m^{-2} s^{-1}-grown plants could be increased in longer nights, the C24/L*er* plants grown under either the standard or doubled irradiance under a light cycle of 8 hr/ 16 hr were analysed (**Figure 4.13**). Under 8hr of illumination at 120 μmol photons m^{-2} s^{-1}, the starch content of both the C24/L*er* reciprocal hybrids was similar to the best parent, C24 (over 4 μg/ mg FW), which was greater than in L*er* (2.5 μg/ mg FW) (**Figure 4.13a**). Starch content of the 240 μmol photons m^{-2} s^{-1}-grown plants was approximately twice that under 120 μmol photons m^{-2} s^{-1} (**Figure 4.13a**). Under 240 μmol photons m^{-2} s^{-1}, both the C24/L*er* reciprocal hybrids and the best parent L*er* contained a similar starch content (9-10 μg/ mg FW), while C24 contained slightly less starch (just over 6 μg/ mg FW) (**Figure 4.13a**). At both 120 μmol photons m^{-2} s^{-1} and 240 μmol photons m^{-2} s^{-1}, plants consumed > 80% of available starch. As a result, the 240 μmol photons m^{-2} s^{-1}-grown plants consumed a greater amount of starch than the 120 μmol photons m^{-2} s^{-1}-grown plants on a unit biomass basis (**Figure 4.13b**). Under both light intensities, the C24/L*er* reciprocal hybrids had a starch consumption no greater than the best parent on a unit biomass basis (**Figure 4.13b**).

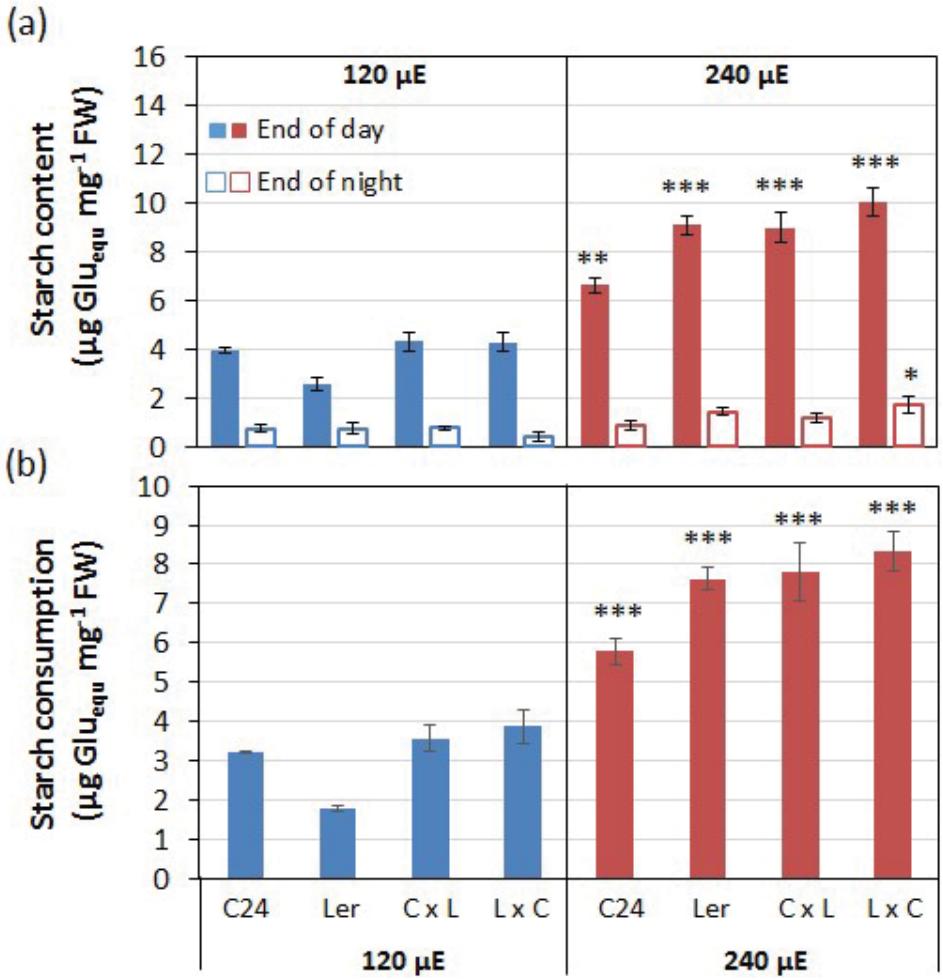

Figure 4.13. (a) Quantitative analyses of starch contents in the 40 DAS, short-day-grown C24/L*er* hybrid and parent plants under control (120 µmol photons m^{-2} s^{-1}) and doubled (240 µmol photons m^{-2} s^{-1}) growth irradiance. Starch content is presented as the equivalent amount of glucose. Data shown were the average and SE of three technical replicates of a pool of n=2-3 rosettes harvested at the end of the day (one hour before lights off) and the end of night (one hour before lights on). **(b) Starch turnover under different light regimes.** The unit biomass starch consumption was calculated by subtracting the average starch content at the end of the night from that at the end of the day. Asterisks indicate significant differences from the standard light conditions (ANOVA; *: $p < 0.05$, **: $p < 0.01$, ***: $p < 0.001$).C x L: C24 x L*er*; L x C: L*er* x C24; µE: µmol photons m^{-2} s^{-1}.

4.10 Heterosis in short daylength

To investigate whether increasing starch utilisation could affect heterosis in biomass, the C24/L*er* seedlings were grown under doubled irradiance in longer nights i.e. shorter days (light cycle 8 hr/ 16 hr). The rosette fresh weights of the short-day-grown plants were determined at 5 weeks after sowing, when they were at a comparable developmental stage as the 3 week-old long-day plants i.e. before L*er* flowering time.

The biomass heterosis in the 240 µmol photons m^{-2} s^{-1}-grown hybrids was greater than that under 120 µmol photons m^{-2} s^{-1} (**Figure 4.14**). The plants grown under doubled irradiance in short days had larger leaves and more compact rosettes than those under standard light, similar to the morphology observed under long daylength (**Figure 4.14a**). As measured by rosette biomass, the 33 DAS 120 µmol photons m^{-2} s^{-1}-grown C24 x L*er* hybrid showed 48% heterosis while the reciprocal hybrid L*er* x C24 showed no heterosis compared with the average of the parents (**Figure 4.14b**). Under 240 µmol photons m^{-2} s^{-1}, parent biomass was more than 3 times greater than that under 120 µmol photons m^{-2} s^{-1} while hybrid biomass increased more than 4.5 times (**Figure 4.13b**). As a result, heterosis in the 240 µmol photons m^{-2} s^{-1}-grown hybrids was greater than that under 120 µmol photons m^{-2} s^{-1}; C24 x L*er* and L*er* x C24 were 91% and 48% greater than the average of the parents respectively (**Figure 4.14c**).

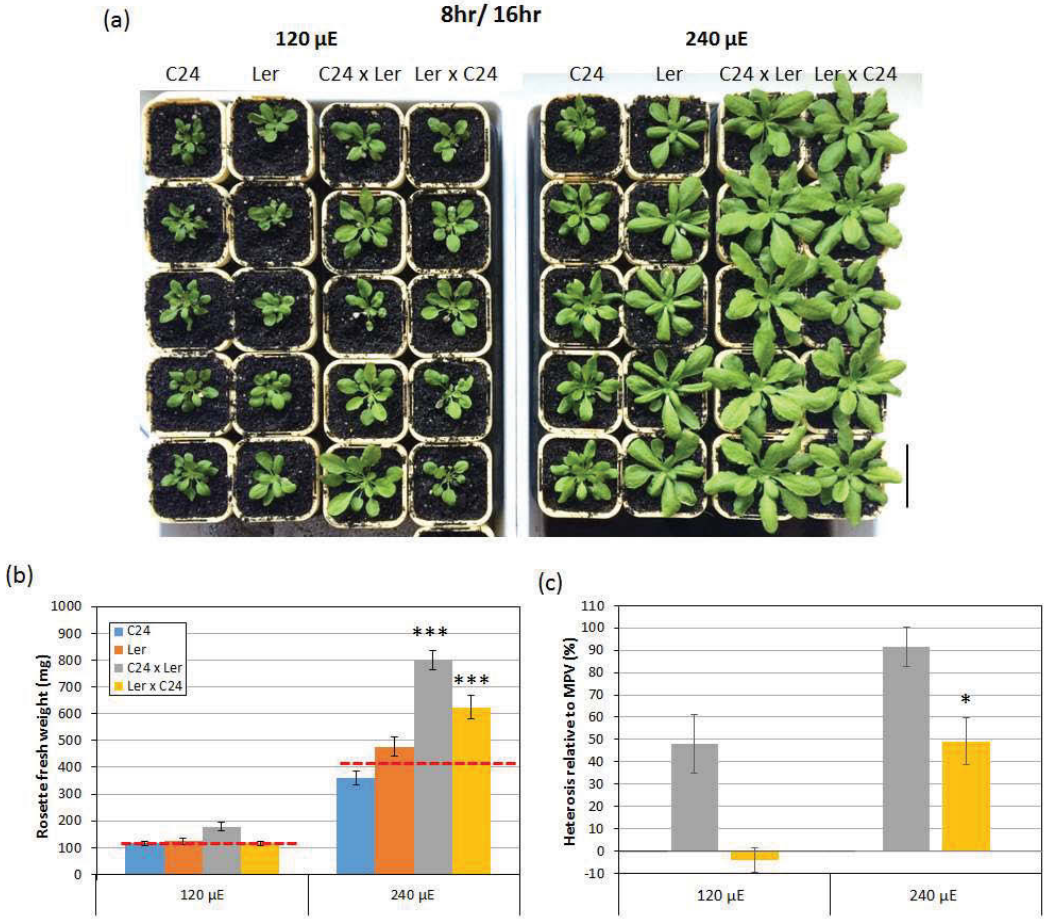

Figure 4.14. Morphology of the C24/L*er* hybrid plants that were grown under a light cycle of 8 hr-light/ 16 hr-dark, under either the standard or doubled light level. (a) A representative image of 5 week-old plants (scale bar: 5 cm). The seedlings were sown and grown on Murashige and Skoog medium (3% sucrose) until transplantation at 10 DAS. Half of the population was randomly selected and transferred to 240 µmol photons m^{-2} s^{-1} while the rest were kept under 120 µmol photons m^{-2} s^{-1}. **(b) Comparison of biomass between the 33 DAS hybrids and parents.** Asterisks indicate significant difference from the average level of the parents (ANOVA; ***: $p < 0.001$). The levels of heterosis relative to the mid-parent value (red dashed line) is shown in **(c)**. Asterisk indicates significant difference from the standard light (ANOVA; *: $p < 0.05$). Data presented are the average and SE of n>15 seedlings collected from 3 experiments. µE: µmol photons m^{-2} s^{-1}.

4.11 Discussion

4.11.1 Photosynthetic properties of parents and hybrids under high growth irradiance

Plants grown under different light regimes make adjustments in photosynthetic properties in response to the growth environment (Boardman, 1977, Bjorkman, 1981, Poorter et al., 2013). In this chapter I showed that the rates of CO_2 assimilation in the plants grown under high irradiance were greater than those under standard light level (**Figure 4.8**). The increased CO_2 assimilation rate may be related to increased leaf thickness (**Figure 4.6**). In studies of sun and shade leaves, it is well documented that the unit leaf area photosynthetic capacity is greater in the sun compared to the shade leaves (Boardman, 1977, Bjorkman, 1981, Terashima et al., 2006). Increased unit leaf area photosynthetic capacity was also found in *Arabidopsis* plants shifted from a moderate (100 µmol photons m^{-2} s^{-1}) to high (400 µmol photons m^{-2} s^{-1}) light conditions although the photosynthetic capacity after the shift was never as high as those that were kept under high light from sowing (Athanasiou et al., 2010). Thicker leaves enable optimisation of the arrangement of chloroplasts in mesophyll cells to maximize the surface area of chloroplasts facing the intercellular air spaces to increase CO_2 diffusion to chloroplasts (Terashima et al., 2011). Although the CO_2 assimilation rate was higher in the plants acclimated to high irradiance, the biochemistry parameters of photosynthesis, V_{cmax} and J, were not altered in response to the growth irradiance (**Figure 4.9**). This increase in the unit area CO_2 assimilation rate may be a result of thicker leaves under high irradiance (**Figure 4.6**) enabling a greater conductance of CO_2 in the surrounding air into the leaf tissue (**Figure 4.10**), rather than alteration of the operational capacity of the photosynthetic pathway.

I have shown that hybrids and parents have a similar response to increasing growth irradiance. Under a growth irradiance double the standard level, hybrids had a similar leaf thickness (**Figure 4.6**), photosynthetic capacity per unit leaf area (**Figure 4.9**), unit biomass chlorophyll content (**Figure 4.11**) and unit biomass starch turnover as the parents (**Figure 4.12**). This indicates that the photosynthetic processes in hybrids and parents were not differentially altered under high growth irradiance.

4.11.2 Increasing light promotes leaf production in both hybrids and parents

Light plays an important role in mediating leaf initiation from the shoot meristem via photoreceptors and hormone networks involving cytokinin and auxin (Yoshida et al., 2011). Changing light intensities directly affects photosynthetic efficiency and the abundance of carbohydrate in the shoot apices has been reported to correlate with leaf initiation rate in cucumber and tomato seedlings under different light regimes (Savvides et al., 2014). The number of leaves per plant was greater when the growth irradiance was double the standard level (**Figure 4.2**). The increased leaf production under high irradiance might be due to more CO_2 being assimilated (**Figure 4.9**) and, therefore, more photosynthate was produced (**Figure 4.12**) for growth. When the growth irradiance was double the standard level, hybrid plants had more leaves compared to the parents (**Figure 4.2**), similar to the observations in the standard light (**Figure 4.2**). These results suggest hybrids may have an increased allocation of carbohydrates to the meristem compared to the parents, probably because the photosynthetic area in hybrids was greater than that of the parents and therefore more photosynthates were made on per plant basis.

4.11.3 Transient effect of doubled-light on hybrid leaf growth

All the doubled-light grown plants had an increased leaf size compared to those under the control level of light. Light plays an important role in mediating both cell expansion and cell division (Okello et al., 2016). It has been reported in tobacco that alterations of final leaf size under high light intensities is correlated with an increased cell number (Granier et al., 2000). In hybrid seedlings, the actively developing leaves at the time of analysis showed increased heterosis levels under doubled-light. This differential response to doubled-light is a transient phenomenon since no significant changes in heterosis levels were found in the other leaves of the same hybrid plant that were at either an earlier or later stage of leaf development. Leaf growth is a complex coordination of cell division and cell expansion (Donnelly et al., 1999, Gonzalez et al., 2012). A further investigation of leaf anatomy of the doubled-light-grown hybrids with transient increased heterosis levels will answer the question of how increased light level promotes hybrid leaf growth. It is not clear how significant is the transient effect on a few leaves on a whole-plant scale since the doubled-light grown hybrids showed no significant increase in heterosis levels compared to the normal light.

4.11.4 Heterosis levels and the correlation to starch contents

I have shown that plants grown under higher irradiance and longer daylength had greater starch content per unit leaf biomass at the end of the day. As shown by the quantitative analyses of starch content, the greatest starch content was found in the plants grown under 16 hr of 240 μmol photons m^{-2} s^{-1}, which was more than those under 16 hr of 120 μmol

photons m^{-2} s^{-1}, and more than those grown under 8hr of 120 µmol photons m^{-2} s^{-1} (**Figure 4.12a; Figure 4.13a**). These results indicate that the greater content of starch at the end of the day reflected more CO_2 being assimilated during the day, as the end-of-day starch content was positively correlated with the total amount of light energy that was available over the photoperiod i.e. photon flux density per unit time multiplied by the daylength; designated as photon dosage (**Table 4.1**). Factors other than photon dose affect starch biosynthetic efficiency. The 8 hr/240 µmol photons m^{-2} s^{-1}-grown plants had a greater starch content than those under 16 hr/120 µmol photons m^{-2} s^{-1} (**Figure 4.2; Figure 4.4**) despite having the same daily photon dosage (**Table 4.1**). This was probably due to an increased partitioning of assimilated CO_2 into starch production under the shorter daylength (Gibon et al., 2009).

Table 4.2. Comparison of daily photon dosage between different light regimes.

Photoperiod (light/ dark)	Photon flux (µmol m^{-2} s^{-1})	Daily photon dosage (Ratio to long-day; 120 µmol m^{-2} s^{-1})
Short-day (8 hr/ 16 hr)	120	0.5
	240	1
Long-day (16 hr/ 8 hr)	120	
	240	2

Although elevating photon dosage increased starch content at the end of the day it did not increase starch turnover. As shown in the plants grown under the 16 hr/ 240 µmol photons m^{-2} s^{-1} light regime, the starch turnover per unit leaf area was the same as that under 16 hr/ 120 µmol photons m^{-2} s^{-1} due to more starch remaining at the end of the night (**Figure 4.12**). The incomplete starch mobilisation was probably due to the supply of assimilated carbon exceeding its use for growth and respiration at night, as shown in plants grown under very high irradiance (Hadrich et al., 2012) or in very long days (Sulpice et al., 2014).

Incomplete starch mobilisation is partly due to feedback inhibition mediated by the sugar-sensing mechanism that starch degradation is down-regulated when the content of trehalose 6-phosphate in the leaf is high (Martins et al., 2013, Lunn et al., 2014). Other regulatory mechanisms must exist to limit accumulation of starch to prevent disruption of chloroplasts by huge starch granules, as shown by the *starch excess* mutants that have defects in starch breakdown but have functional chloroplasts and a mild growth phenotype except for excessive starch storage (Streb and Zeeman, 2012).

To investigate whether biomass heterosis can be increased by elevating starch turnover, the C24/L*er* hybrids and parents were grown under longer nights (short days). Under a light cycle of 8 hr/ 16 hr, both the120 µmol photons m^{-2} s^{-1} and 240 µmol photons m^{-2} s^{-1}-grown plants had low levels of starch content at the end of the night (**Figure 4.13**), indicating more of the accumulated starch can be remobilized under the extended dark period. Starch turnover per unit leaf biomass for the 8 hr/240 µmol photons m^{-2} s^{-1}-grown plants was the greatest amongst all light regimes tested (**Figure 4.13**). However, the unit biomass starch turnover in the hybrids were not greater than the better parent in all light regimes tested (**Figure 4.12, Figure 4.13**). Although starch turnover in hybrids and the parents was the same on per biomass basis, biomass heterosis was increased in 8 hr/ 240 µmol photons m^{-2} s^{-1} (**Figure 4.14**). The coincidence of increased starch turnover per unit biomass and greater biomass heterosis suggests that hybrids contribute more starch into biomass compared to the parents.

Starch is a major carbon source for growth and respiration at night. Whereas the end-of-the-day starch content is similar between *Arabidopsis* ecotypes, the end-of-the-night

starch content is inversely correlated with plant biomass (Cross et al., 2006, Sulpice et al., 2010). This indicates that the more starch being used at night the greater the growth. This is not the case for biomass heterosis, as hybrids have the same unit biomass starch contents and the same unit biomass starch turnover as the parents (**Figure 4.12, Figure 4.13**). This is not consistent with previous reports that show C24/L*er* and C24/Col hybrids have greater end-of-the-day starch content than that of the parents on per unit biomass basis (Ni et al., 2009b, Ng et al., 2014). The authors claimed that biomass heterosis is associated with the greater starch content. However, those studies did not show whether the hybrids have lower end-of-the-night starch contents. This is important for determining whether the starch turnover was greater in the hybrids grown under their conditions.

I have shown that heterosis in biomass can be elevated by increasing starch turnover at night (as discussed above). In *Arabidopsis*, the growth rate changes diurnally. As shown by measurements of leaf expansion, the growth rate peaks at the beginning of the day while moderate growth was observed during the rest of the day (Wiese et al., 2007). In general, the relative growth rate is faster in the day than in the night (Wiese et al., 2007, Poiré et al., 2010). I could not determine whether the differential growth in hybrids occurs only at night. As well as starch, sucrose synthesis under doubled irradiance must have been increased. It can not be excluded that the increased heterosis under doubled-irradiance, short photoperiods may be attributable to the increased sucrose production during the day. The daily growth patterns of hybrids in doubled irradiance, short days could be compared to that under the standard condition; an automated time-lapse rosette imaging technology could be used to document growth curves with high resolution (Vanhaeren et al., 2015).

4.12 Summary

Under long days, doubling the growth irradiance increased plant biomass by two fold, but did not increase the level of heterosis. Under short days, hybrids showed an increased heterosis under doubled light intensity. The greatest starch turnover rate was found in plants grown under doubled irradiance in short daylength. Under all light regimes tested, hybrids showed a starch turnover similar to the best parent on a unit biomass basis.

To investigate the correlation between hybrid vigour and photosynthesis C24/L*er* seedlings grown under either control or doubled-light conditions were analysed for a number of morphological traits and photosynthetic properties. Increasing light increased both parents and hybrid leaf growth, particularly in the newly developing leaves. There was no significant increase in the overall heterosis level when the biomass of the entire rosette was measured as high light only affected a few leaves at a time during development. Under doubled light, both parent and hybrid seedlings showed similar alterations in development, including increased leaf production; increased leaf thickness due to an increased volume of mesophyll cells and a slight reduction in chlorophyll content on a unit leaf biomass basis. No significant difference in the unit leaf area photosynthetic capacity was found between the hybrids and parents grown under doubled irradiance.

5 Chapter V Alterations in hybrid vigour of *Arabidopsis thaliana* hybrids with limited photosynthesis in cotyledons

5.1 Introduction: early establishment of hybrid vigour in the cotyledon stage of seedling development

Arabidopsis thaliana hybrid seedlings show increased biomass relative to their parents as early as the cotyledon stage of the germinating seedlings (Meyer et al., 2004). An up-regulation of expression of genes encoding processes involved in photosynthesis in hybrid cotyledons has been reported at this time of seedling development, suggesting that cotyledons may be an early stage of photosynthate production that contribute to later heterosis (Fujimoto et al., 2012, Zhu et al., 2016). A similar occurrence of early vigour has been reported in the F1 hybrids of *Brassica rapa* (Chinese cabbage) (Saeki et al., 2016). Like *Arabidopsis* hybrids, *Brassica rapa* hybrids have substantial heterosis in growth from early to late-vegetative stage, greater yield and up-regulation of photosynthetic genes in young seedlings (Saeki et al., 2016). In this chapter, the contribution to hybrid vigour of photosynthesis in cotyledons compared to photosynthesis in leaves is examined.

5.2 Experimental design

Two approaches to limit photosynthesis in cotyledons are described: (1) the use of a mutant which has impaired chloroplast biogenesis in cotyledons but not in leaves allowing the assessment of the level of heterosis of hybrids carrying the mutation relative to the wildtype; and (2) growing seedlings under low light intensity, close to the compensation point of photosynthesis, to assess any alteration in heterosis level. The aim of these experiments was to determine whether limiting photosynthesis in cotyledons affects subsequent hybrid vigour.

5.2.1 Cotyledon-specific mutant

Chloroplasts and other functional plastids are derived from proplastids (Jarvis and Lopez-Juez, 2013). The chloroplasts of cotyledons are derived from etioplasts (**Figure 5.1**) (Jarvis and Lopez-Juez, 2013). Etioplasts are chloroplast progenitors that, once illuminated, differentiate into chloroplasts (Jarvis and Lopez-Juez, 2013). In true leaves, chloroplast biogenesis does not proceed via etioplasts under the normal light-dark cycles (Jarvis and Lopez-Juez, 2013). The difference in chloroplast biogenesis between cotyledons and true leaves is demonstrated by the identification of mutants with disrupted chloroplast biogenesis in cotyledons without affecting leaf chloroplasts: *white cotyledon*, *sigma factors2, sigma factors6* and *delayed greening1* have impaired chloroplast gene transcription in cotyledons (Ishizaki et al., 2005, Privat et al., 2003, Yamamoto et al., 2000); *sco1* (*snowy cotyledon1*) has impaired chloroplast protein translation (Albrecht et al., 2006, Ruppel and Hangarter, 2007) and *cyo1* (shi-yo-u, Japanese word for cotyledon), also known as *sco2* (*snowy cotyledon2)*, has impaired thylakoid membrane assembly (Albrecht et al., 2008, Shimada et al., 2007, Tanz et al., 2012). These cotyledon-specific

mutants all exhibit a similar phenotype of albino or pale cotyledons and green true leaves (**Figure 5.2**).

The aim of this experiment was to investigate the effect of lack of photosynthesis, or of reduced photosynthesis, in the cotyledon stage on hybrid vigour by exploiting mutant hybrids with white cotyledons. As the C24/L*er* hybrid was used in most of the experiments, I searched for mutants in both C24 and L*er* backgrounds. No mutant lines were available in a C24 background in the stock centre, but *sco2* was available in a L*er* background and *cyo1* in a Ws background. Here, *cyo1* was crossed to its allelic mutant *sco2* to generate Ws/L*er* hybrids with impaired chloroplast biogenesis in cotyledons. Both *cyo1* and *sco2* carry a mutation in the same locus in chromosome 3 (gene ID At3g19220). The *cyo1* mutant in Ws has a T-DNA insertion in exon 1 at position 19 bp after the predicted transcription start site (Shimada et al., 2007). The *sco2* mutant was identified from an ethyl methanesulfonate mutagenized T1 population of L*er* (Albrecht et al., 2008). The CYO1/SCO2 protein has protein disulfide isomerase activity that might be required for assembly of thylakoid membrane proteins, such as light-harvesting complex B1 (Albrecht et al., 2008, Shimada et al., 2007, Tanz et al., 2012). The two allelic lines are slightly different in phenotype: *cyo1* has albino cotyledons and needs to be grown on Murashige and Skoog medium with sucrose while *sco2* has pale green cotyledons that contain a small amount of chlorophyll (**Figure 2**) (Albrecht et al., 2008, Shimada et al., 2007). No thylakoid membrane structures were found in the small and abnormally shaped plastids in *cyo1* cotyledons (Shimada et al., 2007). In *sco2* cotyledons, etioplasts with large lipid-containing vesicles coexisted with a small number of normal chloroplasts (Tanz et al., 2012). Both allelic lines showed a reduction in growth (Albrecht et al., 2008, Shimada et al., 2007).

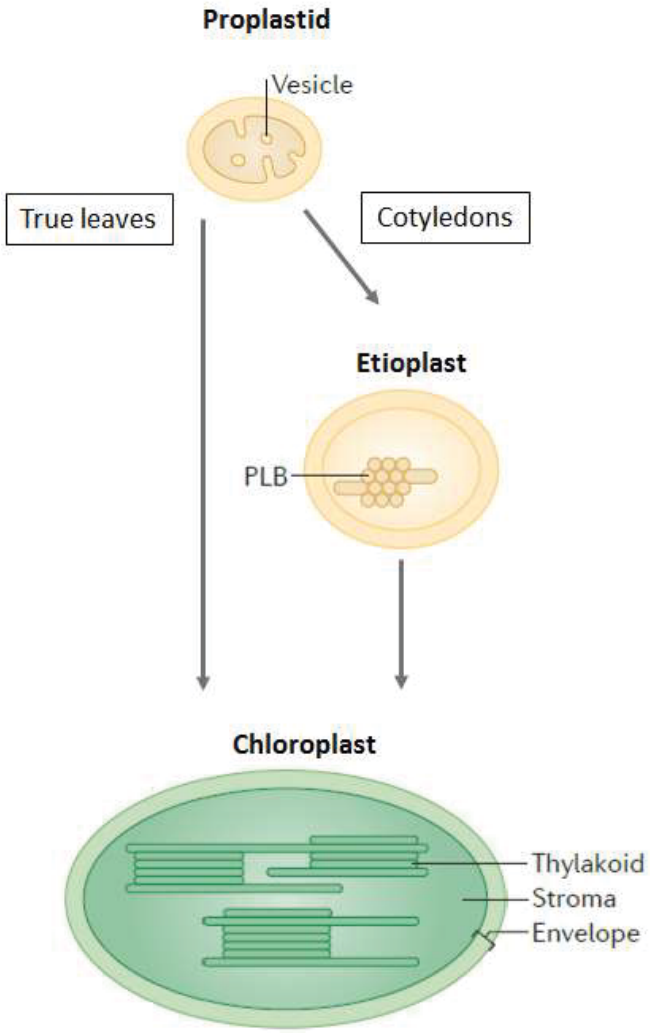

Figure 5.1. Distinct pathways of chloroplast biogenesis in cotyledons and true leaves. PLB: prolamellar bodies, paracrystalline membranous structures containing chlorophyll precursors. (Modified from Jarvis and Lopez-Juez (2013)).

Figure 5.2. The cotyledon-specific chloroplast biogenesis mutants. *snowy cotyledon2* mutant (*sco2*) and wild type L*er* are shown in the top row (images taken from Albrecht et al. (2008)); the allelic *cyo1* mutant and wild type Ws are shown in the bottom row (images taken from Shimada et al. (2007)).

5.2.2 Low light experiment

To investigate the role of cotyledon photosynthesis on hybrid vigour C24/L*er* hybrid seedlings were germinated and grown on Murashige and Skoog medium either with or without sucrose at a low light intensity (30 µmol photons m^{-2} s^{-1}) during the cotyledon stage (0-7 DAS). As the low light level is close to the compensation point of photosynthesis in *Arabidopsis*, it is expected to reduce photosynthesis in cotyledons. Following the period in low light the plants were grown in a control level of light (120 µmol photons m^{-2} s^{-1}) until 21 DAS (**Figure 5.3**). In comparison, seedlings were germinated under the control level of light then shifted to low light in the second week of growth (7-14 DAS); some plants were kept under low light from germination to 14 DAS (**Figure 5.3**). All plants were moved to normal light intensities at 14 DAS and harvested at 21 DAS. To examine changes in seedling growth in a non-destructive way, the rosette area of seedlings was measured. Heterosis in rosette area and biomass under the different light regimes were assessed.

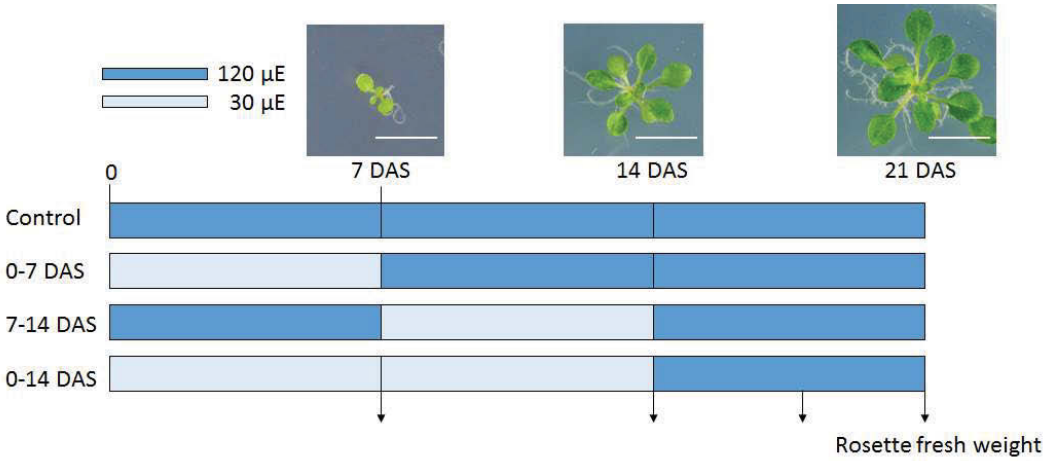

Figure 5.3. Schematic illustration of light regimes used in low light experiment. The C24/L*er* seedlings were germinated and grown under either control light or low light (pale blue shaded) for 7 days. Half of the population were randomly selected and moved to the opposite light condition for another 7 days. All plants were then moves back to control light until 21 DAS. Images of seedlings were taken at different time points (indicated by arrows) for the determination of rosette area using ImageJ. The 21 DAS seedlings were harvested and determined for rosette fresh weights. For each light regime tested, seedlings were grown on Murashige and Skoog growth medium either with or without 3% sucrose in 200 mm diameter petri dish. DAS: days after sowing.

5.3 The validation of sco2 mutants

Two *sco2* lines, *sco2-1* and *sco2-2*, were selected by (Albrecht et al., 2008) and shown to have allelic mutations. Genomic DNA extracted from *sco2* and wildtype seedlings was sequenced using primer pairs complementary to the up-stream or down-stream regions flanking the *SCO2* locus. Four primer sets complementary to either the sense or anti-sense strand were designed to sequence the amplified DNA fragment from either the 3' or 5' regions (**Figure 5.4b**). By aligning the sequencing results of six *sco2* individuals to the wildtype using the sequence analysis software VectorNTI (Thermo Fisher scientific), a cytosine-to-thymine substitution was found in the DNA sequence at position 167 bp after the predicted transcription start site (**Figure 5.4b**). The mutation would result in a shortened protein product as the single nucleic acid mutation is predicted to cause a substitution in the amino acid sequence at position 42, where arginine is replaced by a stop codon (**Figure 5.5**).

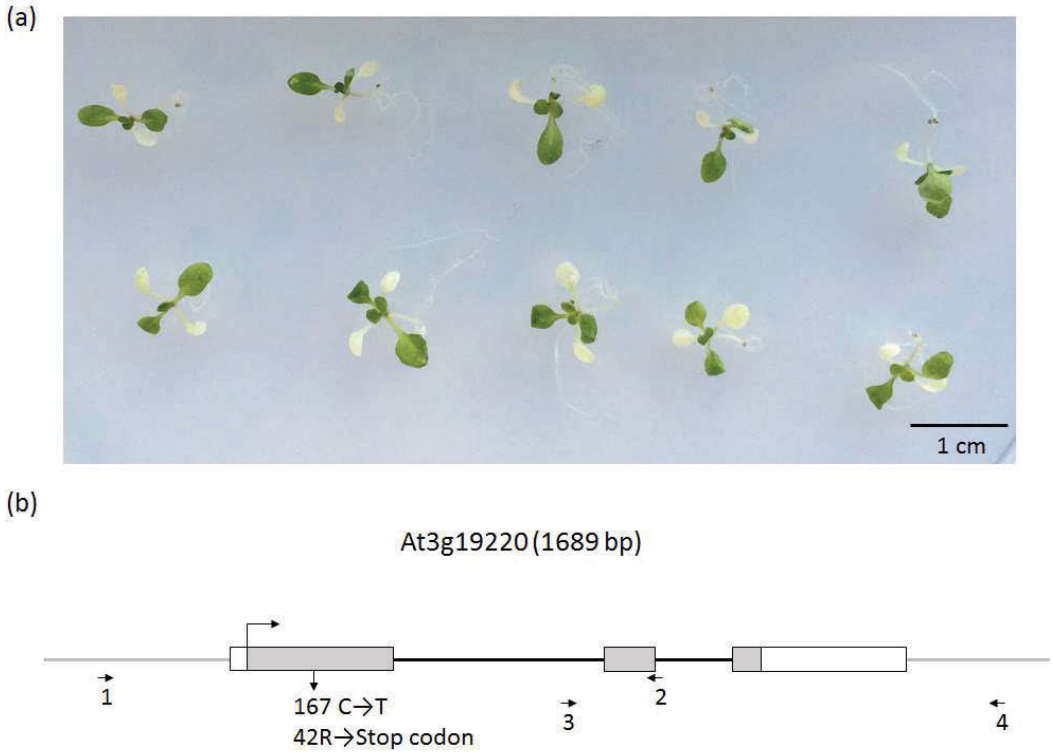

Figure 5.4. (a) Phenotype of the *sco2* mutant. The image was taken of 12 DAS seedlings grown on Murashige and Skoog medium (3% sucrose) under a light cycle of 16hr-light/ 8hr-dark at 21 ˚C in a controlled chamber. Six individual plants were selected randomly and genomic DNA extracted for sequencing. **(b) Schematic illustration of verification of single mutation in the *sco2* mutant.** Arrows indicate the position and direction of primers used for sequencing. The sequencing result showed the *sco2* line used in this experiment has a single nucleic acid substitution of cytosine to thymine at position 167 bp beyond the predicted transcriptional start site (indicated by an upwards arrow with tip rightwards). Prediction of the amino acid sequence suggests an arginine-to-stop codon substitution in the amino acid sequence at position 42. bp: base pair, C: cytosine; T: thymine, R: arginine.

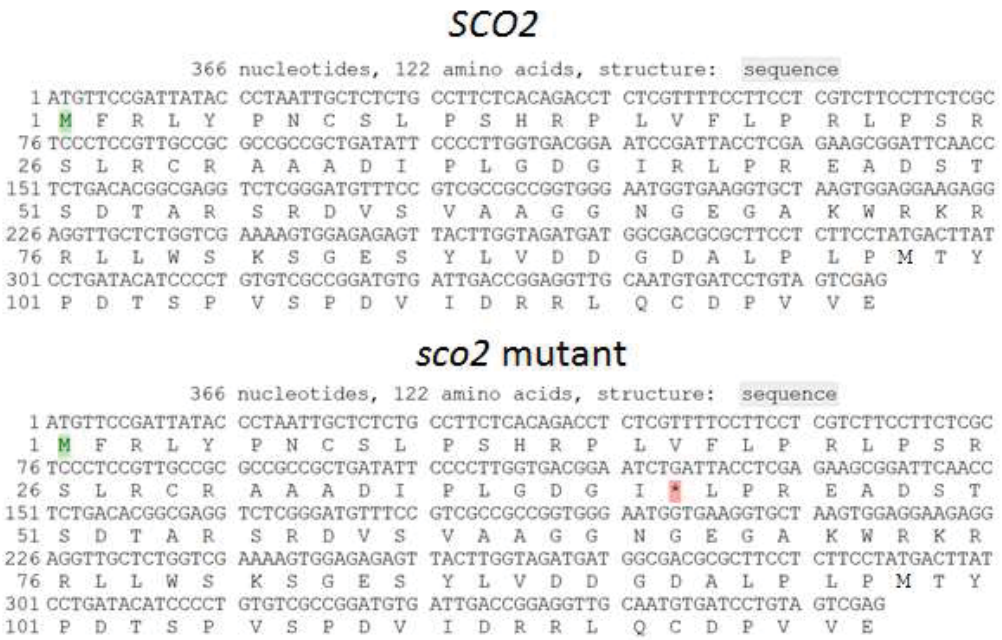

Figure 5.5. The predicted amino acid sequence of *sco2* mutant compared to the wildtype. The *sco2* mutants that had a C-to-T mutation at position 167 resulted in a R-to-stop codon substitution in the amino acid sequence at position 42 (indicated by red shading). The start amino acid (M; methionine) are shaded in green. (Translate, ExPASy, Swiss Institute of Bioinformatics).

5.4 Seed quality of *sco2*/*cyo1* hybrids

Arabidopsis embryos start turning green at the torpedo stage and stay green until shortly before the onset of mature seed dormancy (**Figure 5.6**). These green embryos have chloroplasts capable of photosynthesis, as shown in other oilseeds such as rapeseed and soybean; they operate mainly to refix respiratory carbon and generate metabolic intermediates and reductants for the biosynthesis of seed storage oils (Ruuska et al., 2004, King et al., 1998). It has been reported that mature embryos of *sco2* are green (Albrecht et al., 2008). Different stages of embryos of s*co2*, *cyo1* and both wildtypes were dissected from siliques and examined under a dissecting microscope. All mutant embryos examined showed a greening stage similar to that of the wildtype (**Figure 5.7**), indicating the mutation had no effect on chloroplast development in embryonic cotyledons. Seeds of both *sco2* and *cyo1* mutants were examined for changes in seed size and compared to wildtype. The mutant seeds were smaller than the wildtype, especially *sco2* (**Figure 5.8**).

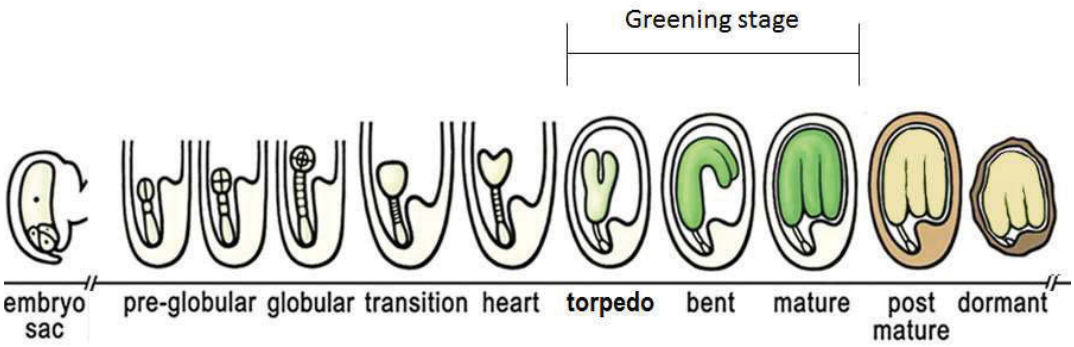

Figure 5.6. Schematic illustration of *Arabidopsis thaliana* seed development. Adapted from Le et al. (2010).

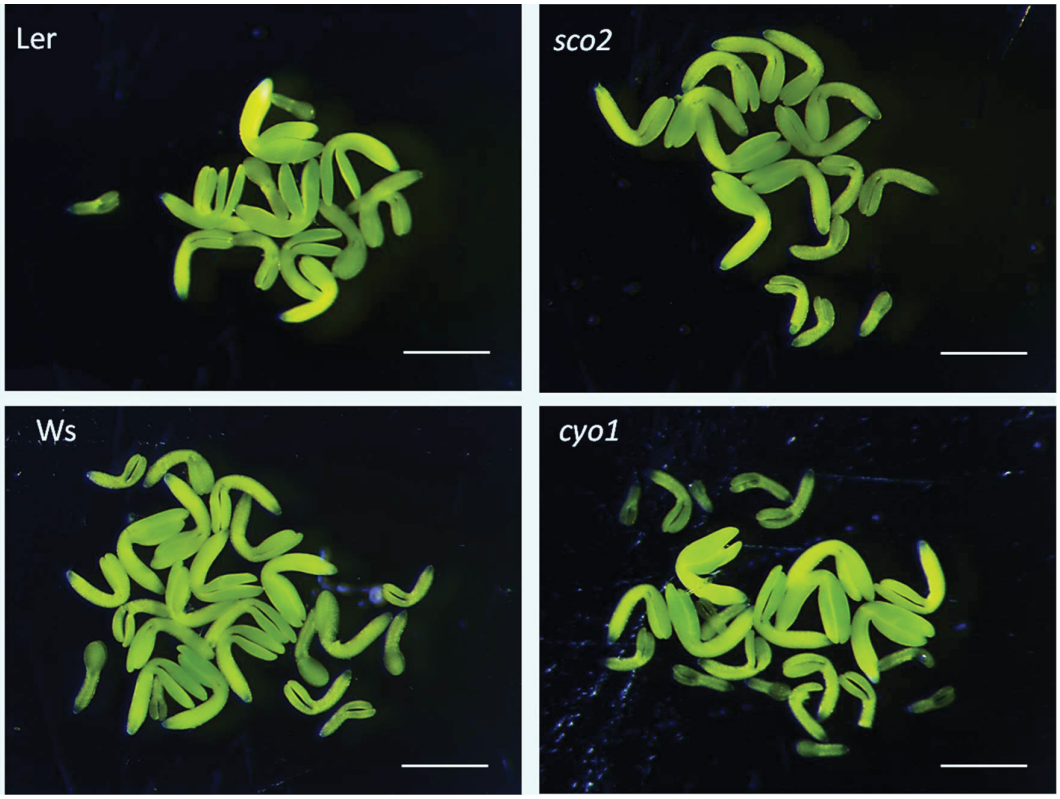

Figure 5.7. Developing embryos isolated from *sco2 and cyo1* mutants undergo a greening stage similar to wildtype. Scale bar represents 0.5 mm.

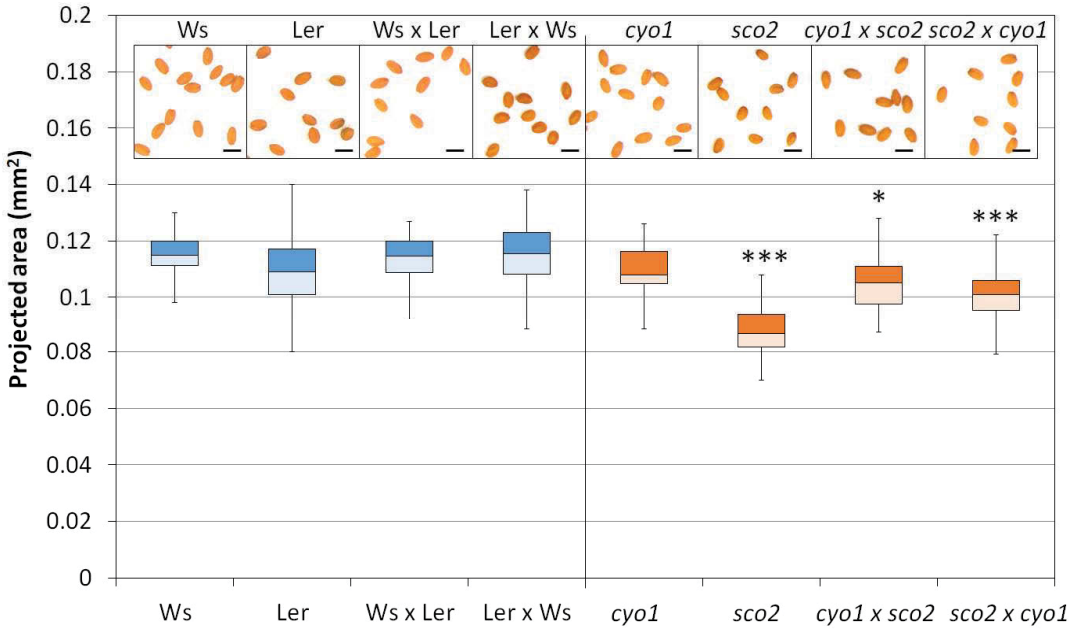

Figure 5.8. Comparisons of seed size between the hybrids and parents of *cyo1*/*sco2* and the wildtype Ws/L*er*. Images integrated above each column are the images of dry seeds taken under a dissecting scope (scale bar: 0.5 mm). The projecting area of seeds were determined as the seed size, using ImageJ. Data presented are the box plot of a population n > 30 seeds. The wildtypes are shown in blue while the mutants are shown in orange. The upper box (dark-shaded) represents the seed size of the third quartile (top 25-50% of the population) while the lower box (light shaded) represents the first quartile (lower 25-50% of the population). The line between two boxes indicates the median value of the population. The ends of the whisker represent the levels of 1.5 times of the interquartile range (third quartile – first quartile) above the third quartile and below the first quartile, respectively. Asterisks indicate significant differences between mutants and the wildtype (ANOVA; *: $p < 0.05$, ***: $p < 0.001$).

5.5 The *cyo1*/*sco2* hybrids had snowy cotyledon phenotypes

The *cyo1/sco2* hybrid seedlings were characterised by a white cotyledon phenotype similar to the homozygous parents (**Figure 5.9**) as expected since both *sco2* and *cyo1* mutations are located in the same gene. To confirm that chloroplast biogenesis in true leaves was not affected, the true leaves of the mutant seedlings were analysed for chlorophyll content and compared to wildtype. The chlorophyll content in the true leaves of both wildtype and mutant were the same, on an average ~1.2 µg chlorophyll per mg fresh weight with a chlorophyll a/ b ratio of 2.2-2.3 (**Figure 5.10**). This indicates that chloroplast biogenesis in true leaves was unaffected by the *sco2* mutation.

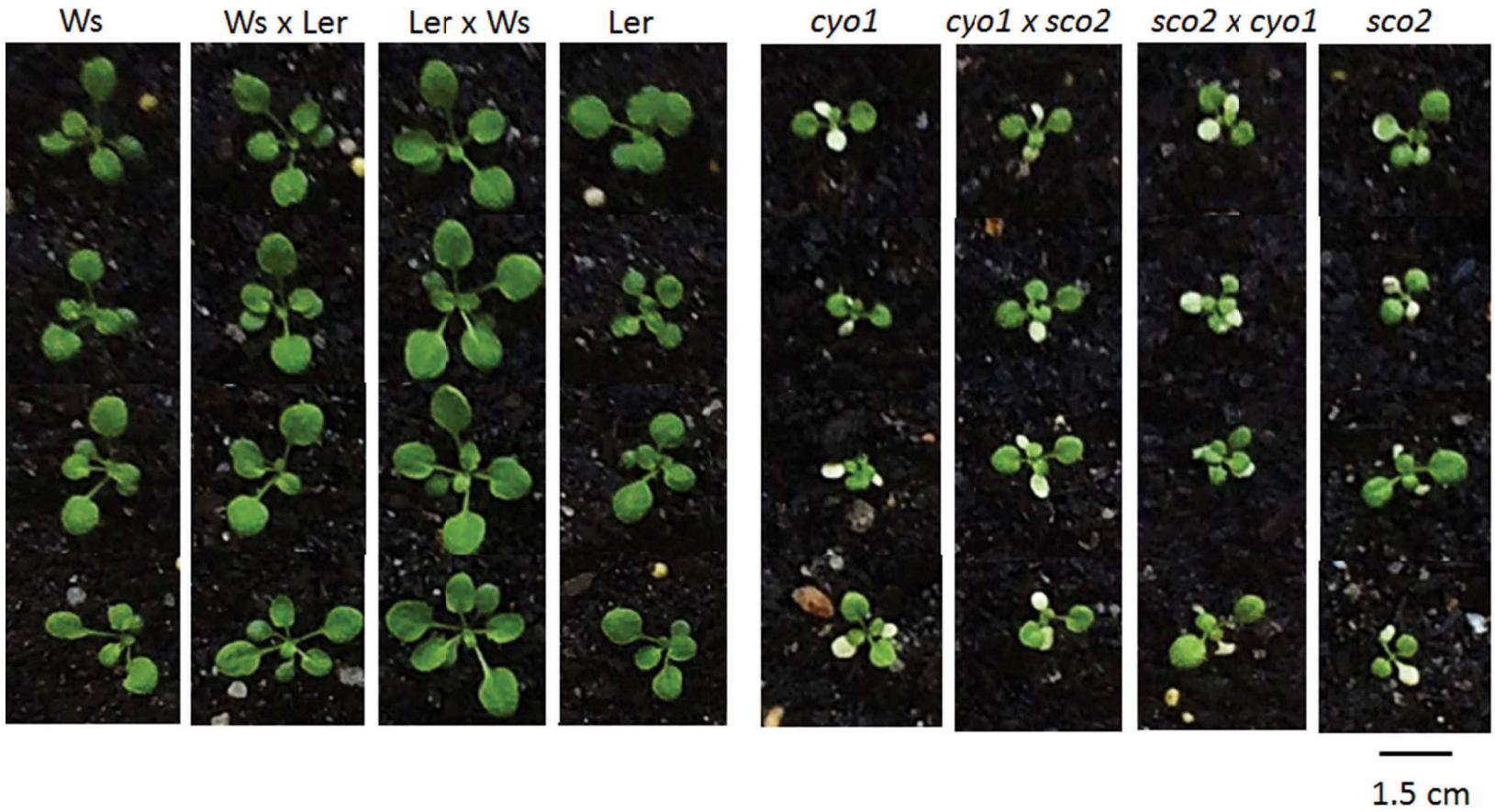

Figure 5.9. Phenotype of *cyo1/sco2* seedlings compared to the wildtype Ws/L*er*. Mutant seedlings have white cotyledons. The mutant seedlings were sown and grown on MS medium (3% sucrose) before transplanting into soil at 10 DAS. Images of seedlings were taken at 14 DAS. The images shown here are representivies of n = 15 plants.

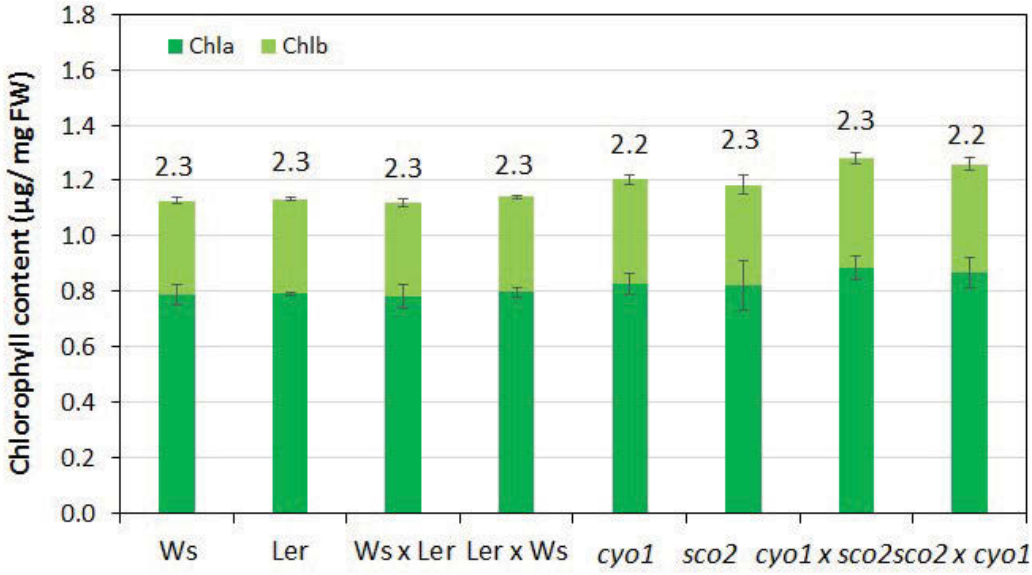

Figure 5.10. Comparison of chlorophyll content of the true leaves between the *cyo1/sco2* and wildtype seedlings. The 19 DAS seedlings were analysed. The cotyledons were removed from sample plants. Data shown were the average and SE of n=3 pools of five seedlings. The number above each column shows the chlorophyll a to b ratio. Chla: chlorophyll a; Chlb: chlorophyll b. Statistical comparisons between mutants and wildtype and no significant differences were found (ANOVA, $p > 0.05$).

5.6 The *cyo1*/*sco2* hybrids seedlings showed a substantial reduction in vigour

Heterosis levels of the 19 DAS Ws x L*er* and L*er* x Ws reciprocal hybrids were 27% and 55% respectively (**Figure 5.11**). Heterosis levels of the *snowy cotyledon* mutant hybrids were substantially reduced. Rosette biomass of wildtype parents and hybrids was on an average greater than 40 mg and 50-60 mg, respectively (**Figure 5.11**). Rosette biomass of the *cyo1/sco2* hybrids and parents was about 15 mg. Rosette biomass of the mutant hybrids was not significantly greater than that of the better parent *sco2*, despite showing a small level of heterosis compared with the average of the parents (**Figure 5.11**). This result showed that impaired chloroplast biogenesis in cotyledons reduced hybrid vigour in seedling growth.

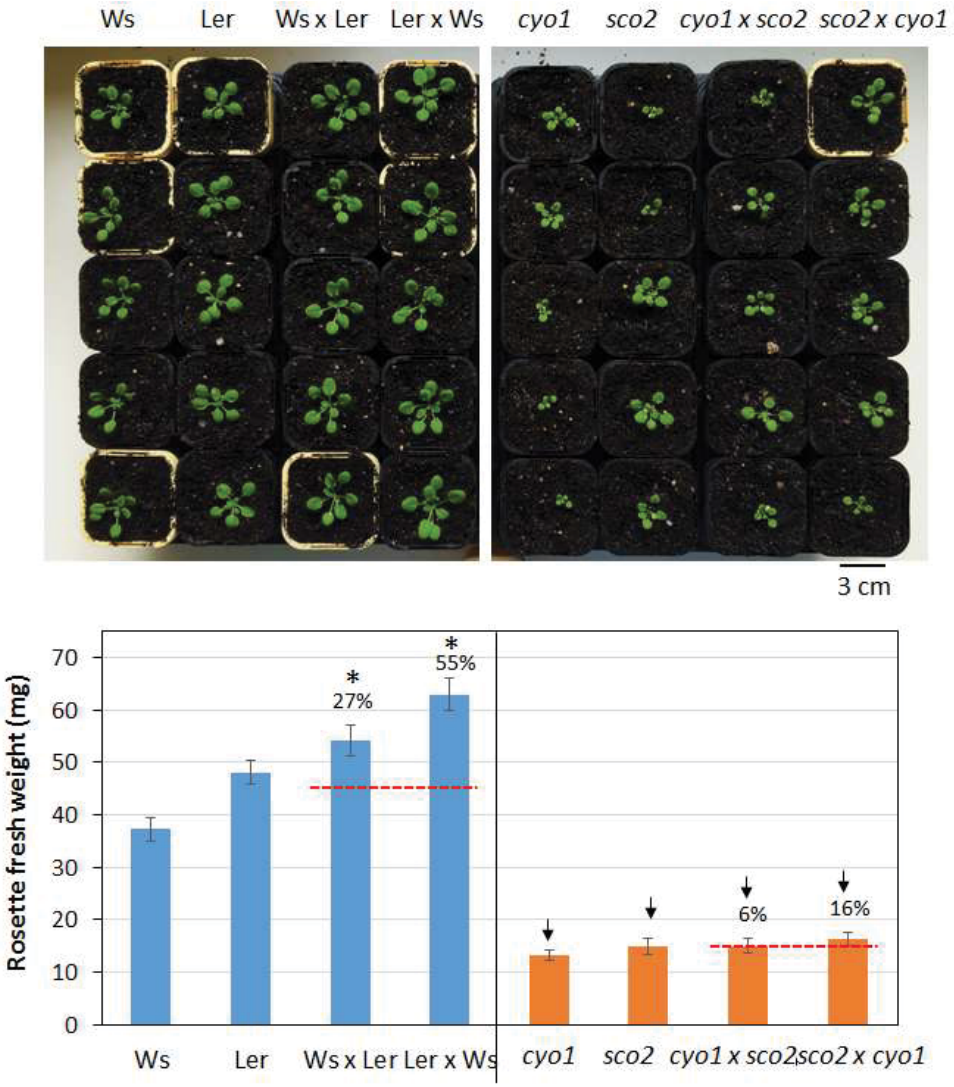

Figure 5.11. Comparisons of fresh weight between the hybrid and parent seedlings in the *snowy cotyledon* mutants (shown in orange) and wildtype (shown in blue). The top panel shows images of the eight genotypes. The seedlings analysed were sown and grown on Murashige and Skoog medium (3% sucrose) for 10 days before transplanting into soil. The soil-grown 19 DAS seedlings were harvested and the rosette fresh weights were determined. Data represent the average and SE of n=47-66 seedlings from four repeats (n ≥ 10 each). The number above each hybrid column represents the percentage of increase from the average of the corresponding parents (red dashed lines). Asterisks indicate significant differences from the average level of the parents (ANOVA, $p < 0.001$). Arrows indicate significant differences between mutants and the wildtype (ANOVA, $p < 0.001$).

5.7 Long-term effects of limited photosynthesis in cotyledons on hybrid vigour

Seedlings grown under low light were characterised by elongated hypocotyls, an increased petiole: leaf blade ratio (Vandenbussche et al., 2003) (**Figure 5.12)** and reduced seedling growth (**Figure 5.13, 5.14**). As measured by rosette area, a ~50% reduction in heterosis was found in the 14 DAS C24/L*er* hybrid plants that were grown under low light for one week, either from 0-7 DAS or from 7-14 DAS (**Figure 5.14**). No significant difference in rosette area was found between the 0-7 DAS and 7-14 DAS samples, but both were lower than the control-light grown plants (**Figure 5.14a**). A further reduction in rosette area was found in plants germinated and kept under low light for two weeks (0-14 DAS) (**Figure 5.14a**), where the lowest heterosis level was found (**Figure 5.14b**). After shifting back to normal light, the reduction in rosette area were not recovered in subsequent time points, showing the same levels of heterosis as observed in the 14 DAS plants (**Figure 5.14b**).

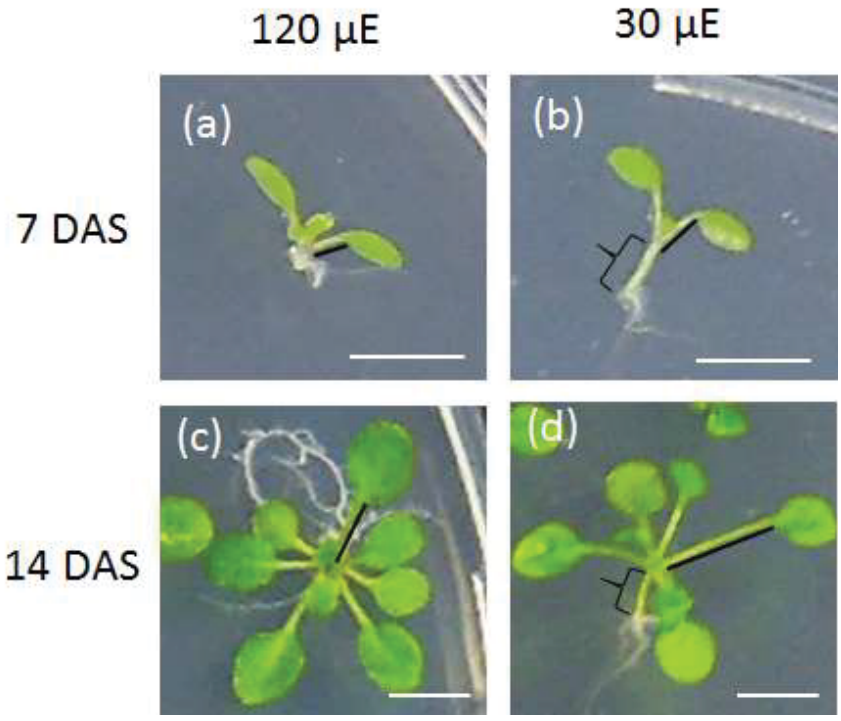

Figure 5.12. Seedlings subjected to low light (b)(d) developed elongated hypocotyls (as indicated by brackets) and petioles (indicated by bold lines). Under the scale the images were taken, the control seedlings **(a)(c)** had hypocotyls that were too short to be seen. Each image shown was a representative of n = 30 C24 seedlings grown on Murashige and Skoog medium in the presence of sucrose. Scale bar represents 5 mm.

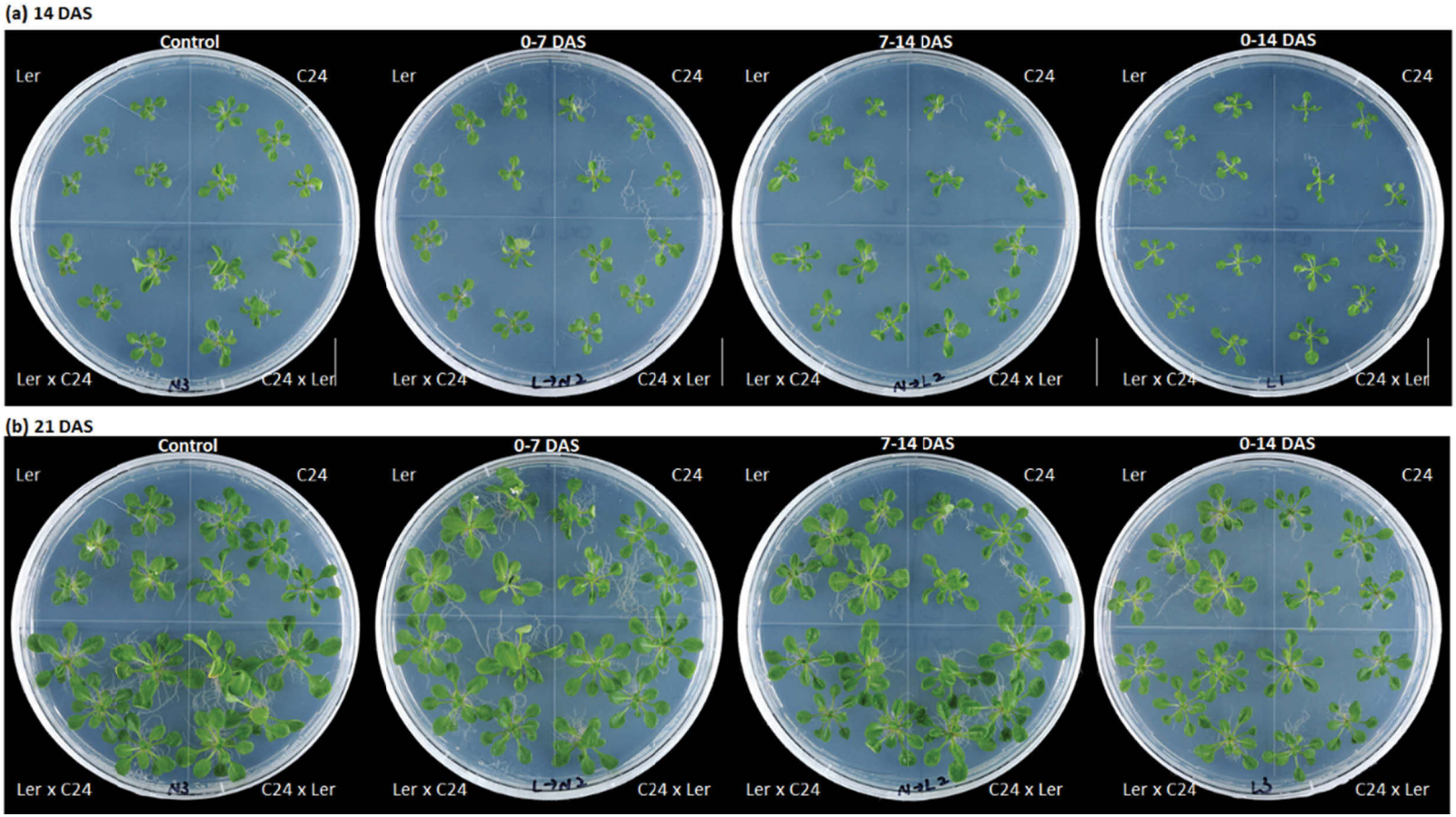

Figure 5.13. Images of the (a) 14 DAS and (b) 21 DAS C24/L*er* seedlings that were grown under low growth irradiance (30 µmol photons m^{-2} s^{-1}) at different times in seedling development. Seedlings were grown on Murashige and Skoog medium (3% sucrose). Each image shown was a representative of three to four replicates. Scale bar represents 2 cm. DAS: days after sowing.

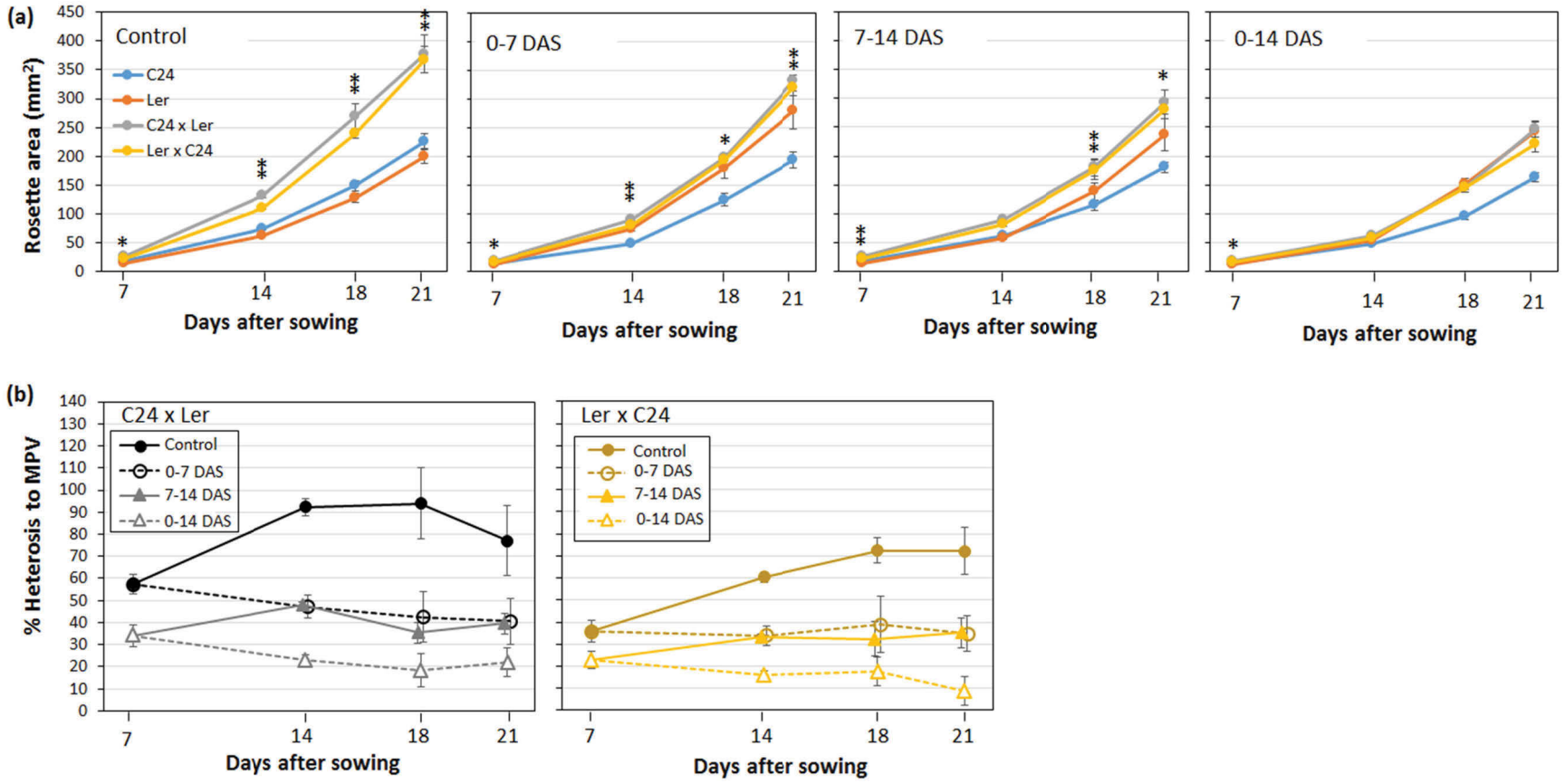

Figure 5.14. See the next page for legend.

Figure 5.14. (a) Rosette area of C24/L*er* seedlings that were grown under low growth irradiance (30 µmol photons m^{-2} s^{-1}) at different stages of seedling development. Plants were grown on Murashige and Skoog medium (3% sucrose) under control irradiance of 120 µmol photons m^{-2} s^{-1}, except for the indicated periods of time. Images of plates were taken at indicated time points and were used to determine the projected area of each rosette using ImageJ. Data presented are the average and SE of n = 7-15 seedlings. Asterisks indicate significant difference from the average level of the parents (ANOVA, $p < 0.01$). As the proximity of the data points, the asterisks for L*er* x C24 hybrid were vertically positioned, beneath those for C24 x L*er*. **(b) Changes of heterosis levels over time.** Heterosis levels were calculated from the percentage of increase relative to the average of parents. Solid or open circles indicate data collected from seedlings growing under control or low light, respectively. See **Appendices** for *p* values. Data points were dispersed to avoid overlapping. Solid lines DAS: days after sowing.

5.8 Long-term effects of limited photosynthesis in cotyledons on hybrid vigour

When sucrose was not added to the growth medium, seedling growth under low light was further reduced, especially in L*er* x C24 and L*er* parent, as shown by the fresh weight measurements of the 21 DAS plants (**Figure 5.15**, **Figure 5.16**). Rosette fresh weights of the 21 DAS plants grown in the absence of sucrose were about half of that in the presence of sucrose (**Figure 5.16a, b**). Heterosis levels of the 21 DAS C24 x L*er* hybrids under all light regimes tested and the control light-grown L*er* x C24 hybrid were comparable to the 14 DAS plants, regardless of the addition of sucrose in the growth medium (**Figure 5.16c, d**). The L*er* x C24 hybrid seedlings that had been grown under low light for one week showed no heterosis in rosette biomass, nor did those grown under low light for two weeks (**Figure 5.16d**).

These results showed that the C24/L*er* hybrids that were grown under low light were not able to regain vigour, even after they were shifted back to the control light for the majority of time in seedling development. The presence of exogenous sucrose was able to promote seedling growth, more so in L*er* x C24 and L*er* than the reciprocal hybrid and C24, but could not reverse the impact of low light on rosette growth or hybrid vigour.

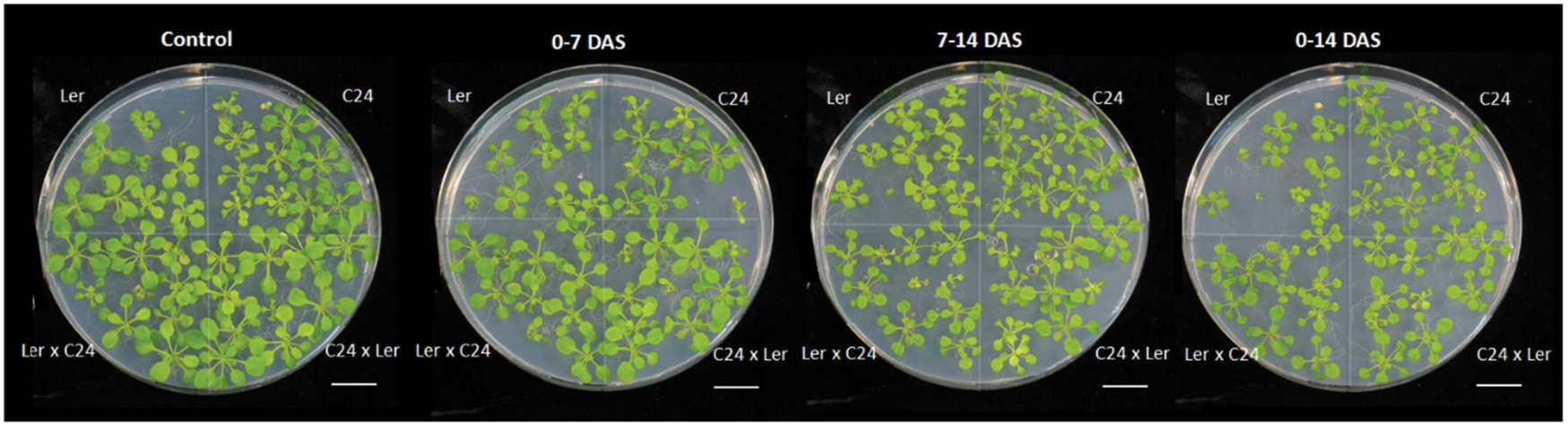

Figure 5.15. Images of the 21 DAS C24/L*er* seedlings that were grown in the absence of sucrose under low growth irradiance (30 µmol photons m^{-2} s^{-1}) at different times in seedling development. Seedlings were grown on Murashige and Skoog medium. Each image shown was a representative of three to four replicates. Scale bar represents 2 cm. DAS: days after sowing.

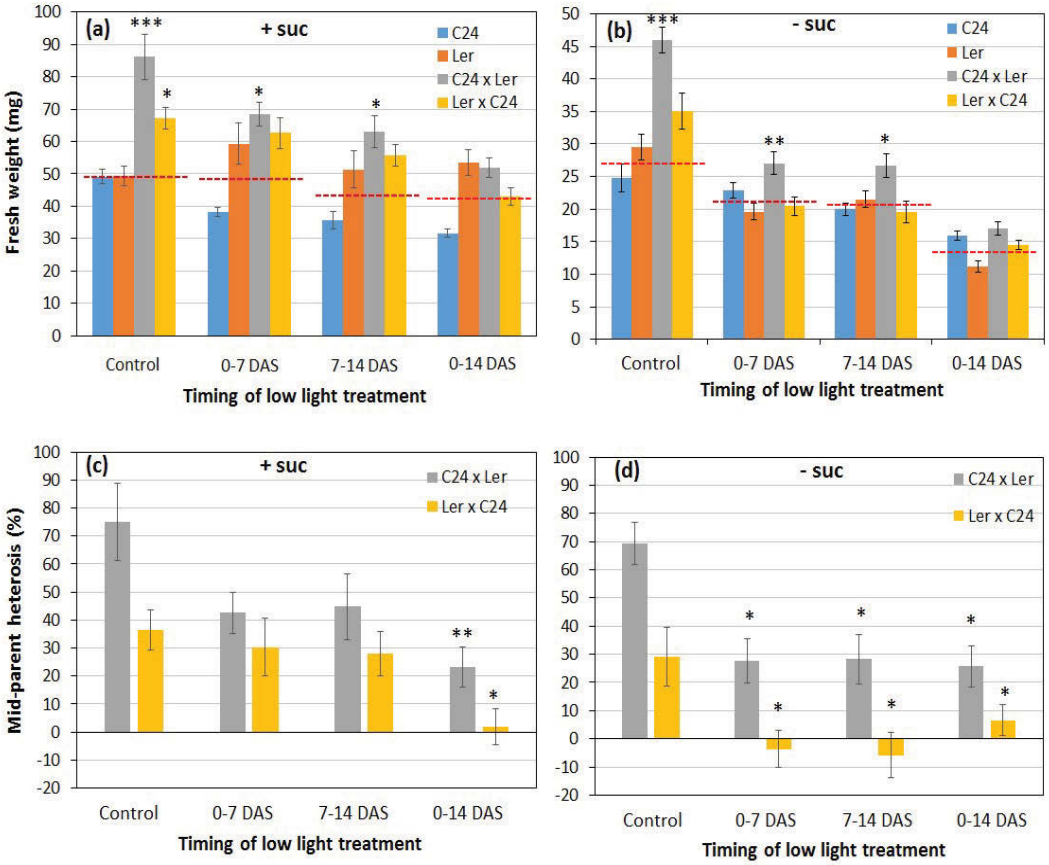

Figure 5.16. Comparisons of (a)(b) rosette fresh weight and (c)(d) heterosis levels between the 21 DAS C24/L*er* seedlings that were grown under low growth irradiance (30 µmol photons m^{-2} s^{-1}) at different stages of seedling development in the presence (a)(c) or absence (b)(d) of sucrose. All seedlings were grown on Murashige and Skoog medium under control irradiance of 120 µmol photons m^{-2} s^{-1}, except for the indicated periods of time. Data presented are the average and SE of n = 7-39 seedlings. Asterisks indicate significant differences from the average levels of the parents (ANOVA; *: $p < 0.05$, **: $p < 0.01$, ***: $p < 0.001$). Heterosis levels shown in **(b)(d)** were calculated from the percentage of increase in hybrid rosette size relative to the average of parents, as indicated by red dashed lines in **(a)(b).** Asterisks in **(b)(c)** indicate significant differences from the control (ANOVA; *: $p < 0.05$, **: $p < 0.01$). DAS: days after sowing; suc: sucrose.

5.9 Discussion

5.9.1 Plant growth and heterosis were reduced when photosynthesis during early seedling development was limited by insufficient light

Heterosis levels of the 21 DAS C24/L*er* hybrids germinated and grown under low light for one week were reduced to half that of continuous growth under control irradiance (summarised in **Figure 5.17**). The low irradiance was close to the compensation point of photosynthesis so very little photosynthesis occurred. Rosette biomass of the low light-grown plants was greater when sucrose was added to the growth medium (**Figure 5.17**). Nevertheless, the addition of sucrose into the growth medium was unable to restore heterosis under low light. These results indicate that photosynthetically derived sucrose is used to fuel plant growth, but heterotic growth is determined by factors in addition to the abundance of photosynthetic sucrose.

For a seed to develop into a photosynthetically competent seedling, early seedling development is fueled by the stored reserves in embryos. Metabolite analysis of 6 DAS C24/Col hybrid cotyledons showed a faster consumption of stored lipids and an increased accumulation of photosynthetically derived lipids relative to the parents (Meyer et al., 2012). Transcriptome analysis of C24/L*er* hybrid seedlings showed that the genes associated with lipid metabolism and photosynthesis, presumably genes for heterotrophic and photoautotrophic growth respectively, were down-regulated and up-regulated earlier than in the parents, respectively (Zhu et al., 2016). These findings suggest the developmental transition from heterotrophic to photoautotrophic growth in hybrid

seedlings is earlier than in the parents. Light is an important component in developmental transitions and alterations in light conditions affect plant growth through an elaborate light signalling network mediated by photoreceptors and light responsive hormones (Chaiwanon et al., 2016, Galvao and Fankhauser, 2015). Low irradiance might have affected heterotic growth by compromising the earlier seed-to-seedlings transition seen in hybrids. This could be determined by transcriptome analyses to see whether earlier changes in the transcriptome in hybrid seedling are compromised under low light.

5.9.2 Reduced hybrid vigour under low light might be attributable to an altered response to low light

The low light-grown seedlings were characterised by an altered leaf growth pattern (elongated petioles and smaller leaf blades), leading to reduced rosette size (**Figure 5.12**), which is in line with the shade avoidance syndrome reported in plants grown under low irradiance and/or low R (red light) to FR (far-red light) ratio (Chaiwanon et al., 2016). The latter is well-studied, as it is one of the key features of the light condition under natural canopy shading. Phytochrome B is the major photoreceptor for sensing low R: FR ratio (Galvao and Fankhauser, 2015). Phytochrome B mediates the shade avoidance mechanism by the activation of a transcription factor network including phytochrome interacting factors that induce biosynthesis of auxin, which promotes hypocotyl elongation and hyponastic growth (leaf movement to a more vertical orientation) (Casal, 2013, Chaiwanon et al., 2016).

Without changing light quality, low irradiance has been reported to induce hypocotyl elongation in *Arabidopsis* seedlings and petiole elongation and leaf inclination to a more vertical orientation (hyponasty) in adult plants (Hornitschek et al., 2012, Millenaar et al., 2009, Mullen et al., 2006, Vandenbussche et al., 2003). In tobacco, low light induces hyponasty and stem elongation (Pierik et al., 2004). Auxin signalling is involved in low irradiance-mediated shade avoidance, as auxin mutants showed severely attenuated hyponastic growth compared with wildtype in response to low irradiance, without changing the R:FR ratio (Vandenbussche et al., 2003). In various *Arabidopsis* hybrids, including C24/L*er*, genes involved in auxin biosynthesis and auxin responsive genes were up-regulated (Groszmann et al., 2015). It has not been verified whether *Arabidopsis* hybrids have a constitutively higher content of auxin or whether hybrids have an altered auxin response compared with the parents. The shade avoidance response might be stronger in hybrids than the parents, as suggested by the greater reduction in rosette area of low light-grown hybrids relative to the parents (**Figure 5.12**). This means that reduction in heterotic growth under low irradiance is attributable to an altered shade avoidance response, in addition to reduced resources due to reduced photosynthesis.

5.9.3 Is having photosynthetically competent cotyledons a prerequisite for hybrid vigour?

In the low light experiment, heterosis levels of the 21 DAS C24/L*er* hybrid plants that were grown under low light for one week, either at the cotyledon stage (first week) or true leaf stage (second week), were reduced to half of that under a control light regime (**Figure 5.17)**. It could not be ruled out that cotyledons also contribute to heterosis at the

first and second true leaf stage, as there is a period of time that cotyledons are still the main photosynthetic tissue in the rosette after the first pair of true leaves are formed. A further attenuation in heterosis levels was found in hybrids with white cotyledons, as seen in *sco2* mutants and by the application of photosynthetic inhibitors (summarised in **Figure 5.18**). These studies and others indicating that photosynthesis in the cotyledon stage is important for the generation of biomass heterosis.

Attenuated hybrid vigour has been reported previously in *Arabidopsi*s C24/Col hybrids treated with norflurazon at an early cotyledon stage (Fujimoto et al., 2012). Norflurazon is an inhibitor of phytoene desaturase in the carotenoid biosynthesis pathway (Breitenbach et al., 2001). A similar reduction in hybrid vigour has been reported in *Brassica rapa* hybrid seedlings when only the cotyledons were treated with norflurazon (Saeki et al., 2016). The treated *Brassica* seedlings were transferred to inhibitor-free conditions where subsequent true leaves reestablished chlorophyll biosynthesis, but hybrids were unable to regain vigour in growth (Saeki et al., 2016) (for detail, see **Figure 5.18**). I have shown a similar attenuation of hybrid vigour in *Arabidopsis* using *sco2* mutants that have impaired chloroplast biogenesis in cotyledons. The growth of the Ws/L*er* hybrids carrying *sco2*/*cyo1* mutant alleles that had white cotyledons with green true leaves were not greater than the homozygous mutant parents (**Figure 5.18**). These results indicate that the presence of intact functional chloroplasts in cotyledons that are photosynthetically competent might be crucial for heterotic growth. Chloroplasts can generate signals that influence nuclear gene expression, although there is no evidence that chloroplast-to-nucleus signalling can directly affect plant growth (Chan et al., 2016).

5.9.4 The *sco2* mutation has other impacts on plant growth

The *sco2* mutants not only prevented chloroplast biogenesis in cotyledons, but also had an impact on the parental level of growth (**Figure 5.17**). This indicates that the *sco2* mutation might affect other biological processes crucial for plant growth, even though chloroplast biogenesis is not affected in the true leaves (**Figure 5.10**, (Shimada et al., 2007). The etiolated (dark-grown) *sco2* seedlings have been reported to have increased accumulation of the chlorophyll precursor, protochlorophyllide, compared with wildtype, which may affect growth in the dark (Tanz et al., 2012). Accumulation of free tetrapyrroles, such as protochlorophyllide, results in the release of singlet oxygen upon illumination and could cause cell death due to oxidative stress (Tripathy and Oelmuller, 2012). It is still unclear how *sco2* affects the tetrapyrrole biosynthetic pathway, and how that might be associated with the reduced growth of *sco2* plants.

5.10 Future work

Both the mutant experiment and the low light experiment show that photosynthesis is important for early hybrid vigour, and can affect hybrid growth in subsequent stages of seedling development. This is in line with inhibitor experiments in *Arabidopsis* and *Brassica* hybrids (Fujimoto et al., 2012, Saeki et al., 2016). These observations show that hybrid vigour appears to be a cumulative result of increased growth in all stages in development so that perturbations at an early stage could have a great impact on hybrid vigour at a subsequent stage. All the attempts to reduce hybrid vigour, either with

inhibitor, reduced light intensity or cotyledon-specific mutants, were unable to attenuate hybrid vigour without decreasing the overall level of growth.

To confirm the causal relation between white cotyledons and reduced heterosis, two experiments should be done. The first question to be answered is whether the mutant experiment can be reproduced using other cotyledon photosynthesis mutants in other hybrid combinations. The T-DNA insertion line of s*co2* mutation in a Col background is available from the stock centre and should be crossed to *sco2* (L*er* background) or *cyo1* (Ws background) to generate other hybrid combinations homozygous for the *sco2* mutation. As most of our analyses were carried out in C24/L*er* hybrids, the *sco2* mutation could be generated in a C24 background by targeted mutagenesis such as CRISPR/Cas9 (Belhaj et al., 2013). To confirm the causal relationship between white cotyledons and reduced hybrid vigour, other cotyledon photosynthesis mutants that have mutations in different loci can be used to repeat the mutant experiment in the future. The *snowy cotyledon1* mutant would be a candidate for further repeats as the SCO1 protein is involved in protein translation, which is affecting a biological process different from that postulated for SCO2. The *sco1* mutants showed entirely white cotyledons. The *sco1* mutation was independently identified by two research groups in L*er* and Col backgrounds that could be crossed to generate mutant hybrids (Albrecht et al., 2006, Ruppel and Hangarter, 2007). To confirm the growth effects on heterosis of limiting photosynthesis in the early cotyledon stage, a low CO_2 condition could be used to limit photosynthesis without affecting other light-dependent pathways that is associated with growth such as photomorphogenesis, the early stage of seedling development after germination (de Wit et al., 2016).

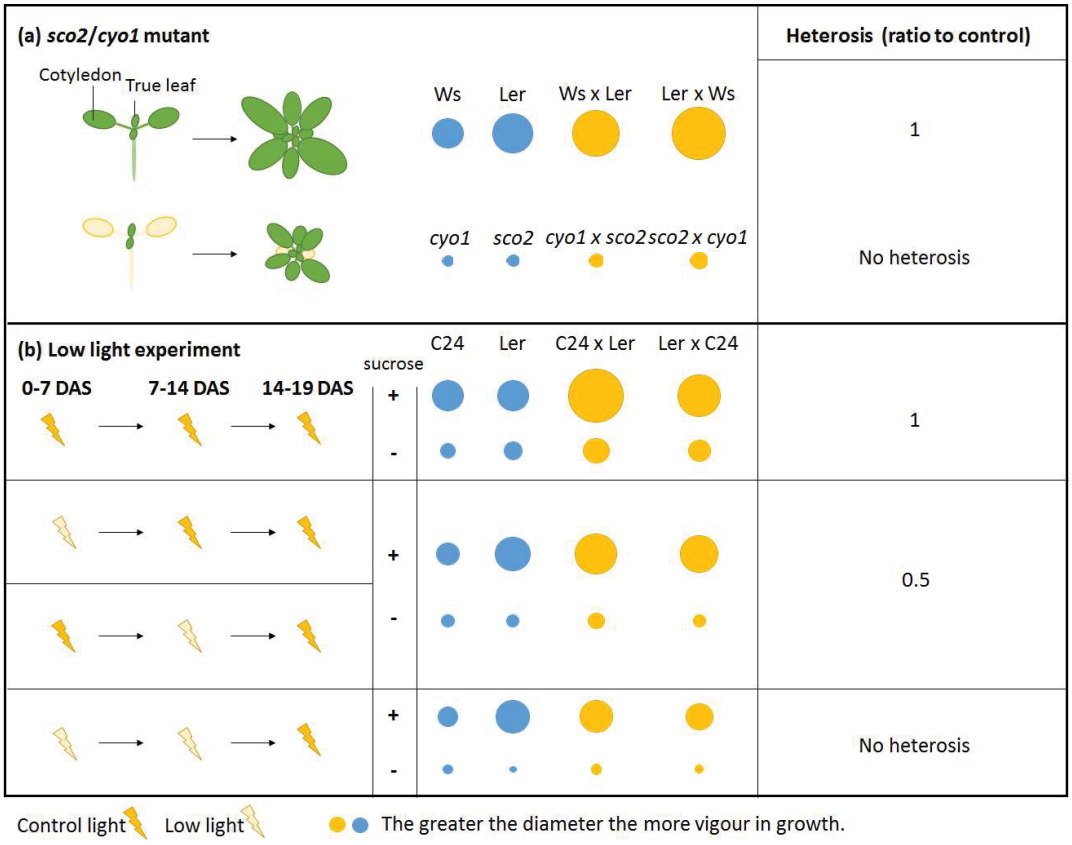

Figure 5.17. Summary of results in (a) mutant and (b) low light experiment. (a)The 19 DAS soil-grown seedlings were measured for rosette fresh weight. (b) Seedlings grown on MS medium either with or without 3% sucrose were measured for rosette biomass at 19 DAS. Circles showed rosette biomass of 19 DAS seedlings (blue: parents, yellow: hybrids). The greater the diameter the greater the biomass.

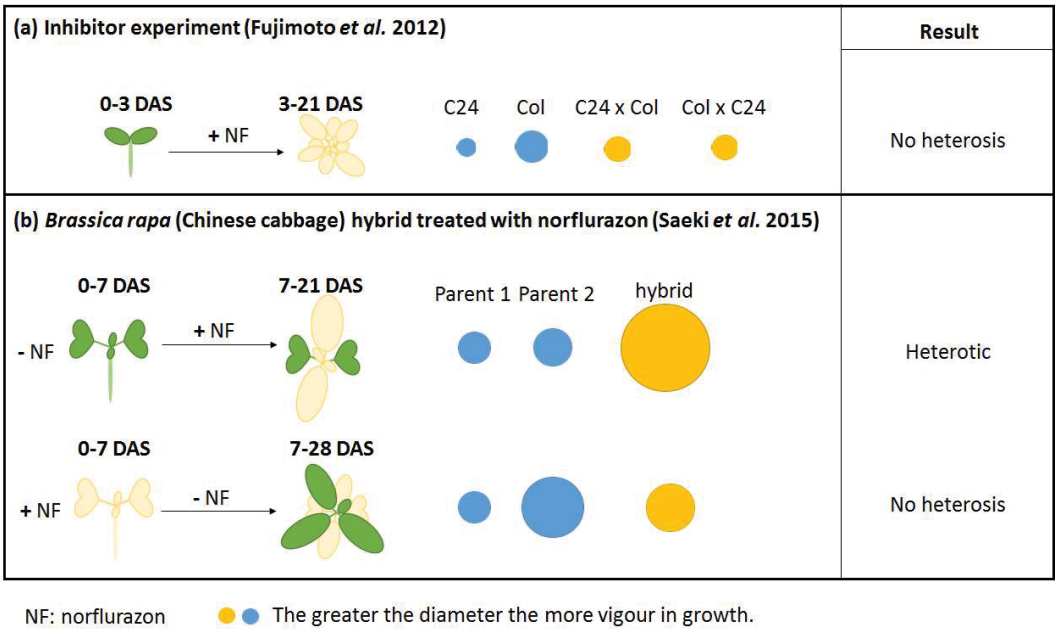

Figure 5.18. Summary of inhibitor results that have been reported in (a) A*rabidopsis thaliana* C24/Col hybrid and (b) *Brassica rapa* hybrid. (a) The 3 DAS *Arabidopsis* seedlings were grown on solid MS medium with norflurazon herbicide (causes photobleaching of green tissues by inhibiting carotenoid biosynthesis) and measured for leaf area of leaves 1 and 2 at 21 DAS. (b) *Brassica* hybrid was germinated and grown on MS medium either with or without norflurazon for one week and transferred on to MS medium in the absence or presence of inhibitor, respectively. Seedlings subjected to the former treatment were measured for the area of leaves 1 and 2 at 21 DAS, while leaves 3 and 4 of the 28 DAS seedling subjected to the latter treatment were measured. No Circles showed rosette biomass of 19 DAS seedlings (blue: parents, yellow: hybrids). The greater the diameter the greater the biomass.

5.11 Summary

Plants carrying the *sco2* mutation having impaired chloroplast biogenesis in cotyledons showed reduced growth. A greater reduction in rosette biomass was found in mutant *cyo1/sco2* hybrids than in the homozygous mutant parents, resulting in a reduced heterosis level compared to wildtype Ws/L*er* hybrids. Impaired chloroplast biogenesis was found only in the cotyledons of *sco2/cyo1* mutant plants, and not in the greening stage of embryos or in the true leaves. As measured by rosette area and fresh weight, the heterosis level of the 21 DAS C24/L*er* hybrids was reduced after growth under low irradiance for one week during early seedling development, either in the cotyledon stage (first week) or in the true leaves stage (second week). A greater reduction in heterosis was found in the 21 DAS hybrids that were germinated and grown continuously under low light for two weeks. When sucrose was added to the growth medium, there was an increase in plant growth, but this did not recover the reduced plant growth and decreased heterosis levels caused by insufficient light.

6 Chapter VI General Discussion

Heterosis, or hybrid vigour, is an important topic in biology. Understanding how hybrids achieve their superior performance relative to their parents could be important for the food industry in improving crop production both in quantity and in quality. Over the last century of use of hybrids in agriculture, the mechanism of heterosis has not been fully elucidated. It has been shown in *Arabidopsis* hybrids that photosynthesis genes in the young seedlings are up-regulated earlier in hybrids than in the parents (Zhu et al., 2016). Heterosis for vegetative biomass is a common trait in hybrids that have a substantial increase in grain yield. The question arises as to whether the hybrids make more vegetative biomass as a result of altered photosynthetic processes.

The aims of this project were to characterise both the light and dark reactions of photosynthesis and growth patterns of eight *Arabidopsis* hybrids derived from four ecotypes, C24, L*er*, Col and Ws, compared to their corresponding parents. This is, to our knowledge, the largest study of photosynthetic gas-exchange and growth parameters for *Arabidopsis* hybrids. Measurements of chlorophyll fluorescence and the CO_2 assimilation rate showed that the photosynthetic properties of hybrids were similar to the parents on a per unit leaf area basis. The maximum electron transport demands for RuBP regeneration (J_{max}) and the maximum velocity of Rubisco in carboxylation (V_{cmax}) in hybrids were at comparable levels to the parents on a per unit leaf area basis (**Chapter 3**). To further investigate if there was an altered amount of photosynthetic apparatus in a unit area of hybrid leaves compared with parent leaves, the C24/L*er* hybrids and the parents were

analysed for chlorophyll content and chloroplast content. Both hybrids and parents had a similar chlorophyll content per unit leaf biomass and a comparable chloroplast content per unit leaf area. These studies and others showed that heterosis in either growth or grain yield is not because of increases in the photosynthetic rates or alterations in basic photosynthetic parameters.

Although there were no changes in photosynthetic parameters on a unit area basis, hybrid leaves were larger than the parent leaves resulting in a greater photosynthetic area to carry out photosynthesis in hybrids than in the parents on a whole plant basis, leading to more photosynthates being produced in hybrid plants than in the parents. Part of the CO_2 assimilated in photosynthesis is stored as starch which is remobilised for respiration and growth at night. To see whether the rates of photosynthate production and consumption were altered in hybrids relative to the parents, starch contents were measured at the end of the day and at the end of the night for the maximum and minimum levels respectively. Starch contents at the end of an irradiance period in the C24/L*er* hybrids were similar to the parents on a leaf biomass basis, and there was a comparable starch consumption per unit biomass at night (**Chapter 4**). These results show that heterosis in biomass is not due to changes in the photosynthetic processes per se, but to the greater photosynthetic area of the leaves in the hybrids. Having larger leaves may be a prerequisite for making more photosynthates to meet the increased demands for carbohydrates sustaining heterotic growth. I propose that heterosis in biomass reflects the ability of hybrids to use a greater amount of the assimilated carbon for growth heterosis.

Heterosis in biomass is not due to increased photosynthetic capacity, but it is a result of a greater area of photosynthetic production

An earlier study in a cohort of hybrids generated from all possible crosses between eight maize inbred lines showed a poor correlation between photosynthetic performance and heterosis in either growth parameters or reproductive traits (Mehta and Sarkar, 1992). Photosynthetic heterosis was only observed when at least one of the parents had relatively lower photosynthetic rates (Mehta and Sarkar, 1992, Morot-Gaudry et al., 1984). A recent study of a single maize hybrid showed that the CO_2 assimilation rates in hybrids were greater than the mid-parent value, but not greater than the better parent (Ko et al., 2016). Similar findings were seen in other crop species, such as wheat (Yang et al., 2007), rice (Zhang et al., 2007, Chang et al., 2016) and Chinese cabbage (Saeki et al., 2016); hybrids have photosynthetic capacities within the range of the parents and not greater than the better parent. This is consistent with our observations in *Arabidopsis* hybrids (**Chapter 3**).

Genetically modified tobacco lines that have increased levels of sedoheptulose-1, 7-biphosphatase (SBPase), a key enzyme involved in the regeneration of RuBP in Calvin cycle, fixed 10% more CO_2 and resulted in 30% increase in biomass compared to the wildtype (Lefebvre et al., 2005). This analysis demonstrated that a subtle increase in photosynthetic rate can have a significant impact on biomass. However, studies on the natural variants for photosynthetic rate in rice (Gu et al., 2014) and wheat (Driever et al., 2014) showed that plants with greater photosynthetic rates do not necessarily have a greater biomass, and vice versa. This indicates that the photosynthetic performance is not

the only factor that determines plant biomass. It is not surprising, as plant biomass is an integrated trait under various regulation processes, such as stress response, hormone, flowering time, defense and environmental cues. Biomass heterosis could be modified by any of the factors mentioned above. For instance, biomass heterosis in *Arabidopsis* hybrids has been associated with differential expression of genes related to the plant hormones, auxin and salicylic acid (Groszmann et al., 2015) .

Chloroplasts are maternally inherited and the photosynthetic machinery in hybrids is a chimeric system with compartments originating from the hybrid nuclear genome and the maternally inherited chloroplast genome. It is not clear how a hybrid nuclear genome interacts with the maternally inherited chloroplast genome and how that affects the capacity of photosynthesis in the hybrid. Despite that, our and others' findings showed that the photosynthetic parameters in hybrids were not different from the parents, indicating that the regulation and cross-talk between the nuclear genome and chloroplast genome were probably the same in hybrids and the parents.

The basis of heterosis in *Arabidopsis* in different light regimes

Heterosis levels can change under some light regimes. It has been reported that the heterosis levels of some *Arabidopsis* hybrids are greater under a doubled irradiance compared to those under standard irradiance (Meyer et al., 2004). In my experiments, doubling irradiance under long daylength increased the plant biomass of both parents and hybrids but did not increase the heterosis level. This was probably because the assimilated

carbon was in excess of that needed for growth, as suggested by my observation of the incomplete degradation of starch at night (**Chapter 4**). To investigate whether heterosis levels can be manipulated by increasing starch turnover under longer night periods, the C24/L*er* hybrids were grown under doubled irradiance in short photoperiods i.e. long nights (light cycle of 8 hr/16 hr). As most of the starch accumulated from the previous day was degraded and remobilised in the longer nights, the starch turnover in doubled irradiance was greater than that in standard light on a per unit biomass basis (**Chapter 4**). The increased starch turnover coincided with an increased level of heterosis in biomass (**Chapter 4**).

I propose that the increased heterotic growth under doubled irradiance in short photoperiods (long nights) is related to greater starch consumption. The unit biomass starch turnover in hybrids was not greater than the better parent in all conditions tested. These results further support the hypothesis for heterosis that hybrid vigour is due to the ability to use more carbon assimilates for growth. To compare carbon partitioning in hybrids and parents, a detailed metabolite profiling will need to be carried out. Isotopically labelled CO_2 can be used to allocate photosynthetically assimilated carbon for specific metabolites or structural components such as proteins and cell wall materials (Kolling et al., 2015, Sulpice et al., 2014).

Heterosis in *Arabidopsis* vegetative growth

In the literature, heterosis in vegetative growth is presented on a per seedling basis; heterosis in individual leaves has not been reported (Groszmann et al., 2014, Meyer et al., 2004). I examined the area of individual leaves of C24/L*er* hybrids and parents and found that heterosis levels in the newly developed leaves were greater than in the older leaves (**Chapter 3**). Measurements of leaf area showed that hybrid biomass is mainly contributed by the largest four to five leaves present at any one time (**Chapter 3**). The developmentally older leaves were outgrown by the newer leaves and contributed less to the total biomass. In addition, the older leaves contributed less to heterosis because the parental leaves matched the greater size of hybrid leaves when they had fully expanded. These results give a new perspective of heterosis in vegetative growth which is a result of the succession of newly developed leaves of hybrids being larger than the corresponding parent leaves.

I further investigated the cellular basis of heterosis in the new leaves by analysing the palisade mesophyll cells at different developmental stages. The results showed that heterosis in hybrid leaves is probably due to a faster and/or an earlier leaf development. The cell size in the new leaves was greater than the parents at a point in time whereas this difference in cell size became less marked in the fully expanded leaves (**Chapter 3**). The larger size of hybrid leaves was also attributable to a greater number of cells per leaf, as shown in most of the hybrid combinations examined. These changes in cell size and cell number suggest that hybrids differ from parents in leaf development, with increased rates of cell expansion and cell division; hybrid leaves may have an earlier commencement or

a prolonged period of cell expansion or division relative to the parents (**Chapter 3**). A more advanced leaf development in hybrids can also be inferred from the earlier leaf emergence in hybrids compared with the parents, as suggested by the measurement of leaf number over a time course (**Chapter 3**). To investigate leaf development between hybrids and parents, a more detailed documentation of leaf area generation and cellular measurements would be justified. Reporter lines for specific cell cycle markers can be used to enable monitoring of leaf development in hybrids (Vanhaeren et al., 2015). Leaf development is mediated by temporal and spatial coordination of cell expansion and cell division by networks of signalling pathways and hormones (Donnelly et al., 1999, Gonzalez et al., 2010, Kalve et al., 2014).

Attempts have been made to identify molecular mechanisms underlying heterosis by analysing alterations in hybrid transcriptomes using pools of leaves of different developmental stages (Fujimoto et al., 2012, Groszmann et al., 2014). Such an approach would be successful in identifying the underlying molecular regulators for hybrid leaf development. The differential leaf development between hybrids and parents would be obvious in comparisons of leaves at the same stage of seedling development.

Effects of early growth stages on heterosis in *Arabidopsis*

Early stages in seedling development have been shown to be critical stages for heterosis in biomass. As shown in *Arabidopsis*, biomass heterosis occurs early in seedling development, as early as in cotyledons (Meyer et al., 2004). The expression of

photosynthesis related genes has been shown to be transiently up-regulated in hybrid cotyledons (Fujimoto et al., 2012, Zhu et al., 2016). As shown in my results and by others, perturbations in photosynthesis in the cotyledon stage have long-term effects on biomass, including heterosis in hybrids. Heterosis levels of the *snowy cotyledon* mutant hybrid plants that have white, photosynthetically incompetent cotyledons were substantially reduced, despite the chlorophyll biosynthesis in the true leaves not being affected (**Chapter 5**). This is consistent with the findings in *Brassica rapa* hybrids when photosynthesis in the cotyledons is compromised by the carotenoid biosynthesis inhibitor, norflurazon (Saeki et al., 2016). The long-lasting impacts of inhibiting photosynthesis in cotyledons on plant growth might be due to the lack of photosynthates production in sustaining the growth of the first pair of true leaves, which in turns affects the growth of the subsequent leaves, leading to a reduced growth and biomass heterosis at subsequent stages. This is in line with our hypothesis of the generation of biomass heterosis is the consequence of advanced growth at the beginning of leaf development.

Conclusions

The current study demonstrates that:

- Hybrids do not have vegetative heterosis because of alterations in the processes of photosynthesis. The rate of photosynthesis per unit leaf area is comparable in parents and hybrids. Hybrids have a greater total photosynthetic capacity because of having larger photosynthetic area (leaf area) with more and larger cells.

- Different leaves contribute different amount of heterosis in biomass. Heterosis in vegetative growth is mainly contributed by the developing leaves in hybrids which are larger than the corresponding parent leaves, probably via more advanced leaf development. This earlier, faster leaf development in hybrids is associated with their greater total photosynthetic capacity of the plant that makes more resources available for plant growth.

- Mutant hybrids that have white, photosynthetically incompetent cotyledons did not have any heterosis in biomass. Reduction in photosynthesis in the cotyledons may have resulted in a reduced production of photosynthate for the growth of subsequent leaves and, consequently, the generation of heterosis was inhibited. This shows that photosynthesis in the cotyledon stage is critical for the establishment of heterosis; and having growth heterosis at the early stages in seedling development is important for the growth heterosis at subsequent stages.

- The present experimental data in *Arabidopsis* hybrids showed many characteristics similar to the hybrids in crop species, such as Chinese cabbage. This suggests that these studies in *Arabidopsis* hybrids may apply in crops to have more understanding in the mechanisms of heterosis.

Appendices

Appendix 3.1c

	p value	
C24/LerMPV-C24	0.677	
C24xLer-C24	0.000	***
Ler-C24	0.054	
LerxC24-C24	0.000	***
C24xLer-C24/LerMPV	0.000	***
Ler-C24/LerMPV	0.623	
LerxC24-C24/LerMPV	0.000	***
Ler-C24xLer	0.005	**
LerxC24-C24xLer	1.000	
LerxC24-Ler	0.010	*

Appendix 3.2b

P value	15 DAS		18 DAS		21 DAS	
C24/LerMPV-C24	0.945		0.998		0.061	
C24xLer-C24	0.583		0.174		0.002	**
Ler-C24	0.583		0.971		0.000	***
LerxC24-C24	0.583		0.046	*	0.041	*
C24xLer-C24/LerMPV	0.204		0.301		0.000	***
Ler-C24/LerMPV	0.945		0.998		0.061	
LerxC24-C24/LerMPV	0.204		0.092		0.000	***
Ler-C24xLer	0.047	*	0.473		0.000	***
LerxC24-C24xLer	1.000		0.971		0.791	
LerxC24-Ler	0.047	*	0.174		0.000	***

Appendix 3.4a

	p value			p value	
C24/LerMPV-C24	0.258		Col/LerMPV-Col	0.907	
C24xLer-C24	0.000	***	ColxLer-Col	0.037	*
Ler-C24	0.000	***	Ler-Col	0.077	
LerxC24-C24	0.597		LerxCol-Col	0.076	

C24xLer-C24/LerMPV	0.000	***	ColxLer-Col/LerMPV	0.016	*
Ler-C24/LerMPV	0.095		Ler-Col/LerMPV	0.811	
LerxC24-C24/LerMPV	0.974		LerxCol-Col/LerMPV	0.032	
Ler-C24xLer	0.000	***	Ler-ColxLer	0.000	***
LerxC24-C24xLer	0.000	***	LerxCol-ColxLer	0.995	
LerxC24-Ler	0.007	**	LerxCol-Ler	0.000	***
C24/ColMPV-C24	0.403		LerxWs-Ler	0.000	***
C24xCol-C24	0.026	*	Ws-Ler	0.995	
Col-C24	0.002	**	Ws/LerMPV-Ler	1.000	
ColxC24-C24	1.000		WsxLer-Ler	0.004	**
C24xCol-C24/ColMPV	0.001	***	Ws-LerxWs	0.000	***
Col-C24/ColMPV	0.649		Ws/LerMPV-LerxWs	0.000	***
ColxC24-C24/ColMPV	0.678		WsxLer-LerxWs	0.000	***
Col-C24xCol	0.000	***	Ws/LerMPV-Ws	1.000	
ColxC24-C24xCol	0.054		WsxLer-Ws	0.058	
ColxC24-Col	0.039	*	WsxLer-Ws/LerMPV	0.038	*

Appendix 3.4b

	p value			p value	
C24xLer-C24	0.048	*	ColxLer-Col	1.000	
C24/LerMPV-C24	0.566		Col/LerMPV-Col	0.816	
Ler-C24	0.019	*	Ler-Col	0.185	
LerxC24-C24	0.039	*	LerxCol-Col	0.940	
C24/LerMPV-C24xLer	0.011	*	Col/LerMPV-ColxLer	0.915	
Ler-C24xLer	0.000	***	Ler-ColxLer	0.526	
LerxC24-C24xLer	0.000	***	LerxCol-ColxLer	0.963	
Ler-C24/LerMPV	0.994		Ler-Col/LerMPV	0.984	
LerxC24-C24/LerMPV	0.946		LerxCol-Col/LerMPV	0.516	
LerxC24-Ler	0.982		LerxCol-Ler	0.081	
C24xCol-C24	0.000	***	LerxWs-Ler	0.000	***
C24/ColMPV-C24	0.998		Ws-Ler	0.652	
Col-C24	0.710		WsxLer-Ler	0.012	*
ColxC24-C24	0.868		Ws/LerMPV-Ler	0.558	
C24/ColMPV-C24xCol	0.000		Ws-LerxWs	0.000	

Col-C24xCol	0.000		WsxLer-LerxWs	0.010	
ColxC24-C24xCol	0.000		Ws/LerMPV-LerxWs	0.000	
Col-C24/ColMPV	0.947		WsxLer-Ws	0.410	
ColxC24-C24/LerMPV	0.972		Ws/LerMPV-Ws	1.000	
ColxC24-Col	1.000		Ws/LerMPV-WsxLer	0.485	

Appendix 3.4ab Comparisons between MS medium supplemented with or without sucrose

	P value	
C24	0.646	
Ler	0.002	**
Col	0.001	***
Ws	0.000	***
C24xLer	0.276	
LerxC24	0.298	
C24xCol	0.216	
ColxC24	0.776	
ColxLer	0.978	
LerxCol	0.159	
WsxLer	0.005	**
LerxWs	0.435	

Appendix 3.5

	p value	
C24/LerMPV-C24	0.003	**
C24xLer-C24	0.000	***
Ler-C24	0.000	***
LerxC24-C24	0.000	***
C24xLer-C24/LerMPV	0.000	***
Ler-C24/LerMPV	0.044	*
LerxC24-C24/LerMPV	0.918	
Ler-C24xLer	0.000	***
LerxC24-C24xLer	0.000	***
LerxC24-Ler	0.351	

Appendix 3.7a

ANOVA comparisons of hybrid and parent combination to see if there is significant difference between the samples (bold). If so, the detail comparisons are shown in the next table.

19 DAS, 120uE	p value
T1	0.2690
T2	0.4160
T3	**0.0006**
T4	**0.0167**
T5	0.0628
T6	0.0542
T7	0.1450
T8	0.3350
T9	0.0927
T10	0.0517

19 DAS, 120uE	T3		T4	
C24xLer-C24	0.0006	***	0.0140	*
Ler-C24	0.0402	*	0.2089	
LerxC24-C24	0.0030	**	0.0832	
MPV-C24	0.4214		0.7857	
Ler-C24xLer	0.0862		0.4366	
LerxC24-C24xLer	0.7511		0.7754	
MPV-C24xLer	0.0071	**	0.0806	
LerxC24-Ler	0.4557		0.9685	
MPV-Ler	0.5145		0.7478	
MPV-LerxC24	0.0447	*	0.4104	

Appendix 3.7b

ANOVA comparisons of hybrid and parent combination to see if there is significant difference between the samples (bold). If so, the detail comparisons are shown in the next table.

30 DAS, 120uE	p value
T1	0.2900
T2	0.6230
T3	**0.0038**
T4	**0.0282**
T5	0.0681
T6	0.2580
T7	0.4030
T8	0.1770
T9	**0.0221**
T10	**0.0016**
T11	**0.0012**
T12	**0.0213**

30 DAS, 120uE	T3		T4		T9		T10		T11		T12	
C24xLer-C24	0.0145	*	0.0444	*	0.0504		0.0038	**	0.0080	**	0.1172	
Ler-C24	0.0069	**	0.0353	*								
LerxC24-C24	0.0063	**	0.0897		0.0248	*	0.0020	**	0.0010	***	0.0179	*
MPV-C24	0.2230		0.4452									
Ler-C24xLer	0.9855		0.9999									
LerxC24-C24xLer	0.9782		0.9898		0.8284		0.7611		0.1251		0.2074	
MPV-C24xLer	0.4259		0.5236									
LerxC24-Ler	1.0000		0.9715									
MPV-Ler	0.2230		0.4452									
MPV-LerxC24	0.2051		0.7753									

Appendix 3.8a

C24xLer	p value		C24xLer	p value		C24xLer	p value	
T2:19DAS-T1:19DAS	1.000		T8:19DAS-T4:19DAS	1.000		T4:30DAS-T8:19DAS	1.000	
T3:19DAS-T1:19DAS	1.000		T9:19DAS-T4:19DAS	1.000		T5:30DAS-T8:19DAS	0.997	
T4:19DAS-T1:19DAS	1.000		T1:30DAS-T4:19DAS	1.000		T6:30DAS-T8:19DAS	0.543	

T5:19DAS-T1:19DAS	1.000		T2:30DAS-T4:19DAS	1.000		T7:30DAS-T8:19DAS	0.000	***
T6:19DAS-T1:19DAS	1.000		T3:30DAS-T4:19DAS	1.000		T8:30DAS-T8:19DAS	0.001	***
T7:19DAS-T1:19DAS	1.000		T4:30DAS-T4:19DAS	1.000		T9:30DAS-T8:19DAS	0.000	***
T8:19DAS-T1:19DAS	1.000		T5:30DAS-T4:19DAS	0.919		T1:30DAS-T9:19DAS	1.000	
T9:19DAS-T1:19DAS	1.000		T6:30DAS-T4:19DAS	0.234		T2:30DAS-T9:19DAS	1.000	
T1:30DAS-T1:19DAS	1.000		T7:30DAS-T4:19DAS	0.000	***	T3:30DAS-T9:19DAS	1.000	
T2:30DAS-T1:19DAS	1.000		T8:30DAS-T4:19DAS	0.000	***	T4:30DAS-T9:19DAS	1.000	
T3:30DAS-T1:19DAS	1.000		T9:30DAS-T4:19DAS	0.000	***	T5:30DAS-T9:19DAS	1.000	
T4:30DAS-T1:19DAS	0.999		T6:19DAS-T5:19DAS	1.000		T6:30DAS-T9:19DAS	0.678	
T5:30DAS-T1:19DAS	0.777		T7:19DAS-T5:19DAS	1.000		T7:30DAS-T9:19DAS	0.000	***
T6:30DAS-T1:19DAS	0.125		T8:19DAS-T5:19DAS	1.000		T8:30DAS-T9:19DAS	0.002	**
T7:30DAS-T1:19DAS	0.000	***	T9:19DAS-T5:19DAS	1.000		T9:30DAS-T9:19DAS	0.000	***
T8:30DAS-T1:19DAS	0.000	***	T1:30DAS-T5:19DAS	1.000		T2:30DAS-T1:30DAS	1.000	
T9:30DAS-T1:19DAS	0.000	***	T2:30DAS-T5:19DAS	1.000		T3:30DAS-T1:30DAS	1.000	
T3:19DAS-T2:19DAS	1.000		T3:30DAS-T5:19DAS	1.000		T4:30DAS-T1:30DAS	0.999	
T4:19DAS-T2:19DAS	1.000		T4:30DAS-T5:19DAS	1.000		T5:30DAS-T1:30DAS	0.793	
T5:19DAS-T2:19DAS	1.000		T5:30DAS-T5:19DAS	0.934		T6:30DAS-T1:30DAS	0.133	
T6:19DAS-T2:19DAS	1.000		T6:30DAS-T5:19DAS	0.256		T7:30DAS-T1:30DAS	0.000	***
T7:19DAS-T2:19DAS	1.000		T7:30DAS-T5:19DAS	0.000	***	T8:30DAS-T1:30DAS	0.000	***
T8:19DAS-T2:19DAS	1.000		T8:30DAS-T5:19DAS	0.000	***	T9:30DAS-T1:30DAS	0.000	***
T9:19DAS-T2:19DAS	1.000		T9:30DAS-T5:19DAS	0.000	***	T3:30DAS-T2:30DAS	1.000	
T1:30DAS-T2:19DAS	1.000		T7:19DAS-T6:19DAS	1.000		T4:30DAS-T2:30DAS	1.000	
T2:30DAS-T2:19DAS	1.000		T8:19DAS-T6:19DAS	1.000		T5:30DAS-T2:30DAS	0.883	
T3:30DAS-T2:19DAS	1.000		T9:19DAS-T6:19DAS	1.000		T6:30DAS-T2:30DAS	0.194	

T4:30DAS-T2:19DAS	0.999		T1:30DAS-T6:19DAS	1.000		T7:30DAS-T2:30DAS	0.000	***
T5:30DAS-T2:19DAS	0.804		T2:30DAS-T6:19DAS	1.000		T8:30DAS-T2:30DAS	0.000	***
T6:30DAS-T2:19DAS	0.139		T3:30DAS-T6:19DAS	1.000		T9:30DAS-T2:30DAS	0.000	***
T7:30DAS-T2:19DAS	0.000	***	T4:30DAS-T6:19DAS	1.000		T4:30DAS-T3:30DAS	1.000	
T8:30DAS-T2:19DAS	0.000	***	T5:30DAS-T6:19DAS	0.999		T5:30DAS-T3:30DAS	0.996	
T9:30DAS-T2:19DAS	0.000	***	T6:30DAS-T6:19DAS	0.601		T6:30DAS-T3:30DAS	0.519	
T4:19DAS-T3:19DAS	1.000		T7:30DAS-T6:19DAS	0.000	***	T7:30DAS-T3:30DAS	0.000	***
T5:19DAS-T3:19DAS	1.000		T8:30DAS-T6:19DAS	0.001	**	T8:30DAS-T3:30DAS	0.001	***
T6:19DAS-T3:19DAS	1.000		T9:30DAS-T6:19DAS	0.000	***	T9:30DAS-T3:30DAS	0.000	***
T7:19DAS-T3:19DAS	1.000		T8:19DAS-T7:19DAS	1.000		T5:30DAS-T4:30DAS	1.000	
T8:19DAS-T3:19DAS	1.000		T9:19DAS-T7:19DAS	1.000		T6:30DAS-T4:30DAS	0.754	
T9:19DAS-T3:19DAS	1.000		T1:30DAS-T7:19DAS	1.000		T7:30DAS-T4:30DAS	0.000	***
T1:30DAS-T3:19DAS	1.000		T2:30DAS-T7:19DAS	1.000		T8:30DAS-T4:30DAS	0.003	**
T2:30DAS-T3:19DAS	1.000		T3:30DAS-T7:19DAS	1.000		T9:30DAS-T4:30DAS	0.000	***
T3:30DAS-T3:19DAS	1.000		T4:30DAS-T7:19DAS	1.000		T6:30DAS-T5:30DAS	0.998	
T4:30DAS-T3:19DAS	1.000		T5:30DAS-T7:19DAS	0.991		T7:30DAS-T5:30DAS	0.004	**
T5:30DAS-T3:19DAS	0.953		T6:30DAS-T7:19DAS	0.457		T8:30DAS-T5:30DAS	0.036	*
T6:30DAS-T3:19DAS	0.293		T7:30DAS-T7:19DAS	0.000		T9:30DAS-T5:30DAS	0.005	**
T7:30DAS-T3:19DAS	0.000	***	T8:30DAS-T7:19DAS	0.001		T7:30DAS-T6:30DAS	0.084	
T8:30DAS-T3:19DAS	0.000	***	T9:30DAS-T7:19DAS	0.000		T8:30DAS-T6:30DAS	0.429	
T9:30DAS-T3:19DAS	0.000	***	T9:19DAS-T8:19DAS	1.000		T9:30DAS-T6:30DAS	0.101	
T5:19DAS-T4:19DAS	1.000		T1:30DAS-T8:19DAS	1.000		T8:30DAS-T7:30DAS	1.000	
T6:19DAS-T4:19DAS	1.000		T2:30DAS-T8:19DAS	1.000		T9:30DAS-T7:30DAS	1.000	
T7:19DAS-T4:19DAS	1.000		T3:30DAS-T8:19DAS	1.000		T9:30DAS-T8:30DAS	1.000	

LerxC24	p value		LerxC24	p value		LerxC24	p value	
T2:19DAS-T1:19DAS	1.000		T8:19DAS-T4:19DAS	1.000		T4:30DAS-T8:19DAS	1.000	
T3:19DAS-T1:19DAS	1.000		T9:19DAS-T4:19DAS	0.686		T5:30DAS-T8:19DAS	1.000	
T4:19DAS-T1:19DAS	1.000		T1:30DAS-T4:19DAS	0.998		T6:30DAS-T8:19DAS	1.000	
T5:19DAS-T1:19DAS	1.000		T2:30DAS-T4:19DAS	1.000		T7:30DAS-T8:19DAS	1.000	
T6:19DAS-T1:19DAS	1.000		T3:30DAS-T4:19DAS	1.000		T8:30DAS-T8:19DAS	1.000	
T7:19DAS-T1:19DAS	1.000		T4:30DAS-T4:19DAS	1.000		T9:30DAS-T8:19DAS	0.998	
T8:19DAS-T1:19DAS	1.000		T5:30DAS-T4:19DAS	1.000		T1:30DAS-T9:19DAS	1.000	
T9:19DAS-T1:19DAS	0.944		T6:30DAS-T4:19DAS	1.000		T2:30DAS-T9:19DAS	0.996	
T1:30DAS-T1:19DAS	1.000		T7:30DAS-T4:19DAS	1.000		T3:30DAS-T9:19DAS	0.496	
T2:30DAS-T1:19DAS	1.000		T8:30DAS-T4:19DAS	1.000		T4:30DAS-T9:19DAS	0.848	
T3:30DAS-T1:19DAS	1.000		T9:30DAS-T4:19DAS	1.000		T5:30DAS-T9:19DAS	0.354	
T4:30DAS-T1:19DAS	1.000		T6:19DAS-T5:19DAS	1.000		T6:30DAS-T9:19DAS	0.654	
T5:30DAS-T1:19DAS	1.000		T7:19DAS-T5:19DAS	1.000		T7:30DAS-T9:19DAS	0.634	
T6:30DAS-T1:19DAS	1.000		T8:19DAS-T5:19DAS	1.000		T8:30DAS-T9:19DAS	0.757	
T7:30DAS-T1:19DAS	1.000		T9:19DAS-T5:19DAS	0.512		T9:30DAS-T9:19DAS	0.121	
T8:30DAS-T1:19DAS	1.000		T1:30DAS-T5:19DAS	0.987		T2:30DAS-T1:30DAS	1.000	
T9:30DAS-T1:19DAS	0.969		T2:30DAS-T5:19DAS	0.998		T3:30DAS-T1:30DAS	0.985	
T3:19DAS-T2:19DAS	1.000		T3:30DAS-T5:19DAS	1.000		T4:30DAS-T1:30DAS	1.000	

T4:19DAS-T2:19DAS	1.000		T4:30DAS-T5:19DAS	1.000		T5:30DAS-T1:30DAS	0.948	
T5:19DAS-T2:19DAS	1.000		T5:30DAS-T5:19DAS	1.000		T6:30DAS-T1:30DAS	0.998	
T6:19DAS-T2:19DAS	1.000		T6:30DAS-T5:19DAS	1.000		T7:30DAS-T1:30DAS	0.997	
T7:19DAS-T2:19DAS	1.000		T7:30DAS-T5:19DAS	1.000		T8:30DAS-T1:30DAS	1.000	
T8:19DAS-T2:19DAS	1.000		T8:30DAS-T5:19DAS	1.000		T9:30DAS-T1:30DAS	0.684	
T9:19DAS-T2:19DAS	0.477		T9:30DAS-T5:19DAS	1.000		T3:30DAS-T2:30DAS	0.998	
T1:30DAS-T2:19DAS	0.982		T7:19DAS-T6:19DAS	1.000		T4:30DAS-T2:30DAS	1.000	
T2:30DAS-T2:19DAS	0.997		T8:19DAS-T6:19DAS	1.000		T5:30DAS-T2:30DAS	0.987	
T3:30DAS-T2:19DAS	1.000		T9:19DAS-T6:19DAS	0.648		T6:30DAS-T2:30DAS	1.000	
T4:30DAS-T2:19DAS	1.000		T1:30DAS-T6:19DAS	0.997		T7:30DAS-T2:30DAS	1.000	
T5:30DAS-T2:19DAS	1.000		T2:30DAS-T6:19DAS	1.000		T8:30DAS-T2:30DAS	1.000	
T6:30DAS-T2:19DAS	1.000		T3:30DAS-T6:19DAS	1.000		T9:30DAS-T2:30DAS	0.830	
T7:30DAS-T2:19DAS	1.000		T4:30DAS-T6:19DAS	1.000		T4:30DAS-T3:30DAS	1.000	
T8:30DAS-T2:19DAS	1.000		T5:30DAS-T6:19DAS	1.000		T5:30DAS-T3:30DAS	1.000	
T9:30DAS-T2:19DAS	1.000		T6:30DAS-T6:19DAS	1.000		T6:30DAS-T3:30DAS	1.000	
T4:19DAS-T3:19DAS	1.000		T7:30DAS-T6:19DAS	1.000		T7:30DAS-T3:30DAS	1.000	
T5:19DAS-T3:19DAS	1.000		T8:30DAS-T6:19DAS	1.000		T8:30DAS-T3:30DAS	1.000	
T6:19DAS-T3:19DAS	1.000		T9:30DAS-T6:19DAS	1.000		T9:30DAS-T3:30DAS	1.000	
T7:19DAS-T3:19DAS	1.000		T8:19DAS-T7:19DAS	1.000		T5:30DAS-T4:30DAS	1.000	

T8:19DAS-T3:19DAS	1.000		T9:19DAS-T7:19DAS	0.948		T6:30DAS-T4:30DAS	1.000	
T9:19DAS-T3:19DAS	0.454		T1:30DAS-T7:19DAS	1.000		T7:30DAS-T4:30DAS	1.000	
T1:30DAS-T3:19DAS	0.978		T2:30DAS-T7:19DAS	1.000		T8:30DAS-T4:30DAS	1.000	
T2:30DAS-T3:19DAS	0.996		T3:30DAS-T7:19DAS	1.000		T9:30DAS-T4:30DAS	0.994	
T3:30DAS-T3:19DAS	1.000		T4:30DAS-T7:19DAS	1.000		T6:30DAS-T5:30DAS	1.000	
T4:30DAS-T3:19DAS	1.000		T5:30DAS-T7:19DAS	1.000		T7:30DAS-T5:30DAS	1.000	
T5:30DAS-T3:19DAS	1.000		T6:30DAS-T7:19DAS	1.000		T8:30DAS-T5:30DAS	1.000	
T6:30DAS-T3:19DAS	1.000		T7:30DAS-T7:19DAS	1.000		T9:30DAS-T5:30DAS	1.000	
T7:30DAS-T3:19DAS	1.000		T8:30DAS-T7:19DAS	1.000		T7:30DAS-T6:30DAS	1.000	
T8:30DAS-T3:19DAS	1.000		T9:30DAS-T7:19DAS	0.967		T8:30DAS-T6:30DAS	1.000	
T9:30DAS-T3:19DAS	1.000		T9:19DAS-T8:19DAS	0.786		T9:30DAS-T6:30DAS	1.000	
T5:19DAS-T4:19DAS	1.000		T1:30DAS-T8:19DAS	1.000		T8:30DAS-T7:30DAS	1.000	
T6:19DAS-T4:19DAS	1.000		T2:30DAS-T8:19DAS	1.000		T9:30DAS-T7:30DAS	1.000	
T7:19DAS-T4:19DAS	1.000		T3:30DAS-T8:19DAS	1.000		T9:30DAS-T8:30DAS	0.999	

Appendix 3.9a

	19 DAS		30 DAS	
C24xLer-C24	1.000		0.084	
Ler-C24	0.369		0.029	*
LerxC24-C24	0.936		0.013	*

Ler-C24xLer	0.369		0.001	***
LerxC24-C24xLer	0.936		0.575	
LerxC24-Ler	0.669		0.000	***

Appendix 3.9b

	19 DAS		30 DAS	
C24xLer-C24	0.001	**	0.000	***
Ler-C24	0.531		0.130	
LerxC24-C24	0.328		0.000	***
MPV-C24	0.916		0.068	
Ler-C24xLer	0.014	*	0.000	***
LerxC24-C24xLer	0.027	*	0.869	
MPV-C24xLer	0.000	***	0.000	***
LerxC24-Ler	0.993		0.000	***
MPV-Ler	0.186		0.992	
MPV-LerxC24	0.101		0.000	***

Appendix 3.10b

	p value	
C24xLer-C24	0.001	***
Ler-C24	0.001	***
LerxC24-C24	0.000	***
Ler-C24xLer	0.000	***
LerxC24-C24xLer	0.756	

LerxC24-Ler	0.000	***

Appendix 3.12a

	p value			p value	
C24/LerMPV-C24	0.003	**	C24/ColMPV-C24	0.568	
C24xLer-C24	0.000	***	C24xCol-C24	0.000	***
Ler-C24	0.000	***	Col-C24	0.019	*
LerxC24-C24	0.000	***	ColxC24-C24	0.000	***
C24xLer-C24/LerMPV	0.000	***	C24xCol-C24/ColMPV	0.000	***
Ler-C24/LerMPV	0.011	*	Col-C24/ColMPV	0.461	
LerxC24-C24/LerMPV	0.017	*	ColxC24-C24/ColMPV	0.000	***
Ler-C24xLer	0.002	**	Col-C24xCol	0.000	***
LerxC24-C24xLer	0.012	*	ColxC24-C24xCol	0.967	
LerxC24-Ler	0.999		ColxC24-Col	0.001	***
Col/LerMPV-Col	0.434		Ler/WsMPV-Ler	0.905	
ColxLer-Col	0.068		LerxWs-Ler	0.815	
Ler-Col	0.014	*	Ws-Ler	0.419	
LerxCol-Col	0.003	**	WsxLer-Ler	0.998	
ColxLer-Col/LerMPV	0.879		LerxWs-Ler/WsMPV	1.000	
Ler-Col/LerMPV	0.701		Ws-Ler/WsMPV	0.905	
LerxCol-Col/LerMPV	0.176		WsxLer-Ler/WsMPV	0.768	
Ler-ColxLer	1.000		Ws-LerxWs	0.963	
LerxCol-ColxLer	0.622		WsxLer-LerxWs	0.644	
LerxCol-Ler	0.606		WsxLer-Ws	0.265	

Appendix 3.12b

	p value			p value	
C24/LerMPV-C24	0.117		C24/ColMPV-C24	0.989	
C24xLer-C24	0.002	**	C24xCol-C24	0.198	
Ler-C24	0.035	*	Col-C24	0.972	
LerxC24-C24	0.009	**	ColxC24-C24	0.014	*
C24xLer-C24/LerMPV	0.500		C24xCol-C24/ColMPV	0.103	
Ler-C24/LerMPV	1.000		Col-C24/ColMPV	1.000	
LerxC24-C24/LerMPV	0.877		ColxC24-C24/ColMPV	0.007	**
Ler-C24xLer	0.436		Col-C24xCol	0.079	
LerxC24-C24xLer	0.951		ColxC24-C24xCol	0.853	
LerxC24-Ler	0.869		ColxC24-Col	0.005	**

Col/LerMPV-Col	0.120		Ler/WsMPV-Ler	0.927	
ColxLer-Col	0.115		LerxWs-Ler	0.471	
Ler-Col	0.017	*	Ws-Ler	0.499	
LerxCol-Col	0.307		WsxLer-Ler	0.975	
ColxLer-Col/LerMPV	1.000		LerxWs-Ler/WsMPV	0.913	
Ler-Col/LerMPV	0.997		Ws-Ler/WsMPV	0.927	
LerxCol-Col/LerMPV	0.993		WsxLer-Ler/WsMPV	1.000	
Ler-ColxLer	0.994		Ws-LerxWs	1.000	
LerxCol-ColxLer	0.995		WsxLer-LerxWs	0.824	
LerxCol-Ler	0.927		WsxLer-Ws	0.845	

Appendix 3.12c

	p value			p value	
C24/LerMPV-C24	0.543		C24/ColMPV-C24	0.405	
C24xLer-C24	0.000	***	C24xCol-C24	0.000	***
Ler-C24	0.000	***	Col-C24	0.009	**
LerxC24-C24	0.004	**	ColxC24-C24	0.000	***
C24xLer-C24/LerMPV	0.002	**	C24xCol-C24/ColMPV	0.001	**
Ler-C24/LerMPV	0.015	*	Col-C24/ColMPV	0.442	
LerxC24-C24/LerMPV	0.226		ColxC24-C24/ColMPV	0.038	*
Ler-C24xLer	0.622		Col-C24xCol	0.083	
LerxC24-C24xLer	0.271		ColxC24-C24xCol	0.626	
LerxC24-Ler	0.893		ColxC24-Col	0.706	
Col/LerMPV-Col	1.000		Ler/WsMPV-Ler	0.985	
ColxLer-Col	0.922		LerxWs-Ler	0.999	
Ler-Col	0.773		Ws-Ler	0.835	
LerxCol-Col	0.147		WsxLer-Ler	0.950	
ColxLer-Col/LerMPV	0.915		LerxWs-Ler/WsMPV	0.998	
Ler-Col/LerMPV	0.758		Ws-Ler/WsMPV	0.985	
LerxCol-Col/LerMPV	0.141		WsxLer-Ler/WsMPV	0.726	
Ler-ColxLer	1.000		Ws-LerxWs	0.922	
LerxCol-ColxLer	0.493		WsxLer-LerxWs	0.879	
LerxCol-Ler	0.466		WsxLer-Ws	0.408	

Appendix 3.13

Leaf area	28 DAS leaf 3/4		19 DAS leaf 3/4		19 DAS leaf 5/6	
C24/LerMPV-C24	0.000	***	0.190		1.000	

C24xLer-C24	0.000	***	0.000	***	0.064	
Ler-C24	0.000	***	0.005	**	0.999	
LerxC24-C24	0.000	***	0.007	**	0.975	
C24xLer-C24/LerMPV	0.000	***	0.000	***	0.085	
Ler-C24/LerMPV	0.000	***	0.190		1.000	
LerxC24-C24/LerMPV	0.000	***	0.281		0.991	
Ler-C24xLer	0.003	**	0.000	***	0.111	
LerxC24-C24xLer	0.000	***	0.000	***	0.200	
LerxC24-Ler	0.913		0.998		0.998	

Cell size	28 DAS leaf 3/4		19 DAS leaf 3/4		19 DAS leaf 5/6	
C24/LerMPV-C24	0.011		0.832		1.000	
C24xLer-C24	0.000	***	0.031	*	0.448	
Ler-C24	0.000	***	0.300		0.998	
LerxC24-C24	0.000	***	0.634		0.997	
C24xLer-C24/LerMPV	0.185		0.154		0.535	
Ler-C24/LerMPV	0.006	**	0.832		1.000	
LerxC24-C24/LerMPV	0.682		0.995		1.000	
Ler-C24xLer	0.718		0.576		0.626	
LerxC24-C24xLer	0.852		0.261		0.653	
LerxC24-Ler	0.138		0.959		1.000	

Cell number	28 DAS leaf 3/4		19 DAS leaf 3/4		19 DAS leaf 5/6	
C24/LerMPV-C24	0.139		0.996		1.000	
C24xLer-C24	0.000	***	0.035	*	0.866	
Ler-C24	0.000	***	0.949		1.000	
LerxC24-C24	0.000	***	0.643		0.968	
C24xLer-C24/LerMPV	0.000	***	0.061		0.858	
Ler-C24/LerMPV	0.176		0.996		1.000	
LerxC24-C24/LerMPV	0.016	*	0.831		0.965	
Ler-C24xLer	0.001	**	0.105		0.850	
LerxC24-C24xLer	0.024	*	0.282		0.997	
LerxC24-Ler	0.832		0.955		0.961	

Appendix 3.14

C24/Ler	P value	Col/Ler	P value	Ws/Ler	P value
C24/LerMPV-C24	1.000	Col/LerMPV-Col	1.000	LerxWs-Ler	0.994
C24xLer-C24	0.667	ColxLer-Col	0.814	Ws-Ler	0.983
Ler-C24	1.000	Ler-Col	0.996	Ws/LerMPV-Ler	0.999
LerxC24-C24	0.998	LerxCol-Col	0.973	WsxLer-Ler	0.996
C24xLer-C24/LerMPV	0.631	ColxLer-Col/LerMPV	0.910	Ws-LerxWs	0.877
Ler-C24/LerMPV	1.000	Ler-Col/LerMPV	1.000	Ws/LerMPV-LerxWs	0.960
LerxC24-C24/LerMPV	0.996	LerxCol-Col/LerMPV	0.952	WsxLer-LerxWs	0.936
Ler-C24xLer	0.595	Ler-ColxLer	0.956	Ws/LerMPV-Ws	0.999
LerxC24-C24xLer	0.834	LerxCol-ColxLer	0.573	WsxLer-Ws	1.000
LerxC24-Ler	0.993	LerxCol-Ler	0.899	WsxLer-Ws/LerMPV	1.000

Appendix 3.15b

	P value
C24xLer-C24	0.409
Ler-C24	0.293
LerxC24-C24	0.388
Ler-C24xLer	0.992
LerxC24-C24xLer	1.000
LerxC24-Ler	0.995

Appendix 3.16a

ANOVA comparisons of hybrid and parent combination to see if there is significant difference between the samples within the dataset (bold). If so, the detail comparisons are shown in the next table.

Combination	Light	p value	Combination	Light	p value
C24/Ler	30 uE	0.565	C24/Col	30 uE	0.554

C24/Ler	140 uE	0.940	C24/Col	140 uE	0.959
C24/Ler	200 uE	0.485	C24/Col	200 uE	0.812
C24/Ler	330 uE	0.425	C24/Col	330 uE	**0.005**
C24/Ler	440 uE	**0.003**	C24/Col	440 uE	**0.003**
C24/Ler	550 uE	**0.000**	C24/Col	550 uE	0.001
C24/Ler	640 uE	**0.000**	C24/Col	640 uE	**0.000**
C24/Ler	720 uE	**0.000**	C24/Col	720 uE	**0.000**
C24/Ler	850 uE	**0.000**	C24/Col	850 uE	**0.003**
C24/Ler	950 uE	**0.007**	Col/Ler	30 uE	0.120
C24/Ler	1000 uE	**0.006**	Col/Ler	200 uE	0.053
Ws/Ler	30 uE	0.139	Col/Ler	330 uE	0.622
Ws/Ler	200 uE	0.510	Col/Ler	440 uE	0.366
Ws/Ler	330 uE	0.157	Col/Ler	550 uE	0.571
Ws/Ler	440 uE	0.581	Col/Ler	640 uE	0.486
Ws/Ler	550 uE	0.346	Col/Ler	720 uE	0.284
Ws/Ler	640 uE	0.982	Col/Ler	850 uE	0.934
Ws/Ler	720 uE	0.343			
Ws/Ler	850 uE	0.812			

C24/Ler 440uE	p value		C24/Col 330uE	p value	
C24xLer-C24	0.007	**	C24xCol-C24	0.897	
Ler-C24	0.008	**	Col-C24	0.004	**
LerxC24-C24	0.231		ColxC24-C24	0.256	
Ler-C24xLer	0.691		Col-C24xCol	0.091	
LerxC24-C24xLer	0.745		ColxC24-C24xCol	0.744	
LerxC24-Ler	0.995		ColxC24-Col	0.565	
C24/Ler 550uE	p value		C24/Col 440uE	p value	
C24xLer-C24	0.031	*	C24xCol-C24	0.731	
Ler-C24	0.000	***	Col-C24	0.048	*
LerxC24-C24	0.006	**	ColxC24-C24	0.003	**
Ler-C24xLer	1.000		Col-C24xCol	0.577	
LerxC24-C24xLer	0.982		ColxC24-C24xCol	0.097	
LerxC24-Ler	0.937		ColxC24-Col	0.527	
C24/Ler 640uE	pvalue		C24/Col 550uE	p value	
C24xLer-C24	0.000	***	C24xCol-C24	0.023	*
Ler-C24	0.000	***	Col-C24	0.000	***
LerxC24-C24	0.002	**	ColxC24-C24	0.336	
Ler-C24xLer	0.976		Col-C24xCol	0.976	

LerxC24-C24xLer	0.805		ColxC24-C24xCol	0.537	
LerxC24-Ler	0.887		ColxC24-Col	0.171	
C24/Ler 720uE	p value		C24/Col 720uE	p value	
C24xLer-C24	0.029	*	C24xCol-C24	0.796	
Ler-C24	0.000	***	Col-C24	0.000	***
LerxC24-C24	0.008	**	ColxC24-C24	0.046	*
Ler-C24xLer	0.984		Col-C24xCol	0.009	**
LerxC24-C24xLer	0.961		ColxC24-C24xCol	0.236	
LerxC24-Ler	0.992		ColxC24-Col	0.978	
C24/Ler 850uE	p value		C24/Col 850uE	p	
C24xLer-C24	0.002	**	C24xCol-C24	0.363	
Ler-C24	0.000	***	Col-C24	0.002	**
LerxC24-C24	0.028	*	ColxC24-C24	0.085	
Ler-C24xLer	1.000		Col-C24xCol	0.238	
LerxC24-C24xLer	0.807		ColxC24-C24xCol	0.887	
LerxC24-Ler	0.679		ColxC24-Col	0.656	
C24/Ler 950 uE	p value		C24/Ler 1000uE	p value	
C24xLer-C24	0.011	*	C24xLer-C24	0.006	**
Ler-C24	0.023	*	Ler-C24	0.079	
LerxC24-C24	0.017	*	LerxC24-C24	0.227	
Ler-C24xLer	0.929		Ler-C24xLer	0.641	
LerxC24-C24xLer	0.988		LerxC24-C24xLer	0.372	
LerxC24-Ler	0.992		LerxC24-Ler	0.959	

Appendix 3.16b

ANOVA comparisons of hybrid and parent combination to see if there is significant difference between the samples within the dataset (bold). If so, the detail comparisons are shown in the next table.

Combination	Light	p value	Combination	Light	p value
C24/Ler	30 uE	0.018	C24/Col	30 uE	0.232

C24/Ler	200 uE	0.120	C24/Col	200 uE	0.942
C24/Ler	330 uE	0.014	C24/Col	330 uE	0.279
C24/Ler	440 uE	0.000	C24/Col	440 uE	**0.047**
C24/Ler	550 uE	0.004	C24/Col	550 uE	0.269
C24/Ler	640 uE	0.364	C24/Col	640 uE	0.056
C24/Ler	720 uE	0.055	C24/Col	720 uE	**0.027**
C24/Ler	850 uE	0.011	C24/Col	850 uE	**0.018**
Col/Ler	30 uE	0.603	Ws/Ler	30 uE	0.276
Col/Ler	200 uE	0.197	Ws/Ler	200 uE	0.928
Col/Ler	330 uE	0.267	Ws/Ler	330 uE	0.259
Col/Ler	440 uE	0.526	Ws/Ler	440 uE	0.568
Col/Ler	550 uE	0.699	Ws/Ler	550 uE	0.603
Col/Ler	640 uE	0.643	Ws/Ler	640 uE	0.403
Col/Ler	720 uE	0.838	Ws/Ler	720 uE	0.677
Col/Ler	850 uE	0.592	Ws/Ler	850 uE	0.440

C24/Ler 30uE	pvalue		C24/Col 330uE	p value	
C24xLer-C24	0.621		C24xCol-C24	0.550	
Ler-C24	0.976		Col-C24	0.119	
LerxC24-C24	0.169		ColxC24-C24	0.045	*
Ler-C24xLer	0.277		Col-C24xCol	0.800	
LerxC24-C24xLer	0.011	*	ColxC24-C24xCol	0.394	
LerxC24-Ler	0.171		ColxC24-Col	0.806	
C24/Ler 200uE	p value		C24/Col 720uE	p value	
C24xLer-C24	0.464		C24xCol-C24	0.840	
Ler-C24	0.415		Col-C24	0.112	
LerxC24-C24	0.555		ColxC24-C24	0.038	*
Ler-C24xLer	0.996		Col-C24xCol	0.444	
LerxC24-C24xLer	0.042	*	ColxC24-C24xCol	0.160	
LerxC24-Ler	0.017	*	ColxC24-Col	0.779	
C24/Ler 330uE	p value			p value	
C24xLer-C24	0.001	**	C24xCol-C24	0.648	
Ler-C24	0.064		Col-C24	0.024	*
LerxC24-C24	0.998		ColxC24-C24	0.065	
Ler-C24xLer	0.110		Col-C24xCol	0.275	
LerxC24-C24xLer	0.001	***	ColxC24-C24xCol	0.407	

LerxC24-Ler	0.040	*	ColxC24-Col	1.000	
C24/Ler 440uE	p value		C24/Ler 850uE	p value	
C24xLer-C24	0.908		C24xLer-C24	0.912	
Ler-C24	0.616		Ler-C24	0.245	
LerxC24-C24	0.126		LerxC24-C24	0.465	
Ler-C24xLer	0.979		Ler-C24xLer	0.715	
LerxC24-C24xLer	0.032	*	LerxC24-C24xLer	0.185	
LerxC24-Ler	0.002	**	LerxC24-Ler	0.007	**

Appendix 3.17

ANOVA comparisons of hybrid and parent combination to see if there is significant difference between the samples within the dataset (bold). If so, the detail comparisons are shown in the next table.

Combination	Suc	p value
C24/Ler	with	**0.000**
C24/Ler	without	**0.017**
C24/Col	with	**0.000**
C24/Col	without	0.289
Col/Ler	with	0.254
Col/Ler	without	0.782
Ws/Ler	with	0.997
Ws/Ler	without	0.231

with sucrose	p		without sucrose	p	
C24xLer-C24	0.001	***	C24xLer-C24	0.960	
Ler-C24	0.000	***	Ler-C24	0.138	
LerxC24-C24	0.004	**	LerxC24-C24	0.661	
Ler-C24xLer	0.999		Ler-C24xLer	0.109	
LerxC24-C24xLer	0.912		LerxC24-C24xLer	0.919	
LerxC24-Ler	0.892		LerxC24-Ler	0.039	*
C24xCol-C24	0.141				
Col-C24	0.000	***			

ColxC24-C24	0.019	*
Col-C24xCol	0.106	
ColxC24-C24xCol	0.880	
ColxC24-Col	0.458	

Appendix 3.18

Comparison of net CO_2 assimilation rate

C24/Ler	p value	C24/Col	p value
Ca=50	**0.000**	Ca=50	0.155
Ca=100	0.202	Ca=100	0.158
Ca=200	0.377	Ca=200	0.294
Ca=400	0.080	Ca=400	0.091
Ca=600	**0.020**	Ca=600	0.056
Ca=800	**0.006**	Ca=800	**0.029**
Ca=1000	**0.012**	Ca=1000	**0.017**
Ca=1200	**0.006**	Ca=1200	**0.033**
Ca=1500	**0.005**	Ca=1500	**0.041**
Col/Ler	p value	Ws/Ler	p value
Ca=50	0.186	Ca=50	0.051
Ca=100	0.234	Ca=100	0.161
Ca=200	0.817	Ca=200	0.496
Ca=400	0.816	Ca=400	0.209
Ca=600	0.689	Ca=600	0.251
Ca=800	0.393	Ca=800	0.245
Ca=1000	0.533	Ca=1000	0.266
Ca=1200	0.323	Ca=1200	0.258
Ca=1500	0.368	Ca=1500	0.196

Ca=50, C24/Ler	p value		Ca=800, C24/Col	p value	
C24xLer-C24	0.000	***	C24xCol-C24	0.486	
Ler-C24	0.564		Col-C24	0.022	*
LerxC24-C24	0.000	***	ColxC24-C24	0.155	
Ler-C24xLer	0.001	***	Col-C24xCol	0.173	
LerxC24-C24xLer	0.993		ColxC24-C24xCol	0.801	
LerxC24-Ler	0.001	**	ColxC24-Col	0.528	

Ca=600, C24/Ler	p value		Ca=1000, C24/Col	p value	
C24xLer-C24	0.687		C24xCol-C24	0.389	
Ler-C24	0.020	*	Col-C24	0.012	*
LerxC24-C24	0.934		ColxC24-C24	0.113	
Ler-C24xLer	0.071		Col-C24xCol	0.128	
LerxC24-C24xLer	0.958		ColxC24-C24xCol	0.786	
LerxC24-Ler	0.047	*	ColxC24-Col	0.431	

Ca=800, C24/Ler	p value		Ca=1200, C24/Col	p value	
C24xLer-C24	0.360		C24xCol-C24	0.402	
Ler-C24	0.005	**	Col-C24	0.026	*
LerxC24-C24	0.812		ColxC24-C24	0.125	
Ler-C24xLer	0.039	*	Col-C24xCol	0.257	
LerxC24-C24xLer	0.858		ColxC24-C24xCol	0.809	
LerxC24-Ler	0.018	*	ColxC24-Col	0.683	

Ca=1000, C24/Ler	p value		Ca=1500, C24/Col	p value	
C24xLer-C24	0.384		C24xCol-C24	0.261	
Ler-C24	0.010	**	Col-C24	0.035	*
LerxC24-C24	0.812		ColxC24-C24	0.097	
Ler-C24xLer	0.077		Col-C24xCol	0.508	
LerxC24-C24xLer	0.880		ColxC24-C24xCol	0.883	
LerxC24-Ler	0.036	*	ColxC24-Col	0.887	

Ca=1200, C24/Ler	p value	
C24xLer-C24	0.237	
Ler-C24	0.005	**
LerxC24-C24	0.759	
Ler-C24xLer	0.056	
LerxC24-C24xLer	0.753	
LerxC24-Ler	0.019	*

Ca=1500, C24/Ler	p value	
C24xLer-C24	0.104	
Ler-C24	0.003	**

LerxC24-C24	0.483	
Ler-C24xLer	0.089	
LerxC24-C24xLer	0.728	
LerxC24-Ler	0.027	*

Appendix 3.19

	p value			p value	
C24/ColMPV-C24	0.969		LerxCol-C24xLer	1.000	
C24/LerMPV-C24	1.000		LerxWs-C24xLer	0.948	
C24xCol-C24	1.000		Ws-C24xLer	1.000	
C24xLer-C24	0.800		Ws/LerMPV-C24xLer	1.000	
Col-C24	0.924		WsxLer-C24xLer	1.000	
Col/LerMPV-C24	1.000		Col/LerMPV-Col	1.000	
ColxC24-C24	0.950		ColxC24-Col	0.240	
ColxLer-C24	0.344		ColxLer-Col	0.023	*
Ler-C24	0.759		Ler-Col	0.074	
LerxC24-C24	0.990		LerxC24-Col	0.369	
LerxCol-C24	0.542		LerxCol-Col	0.046	*
LerxWs-C24	1.000		LerxWs-Col	0.892	
Ws-C24	0.543		Ws-Col	0.047	*
Ws/LerMPV-C24	0.463		Ws/LerMPV-Col	0.041	*
WsxLer-C24	0.995		WsxLer-Col	0.375	
C24/LerMPV-C24/ColMPV	0.700		ColxC24-Col/LerMPV	0.792	
C24xCol-C24/ColMPV	0.874		ColxLer-Col/LerMPV	0.227	
C24xLer-C24/ColMPV	0.173		Ler-Col/LerMPV	0.550	
Col-C24/ColMPV	1.000		LerxC24-Col/LerMPV	0.906	
Col/LerMPV-C24/ColMPV	1.000		LerxCol-Col/LerMPV	0.362	
ColxC24-C24/ColMPV	0.322		LerxWs-Col/LerMPV	1.000	
ColxLer-C24/ColMPV	0.037	*	Ws-Col/LerMPV	0.363	
Ler-C24/ColMPV	0.117		Ws/LerMPV-Col/LerMPV	0.301	
LerxC24-C24/ColMPV	0.472		WsxLer-Col/LerMPV	0.930	
LerxCol-C24/ColMPV	0.072		ColxLer-ColxC24	1.000	
LerxWs-C24/ColMPV	0.948		Ler-ColxC24	1.000	
Ws-C24/ColMPV	0.072		LerxC24-ColxC24	1.000	
Ws/LerMPV-C24/ColMPV	0.062		LerxCol-ColxC24	1.000	
WsxLer-C24/ColMPV	0.487		LerxWs-ColxC24	0.994	
C24xCol-C24/LerMPV	1.000		Ws-ColxC24	1.000	

C24xLer-C24/LerMPV	0.988		Ws/LerMPV-ColxC24	1.000	
Col-C24/LerMPV	0.574		WsxLer-ColxC24	1.000	
Col/LerMPV-C24/LerMPV	0.992		Ler-ColxLer	1.000	
ColxC24-C24/LerMPV	1.000		LerxC24-ColxLer	0.999	
ColxLer-C24/LerMPV	0.793		LerxCol-ColxLer	1.000	
Ler-C24/LerMPV	0.995		LerxWs-ColxLer	0.654	
LerxC24-C24/LerMPV	1.000		Ws-ColxLer	1.000	
LerxCol-C24/LerMPV	0.928		Ws/LerMPV-ColxLer	1.000	
LerxWs-C24/LerMPV	1.000		WsxLer-ColxLer	0.992	
Ws-C24/LerMPV	0.928		LerxC24-Ler	1.000	
Ws/LerMPV-C24/LerMPV	0.860		LerxCol-Ler	1.000	
WsxLer-C24/LerMPV	1.000		LerxWs-Ler	0.961	
C24xLer-C24xCol	0.997		Ws-Ler	1.000	
Col-C24xCol	0.792		Ws/LerMPV-Ler	1.000	
Col/LerMPV-C24xCol	0.998		WsxLer-Ler	1.000	
ColxC24-C24xCol	1.000		LerxCol-LerxC24	1.000	
ColxLer-C24xCol	0.923		LerxWs-LerxC24	0.999	
Ler-C24xCol	0.999		Ws-LerxC24	1.000	
LerxC24-C24xCol	1.000		Ws/LerMPV-LerxC24	1.000	
LerxCol-C24xCol	0.979		WsxLer-LerxC24	1.000	
LerxWs-C24xCol	1.000		LerxWs-LerxCol	0.825	
Ws-C24xCol	0.979		Ws-LerxCol	1.000	
Ws/LerMPV-C24xCol	0.944		Ws/LerMPV-LerxCol	1.000	
WsxLer-C24xCol	1.000		WsxLer-LerxCol	0.999	
Col-C24xLer	0.122		Ws-LerxWs	0.826	
Col/LerMPV-C24xLer	0.583		Ws/LerMPV-LerxWs	0.735	
ColxC24-C24xLer	1.000		WsxLer-LerxWs	1.000	
ColxLer-C24xLer	1.000		Ws/LerMPV-Ws	1.000	
Ler-C24xLer	1.000		WsxLer-Ws	0.999	
LerxC24-C24xLer	1.000		WsxLer-Ws/LerMPV	0.995	

Appendix 3.20

Comparisons	p value
Chla	0.731
Chlb	**0.014**
a/b ratio	0.302

Chlb	p value				
C24/LerMPV-C24	0.887		Ler-C24/LerMPV	0.887	
C24xLer-C24	0.333		LerxC24-C24/LerMPV	0.141	
Ler-C24	0.415		Ler-C24xLer	0.022	*
LerxC24-C24	0.472		LerxC24-C24xLer	0.998	
C24xLer-C24/LerMPV	0.091		LerxC24-Ler	0.035	*

Appendix 3.21a

10 DAS	p value
C24xLer-C24	0.994
Ler-C24	0.923
LerxC24-C24	1.000
Ler-C24xLer	0.694
LerxC24-C24xLer	0.981
LerxC24-Ler	0.917

19DAS	p value
C24xLer-C24	0.599
Ler-C24	0.166
LerxC24-C24	0.924
Ler-C24xLer	0.768
LerxC24-C24xLer	0.345
LerxC24-Ler	0.088

Appendix 4.1b

120uE	p value		240uE	p value	
C24/LerMPV-C24	0.860		C24/LerMPV-C24	0.999	
C24xLer-C24	0.000	***	C24xLer-C24	0.000	***
Ler-C24	0.286		Ler-C24	0.999	
LerxC24-C24	0.000	***	LerxC24-C24	0.000	***
C24xLer-C24/LerMPV	0.000	***	C24xLer-C24/LerMPV	0.000	***
Ler-C24/LerMPV	0.860		Ler-C24/LerMPV	0.999	
LerxC24-C24/LerMPV	0.000	***	LerxC24-C24/LerMPV	0.000	***
Ler-C24xLer	0.003	**	Ler-C24xLer	0.000	***
LerxC24-C24xLer	0.916		LerxC24-C24xLer	0.429	
LerxC24-Ler	0.000	***	LerxC24-Ler	0.000	***

Appendix 4.1c

120uE vs 240uE	p value

C24xLer	0.091
LerxC24	0.735

Appendix 4.2

	15 DAS		18 DAS		21 DAS	
C24xLer:120uE-C24:120uE	0.933		0.228		0.003	**
Ler:120uE-C24:120uE	0.933		0.997		0.000	***
LerxC24:120uE-C24:120uE	0.933		0.050	*	0.091	
C24:240uE-C24:120uE	0.136		0.001		0.000	**
C24xLer:240uE-C24:120uE	0.007	**	0.000	***	0.000	***
Ler:240uE-C24:120uE	0.287		0.877		0.341	
LerxC24:240uE-C24:120uE	0.002	**	0.000	***	0.000	***
Ler:120uE-C24xLer:120uE	0.287		0.625		0.000	***
LerxC24:120uE-C24xLer:120uE	1.000		0.997		0.951	
C24:240uE-C24xLer:120uE	0.762		0.303		0.002	**
C24xLer:240uE-C24xLer:120uE	0.136		0.000	***	0.000	***
Ler:240uE-C24xLer:120uE	0.933		0.949		0.000	***
LerxC24:240uE-C24xLer:120uE	0.056		0.007	**	0.000	***
LerxC24:120uE-Ler:120uE	0.287		0.228		0.000	***
C24:240uE-Ler:120uE	0.007	**	0.007	**	0.000	***
C24xLer:240uE-Ler:120uE	0.000	***	0.000	***	0.000	***
Ler:240uE-Ler:120uE	0.021	*	0.997		0.039	*
LerxC24:240uE-Ler:120uE	0.000	***	0.000	***	0.000	***
C24:240uE-LerxC24:120uE	0.762		0.658		0.000	***
C24xLer:240uE-LerxC24:120uE	0.136		0.000	***	0.000	***
Ler:240uE-LerxC24:120uE	0.933		0.625		0.000	***
LerxC24:240uE-LerxC24:120uE	0.056		0.050	*	0.000	***
C24xLer:240uE-C24:240uE	0.933		0.344		0.052	
Ler:240uE-C24:240uE	1.000		0.036	*	0.000	***
LerxC24:240uE-C24:240uE	0.762		0.984		0.440	
Ler:240uE-C24xLer:240uE	0.762		0.000	***	0.000	***
LerxC24:240uE-C24xLer:240uE	1.000		0.765		0.973	
LerxC24:240uE-Ler:240uE	0.515		0.000	***	0.000	***

Appendix 4.3b

ANOVA comparisons of hybrid and parent combination to see if there is significant difference between the samples within the dataset (bold). If so, the detail comparisons are shown in the next table.

19 DAS, 240uE	p value
T1	0.104
T2	**0.011**
T3	**0.002**
T4	**0.007**
T5	**0.002**
T6	**0.001**
T7	**0.001**
T8	**0.005**
T9	**0.034**
T10	0.372
T11	0.200
T12	0.381
T13	0.212

19 DAS, 240uE	T2		T3		T4		T5		T6	
C24xLer-C24	0.0114	*	0.0016	**	0.0221	*	0.0185	*	0.0112	*
Ler-C24	0.0286	*	0.0228	*	0.4765		0.2731		0.9444	
LerxC24-C24	0.0604		0.0178	*	0.0131	*	0.0022	**	0.0059	**
MPV-C24	0.4114		0.3762		0.9090		0.8156		0.9956	
Ler-C24xLer	0.9714		0.4171		0.2829		0.4319		0.0343	*
LerxC24-C24xLer	0.8107		0.4998		0.9967		0.6015		0.9919	
MPV-C24xLer	0.1846		0.0260	*	0.0821		0.0975		0.0195	*
LerxC24-Ler	0.9874		0.9998		0.1762		0.0530		0.0177	
MPV-Ler	0.4114		0.3762		0.9090		0.8156		0.9956	
MPV-LerxC24	0.6725		0.3070		0.0486	*	0.0102	*	0.0102	*

19 DAS, 240uE	T7		T8		T9	
C24xLer-C24	0.0369	*	0.0674		0.2166	
Ler-C24	0.7407		0.4000		0.6431	
LerxC24-C24	0.0256	*	0.8772		0.9790	
MPV-C24	0.9702		0.8811		0.9523	
Ler-C24xLer	0.0058	**	0.0041	**	0.0260	*
LerxC24-C24xLer	0.9992		0.2673		0.4427	
MPV-C24xLer	0.0144	*	0.0161	*	0.0767	
LerxC24-Ler	0.0041	**	0.1092		0.3533	
MPV-Ler	0.9702		0.8811		0.9523	
MPV-LerxC24	0.0101	*	0.3953		0.7238	

Appendix 4.3c, d

	p value		p value
T2:120uE-T1:120uE	1.000	T9:120uE-T6:120uE	1.000
T3:120uE-T1:120uE	1.000	T1:240uE-T6:120uE	1.000
T4:120uE-T1:120uE	1.000	T2:240uE-T6:120uE	1.000
T5:120uE-T1:120uE	1.000	T3:240uE-T6:120uE	1.000
T6:120uE-T1:120uE	1.000	T4:240uE-T6:120uE	1.000
T7:120uE-T1:120uE	1.000	T5:240uE-T6:120uE	1.000
T8:120uE-T1:120uE	1.000	T6:240uE-T6:120uE	0.613
T9:120uE-T1:120uE	1.000	T7:240uE-T6:120uE	0.999
T1:240uE-T1:120uE	1.000	T8:240uE-T6:120uE	1.000
T2:240uE-T1:120uE	1.000	T9:240uE-T6:120uE	1.000
T3:240uE-T1:120uE	1.000	T8:120uE-T7:120uE	1.000
T4:240uE-T1:120uE	1.000	T9:120uE-T7:120uE	1.000
T5:240uE-T1:120uE	1.000	T1:240uE-T7:120uE	1.000
T6:240uE-T1:120uE	0.890	T2:240uE-T7:120uE	1.000
T7:240uE-T1:120uE	1.000	T3:240uE-T7:120uE	1.000
T8:240uE-T1:120uE	1.000	T4:240uE-T7:120uE	1.000
T9:240uE-T1:120uE	1.000	T5:240uE-T7:120uE	1.000
T3:120uE-T2:120uE	1.000	T6:240uE-T7:120uE	0.921
T4:120uE-T2:120uE	1.000	T7:240uE-T7:120uE	1.000
T5:120uE-T2:120uE	1.000	T8:240uE-T7:120uE	1.000
T6:120uE-T2:120uE	1.000	T9:240uE-T7:120uE	1.000
T7:120uE-T2:120uE	1.000	T9:120uE-T8:120uE	1.000

T8:120uE-T2:120uE	1.000	T1:240uE-T8:120uE	1.000
T9:120uE-T2:120uE	1.000	T2:240uE-T8:120uE	1.000
T1:240uE-T2:120uE	1.000	T3:240uE-T8:120uE	1.000
T2:240uE-T2:120uE	1.000	T4:240uE-T8:120uE	1.000
T3:240uE-T2:120uE	1.000	T5:240uE-T8:120uE	1.000
T4:240uE-T2:120uE	1.000	T6:240uE-T8:120uE	0.901
T5:240uE-T2:120uE	1.000	T7:240uE-T8:120uE	1.000
T6:240uE-T2:120uE	0.930	T8:240uE-T8:120uE	1.000
T7:240uE-T2:120uE	1.000	T9:240uE-T8:120uE	1.000
T8:240uE-T2:120uE	1.000	T1:240uE-T9:120uE	1.000
T9:240uE-T2:120uE	1.000	T2:240uE-T9:120uE	1.000
T4:120uE-T3:120uE	1.000	T3:240uE-T9:120uE	1.000
T5:120uE-T3:120uE	1.000	T4:240uE-T9:120uE	1.000
T6:120uE-T3:120uE	1.000	T5:240uE-T9:120uE	1.000
T7:120uE-T3:120uE	1.000	T6:240uE-T9:120uE	0.911
T8:120uE-T3:120uE	1.000	T7:240uE-T9:120uE	1.000
T9:120uE-T3:120uE	1.000	T8:240uE-T9:120uE	1.000
T1:240uE-T3:120uE	0.999	T9:240uE-T9:120uE	1.000
T2:240uE-T3:120uE	1.000	T2:240uE-T1:240uE	1.000
T3:240uE-T3:120uE	1.000	T3:240uE-T1:240uE	1.000
T4:240uE-T3:120uE	1.000	T4:240uE-T1:240uE	1.000
T5:240uE-T3:120uE	1.000	T5:240uE-T1:240uE	0.999
T6:240uE-T3:120uE	0.991	T6:240uE-T1:240uE	0.483
T7:240uE-T3:120uE	1.000	T7:240uE-T1:240uE	0.996
T8:240uE-T3:120uE	1.000	T8:240uE-T1:240uE	1.000
T9:240uE-T3:120uE	0.996	T9:240uE-T1:240uE	1.000
T5:120uE-T4:120uE	1.000	T3:240uE-T2:240uE	1.000
T6:120uE-T4:120uE	1.000	T4:240uE-T2:240uE	1.000
T7:120uE-T4:120uE	1.000	T5:240uE-T2:240uE	1.000
T8:120uE-T4:120uE	1.000	T6:240uE-T2:240uE	0.710
T9:120uE-T4:120uE	1.000	T7:240uE-T2:240uE	1.000
T1:240uE-T4:120uE	0.999	T8:240uE-T2:240uE	1.000
T2:240uE-T4:120uE	1.000	T9:240uE-T2:240uE	1.000
T3:240uE-T4:120uE	1.000	T4:240uE-T3:240uE	1.000
T4:240uE-T4:120uE	1.000	T5:240uE-T3:240uE	1.000
T5:240uE-T4:120uE	1.000	T6:240uE-T3:240uE	0.927
T6:240uE-T4:120uE	0.989	T7:240uE-T3:240uE	1.000
T7:240uE-T4:120uE	1.000	T8:240uE-T3:240uE	1.000
T8:240uE-T4:120uE	1.000	T9:240uE-T3:240uE	1.000
T9:240uE-T4:120uE	0.997	T5:240uE-T4:240uE	1.000
T6:120uE-T5:120uE	1.000	T6:240uE-T4:240uE	0.773
T7:120uE-T5:120uE	1.000	T7:240uE-T4:240uE	1.000
T8:120uE-T5:120uE	1.000	T8:240uE-T4:240uE	1.000
T9:120uE-T5:120uE	1.000	T9:240uE-T4:240uE	1.000

T1:240uE-T5:120uE	1.000	T6:240uE-T5:240uE	0.992
T2:240uE-T5:120uE	1.000	T7:240uE-T5:240uE	1.000
T3:240uE-T5:120uE	1.000	T8:240uE-T5:240uE	1.000
T4:240uE-T5:120uE	1.000	T9:240uE-T5:240uE	0.995
T5:240uE-T5:120uE	1.000	T7:240uE-T6:240uE	0.998
T6:240uE-T5:120uE	0.898	T8:240uE-T6:240uE	0.835
T7:240uE-T5:120uE	1.000	T9:240uE-T6:240uE	0.380
T8:240uE-T5:120uE	1.000	T8:240uE-T7:240uE	1.000
T9:240uE-T5:120uE	1.000	T9:240uE-T7:240uE	0.986
T7:120uE-T6:120uE	1.000	T9:240uE-T8:240uE	1.000
T8:120uE-T6:120uE	1.000		

LerxC24	p value		LerxC24	p value	
T2:120uE-T1:120uE	1.000		T3:240uE-T6:120uE	1.000	
T3:120uE-T1:120uE	0.788		T4:240uE-T6:120uE	1.000	
T4:120uE-T1:120uE	0.997		T5:240uE-T6:120uE	0.901	
T5:120uE-T1:120uE	0.573		T6:240uE-T6:120uE	0.707	
T6:120uE-T1:120uE	0.937		T7:240uE-T6:120uE	1.000	
T7:120uE-T1:120uE	0.924		T8:240uE-T6:120uE	1.000	
T8:120uE-T1:120uE	0.982		T9:240uE-T6:120uE	0.991	
T9:120uE-T1:120uE	0.142		T8:120uE-T7:120uE	1.000	
T1:240uE-T1:120uE	0.999		T9:120uE-T7:120uE	0.993	
T10:240uE-T1:120uE	0.000	***	T1:240uE-T7:120uE	1.000	
T2:240uE-T1:120uE	1.000		T10:240uE-T7:120uE	0.000	
T3:240uE-T1:120uE	1.000		T2:240uE-T7:120uE	0.772	
T4:240uE-T1:120uE	0.978		T3:240uE-T7:120uE	1.000	
T5:240uE-T1:120uE	1.000		T4:240uE-T7:120uE	1.000	
T6:240uE-T1:120uE	1.000		T5:240uE-T7:120uE	0.884	
T7:240uE-T1:120uE	1.000		T6:240uE-T7:120uE	0.678	
T8:240uE-T1:120uE	1.000		T7:240uE-T7:120uE	1.000	
T9:240uE-T1:120uE	0.145		T8:240uE-T7:120uE	1.000	
T3:120uE-T2:120uE	0.942		T9:240uE-T7:120uE	0.994	
T4:120uE-T2:120uE	1.000		T9:120uE-T8:120uE	0.961	
T5:120uE-T2:120uE	0.805		T1:240uE-T8:120uE	1.000	
T6:120uE-T2:120uE	0.992		T10:240uE-T8:120uE	0.000	***
T7:120uE-T2:120uE	0.989		T2:240uE-T8:120uE	0.907	
T8:120uE-T2:120uE	0.999		T3:240uE-T8:120uE	1.000	
T9:120uE-T2:120uE	0.289		T4:240uE-T8:120uE	1.000	
T1:240uE-T2:120uE	1.000		T5:240uE-T8:120uE	0.966	
T10:240uE-T2:120uE	0.000	***	T6:240uE-T8:120uE	0.844	
T2:240uE-T2:120uE	1.000		T7:240uE-T8:120uE	1.000	
T3:240uE-T2:120uE	1.000		T8:240uE-T8:120uE	1.000	

T4:240uE-T2:120uE	0.999		T9:240uE-T8:120uE	0.963	
T5:240uE-T2:120uE	1.000		T1:240uE-T9:120uE	0.845	
T6:240uE-T2:120uE	1.000		T10:240uE-T9:120uE	0.008	**
T7:240uE-T2:120uE	1.000		T2:240uE-T9:120uE	0.067	
T8:240uE-T2:120uE	1.000		T3:240uE-T9:120uE	0.794	
T9:240uE-T2:120uE	0.295		T4:240uE-T9:120uE	0.966	
T4:120uE-T3:120uE	1.000		T5:240uE-T9:120uE	0.112	
T5:120uE-T3:120uE	1.000		T6:240uE-T9:120uE	0.046	*
T6:120uE-T3:120uE	1.000		T7:240uE-T9:120uE	0.680	
T7:120uE-T3:120uE	1.000		T8:240uE-T9:120uE	0.552	
T8:120uE-T3:120uE	1.000		T9:240uE-T9:120uE	1.000	
T9:120uE-T3:120uE	1.000		T10:240uE-T1:240uE	0.000	***
T1:240uE-T3:120uE	1.000		T2:240uE-T1:240uE	0.983	
T10:240uE-T3:120uE	0.000		T3:240uE-T1:240uE	1.000	
T2:240uE-T3:120uE	0.575		T4:240uE-T1:240uE	1.000	
T3:240uE-T3:120uE	1.000		T5:240uE-T1:240uE	0.997	
T4:240uE-T3:120uE	1.000		T6:240uE-T1:240uE	0.960	
T5:240uE-T3:120uE	0.723		T7:240uE-T1:240uE	1.000	
T6:240uE-T3:120uE	0.475		T8:240uE-T1:240uE	1.000	
T7:240uE-T3:120uE	0.999		T9:240uE-T1:240uE	0.851	
T8:240uE-T3:120uE	0.996		T2:240uE-T10:240uE	0.000	***
T9:240uE-T3:120uE	1.000		T3:240uE-T10:240uE	0.000	***
T5:120uE-T4:120uE	1.000		T4:240uE-T10:240uE	0.000	***
T6:120uE-T4:120uE	1.000		T5:240uE-T10:240uE	0.000	***
T7:120uE-T4:120uE	1.000		T6:240uE-T10:240uE	0.000	***
T8:120uE-T4:120uE	1.000		T7:240uE-T10:240uE	0.000	***
T9:120uE-T4:120uE	0.886		T8:240uE-T10:240uE	0.000	***
T1:240uE-T4:120uE	1.000		T9:240uE-T10:240uE	0.008	**
T10:240uE-T4:120uE	0.000		T3:240uE-T2:240uE	0.991	
T2:240uE-T4:120uE	0.971		T4:240uE-T2:240uE	0.896	
T3:240uE-T4:120uE	1.000		T5:240uE-T2:240uE	1.000	
T4:240uE-T4:120uE	1.000		T6:240uE-T2:240uE	1.000	
T5:240uE-T4:120uE	0.993		T7:240uE-T2:240uE	0.998	
T6:240uE-T4:120uE	0.938		T8:240uE-T2:240uE	1.000	
T7:240uE-T4:120uE	1.000		T9:240uE-T2:240uE	0.069	
T8:240uE-T4:120uE	1.000		T4:240uE-T3:240uE	1.000	
T9:240uE-T4:120uE	0.891		T5:240uE-T3:240uE	0.999	
T6:120uE-T5:120uE	1.000		T6:240uE-T3:240uE	0.976	
T7:120uE-T5:120uE	1.000		T7:240uE-T3:240uE	1.000	
T8:120uE-T5:120uE	1.000		T8:240uE-T3:240uE	1.000	
T9:120uE-T5:120uE	1.000		T9:240uE-T3:240uE	0.800	
T1:240uE-T5:120uE	0.999		T5:240uE-T4:240uE	0.961	
T10:240uE-T5:120uE	0.001	**	T6:240uE-T4:240uE	0.828	
T2:240uE-T5:120uE	0.360		T7:240uE-T4:240uE	1.000	

T3:240uE-T5:120uE	0.997		T8:240uE-T4:240uE	1.000	
T4:240uE-T5:120uE	1.000		T9:240uE-T4:240uE	0.968	
T5:240uE-T5:120uE	0.500		T6:240uE-T5:240uE	1.000	
T6:240uE-T5:120uE	0.279		T7:240uE-T5:240uE	1.000	
T7:240uE-T5:120uE	0.988		T8:240uE-T5:240uE	1.000	
T8:240uE-T5:120uE	0.963		T9:240uE-T5:240uE	0.115	
T9:240uE-T5:120uE	1.000		T7:240uE-T6:240uE	0.993	
T7:120uE-T6:120uE	1.000		T8:240uE-T6:240uE	0.999	
T8:120uE-T6:120uE	1.000		T9:240uE-T6:240uE	0.048	
T9:120uE-T6:120uE	0.991		T8:240uE-T7:240uE	1.000	
T1:240uE-T6:120uE	1.000		T9:240uE-T7:240uE	0.687	
T10:240uE-T6:120uE	0.000	***	T9:240uE-T8:240uE	0.560	
T2:240uE-T6:120uE	0.797				

C24xLer	p value	C24xLer	p value	C24xLer	p value	
T2:120uE-T1:120uE	1.000	T7:240uE-T3:120uE	0.878	T1:240uE-T7:120uE	0.969	
T3:120uE-T1:120uE	1.000	T8:240uE-T3:120uE	0.262	T2:240uE-T7:120uE	1.000	
T4:120uE-T1:120uE	1.000	T5:120uE-T4:120uE	1.000	T7:240uE-T7:120uE	0.992	
T5:120uE-T1:120uE	1.000	T6:120uE-T4:120uE	0.998	T8:240uE-T7:120uE	0.570	
T6:120uE-T1:120uE	0.917	T7:120uE-T4:120uE	1.000	T1:240uE-T8:120uE	0.906	
T7:120uE-T1:120uE	0.991	T8:120uE-T4:120uE	1.000	T2:240uE-T8:120uE	0.998	
T8:120uE-T1:120uE	0.960	T1:240uE-T4:120uE	1.000	T3:240uE-T8:120uE	1.000	
T1:240uE-T1:120uE	1.000	T2:240uE-T4:120uE	1.000	T4:240uE-T8:120uE	1.000	
T2:240uE-T1:120uE	1.000	T3:240uE-T4:120uE	1.000	T5:240uE-T8:120uE	1.000	
T3:240uE-T1:120uE	0.998	T4:240uE-T4:120uE	1.000	T6:240uE-T8:120uE	0.995	
T4:240uE-T1:120uE	1.000	T5:240uE-T4:120uE	1.000	T7:240uE-T8:120uE	0.999	
T5:240uE-T1:120uE	0.998	T6:240uE-T4:120uE	0.652	T8:240uE-T8:120uE	0.728	
T6:240uE-T1:120uE	0.296	T7:240uE-T4:120uE	0.762	T2:240uE-T1:240uE	1.000	
T7:240uE-T1:120uE	0.393	T8:240uE-T4:120uE	0.170	T3:240uE-T1:240uE	0.992	

T8:240uE-T1:120uE	0.048	T6:120uE-T5:120uE	0.999	T4:240uE-T1:240uE	1.000	
T3:120uE-T2:120uE	1.000	T7:120uE-T5:120uE	1.000	T5:240uE-T1:240uE	0.992	
T4:120uE-T2:120uE	1.000	T8:120uE-T5:120uE	1.000	T6:240uE-T1:240uE	0.209	
T5:120uE-T2:120uE	1.000	T1:240uE-T5:120uE	1.000	T7:240uE-T1:240uE	0.287	
T6:120uE-T2:120uE	0.943	T2:240uE-T5:120uE	1.000	T8:240uE-T1:240uE	0.030	*
T7:120uE-T2:120uE	0.995	T3:240uE-T5:120uE	1.000	T3:240uE-T2:240uE	1.000	
T8:120uE-T2:120uE	0.975	T3:240uE-T7:120uE	1.000	T4:240uE-T2:240uE	1.000	
T1:240uE-T2:120uE	1.000	T4:240uE-T7:120uE	1.000	T5:240uE-T2:240uE	1.000	
T2:240uE-T2:120uE	1.000	T5:240uE-T7:120uE	1.000	T6:240uE-T2:240uE	0.571	
T3:240uE-T2:120uE	0.999	T6:240uE-T7:120uE	0.974	T7:240uE-T2:240uE	0.686	
T4:240uE-T2:120uE	1.000	T4:240uE-T5:120uE	1.000	T8:240uE-T2:240uE	0.133	
T5:240uE-T2:120uE	0.999	T5:240uE-T5:120uE	1.000	T4:240uE-T3:240uE	1.000	
T6:240uE-T2:120uE	0.343	T6:240uE-T5:120uE	0.709	T5:240uE-T3:240uE	1.000	
T7:240uE-T2:120uE	0.447	T7:240uE-T5:120uE	0.812	T6:240uE-T3:240uE	0.925	
T8:240uE-T2:120uE	0.059	T8:240uE-T5:120uE	0.203	T7:240uE-T3:240uE	0.967	
T4:120uE-T3:120uE	1.000	T7:120uE-T6:120uE	1.000	T8:240uE-T3:240uE	0.428	
T5:120uE-T3:120uE	1.000	T8:120uE-T6:120uE	1.000	T5:240uE-T4:240uE	1.000	
T6:120uE-T3:120uE	1.000	T1:240uE-T6:120uE	0.837	T6:240uE-T4:240uE	0.783	
T7:120uE-T3:120uE	1.000	T2:240uE-T6:120uE	0.993	T7:240uE-T4:240uE	0.871	
T8:120uE-T3:120uE	1.000	T3:240uE-T6:120uE	1.000	T8:240uE-T4:240uE	0.254	
T1:240uE-T3:120uE	1.000	T4:240uE-T6:120uE	1.000	T6:240uE-T5:240uE	0.926	
T2:240uE-T3:120uE	1.000	T5:240uE-T6:120uE	1.000	T7:240uE-T5:240uE	0.968	
T3:240uE-T3:120uE	1.000	T6:240uE-T6:120uE	0.999	T8:240uE-T5:240uE	0.429	
T4:240uE-T3:120uE	1.000	T7:240uE-T6:120uE	1.000	T7:240uE-T6:240uE	1.000	

T5:240uE-T3:120uE	1.000	T8:240uE-T6:120uE	0.820	T8:240uE-T6:240uE	1.000	
T6:240uE-T3:120uE	0.792	T8:120uE-T7:120uE	1.000	T8:240uE-T7:240uE	0.999	

LerxC24	p value	LerxC24	p value	LerxC24	p value
T2:120uE-T1:120uE	1.000	T7:240uE-T3:120uE	0.831	T5:240uE-T7:120uE	0.4103
T3:120uE-T1:120uE	1.000	T8:240uE-T3:120uE	1.000	T6:240uE-T7:120uE	0.1687
T4:120uE-T1:120uE	1.000	T5:120uE-T4:120uE	1.000	T7:240uE-T7:120uE	0.2935
T5:120uE-T1:120uE	1.000	T6:120uE-T4:120uE	1.000	T8:240uE-T7:120uE	0.9914
T6:120uE-T1:120uE	1.000	T7:120uE-T4:120uE	1.000	T1:240uE-T8:120uE	1.0000
T7:120uE-T1:120uE	1.000	T8:120uE-T4:120uE	1.000	T2:240uE-T8:120uE	1.0000
T8:120uE-T1:120uE	1.000	T1:240uE-T4:120uE	1.000	T3:240uE-T8:120uE	1.0000
T1:240uE-T1:120uE	1.000	T2:240uE-T4:120uE	1.000	T4:240uE-T8:120uE	0.9975
T2:240uE-T1:120uE	1.000	T3:240uE-T4:120uE	1.000	T5:240uE-T8:120uE	0.6596
T3:240uE-T1:120uE	1.000	T4:240uE-T4:120uE	1.000	T6:240uE-T8:120uE	0.3381
T4:240uE-T1:120uE	0.967	T5:240uE-T4:120uE	0.760	T7:240uE-T8:120uE	0.5205
T5:240uE-T1:120uE	0.420	T6:240uE-T4:120uE	0.4322	T8:240uE-T8:120uE	0.9998
T6:240uE-T1:120uE	0.174	T7:240uE-T4:120uE	0.6272	T2:240uE-T1:240uE	1.0000
T7:240uE-T1:120uE	0.302	T8:240uE-T4:120uE	1.0000	T3:240uE-T1:240uE	1.0000
T8:240uE-T1:120uE	0.992	T6:120uE-T5:120uE	1.0000	T4:240uE-T1:240uE	0.9864
T3:120uE-T2:120uE	1.000	T7:120uE-T5:120uE	1.0000	T5:240uE-T1:240uE	0.5140
T4:120uE-T2:120uE	1.000	T8:120uE-T5:120uE	1.0000	T6:240uE-T1:240uE	0.2309
T5:120uE-T2:120uE	1.000	T1:240uE-T5:120uE	1.0000	T7:240uE-T1:240uE	0.3826
T6:120uE-T2:120uE	1.000	T2:240uE-T5:120uE	1.0000	T8:240uE-T1:240uE	0.9977

T7:120uE-T2:120uE	1.000	T3:240uE-T5:120uE	1.0000	T3:240uE-T2:240uE	1.0000
T8:120uE-T2:120uE	1.000	T4:240uE-T5:120uE	1.0000	T4:240uE-T2:240uE	0.9980
T1:240uE-T2:120uE	1.000	T5:240uE-T5:120uE	0.8871	T5:240uE-T2:240uE	0.6746
T2:240uE-T2:120uE	1.000	T6:240uE-T5:120uE	0.5975	T6:240uE-T2:240uE	0.3509
T3:240uE-T2:120uE	1.000	T7:240uE-T5:120uE	0.7851	T7:240uE-T2:240uE	0.5358
T4:240uE-T2:120uE	1.000	T8:240uE-T5:120uE	1.0000	T8:240uE-T2:240uE	0.9998
T5:240uE-T2:120uE	0.906	T7:120uE-T6:120uE	1.0000	T4:240uE-T3:240uE	0.9999
T6:240uE-T2:120uE	0.631	T8:120uE-T6:120uE	1.0000	T5:240uE-T3:240uE	0.8261
T7:240uE-T2:120uE	0.813	T1:240uE-T6:120uE	1.0000	T6:240uE-T3:240uE	0.5090
T8:240uE-T2:120uE	1.000	T2:240uE-T6:120uE	1.0000	T7:240uE-T3:240uE	0.7051
T4:120uE-T3:120uE	1.000	T3:240uE-T6:120uE	1.0000	T8:240uE-T3:240uE	1.0000
T5:120uE-T3:120uE	1.000	T4:240uE-T6:120uE	0.9997	T5:240uE-T4:240uE	0.9990
T6:120uE-T3:120uE	1.000	T5:240uE-T6:120uE	0.7921	T6:240uE-T4:240uE	0.9593
T7:120uE-T3:120uE	1.000	T6:240uE-T6:120uE	0.4676	T7:240uE-T4:240uE	0.9937
T8:120uE-T3:120uE	1.000	T7:240uE-T6:120uE	0.6641	T8:240uE-T4:240uE	1.0000
T1:240uE-T3:120uE	1.000	T8:240uE-T6:120uE	1.0000	T6:240uE-T5:240uE	1.0000
T2:240uE-T3:120uE	1.000	T8:120uE-T7:120uE	1.0000	T7:240uE-T5:240uE	1.0000
T3:240uE-T3:120uE	1.000	T1:240uE-T7:120uE	1.0000	T8:240uE-T5:240uE	0.9926
T4:240uE-T3:120uE	1.000	T2:240uE-T7:120uE	1.0000	T7:240uE-T6:240uE	1.0000
T5:240uE-T3:120uE	0.919	T3:240uE-T7:120uE	1.0000	T8:240uE-T6:240uE	0.8905
T6:240uE-T3:120uE	0.655	T4:240uE-T7:120uE	0.9644	T8:240uE-T7:240uE	0.9714

Appendix 4.4a, b

ANOVA comparisons of hybrid and parent combination to see if there is significant difference between the samples (bold). If so, the detail comparisons are shown in the next table.

30 DAS, 120uE	p value
T1	0.2900
T2	0.6230
T3	**0.0038**
T4	**0.0282**
T5	0.0681
T6	0.2580
T7	0.4030
T8	0.1770
T9	**0.0221**
T10	**0.0016**
T11	**0.0012**
T12	**0.0213**

30 DAS, 120uE	T3		T4		T9		T10		T11		T12	
C24xLer-C24	0.0145	*	0.0444	*	0.0504		0.0038	**	0.0080	**	0.1172	
Ler-C24	0.0069	**	0.0353	*								
LerxC24-C24	0.0063	**	0.0897		0.0248	*	0.0020	**	0.0010	***	0.0179	*
MPV-C24	0.2230		0.4452									
Ler-C24xLer	0.9855		0.9999									
LerxC24-C24xLer	0.9782		0.9898		0.8284		0.7611		0.1251		0.2074	
MPV-C24xLer	0.4259		0.5236									
LerxC24-Ler	1.0000		0.9715									
MPV-Ler	0.2230		0.4452									
MPV-LerxC24	0.2051		0.7753									

30 DAS, 240uE	p value
T1	0.344
T2	**0.006**
T3	**0.008**
T4	**0.005**
T5	**0.016**

T6	0.289
T7	**0.015**
T8	**0.030**
T9	**0.001**
T10	**0.000**
T11	**0.000**
T12	**0.000**
T13	**0.008**
T14	**0.047**
T15	**0.075**
T16	0.302
T17	0.257
T18	0.338
T19	0.730
T20	0.390

30 DAS, 240uE	T2		T3		T4		T5		T7		T8	
C24xLer-C24	0.0141	*	0.0084	**	0.0031	**	0.0301	*	0.0363	*	0.0330	*
Ler-C24	0.9977		0.0144	*	0.0483	*	0.0163	*	0.0119	*	0.0408	*
LerxC24-C24	0.9925		0.0667		0.0432	*	0.4116		0.0720		0.2523	
MPV-C24	0.9998		0.3110		0.4982		0.3284		0.2862		0.4692	
Ler-C24xLer	0.0226	*	0.9960		0.4126		0.9938		0.9450		0.9999	
LerxC24-C24xLer	0.0075	**	0.6699		0.4491		0.4277		0.9908		0.6685	
MPV-C24xLer	0.0178	*	0.1911		0.0373	*	0.5236		0.6499		0.4011	
LerxC24-Ler	0.9453		0.8521		1.0000		0.2578		0.7673		0.7432	
MPV-Ler	0.9998		0.3110		0.4982		0.3284		0.2862		0.4692	
MPV-LerxC24	0.9762		0.8244		0.4597		0.9997		0.8740		0.9860	

30 DAS, 240uE	T9		T10		T11		T12		T13		T14	
C24xLer-C24	0.000	***	0.000	***	0.000	***	0.000	***	0.001	**	0.043	*
LerxC24-C24	0.001	**	0.000	***	0.000	***	0.000	***	0.002	**	0.146	
LerxC24-C24xLer	0.648		0.669		0.012	*	0.493		0.666		0.620	

Appendix 4.4c, d

C24xLer	p value		C24xLer	p value	
T11:120uE-T10:120uE	0.998		T12:240uE-T12:120uE	0.063	
T12:120uE-T10:120uE	0.393		T13:240uE-T12:120uE	0.219	
T13:120uE-T10:120uE	0.665		T14:240uE-T12:120uE	0.246	
T14:120uE-T10:120uE	0.152		T14:120uE-T13:120uE	0.981	
T11:240uE-T10:120uE	0.267		T11:240uE-T13:120uE	0.007	**
T12:240uE-T10:120uE	0.979		T12:240uE-T13:120uE	0.148	
T13:240uE-T10:120uE	1.000		T13:240uE-T13:120uE	0.432	
T14:240uE-T10:120uE	1.000		T14:240uE-T13:120uE	0.474	
T12:120uE-T11:120uE	0.842		T11:240uE-T14:120uE	0.001	**
T13:120uE-T11:120uE	0.977		T12:240uE-T14:120uE	0.019	*
T14:120uE-T11:120uE	0.496		T13:240uE-T14:120uE	0.074	
T11:240uE-T11:120uE	0.067		T14:240uE-T14:120uE	0.085	
T12:240uE-T11:120uE	0.677		T12:240uE-T11:240uE	0.854	
T13:240uE-T11:120uE	0.965		T13:240uE-T11:240uE	0.463	
T14:240uE-T11:120uE	0.976		T14:240uE-T11:240uE	0.421	
T13:120uE-T12:120uE	1.000		T13:240uE-T12:240uE	0.999	
T14:120uE-T12:120uE	1.000		T14:240uE-T12:240uE	0.998	
T11:240uE-T12:120uE	0.003	**	T14:240uE-T13:240uE	1.000	

LerxC24	p value		LerxC24	p value	
T12:120uE-T11:120uE	0.266		T11:240uE-T13:120uE	0.004	**
T13:120uE-T11:120uE	0.029	*	T12:240uE-T13:120uE	0.066	
T14:120uE-T11:120uE	0.008	**	T13:240uE-T13:120uE	0.219	
T11:240uE-T11:120uE	0.969		T14:240uE-T13:120uE	0.622	
T12:240uE-T11:120uE	1.000		T11:240uE-T14:120uE	0.001	**
T13:240uE-T11:120uE	0.939		T12:240uE-T14:120uE	0.019	*
T14:240uE-T11:120uE	0.546		T13:240uE-T14:120uE	0.071	
T13:120uE-T12:120uE	0.901		T14:240uE-T14:120uE	0.277	
T14:120uE-T12:120uE	0.563		T12:240uE-T11:240uE	0.829	
T11:240uE-T12:120uE	0.048	*	T13:240uE-T11:240uE	0.439	
T12:240uE-T12:120uE	0.482		T14:240uE-T11:240uE	0.130	
T13:240uE-T12:120uE	0.863		T13:240uE-T12:240uE	0.996	
T14:240uE-T12:120uE	0.999		T14:240uE-T12:240uE	0.798	
T14:120uE-T13:120uE	0.997		T14:240uE-T13:240uE	0.990	

Appendix 4.5a (refer to Appendix 4.3b)

Appendix 4.5b (refer to Appendix 4.4b)

Appendix 4.6

	p value	
C24xLer:120uE-C24:120uE	0.917	
Ler:120uE-C24:120uE	0.838	
LerxC24:120uE-C24:120uE	0.906	
C24:240uE-C24:120uE	0.181	
C24xLer:240uE-C24:120uE	0.022	*
Ler:240uE-C24:120uE	0.006	**
LerxC24:240uE-C24:120uE	0.002	**
Ler:120uE-C24xLer:120uE	1.000	
LerxC24:120uE-C24xLer:120uE	1.000	
C24:240uE-C24xLer:120uE	0.784	
C24xLer:240uE-C24xLer:120uE	0.197	
Ler:240uE-C24xLer:120uE	0.062	
LerxC24:240uE-C24xLer:120uE	0.022	*
LerxC24:120uE-Ler:120uE	1.000	
C24:240uE-Ler:120uE	0.878	
C24xLer:240uE-Ler:120uE	0.270	
Ler:240uE-Ler:120uE	0.090	
LerxC24:240uE-Ler:120uE	0.032	*
C24:240uE-LerxC24:120uE	0.801	
C24xLer:240uE-LerxC24:120uE	0.208	
Ler:240uE-LerxC24:120uE	0.066	
LerxC24:240uE-LerxC24:120uE	0.023	
C24xLer:240uE-C24:240uE	0.933	
Ler:240uE-C24:240uE	0.617	
LerxC24:240uE-C24:240uE	0.313	
Ler:240uE-C24xLer:240uE	0.997	
LerxC24:240uE-C24xLer:240uE	0.914	
LerxC24:240uE-Ler:240uE	0.999	

Appendix 4.8a

ANOVA comparisons of hybrid and parent combination to see if there is significant difference between the samples (bold). If so, the detail comparisons are shown in the next table.

	p value
Ci=50	**0.006**
Ci=100	**0.015**
Ci=150	0.109
Ci=200	0.405
Ci=300	0.106
Ci=400	0.089
Ci=500	0.471
Ci=600	0.582
Ci=800	0.718

	Ci=50		Ci=100	
C24xLer-C24	0.013	*	0.018	*
Ler-C24	0.499		0.065	
LerxC24-C24	0.009	**	0.028	*
Ler-C24xLer	0.102		0.787	
LerxC24-C24xLer	0.992		0.987	
LerxC24-Ler	0.069		0.926	

Appendix 4.8b

	p value
Ci=50	0.058
Ci=100	0.774
Ci=150	0.436
Ci=200	0.418
Ci=300	0.238
Ci=400	0.278
Ci=500	0.197
Ci=600	0.094
Ci=800	0.130

Appendix 4.8c

ANOVA comparisons of hybrid and parent combination to see if there is significant difference between the samples (bold). If so, the detail comparisons are shown in the next table.

	p value
Ci=50	**0.000**
Ci=100	0.058
Ci=200	0.407
Ci=400	0.051
Ci=600	**0.003**
Ci=800	**0.000**
Ci=1000	**0.000**
Ci=1200	**0.000**
Ci=1500	**0.000**

	Ci=50		Ci=600		Ci=800	
C24xLer-C24	0.000	***	0.809		0.410	
Ler-C24	0.311		0.004	**	0.000	***
LerxC24-C24	0.000	***	0.967		0.788	
Ler-C24xLer	0.007	**	0.018	*	0.008	**
LerxC24-C24xLer	0.996		0.982		0.948	
LerxC24-Ler	0.022	*	0.015	*	0.005	**

	Ci=1000		Ci=1200		Ci=1500	
C24xLer-C24	0.410		0.178		0.050	*
Ler-C24	0.000	***	0.000	***	0.000	***
LerxC24-C24	0.788		0.626		0.401	
Ler-C24xLer	0.008	**	0.011	*	0.039	*
LerxC24-C24xLer	0.948		0.867		0.749	
LerxC24-Ler	0.005	**	0.004	**	0.008	**

Appendix 4.8d

ANOVA comparisons of hybrid and parent combination to see if there is significant difference between the samples (bold). If so, the detail comparisons are shown in the next table.

	p value
Ci=50	**0.023**
Ci=100	**0.030**
Ci=200	0.104
Ci=400	0.127
Ci=600	0.079
Ci=800	0.071
Ci=1000	0.079
Ci=1200	0.087
Ci=1500	0.170

	Ci=50		Ci=100	
C24xLer-C24	0.046	*	0.092	
Ler-C24	0.923		0.356	
LerxC24-C24	0.071		0.028	*
Ler-C24xLer	0.114		0.716	
LerxC24-C24xLer	0.994		0.897	
LerxC24-Ler	0.172		0.324	

Appendix 4.9

Vcmax	P value
C24xLer:120uE-C24:120uE	0.501
Ler:120uE-C24:120uE	0.738
LerxC24:120uE-C24:120uE	0.738
C24:240uE-C24:120uE	0.977
C24xLer:240uE-C24:120uE	0.962
Ler:240uE-C24:120uE	0.961
LerxC24:240uE-C24:120uE	0.995
Ler:120uE-C24xLer:120uE	1.000
LerxC24:120uE-C24xLer:120uE	1.000
C24:240uE-C24xLer:120uE	0.141
C24xLer:240uE-C24xLer:120uE	0.999
Ler:240uE-C24xLer:120uE	0.997
LerxC24:240uE-C24xLer:120uE	0.216

LerxC24:120uE-Ler:120uE	1.000
C24:240uE-Ler:120uE	0.272
C24xLer:240uE-Ler:120uE	1.000
Ler:240uE-Ler:120uE	1.000
LerxC24:240uE-Ler:120uE	0.384
C24:240uE-LerxC24:120uE	0.272
C24xLer:240uE-LerxC24:120uE	1.000
Ler:240uE-LerxC24:120uE	1.000
LerxC24:240uE-LerxC24:120uE	0.384
C24xLer:240uE-C24:240uE	0.631
Ler:240uE-C24:240uE	0.596
LerxC24:240uE-C24:240uE	1.000
Ler:240uE-C24xLer:240uE	1.000
LerxC24:240uE-C24xLer:240uE	0.743
LerxC24:240uE-Ler:240uE	0.719

	P value	
C24xLer:120uE-C24:120uE	0.186	
Ler:120uE-C24:120uE	0.190	
LerxC24:120uE-C24:120uE	0.333	
C24:240uE-C24:120uE	1.000	
C24xLer:240uE-C24:120uE	0.990	
Ler:240uE-C24:120uE	0.744	
LerxC24:240uE-C24:120uE	0.877	
Ler:120uE-C24xLer:120uE	1.000	
LerxC24:120uE-C24xLer:120uE	1.000	
C24:240uE-C24xLer:120uE	0.179	
C24xLer:240uE-C24xLer:120uE	0.904	
Ler:240uE-C24xLer:120uE	0.997	
LerxC24:240uE-C24xLer:120uE	0.016	*
LerxC24:120uE-Ler:120uE	1.000	
C24:240uE-Ler:120uE	0.179	
C24xLer:240uE-Ler:120uE	0.889	
Ler:240uE-Ler:120uE	0.995	
LerxC24:240uE-Ler:120uE	0.017	*
C24:240uE-LerxC24:120uE	0.301	
C24xLer:240uE-LerxC24:120uE	0.964	
Ler:240uE-LerxC24:120uE	1.000	
LerxC24:240uE-LerxC24:120uE	0.036	
C24xLer:240uE-C24:240uE	0.968	
Ler:240uE-C24:240uE	0.661	
LerxC24:240uE-C24:240uE	0.979	
Ler:240uE-C24xLer:240uE	0.999	

LerxC24:240uE-C24xLer:240uE	0.565	
LerxC24:240uE-Ler:240uE	0.163	

Table 4.1

	p value		p value
C24xLer:120uE-C24:120uE	0.997	C24:240uE-Ler:120uE	1.000
Ler:120uE-C24:120uE	0.984	C24xLer:240uE-Ler:120uE	0.868
LerxC24:120uE-C24:120uE	1.000	Ler:240uE-Ler:120uE	1.000
C24:240uE-C24:120uE	0.992	LerxC24:240uE-Ler:120uE	0.881
C24xLer:240uE-C24:120uE	0.998	C24:240uE-LerxC24:120uE	0.999
Ler:240uE-C24:120uE	1.000	C24xLer:240uE-LerxC24:120uE	0.989
LerxC24:240uE-C24:120uE	0.999	Ler:240uE-LerxC24:120uE	1.000
Ler:120uE-C24xLer:120uE	1.000	LerxC24:240uE-LerxC24:120uE	0.994
LerxC24:120uE-C24xLer:120uE	1.000	C24xLer:240uE-C24:240uE	0.908
C24:240uE-C24xLer:120uE	1.000	Ler:240uE-C24:240uE	1.000
C24xLer:240uE-C24xLer:120uE	0.932	LerxC24:240uE-C24:240uE	0.924
Ler:240uE-C24xLer:120uE	1.000	Ler:240uE-C24xLer:240uE	0.975
LerxC24:240uE-C24xLer:120uE	0.945	LerxC24:240uE-C24xLer:240uE	1.000
LerxC24:120uE-Ler:120uE	0.998	LerxC24:240uE-Ler:240uE	0.984

Appendix 4.10

p value	A		Ci/Ca		g_s		VPD	
C24xLer:120uE-C24:120uE	1.000		1.000		0.999		0.635	
Ler:120uE-C24:120uE	0.995		0.011	*	0.032	*	0.215	
LerxC24:120uE-C24:120uE	0.985		0.997		1.000		1.000	
C24:240uE-C24:120uE	0.995		0.997		1.000		1.000	

C24xLer:240uE-C24:120uE	0.289		1.000		0.120		0.358	
Ler:240uE-C24:120uE	0.684		0.978		0.718		0.910	
LerxC24:240uE-C24:120uE	0.016	*	1.000		0.002	**	0.949	
Ler:120uE-C24xLer:120uE	0.994		0.006	**	0.088		0.990	
LerxC24:120uE-C24xLer:120uE	0.981		1.000		0.993		0.761	
C24:240uE-C24xLer:120uE	0.996		1.000		1.000		0.667	
C24xLer:240uE-C24xLer:120uE	0.302		0.994		0.286		1.000	
Ler:240uE-C24xLer:120uE	0.703		0.920		0.942		0.997	
LerxC24:240uE-C24xLer:120uE	0.017	*	0.999		0.006	**	0.990	
LerxC24:120uE-Ler:120uE	1.000		0.003	**	0.019	*	0.303	
C24:240uE-Ler:120uE	0.795		0.001	**	0.022	*	0.214	
C24xLer:240uE-Ler:120uE	0.082		0.029	*	0.996		1.000	
Ler:240uE-Ler:120uE	0.262		0.071		0.514		0.777	
LerxC24:240uE-Ler:120uE	0.003	**	0.010	**	0.949		0.700	
C24:240uE-LerxC24:120uE	0.704		1.000		1.000		1.000	
C24xLer:240uE-LerxC24:120uE	0.060		0.932		0.076		0.476	
Ler:240uE-LerxC24:120uE	0.200		0.736		0.572		0.968	
LerxC24:240uE-LerxC24:120uE	0.002	**	0.972		0.001	***	0.986	
C24xLer:240uE-C24:240uE	0.597		0.923		0.093		0.368	

Ler:240uE-C24:240uE	0.959		0.701		0.691		0.937	
LerxC24:240uE-C24:240uE	0.043	*	0.969		0.001	***	0.969	
Ler:240uE-C24xLer:240uE	0.985		1.000		0.887		0.926	
LerxC24:240uE-C24xLer:240uE	0.867		1.000		0.608		0.878	
LerxC24:240uE-Ler:240uE	0.292		0.994		0.072		1.000	

Appendix 4.11

p value	chla	chlb	a/b ratio
C24xLer:120uE-C24:120uE	0.959	0.990	1.000
Ler:120uE-C24:120uE	0.983	0.996	1.000
LerxC24:120uE-C24:120uE	0.863	0.965	1.000
C24:240uE-C24:120uE	0.683	0.519	0.918
C24xLer:240uE-C24:120uE	0.996	1.000	1.000
Ler:240uE-C24:120uE	0.687	0.962	1.000
LerxC24:240uE-C24:120uE	0.928	0.650	0.872
Ler:120uE-C24xLer:120uE	1.000	1.000	1.000
LerxC24:120uE-C24xLer:120uE	1.000	1.000	1.000
C24:240uE-C24xLer:120uE	0.176	0.164	0.851
C24xLer:240uE-C24xLer:120uE	0.671	0.998	1.000
Ler:240uE-C24xLer:120uE	0.178	0.603	1.000
LerxC24:240uE-C24xLer:120uE	0.389	0.234	0.790
LerxC24:120uE-Ler:120uE	1.000	1.000	1.000
C24:240uE-Ler:120uE	0.225	0.197	0.878
C24xLer:240uE-Ler:120uE	0.758	1.000	1.000
Ler:240uE-Ler:120uE	0.228	0.671	1.000
LerxC24:240uE-Ler:120uE	0.472	0.278	0.823
C24:240uE-LerxC24:120uE	0.103	0.115	0.857
C24xLer:240uE-LerxC24:120uE	0.487	0.991	1.000
Ler:240uE-LerxC24:120uE	0.104	0.482	1.000
LerxC24:240uE-LerxC24:120uE	0.249	0.168	0.797
C24xLer:240uE-C24:240uE	0.963	0.399	0.691
Ler:240uE-C24:240uE	1.000	0.975	0.917
LerxC24:240uE-C24:240uE	0.999	1.000	1.000
Ler:240uE-C24xLer:240uE	0.965	0.904	1.000
LerxC24:240uE-C24xLer:240uE	1.000	0.522	0.616

LerxC24:240uE-Ler:240uE	0.999	0.994	0.871

Appendix 4.12bc

P value	ED		EN		Turnover	
C24xLer:120uE-C24:120uE	1.000		1.000		1.000	
Ler:120uE-C24:120uE	0.871		0.997		0.722	
LerxC24:120uE-C24:120uE	1.000		0.997		0.984	
C24:240uE-C24:120uE	0.000	***	0.000	***	0.157	
C24xLer:240uE-C24:120uE	0.000	***	0.000	***	1.000	
Ler:240uE-C24:120uE	0.000	***	0.000	***	0.975	
LerxC24:240uE-C24:120uE	0.000	***	0.000	***	0.027	*
Ler:120uE-C24xLer:120uE	0.630		0.995		0.461	
LerxC24:120uE-C24xLer:120uE	1.000		0.999		1.000	
C24:240uE-C24xLer:120uE	0.000	***	0.000	**	0.315	
C24xLer:240uE-C24xLer:120uE	0.000	***	0.000	***	1.000	
Ler:240uE-C24xLer:120uE	0.000	***	0.000	***	0.843	
LerxC24:240uE-C24xLer:120uE	0.000	***	0.000	***	0.063	
LerxC24:120uE-Ler:120uE	0.644		0.889		0.255	
C24:240uE-Ler:120uE	0.000	***	0.000	**	0.007	*
C24xLer:240uE-Ler:120uE	0.000	***	0.000	***	0.520	
Ler:240uE-Ler:120uE	0.000	***	0.000	***	0.996	
LerxC24:240uE-Ler:120uE	0.000	***	0.000	***	0.001	***
C24:240uE-LerxC24:120uE	0.000	***	0.000	**	0.544	
C24xLer:240uE-LerxC24:120uE	0.000	***	0.000	***	0.999	
Ler:240uE-LerxC24:120uE	0.000	***	0.000	***	0.608	
LerxC24:240uE-LerxC24:120uE	0.000	***	0.000	***	0.137	
C24xLer:240uE-C24:240uE	0.787		0.793		0.271	
Ler:240uE-C24:240uE	0.569		0.183		0.027	*
LerxC24:240uE-C24:240uE	0.012	*	0.001	****	0.974	
Ler:240uE-C24xLer:240uE	1.000		0.913		0.886	
LerxC24:240uE-C24xLer:240uE	0.194		0.000	***	0.052	
LerxC24:240uE-Ler:240uE	0.344		0.000	***	0.004	**

Appendix 4.13

P value	ED		EN		Turnover	
C24xLer:120uE-C24:120uE	0.998		1.000		0.994	
Ler:120uE-C24:120uE	0.309		1.000		0.109	
LerxC24:120uE-C24:120uE	0.999		0.961		0.852	
C24:240uE-C24:120uE	0.006	**	1.000		0.001	***

C24xLer:240uE-C24:120uE	0.000	***	0.800		0.000	***
Ler:240uE-C24:120uE	0.000	***	0.287		0.000	***
LerxC24:240uE-C24:120uE	0.000	***	0.063		0.000	***
Ler:120uE-C24xLer:120uE	0.111		1.000		0.028	*
LerxC24:120uE-C24xLer:120uE	1.000		0.937		0.997	
C24:240uE-C24xLer:120uE	0.021	*	1.000		0.004	**
C24xLer:240uE-C24xLer:120uE	0.000	***	0.849		0.000	***
Ler:240uE-C24xLer:120uE	0.000	***	0.334		0.000	***
LerxC24:240uE-C24xLer:120uE	0.000	***	0.076		0.000	***
LerxC24:120uE-Ler:120uE	0.122		0.956		0.008	***
C24:240uE-Ler:120uE	0.000	***	1.000		0.000	***
C24xLer:240uE-Ler:120uE	0.000	***	0.811		0.000	***
Ler:240uE-Ler:120uE	0.000	***	0.297		0.000	***
LerxC24:240uE-Ler:120uE	0.000	***	0.066		0.000	***
C24:240uE-LerxC24:120uE	0.019	*	0.817		0.015	*
C24xLer:240uE-LerxC24:120uE	0.000	***	0.249		0.000	***
Ler:240uE-LerxC24:120uE	0.000	***	0.049	*	0.000	***
LerxC24:240uE-LerxC24:120uE	0.000	***	0.009	**	0.000	***
C24xLer:240uE-C24:240uE	0.018	*	0.954		0.009	**
Ler:240uE-C24:240uE	0.014	*	0.500		0.019	*
LerxC24:240uE-C24:240uE	0.001	***	0.134		0.001	**
Ler:240uE-C24xLer:240uE	1.000		0.976		1.000	
LerxC24:240uE-C24xLer:240uE	0.639		0.603		0.947	
LerxC24:240uE-Ler:240uE	0.727		0.982		0.796	

Appendix 4.14b

	p value	
C24/LerMPV:120uE-C24:120uE	1.0000	
C24xLer:120uE-C24:120uE	0.9605	
Ler:120uE-C24:120uE	1.0000	
LerxC24:120uE-C24:120uE	1.0000	
C24:240uE-C24:120uE	0.0144	*
C24/LerMPV:240uE-C24:120uE	0.0001	***
C24xLer:240uE-C24:120uE	0.0000	***
Ler:240uE-C24:120uE	0.0000	***
LerxC24:240uE-C24:120uE	0.0000	***
C24xLer:120uE-C24/LerMPV:120uE	0.9588	
Ler:120uE-C24/LerMPV:120uE	1.0000	
LerxC24:120uE-C24/LerMPV:120uE	1.0000	

C24:240uE-C24/LerMPV:120uE	0.0139	*
C24/LerMPV:240uE-C24/LerMPV:120uE	0.0001	***
C24xLer:240uE-C24/LerMPV:120uE	0.0000	***
Ler:240uE-C24/LerMPV:120uE	0.0000	***
LerxC24:240uE-C24/LerMPV:120uE	0.0000	***
Ler:120uE-C24xLer:120uE	0.9571	
LerxC24:120uE-C24xLer:120uE	0.9579	
C24:240uE-C24xLer:120uE	0.4371	
C24/LerMPV:240uE-C24xLer:120uE	0.0157	*
C24xLer:240uE-C24xLer:120uE	0.0000	***
Ler:240uE-C24xLer:120uE	0.0001	***
LerxC24:240uE-C24xLer:120uE	0.0000	***
LerxC24:120uE-Ler:120uE	1.0000	
C24:240uE-Ler:120uE	0.0135	*
C24/LerMPV:240uE-Ler:120uE	0.0001	***
C24xLer:240uE-Ler:120uE	0.0000	***
Ler:240uE-Ler:120uE	0.0000	***
LerxC24:240uE-Ler:120uE	0.0000	***
C24:240uE-LerxC24:120uE	0.0137	*
C24/LerMPV:240uE-LerxC24:120uE	0.0001	***
C24xLer:240uE-LerxC24:120uE	0.0000	***
Ler:240uE-LerxC24:120uE	0.0000	***
LerxC24:240uE-LerxC24:120uE	0.0000	***
C24/LerMPV:240uE-C24:240uE	0.7995	*
C24xLer:240uE-C24:240uE	0.0000	***
Ler:240uE-C24:240uE	0.0489	*
LerxC24:240uE-C24:240uE	0.0000	***
C24xLer:240uE-C24/LerMPV:240uE	0.0000	***
Ler:240uE-C24/LerMPV:240uE	0.8883	
LerxC24:240uE-C24/LerMPV:240uE	0.0001	***
Ler:240uE-C24xLer:240uE	0.0000	***
LerxC24:240uE-C24xLer:240uE	0.0261	*
LerxC24:240uE-Ler:240uE	0.0236	*

Appendix 4.14c

	p value	

LerxC24:120uE-C24xLer:120uE	0.023	*
C24xLer:240uE-C24xLer:120uE	0.464	
LerxC24:240uE-C24xLer:120uE	0.975	
C24xLer:240uE-LerxC24:120uE	0.000	***
LerxC24:240uE-LerxC24:120uE	0.029	*
LerxC24:240uE-C24xLer:240uE	0.137	

Appendix 5.8

	p value	
cyoxsco-cyo	0.771	
Ler-cyo	1.000	
LerxWs-cyo	0.013	*
sco-cyo	0.000	***
scoxcyo-cyo	0.013	*
Ws-cyo	0.088	
WsxLer-cyo	0.424	
Ler-cyoxsco	0.779	
LerxWs-cyoxsco	0.000	***
sco-cyoxsco	0.000	***
scoxcyo-cyoxsco	0.754	
Ws-cyoxsco	0.001	***
WsxLer-cyoxsco	0.011	*
LerxWs-Ler	0.002	**
sco-Ler	0.000	***
scoxcyo-Ler	0.007	**
Ws-Ler	0.029	*
WsxLer-Ler	0.248	
sco-LerxWs	0.000	***
scoxcyo-LerxWs	0.000	***
Ws-LerxWs	1.000	
WsxLer-LerxWs	0.925	
scoxcyo-sco	0.000	***
Ws-sco	0.000	***
WsxLer-sco	0.000	***
Ws-scoxcyo	0.000	***
WsxLer-scoxcyo	0.000	***
WsxLer-Ws	0.997	

Appendix 5.10

	Chla	Chlb	a/b ratio	
cyoxsco-cyo	0.986	0.998	0.864	
Ler-cyo	0.998	0.880	0.117	
LerxWs-cyo	1.000	0.881	0.050	*
sco-cyo	1.000	0.999	0.562	
scoxcyo-cyo	0.999	0.999	0.997	
Ws-cyo	0.998	0.820	0.076	
WsxLer-cyo	0.996	0.790	0.089	
Ler-cyoxsco	0.817	0.536	0.723	
LerxWs-cyoxsco	0.883	0.537	0.448	
sco-cyoxsco	0.975	0.917	0.999	
scoxcyo-cyoxsco	1.000	1.000	0.996	
Ws-cyoxsco	0.817	0.457	0.581	
WsxLer-cyoxsco	0.766	0.424	0.632	
LerxWs-Ler	1.000	1.000	1.000	
sco-Ler	0.999	0.994	0.952	
scoxcyo-Ler	0.933	0.598	0.335	
Ws-Ler	1.000	1.000	1.000	
WsxLer-Ler	1.000	1.000	1.000	
sco-LerxWs	1.000	0.994	0.768	
scoxcyo-LerxWs	0.967	0.599	0.162	
Ws-LerxWs	1.000	1.000	1.000	
WsxLer-LerxWs	1.000	1.000	1.000	
scoxcyo-sco	0.997	0.946	0.905	
Ws-sco	0.999	0.984	0.877	
WsxLer-sco	0.998	0.976	0.908	
Ws-scoxcyo	0.933	0.516	0.234	
WsxLer-scoxcyo	0.901	0.481	0.267	
WsxLer-Ws	1.000	1.000	1.000	

Appendix 5.11

	p value			p value	
cyo/scoMPV-cyo	1.000		WsxLer-cyoxsco	0.000	***
cyoxsco-cyo	0.710		LerxWs-Ler	0.000	***
Ler-cyo	0.000	***	sco-Ler	0.000	***
LerxWs-cyo	0.000	***	scoxcyo-Ler	0.000	***
sco-cyo	1.000		Ws-Ler	0.000	***
scoxcyo-cyo	0.925		Ws/LerMPV-Ler	0.120	
Ws-cyo	0.000	***	WsxLer-Ler	0.204	
Ws/LerMPV-cyo	0.000	***	sco-LerxWs	0.000	***
WsxLer-cyo	0.000	***	scoxcyo-LerxWs	0.000	***

cyoxsco-cyo/scoMPV	0.938		Ws-LerxWs	0.000	***
Ler-cyo/scoMPV	0.000	***	Ws/LerMPV-LerxWs	0.000	***
LerxWs-cyo/scoMPV	0.000	***	WsxLer-LerxWs	0.000	***
sco-cyo/scoMPV	1.000		scoxcyo-sco	0.999	
scoxcyo-cyo/scoMPV	0.996		Ws-sco	0.000	***
Ws-cyo/scoMPV	0.000	***	Ws/LerMPV-sco	0.000	***
Ws/LerMPV-cyo/scoMPV	0.000	***	WsxLer-sco	0.000	***
WsxLer-cyo/scoMPV	0.000	***	Ws-scoxcyo	0.000	***
Ler-cyoxsco	0.000	***	Ws/LerMPV-scoxcyo	0.000	***
LerxWs-cyoxsco	0.000	***	WsxLer-scoxcyo	0.000	***
sco-cyoxsco	0.976		Ws/LerMPV-Ws	0.118	
scoxcyo-cyoxsco	1.000		WsxLer-Ws	0.000	***
Ws-cyoxsco	0.000	***	WsxLer-Ws/LerMPV	0.000	***
Ws/LerMPV-cyoxsco	0.000	***			

Appendix 5.14a

Control	7 DAS		14 DAS		18 DAS		21DAS	
C24xLer-C24	0.0052	**	0.0000	***	0.0000	***	0.0002	***
Ler-C24	0.0060	**	0.5098		0.6873		0.9213	
LerxC24-C24	0.8179		0.0001	***	0.0000	***	0.0005	***
MPV-C24	0.5310		0.9304		0.9952		0.9969	
Ler-C24xLer	0.0000	***	0.0000	***	0.0000	***	0.0000	***
LerxC24-C24xLer	0.0903		0.0506		0.3610		0.9968	
MPV-C24xLer	0.0000	***	0.0000	***	0.0000	***	0.0001	***
LerxC24-Ler	0.0002	***	0.0000	***	0.0000	***	0.0000	***
MPV-Ler	0.2779		0.9304		0.8944		0.9896	
MPV-LerxC24	0.0831		0.0000	***	0.0000	***	0.0002	***
0-7 DAS	7 DAS		14 DAS		18 DAS		21DAS	
C24xLer-C24	0.0453	*	0.0000	***	0.0043	**	0.0002	***
Ler-C24	0.3885		0.0019	**	0.1609		0.3175	
LerxC24-C24	0.4483		0.0001	***	0.0080	**	0.0007	***
MPV-C24	0.9002		0.3141		0.9096		0.8710	
Ler-C24xLer	0.0001	***	0.1602		0.5650		0.0627	
LerxC24-C24xLer	0.7691		0.6377		0.9995		0.9966	
MPV-C24xLer	0.0046	**	0.0004	***	0.0457	*	0.0045	**
LerxC24-Ler	0.0069	**	0.8697		0.7018		0.1379	
MPV-Ler	0.9203		0.2194		0.6163		0.8710	
MPV-LerxC24	0.0961		0.0204	*	0.0762		0.0128	*

7-14 DAS	7 DAS		14 DAS		18 DAS		21DAS	
C24xLer-C24	0.0000	***	0.2399		0.0320	*	0.0016	**
Ler-C24	0.0276	*	0.9980		0.7820		0.2697	
LerxC24-C24	0.0069	**	0.5337		0.0524		0.0059	**
MPV-C24	0.5195		0.9999		0.9999		0.8700	
Ler-C24xLer	0.0000	***	0.0535		0.1918		0.2547	
LerxC24-C24xLer	0.2176		0.9392		0.9994		0.9924	
MPV-C24xLer	0.0000	***	0.1464		0.0215	*	0.0283	*
LerxC24-Ler	0.0000	***	0.1791		0.2891		0.4906	
MPV-Ler	0.5587		0.9841		0.6886		0.8368	
MPV-LerxC24	0.0000	***	0.4155		0.0359	*	0.0804	

0-14 DAS	7 DAS		14 DAS		18 DAS		21DAS	
C24xLer-C24	0.0286	*	0.0215	*	0.0002	***	0.0001	***
Ler-C24	0.0986		0.7228		0.0000	***	0.0004	***
LerxC24-C24	0.5915		0.1352		0.0003	***	0.0150	*
MPV-C24	0.8573		0.9785		0.1111		0.1987	
Ler-C24xLer	0.0000	***	0.3659		0.9909		0.9988	
LerxC24-C24xLer	0.4891		0.9392		1.0000		0.5468	
MPV-C24xLer	0.0021	**	0.1038		0.2381		0.1017	
LerxC24-Ler	0.0031	**	0.8139		0.9770		0.7357	
MPV-Ler	0.5034		0.9635		0.0953		0.1955	
MPV-LerxC24	0.1264		0.4071		0.2703		0.8448	

Appendix 5.14b

N: Control; L: 0-14 DAS in low light; L-N: 0-7 DAS in low light; N-L: 7-14 DAS in low light

Comparisons of Heterosis Levels on indicated DAS	7 DAS		14 DAS		18 DAS		21 DAS	
LerxC24:L-C24xLer:L	0.849		0.998		1.000		0.941	
C24xLer:L-N-C24xLer:L	1.000		0.304		0.862		0.793	
LerxC24:L-N-C24xLer:L	0.763		0.979		0.944		0.946	
C24xLer:N-C24xLer:L	0.666		0.000	***	0.000	***	0.001	**
LerxC24:N-C24xLer:L	0.980		0.044	*	0.003	**	0.004	**
C24xLer:N-L-C24xLer:L	0.131		0.574		0.542		0.743	
LerxC24:N-L-C24xLer:L	0.993		0.983		0.722		0.952	
C24xLer:L-N-LerxC24:L	0.976		0.076		0.804		0.143	

LerxC24:L-N-LerxC24:L	1.000		0.736		0.911		0.306	
C24xLer:N-LerxC24:L	0.037	*	0.000	***	0.000	***	0.000	***
LerxC24:N-LerxC24:L	1.000		0.008	**	0.002	**	0.000	***
C24xLer:N-L-LerxC24:L	0.002	**	0.250		0.460		0.117	
LerxC24:N-L-LerxC24:L	0.333		0.796		0.647		0.321	
LerxC24:L-N-C24xLer:L-N	0.945		0.866		1.000		1.000	
C24xLer:N-C24xLer:L-N	0.340		0.007	**	0.003	**	0.080	
LerxC24:N-C24xLer:L-N	1.000		0.966		0.112		0.188	
C24xLer:N-L-C24xLer:L-N	0.034	*	1.000		0.999		1.000	
LerxC24:N-L-C24xLer:L-N	0.906		0.938		1.000		1.000	
C24xLer:N-LerxC24:L-N	0.023	*	0.000	***	0.002	**	0.032	*
LerxC24:N-LerxC24:L-N	0.998		0.300		0.066		0.087	
C24xLer:N-L-LerxC24:L-N	0.001	***	0.956		0.992		1.000	
LerxC24:N-L-LerxC24:L-N	0.246		1.000		1.000		1.000	
LerxC24:N-C24xLer:N	0.125		0.195		0.857		1.000	
C24xLer:N-L-C24xLer:N	0.972		0.030	*	0.018	*	0.097	
LerxC24:N-L-C24xLer:N	0.978		0.000	***	0.009	**	0.030	*
C24xLer:N-L-LerxC24:N	0.007	**	0.980		0.355		0.220	
LerxC24:N-L-LerxC24:N	0.639		0.455		0.225		0.082	
LerxC24:N-L-C24xLer:N-L	0.505		0.979		1.000		1.000	

Appendix 5.16a

P value	Control		0-7 DAS		7-14 DAS		0-14 DAS	
C24xLer-C24	0.000	***	0.000	***	0.000	***	0.000	***
Ler-C24	1.000		0.005	**	0.072		0.000	***
LerxC24-C24	0.032	*	0.001	***	0.009	**	0.033	*
MPV-C24	1.000		0.308		0.672		0.053	
Ler-C24xLer	0.000	***	0.562		0.290		0.993	
LerxC24-C24xLer	0.016	*	0.866		0.715		0.132	
MPV-C24xLer	0.000	***	0.021	*	0.014	*	0.114	
LerxC24-Ler	0.025	*	0.983		0.942		0.057	
MPV-Ler	1.000		0.477		0.672		0.049	*
MPV-LerxC24	0.023	*	0.203		0.228		1.000	

Appendix 5.16b

P value	Control		0-7 DAS		7-14 DAS		0-14 DAS	

C24xLer-C24	0.0000	***	0.0361	*	0.0033	**	0.8488	
Ler-C24	0.4412		0.6218		0.9270		0.0009	***
LerxC24-C24	0.0077	**	0.8663		0.9993		0.6513	
MPV-C24	0.6483		0.9700		0.9448		0.6533	
Ler-C24xLer	0.0000	***	0.0005	***	0.0649		0.0000	***
LerxC24-C24xLer	0.0067	**	0.0016	**	0.0034	**	0.1281	
MPV-C24xLer	0.0000	***	0.0078	**	0.0554		0.1509	
LerxC24-Ler	0.4241		0.9900		0.8613		0.0508	
MPV-Ler	0.9982		0.9446		1.0000		0.0968	
MPV-LerxC24	0.2695		0.9981		0.8861		1.0000	

Appendix 5.16c

P value	C24xLer		LerxC24	
0-7DAS-0-14DAS	0.4784		0.0727	
7-14DAS-0-14DAS	0.3853		0.1032	
Control-0-14DAS	0.0067	**	0.0442	*
7-14DAS-0-7DAS	0.9985		0.9966	
Control-0-7DAS	0.1476		0.9627	
Control-7-14DAS	0.1940		0.9047	

Appendix 5.16d

P value	C24xLer		LerxC24	
0-7DAS-0-14DAS	0.9981		0.9981	
7-14DAS-0-14DAS	0.9962		0.9962	
Control-0-14DAS	0.0029	**	0.0029	**
7-14DAS-0-7DAS	0.9999		0.9999	
Control-0-7DAS	0.0024	**	0.0024	**
Control-7-14DAS	0.0062	**	0.0062	**

Bibliography

ALABADI, D., OYAMA, T., YANOVSKY, M. J., HARMON, F. G., MAS, P. & KAY, S. A. 2001. Reciprocal regulation between TOC1 and LHY/CCA1 within the *Arabidopsis* circadian clock. *Science,* 293**,** 880-883.

ALBRECHT, V., INGENFELD, A. & APEL, K. 2006. Characterization of the *snowy cotyledon 1* mutant of *Arabidopsis thaliana*: the impact of chloroplast elongation factor G on chloroplast development and plant vitality. *Plant Mol Biol,* 60**,** 507-18.

ALBRECHT, V., INGENFELD, A. & APEL, K. 2008. Snowy cotyledon 2: the identification of a zinc finger domain protein essential for chloroplast development in cotyledons but not in true leaves. *Plant Mol Biol,* 66**,** 599-608.

ANDERSON, L. E. 1971. Chloroplast and cytoplasmic enzymes II. Pea leaf triose phosphate isomerases. *Biochimica et Biophysica Acta (BBA)-Enzymology,* 235**,** 237-244.

ARABIDOPSIS GENOME, I. 2000. Analysis of the genome sequence of the flowering plant *Arabidopsis thaliana*. *Nature,* 408**,** 796-815.

ATHANASIOU, K., DYSON, B. C., WEBSTER, R. E. & JOHNSON, G. N. 2010. Dynamic acclimation of photosynthesis increases plant fitness in changing environments. *Plant Physiology,* 152**,** 366-373.

BAKER, N. R. 2008. Chlorophyll fluorescence: a probe of photosynthesis *in vivo*. *Annu Rev Plant Biol,* 59**,** 89-113.

BAKER, N. R., HARBINSON, J. & KRAMER, D. M. 2007. Determining the limitations and regulation of photosynthetic energy transduction in leaves. *Plant Cell Environ,* 30**,** 1107-25.

BAUWE, H., HAGEMANN, M. & FERNIE, A. R. 2010. Photorespiration: players, partners and origin. *Trends in Plant Science,* 15**,** 330-336.

BELHAJ, K., CHAPARRO-GARCIA, A., KAMOUN, S. & NEKRASOV, V. 2013. Plant genome editing made easy: targeted mutagenesis in model and crop plants using the CRISPR/Cas system. *Plant Methods,* 9**,** 39.

BIRCHLER, J. A., AUGER, D. L. & RIDDLE, N. C. 2003. In search of the molecular basis of heterosis. *Plant Cell,* 15**,** 2236-2239.

BJORKMAN, O. 1981. Responses to different quantum flux densities. *In:* LANGE, O. L., NOBEL, P. S., OSMOND, C. B. & ZIEGLER, H. (eds.) *Physiological Plant Ecology I: Responses to the Physical Environment.* Berlin, Heidelberg: Springer Berlin Heidelberg.

BOARDMAN, N. K. 1977. Comparative photosynthesis of sun and shade plants *Annual Review of Plant Physiology and Plant Molecular Biology,* 28**,** 355-377.

BREITENBACH, J., ZHU, C. & SANDMANN, G. 2001. Bleaching herbicide Norflurazon inhibits phytoene desaturase by competition with the cofactors. *Journal of Agricultural and Food Chemistry,* 49**,** 5270-5272.

BRUCE, A. B. 1910. The Mendelian theory of heredity and the augmentation of vigor. *Science,* 32**,** 627-628.

CASAL, J. J. 2013. Photoreceptor signaling networks in plant responses to shade. *Annu Rev Plant Biol,* 64**,** 403-27.

CASSADY, J. P., YOUNG, L. D. & LEYMASTER, K. A. 2002. Heterosis and recombination effects on pig growth and carcass traits. *Journal of Animal Science,* 80**,** 2286-2302.

CHAIWANON, J., WANG, W., ZHU, J.-Y., OH, E. & WANG, Z.-Y. 2016. Information integration and communication in plant growth regulation. *Cell,* 164**,** 1257-1268.

CHAN, K. X., PHUA, S. Y., CRISP, P., MCQUINN, R. & POGSON, B. J. 2016. Learning the languages of the chloroplast: retrograde signaling and beyond. *Annu Rev Plant Biol,* 67**,** 25-53.

CHANG, S. Q., CHANG, T. G., SONG, Q. F., ZHU, X. G. & DENG, Q. Y. 2016. Photosynthetic and agronomic traits of an elite hybrid rice Y-Liang-You 900 with a record-high yield. *Field Crops Research,* 187**,** 49-57.

CHEN, Z. J. 2013. Genomic and epigenetic insights into the molecular bases of heterosis. *Nature Reviews Genetics,* 14**,** 471-482.

CHINNUSAMY, V. & ZHU, J. K. 2009. Epigenetic regulation of stress responses in plants. *Current Opinion in Plant Biology,* 12**,** 133-139.

CONDON, A. G., RICHARDS, R. A., REBETZKE, G. J. & FARQUHAR, G. D. 2004. Breeding for high water-use efficiency. *Journal of Experimental Botany,* 55**,** 2447-2460.

CROSS, J. M., VON KORFF, M., ALTMANN, T., BARTZETKO, L., SULPICE, R., GIBON, Y., PALACIOS, N. & STITT, M. 2006. Variation of enzyme activities and metabolite levels in 24 *Arabidopsis* accessions growing in carbon-limited conditions. *Plant Physiology,* 142**,** 1574-1588.

CROW, J. F. 1948. Alternative hypotheses of hybrid vigor. *Genetics,* 33**,** 477-487.

CROW, J. F. 1998. 90 years ago: the beginning of hybrid maize. *Genetics,* 148**,** 923-928.

DE WIT, M., GALVAO, V. C. & FANKHAUSER, C. 2016. Light-mediated hormonal regulation of plant growth and development. *Annu Rev Plant Biol,* 67**,** 513-37.

DEMMIG, B. & BJORKMAN, O. 1987. Comparison of the effect of excessive light on chlorophyll fluorescence (77K) and photon yield of O_2 evolution in leaves of higher plants. *Planta,* 171**,** 171-184.

DONNELLY, P. M., BONETTA, D., TSUKAYA, H., DENGLER, R. E. & DENGLER, N. G. 1999. Cell cycling and cell enlargement in developing leaves of *Arabidopsis*. *Developmental Biology,* 215**,** 407-419.

DRIEVER, S. M., LAWSON, T., ANDRALOJC, P. J., RAINES, C. A. & PARRY, M. A. J. 2014. Natural variation in photosynthetic capacity, growth, and yield in 64 field-grown wheat genotypes. *Journal of Experimental Botany,* 65**,** 4959-4973.

DYSON, B. C., ALLWOOD, J. W., FEIL, R., XU, Y., MILLER, M., BOWSHER, C. G., GOODACRE, R., LUNN, J. E. & JOHNSON, G. N. 2015. Acclimation of metabolism to light in *Arabidopsis thaliana*: the glucose 6-phosphate/phosphate translocator GPT2 directs metabolic acclimation. *Plant Cell and Environment,* 38**,** 1404-1417.

EAST, E. M. 1936. Heterosis. *Genetics,* 21**,** 375-397.

EDWARDS, G. E. & BAKER, N. R. 1993. Can CO_2 assimilation in maize leaves be predicted accurately from chlorophyll fluorescence analysis? *Photosynthesis Research,* 37**,** 89-102.

FARQUHAR, G. D., VON CAEMMERER, S. & BERRY, J. A. 1980. A biochemical model of photosynthetic CO_2 assimilation in leaves of C_3 species. *Planta,* 149**,** 78-90.

FISCHER, R., BYERLEE, D. & EDMEADES, G. 2014. Crop yields and global food security. *ACIAR: Canberra, ACT*.

FUJIMOTO, R., TAYLOR, J. M., SHIRASAWA, S., PEACOCK, W. J. & DENNIS, E. S. 2012. Heterosis of *Arabidopsis* hybrids between C24 and Col is associated with increased photosynthesis capacity. *Proceedings of the National Academy of Sciences,* 109**,** 7109-7114.

GALBRAITH, D. W., HARKINS, K. R. & KNAPP, S. 1991. Systemic endopolyploidy in *Arabidopsis thaliana*. *Plant Physiology,* 96**,** 985-989.

GALVAO, V. C. & FANKHAUSER, C. 2015. Sensing the light environment in plants: photoreceptors and early signaling steps. *Curr Opin Neurobiol,* 34**,** 46-53.

GENTY, B., BRIANTAIS, J. M. & BAKER, N. R. 1989. The relationship between the quantum yield of photosynthetic electron transport and quenching of chlorophyll fluorescence. *Biochimica et Biophysica Acta,* 990**,** 87-92.

GIBON, Y., PYL, E. T., SULPICE, R., LUNN, J. E., HOHNE, M., GUNTHER, M. & STITT, M. 2009. Adjustment of growth, starch turnover, protein content and central metabolism to a decrease of the carbon supply when *Arabidopsis* is grown in very short photoperiods. *Plant Cell and Environment,* 32**,** 859-874.

GONZALEZ, N., DE BODT, S., SULPICE, R., JIKUMARU, Y., CHAE, E., DHONDT, S., VAN DAELE, T., DE MILDE, L., WEIGEL, D., KAMIYA, Y., STITT, M., BEEMSTER, G. T. S. & INZE, D. 2010. Increased leaf size: different means to an end. *Plant Physiology,* 153**,** 1261-1279.

GONZALEZ, N., VANHAEREN, H. & INZE, D. 2012. Leaf size control: complex coordination of cell division and expansion. *Trends in Plant Science,* 17**,** 332-340.

GRANIER, C., TURC, O. & TARDIEU, F. 2000. Co-ordination of cell division and tissue expansion in sunflower, tobacco, and pea leaves: Dependence or independence of both processes? *Journal of Plant Growth Regulation,* 19**,** 45-54.

GREAVES, I. K., GROSZMANN, M., YING, H., TAYLOR, J. M., PEACOCK, W. J. & DENNIS, E. S. 2012. Trans chromosomal methylation in *Arabidopsis* hybrids. *Proceedings of the National Academy of Sciences of the United States of America,* 109**,** 3570-3575.

GROSZMANN, M., GONZALEZ-BAYON, R., GREAVES, I. K., WANG, L., HUEN, A. K., PEACOCK, W. J. & DENNIS, E. S. 2014. Intraspecific *Arabidopsis* hybrids show different patterns of heterosis despite the close relatedness of the parental genomes. *Plant Physiology,* 166**,** 265-280.

GROSZMANN, M., GONZALEZ-BAYON, R., LYONS, R. L., GREAVES, I. K., KAZAN, K., PEACOCK, W. J. & DENNIS, E. S. 2015. Hormone-regulated defense and stress response networks contribute to heterosis in *Arabidopsis* F1 hybrids. *Proceedings of the National Academy of Sciences of the United States of America,* 112**,** E6397-E6406.

GROSZMANN, M., GREAVES, I. K., FUJIMOTO, R., PEACOCK, W. J. & DENNIS, E. S. 2013. The role of epigenetics in hybrid vigour. *Trends Genet,* 29**,** 684-90.

GU, J. F., YIN, X. Y., STOMPH, T. J. & STRUIK, P. C. 2014. Can exploiting natural genetic variation in leaf photosynthesis contribute to increasing rice productivity? A simulation analysis. *Plant Cell and Environment,* 37**,** 22-34.

GUO, M., RUPE, M. A., DIETER, J. A., ZOU, J. J., SPIELBAUER, D., DUNCAN, K. E., HOWARD, R. J., HOU, Z. L. & SIMMONS, C. R. 2010. Cell Number Regulator1 affects plant and organ size in maize: implications for crop yield enhancement and heterosis. *Plant Cell,* 22**,** 1057-1073.

HADRICH, N., HENDRIKS, J. H., KOTTING, O., ARRIVAULT, S., FEIL, R., ZEEMAN, S. C., GIBON, Y., SCHULZE, W. X., STITT, M. & LUNN, J. E. 2012. Mutagenesis of cysteine 81 prevents dimerization of the APS1 subunit of ADP-glucose pyrophosphorylase and alters diurnal starch turnover in *Arabidopsis thaliana* leaves. *The Plant Journal,* 70**,** 231-242.

HE, G., ZHU, X., ELLING, A. A., CHEN, L., WANG, X., GUO, L., LIANG, M., HE, H., ZHANG, H. & CHEN, F. 2010. Global epigenetic and transcriptional trends among two rice subspecies and their reciprocal hybrids. *The Plant Cell,* 22**,** 17-33.

HEYNEKE, E., LUSCHIN-EBENGREUTH, N., KRAJCER, I., WOLKINGER, V., MULLER, M. & ZECHMANN, B. 2013. Dynamic compartment specific changes in glutathione and ascorbate levels in *Arabidopsis* plants exposed to different light intensities. *Bmc Plant Biology,* 13.

HORNITSCHEK, P., KOHNEN, M. V., LORRAIN, S., ROUGEMONT, J., LJUNG, K., LOPEZ-VIDRIERO, I., FRANCO-ZORRILLA, J. M., SOLANO, R., TREVISAN, M., PRADERVAND, S., XENARIOS, I. & FANKHAUSER, C. 2012. Phytochrome interacting factors 4 and 5 control seedling growth in changing light conditions by directly controlling auxin signaling. *Plant J,* 71**,** 699-711.

INZE, D. & DE VEYLDER, L. 2006. Cell cycle regulation in plant development. *Annual Review of Genetics,* 40**,** 77-105.

ISHIZAKI, Y., TSUNOYAMA, Y., HATANO, K., ANDO, K., KATO, K., SHINMYO, A., KOBORI, M., TAKEBA, G., NAKAHIRA, Y. & SHIINA, T. 2005. A nuclear-encoded sigma factor, *Arabidopsis* SIG6, recognizes sigma-70 type chloroplast promoters and regulates early chloroplast development in cotyledons. *Plant J,* 42**,** 133-44.

JAHNS, P. & HOLZWARTH, A. R. 2012. The role of the xanthophyll cycle and of lutein in photoprotection of photosystem II. *Biochim Biophys Acta,* 1817**,** 182-193.

JARVIS, P. & LOPEZ-JUEZ, E. 2013. Biogenesis and homeostasis of chloroplasts and other plastids. *Nature Reviews Molecular Cell Biology,* 14**,** 787-802.

KALVE, S., FOTSCHKI, J., BEECKMAN, T., VISSENBERG, K. & BEEMSTER, G. T. S. 2014. Three-dimensional patterns of cell division and expansion throughout the development of *Arabidopsis thaliana* leaves. *Journal of Experimental Botany,* 65**,** 6385-6397.

KARPECHENKO, G. D. 1928. Polyploid hybrids of *Raphanus sativus L.* X *Brassica oleracea L. Zeitschrift für Induktive Abstammungs- und Vererbungslehre,* 48**,** 1-85.

KATAGIRI, Y., HASEGAWA, J., FUJIKURA, U., HOSHINO, R., MATSUNAGA, S. & TSUKAYA, H. 2016. The coordination of ploidy and cell size differs between cell layers in leaves. *Development,* 143**,** 1120-1125.

KING, S. P., BADGER, M. R. & FURBANK, R. T. 1998. CO_2 refixation characteristics of developing canola seeds and silique wall. *Australian Journal of Plant Physiology,* 25**,** 377-386.

KO, D. K., ROHOZINSKI, D., SONG, Q., TAYLOR, S. H., JUENGER, T. E., HARMON, F. G. & CHEN, Z. J. 2016. Temporal Shift of Circadian-Mediated Gene Expression and Carbon Fixation Contributes to Biomass Heterosis in Maize Hybrids. *PLoS Genet,* 12**,** e1006197.

KOLLING, K., THALMANN, M., MULLER, A., JENNY, C. & ZEEMAN, S. C. 2015. Carbon partitioning in *Arabidopsis thaliana* is a dynamic process controlled by the plants metabolic status and its circadian clock. *Plant Cell and Environment,* 38**,** 1965-1979.

KUSTERER, B., PIEPHO, H. P., UTZ, H. F., SCHON, C. C., MUMINOVIC, J., MEYER, R. C., ALTMANN, T. & MELCHINGER, A. E. 2007. Heterosis for biomass-related traits in *Arabidopsis* investigated by quantitative trait loci analysis of the triple testcross design with recombinant inbred lines. *Genetics,* 177**,** 1839-1850.

LE, B. H., CHENG, C., BUI, A. Q., WAGMAISTER, J. A., HENRY, K. F., PELLETIER, J., KWONG, L., BELMONTE, M., KIRKBRIDE, R., HORVATH, S., DREWS, G. N., FISCHER, R. L., OKAMURO, J. K., HARADA, J. J. & GOLDBERG, R. B. 2010. Global analysis of gene activity during *Arabidopsis* seed development and identification of seed-specific transcription factors. *Proc Natl Acad Sci U S A,* 107**,** 8063-70.

LEFEBVRE, S., LAWSON, T., ZAKHLENIUK, O. V., LLOYD, J. C., RAINES, C. A. & FRYER, M. 2005. Increased sedoheptulose-1,7-bisphosphatase activity in transgenic tobacco plants stimulates photosynthesis and growth from an early stage in development. *Plant Physiol,* 138**,** 451-60.

LEISTER, D. 2003. Chloroplast research in the genomic age. *Trends in Genetics,* 19**,** 47-56.

LEISTER, D. 2012. Retrograde signaling in plants: from simple to complex scenarios. *Frontiers in Plant Science,* 3**,** 9.

LICHTENTHALER, H. K. & BUSCHMANN, C. 2001. Chlorophylls and Carotenoids: Measurement and Characterization by UV-VIS Spectroscopy. *Current Protocols in Food Analytical Chemistry.* John Wiley & Sons, Inc.

LIU, Z., YAN, H., WANG, K., KUANG, T., ZHANG, J., GUI, L., AN, X. & CHANG, W. 2004. Crystal structure of spinach major light-harvesting complex at 2.72 A resolution. *Nature,* 428**,** 287-92.

LUNN, J. E., DELORGE, I., FIGUEROA, C. M., VAN DIJCK, P. & STITT, M. 2014. Trehalose metabolism in plants. *The Plant Journal,* 79**,** 544-567.

MARTINS, M. C. M., HEJAZI, M., FETTKE, J., STEUP, M., FEIL, R., KRAUSE, U., ARRIVAULT, S., VOSLOH, D., FIGUEROA, C. M. & IVAKOV, A. 2013. Feedback inhibition of starch degradation in *Arabidopsis* leaves mediated by trehalose 6-phosphate. *Plant physiology,* 163**,** 1142-1163.

MASLE, J., GILMORE, S. R. & FARQUHAR, G. D. 2005. The ERECTA gene regulates plant transpiration efficiency in *Arabidopsis*. *Nature,* 436**,** 866-870.

MEHTA, H. & SARKAR, K. R. 1992. Heterosis for Leaf Photosynthesis, Grain-Yield and Yield Components in Maize. *Euphytica,* 61**,** 161-168.

MEYER, R., KUSTERER, B., LISEC, J., STEINFATH, M., BECHER, M., SCHARR, H., MELCHINGER, A., SELBIG, J., SCHURR, U., WILLMITZER, L. & ALTMANN, T. 2010. QTL analysis of early stage heterosis for biomass in *Arabidopsis*. *Theoretical and Applied Genetics,* 120**,** 227-237.

MEYER, R. C., TORJEK, O., BECHER, M. & ALTMANN, T. 2004. Heterosis of biomass production in *Arabidopsis* establishment during early development. *Plant Physiology,* 134**,** 1813-1823.

MEYER, R. C., WITUCKA-WALL, H., BECHER, M., BLACHA, A., BOUDICHEVSKAIA, A., DORMANN, P., FIEHN, O., FRIEDEL, S., VON KORFF, M., LISEC, J., MELZER, M., REPSILBER, D., SCHMIDT, R., SCHOLZ, M., SELBIG, J., WILLMITZER, L. & ALTMANN, T. 2012. Heterosis manifestation during early *Arabidopsis* seedling development is characterized by intermediate gene expression and enhanced metabolic activity in the hybrids. *Plant Journal,* 71**,** 669-683.

MILLENAAR, F. F., VAN ZANTEN, M., COX, M. C., PIERIK, R., VOESENEK, L. A. & PEETERS, A. J. 2009. Differential petiole growth in *Arabidopsis thaliana*: photocontrol and hormonal regulation. *New Phytol,* 184**,** 141-52.

MILLER, M., ZHANG, C. Q. & CHEN, Z. J. 2012. Ploidy and Hybridity Effects on Growth Vigor and Gene Expression in Arabidopsis thaliana Hybrids and Their Parents. *G3-Genes Genomes Genetics,* 2**,** 505-513.

MOCHIZUKI, N., BRUSSLAN, J. A., LARKIN, R., NAGATANI, A. & CHORY, J. 2001. *Arabidopsis* genomes uncoupled 5 (GUN5) mutant reveals the involvement of Mg-chelatase H subunit in plastid-to-nucleus signal transduction. *Proceedings of the National Academy of Sciences,* 98**,** 2053-2058.

MOCHIZUKI, N., TANAKA, R., TANAKA, A., MASUDA, T. & NAGATANI, A. 2008. The steady-state level of Mg-protoporphyrin IX is not a determinant of plastid-to-nucleus signaling in *Arabidopsis*. *Proceedings of the National Academy of Sciences,* 105**,** 15184-15189.

MOROT-GAUDRY, J.-F., CARRAYOL, E., WUILLEME, S., MOUTOT, F., DEROCHE, M.-E. & JOLIVET, E. 1984. Heterosis and Photosynthesis in Maize (*Zea Mays L.*). *In:* SYBESMA, C. (ed.) *Advances in Photosynthesis Research: Proceedings of the VIth International Congress on Photosynthesis, Brussels, Belgium, August 1–6, 1983. Volume IV.* Dordrecht: Springer Netherlands.

MULLEN, J. L., WEINIG, C. & HANGARTER, R. P. 2006. Shade avoidance and the regulation of leaf inclination in *Arabidopsis*. *Plant Cell Environ,* 29**,** 1099-106.

NEBRASKA AGRICULTURAL EXPERIMENT, S. & KIESSELBACH, T. A. 1922. *Corn Investigations*.

NG, D. W.-K., MILLER, M., HELEN, H. Y., HUANG, T.-Y., KIM, E.-D., LU, J., XIE, Q., MCCLUNG, C. R. & CHEN, Z. J. 2014. A role for CHH methylation in the parent-of-origin effect on altered circadian rhythms and biomass heterosis in *Arabidopsis* intraspecific hybrids. *The Plant Cell,* 26**,** 2430-2440.

NI, Z., KIM, E.-D. & CHEN, Z. J. 2009a. Chlorophyll and starch assays.

NI, Z. F., KIM, E. D., HA, M. S., LACKEY, E., LIU, J. X., ZHANG, Y. R., SUN, Q. X. & CHEN, Z. J. 2009b. Altered circadian rhythms regulate growth vigour in hybrids and allopolyploids. *Nature,* 457**,** 327-331.

OGUCHI, R., HIKOSAKA, K. & HIROSE, T. 2003. Does the photosynthetic light-acclimation need change in leaf anatomy? *Plant, Cell & Environment,* 26**,** 505-512.

OKAZAKI, K., KABEYA, Y., SUZUKI, K., MORI, T., ICHIKAWA, T., MATSUI, M., NAKANISHI, H. & MIYAGISHIMA, S. Y. 2009. The PLASTID DIVISION1 and 2 components of the chloroplast division machinery determine the rate of chloroplast division in land plant cell differentiation. *Plant Cell,* 21**,** 1769-1780.

OKELLO, R. C. O., DE VISSER, P. H. B., HEUVELINK, E., MARCELIS, L. F. M. & STRUIK, P. C. 2016. Light mediated regulation of cell division, endoreduplication and cell expansion. *Environmental and Experimental Botany,* 121**,** 39-47.

OLEJNICZAK, S. A., ŁOJEWSKA, E., KOWALCZYK, T. & SAKOWICZ, T. 2016. Chloroplasts: state of research and practical applications of plastome sequencing. *Planta,* 244**,** 517-527.

PAVLIKOVA, E. & ROOD, S. B. 1987. Cellular basis of heterosis for leaf area in maize. *Canadian Journal of Plant Science,* 67**,** 99-104.

PIERIK, R., WHITELAM, G. C., VOESENEK, L. A., DE KROON, H. & VISSER, E. J. 2004. Canopy studies on ethylene-insensitive tobacco identify ethylene as a novel element in blue light and plant-plant signalling. *Plant J,* 38**,** 310-9.

POIRÉ, R., WIESE-KLINKENBERG, A., PARENT, B., MIELEWCZIK, M., SCHURR, U., TARDIEU, F. & WALTER, A. 2010. Diel time-courses of leaf growth in monocot and dicot species: endogenous rhythms and temperature effects. *Journal of Experimental Botany,* 61**,** 1751-1759.

POORTER, H., ANTEN, N. P. R. & MARCELIS, L. F. M. 2013. Physiological mechanisms in plant growth models: do we need a supra-cellular systems biology approach? *Plant, Cell & Environment,* 36**,** 1673-1690.

POORTER, H., LAMBERS, H. & EVANS, J. R. 2014. Trait correlation networks: a whole-plant perspective on the recently criticized leaf economic spectrum. *New Phytologist,* 201**,** 378-382.

PORRA, R. J., THOMPSON, W. A. & KRIEDEMANN, P. E. 1989. Determination of accurate extinction coefficients and simultaneous equations for assaying chlorophylls a and b extracted with four different solvents: verification of the concentration of chlorophyll standards by atomic absorption spectroscopy. *Biochimica et Biophysica Acta,* 975**,** 384-394.

PRIVAT, I., HAKIMI, M. A., BUHOT, L., FAVORY, J. J. & MACHE-LERBS, S. 2003. Characterization of *Arabidopsis* plastid sigma-like transcription factors SIG1, SIG2 and SIG3. *Plant Mol Biol,* 51**,** 385-99.

PYKE, K. A. & LEECH, R. M. 1991. Rapid Image Analysis Screening Procedure for Identifying Chloroplast Number Mutants in Mesophyll Cells of *Arabidopsis thaliana* (L.) Heynh. *Plant Physiology,* 96**,** 1193-1195.

REIK, W. 2007. Stability and flexibility of epigenetic gene regulation in mammalian development. *Nature,* 447**,** 425-432.

RUPPEL, N. J. & HANGARTER, R. P. 2007. Mutations in a plastid-localized elongation factor G alter early stages of plastid development in *Arabidopsis thaliana*. *BMC Plant Biol,* 7**,** 37.

RUUSKA, S. A., SCHWENDER, J. & OHLROGGE, J. B. 2004. The capacity of green oilseeds to utilize photosynthesis to drive biosynthetic processes. *Plant Physiology,* 136**,** 2700-2709.

RYMEN, B., COPPENS, F., DHONDT, S., FIORANI, F. & BEEMSTER, G. T. 2010. Kinematic analysis of cell division and expansion. *Plant developmental biology: methods and protocols***,** 203-227.

SAEKI, N., KAWANABE, T., YING, H., SHIMIZU, M., KOJIMA, M., ABE, H., OKAZAKI, K., KAJI, M., TAYLOR, J. M. & SAKAKIBARA, H. 2016. Molecular and cellular characteristics of hybrid vigour in a commercial hybrid of Chinese cabbage. *BMC plant biology,* 16**,** 1.

SAVVIDES, A., NTAGKAS, N., VAN IEPEREN, W., DIELEMAN, J. A. & MARCELIS, L. F. M. 2014. Impact of light on leaf initiation: a matter of photosynthate availability in the apical bud? *Functional Plant Biology,* 41**,** 547-556.

SCHREIBER, U. 2004. Pulse-Amplitude-Modulation (PAM) Fluorometry and Saturation Pulse Method: An Overview. *In:* PAPAGEORGIOU, G. C. & GOVINDJEE (eds.) *Chlorophyll a Fluorescence: A Signature of Photosynthesis.* Dordrecht, Netherlands: Springer

SEMEL, Y., NISSENBAUM, J., MENDA, N., ZINDER, M., KRIEGER, U., ISSMAN, N., PLEBAN, T., LIPPMAN, Z., GUR, A. & ZAMIR, D. 2006. Overdominant quantitative trait loci for yield and fitness in tomato. *Proc Natl Acad Sci U S A,* 103**,** 12981-12986.

SHARKEY, T. D. 1985. Steady-state room temperature fluorescence and CO_2 assimilation rates in intact leaves. *Photosynthesis Research,* 7**,** 163-174.

SHARKEY, T. D., BERNACCHI, C. J., FARQUHAR, G. D. & SINGSAAS, E. L. 2007. Fitting photosynthetic carbon dioxide response curves for C_3 leaves. *Plant, Cell & Environment,* 30**,** 1035-1040.

SHEN, H., HE, H., LI, J., CHEN, W., WANG, X., GUO, L., PENG, Z., HE, G., ZHONG, S., QI, Y., TERZAGHI, W. & DENG, X. W. 2012. Genome-wide analysis of DNA methylation and gene expression changes in two *Arabidopsis* ecotypes and their reciprocal hybrids. *Plant Cell,* 24**,** 875-892.

SHIMADA, H., MOCHIZUKI, M., OGURA, K., FROEHLICH, J. E., OSTERYOUNG, K. W., SHIRANO, Y., SHIBATA, D., MASUDA, S., MORI, K. & TAKAMIYA, K. 2007. *Arabidopsis* cotyledon-specific chloroplast biogenesis factor CYO1 is a protein disulfide isomerase. *Plant Cell,* 19**,** 3157-69.

SHULL, G. H. 1948. WHAT IS "HETEROSIS"? *Genetics,* 33**,** 439-446.

SMITH, A. M. 2012. Starch in the *Arabidopsis* plant. *Starch - Stärke,* 64**,** 421-434.

SPRINGER, N. M. & STUPAR, R. M. 2007. Allelic variation and heterosis in maize: How do two halves make more than a whole? *Genome Research,* 17**,** 264-275.

STREB, S. & ZEEMAN, S. C. 2012. Starch Metabolism in *Arabidopsis*. *The Arabidopsis Book***,** e0160.

SULPICE, R., FLIS, A., IVAKOV, A. A., APELT, F., KROHN, N., ENCKE, B., ABEL, C., FEIL, R., LUNN, J. E. & STITT, M. 2014. *Arabidopsis* Coordinates the Diurnal Regulation of Carbon Allocation and Growth across a Wide Range of Photoperiods. *Molecular Plant,* 7**,** 137-155.

SULPICE, R., TRENKAMP, S., STEINFATH, M., USADEL, B., GIBON, Y., WITUCKA-WALL, H., PYL, E. T., TSCHOEP, H., STEINHAUSER, M. C., GUENTHER, M., HOEHNE, M., ROHWER, J. M., ALTMANN, T., FERNIE, A. R. & STITT, M. 2010. Network Analysis of Enzyme Activities and Metabolite Levels and Their Relationship to Biomass in a Large Panel of *Arabidopsis* Accessions. *Plant Cell,* 22**,** 2872-2893.

TAIZ, L. & ZEIGER, E. 2010. *Plant physiology,* Sunderland, MA, Sinauer Associates.

TANAKA, R., KOSHINO, Y., SAWA, S., ISHIGURO, S., OKADA, K. & TANAKA, A. 2001. Overexpression of chlorophyllide a oxygenase (CAO) enlarges the antenna size of photosystem II in *Arabidopsis thaliana*. *The Plant Journal,* 26**,** 365-373.

TANZ, S. K., KILIAN, J., JOHNSSON, C., APEL, K., SMALL, I., HARTER, K., WANKE, D., POGSON, B. & ALBRECHT, V. 2012. The SCO2 protein disulphide isomerase is required for thylakoid biogenesis and interacts with LHCB1 chlorophyll a/b binding proteins which affects chlorophyll biosynthesis in *Arabidopsis* seedlings. *Plant J,* 69**,** 743-754.

TERASHIMA, I., HANBA, Y. T., TAZOE, Y., VYAS, P. & YANO, S. 2006. Irradiance and phenotype: comparative eco-development of sun and shade leaves in relation to photosynthetic CO_2 diffusion. *Journal of Experimental Botany,* 57**,** 343-354.

TERASHIMA, I., HANBA, Y. T., THOLEN, D. & NIINEMETS, Ü. 2011. Leaf Functional Anatomy in Relation to Photosynthesis. *Plant Physiology,* 155**,** 108-116.

TRIPATHY, B. C. & OELMULLER, R. 2012. Reactive oxygen species generation and signaling in plants. *Plant Signal Behav,* 7**,** 1621-1633.

VANDENBUSSCHE, F., VRIEZEN, W. H., SMALLE, J., LAARHOVEN, L. J., HARREN, F. J. & VAN DER STRAETEN, D. 2003. Ethylene and auxin control the *Arabidopsis* response to decreased light intensity. *Plant Physiol,* 133**,** 517-527.

VANHAEREN, H., GONZALEZ, N. & INZÉ, D. 2015. A Journey Through a Leaf: Phenomics Analysis of Leaf Growth in *Arabidopsis thaliana*. *The Arabidopsis Book,* 13**,** 19.

VICENTE, M. R. S. & PLASENCIA, J. 2011. Salicylic acid beyond defence: its role in plant growth and development. *Journal of Experimental Botany,* 62**,** 3321-3338.

VON CAEMMERER, S. 2000. *Biochemical models of leaf photosynthesis,* Collingwood, VIC, Australia, CSIRO Publishing.

VON CAEMMERER, S. & FARQUHAR, G. D. 1981. Some relationships between the biochemistry of photosynthesis and the gas exchange of leaves. *Planta,* 153**,** 376-387.

WANG, L. & RUAN, Y.-L. 2013. Regulation of cell division and expansion by sugar and auxin signaling. *Frontiers in Plant Science,* 4**,** 9.

WICKE, S., SCHNEEWEISS, G. M., DEPAMPHILIS, C. W., MÜLLER, K. F. & QUANDT, D. 2011. The evolution of the plastid chromosome in land plants: gene content, gene order, gene function. *Plant Molecular Biology,* 76**,** 273-297.

WIESE, A., CHRIST, M. M., VIRNICH, O., SCHURR, U. & WALTER, A. 2007. Spatio-temporal leaf growth patterns of *Arabidopsis thaliana* and evidence for sugar control of the diel leaf growth cycle. *New Phytologist,* 174**,** 752-761.

XIAO, J., LI, J., YUAN, L. & TANKSLEY, S. D. 1995. Dominance is the major genetic basis of heterosis in rice as revealed by QTL analysis using molecular markers. *Genetics,* 140**,** 745-754.

YAMAMOTO, Y. Y., PUENTE, P. & DENG, X. W. 2000. An *Arabidopsis* cotyledon-specific albino locus: a possible role in 16S rRNA maturation. *Plant Cell Physiol,* 41**,** 68-76.

YANG, X. H., XIAOYING, C. Y., GE, Q. Y., LI, B., TONG, Y. P., LI, Z. S., KUANG, T. Y. & LU, C. M. 2007. Characterization of photosynthesis of flag leaves in a wheat hybrid and its parents grown under field conditions. *Journal of Plant Physiology,* 164**,** 318-326.

YOSHIDA, S., MANDEL, T. & KUHLEMEIER, C. 2011. Stem cell activation by light guides plant organogenesis. *Genes & Development,* 25**,** 1439-1450.

YU, S. B., LI, J. X., XU, C. G., TAN, Y. F., GAO, Y. J., LI, X. H., ZHANG, Q. & MAROOF, M. A. S. 1997. Importance of epistasis as the genetic basis of heterosis in an elite

rice hybrid. *Proceedings of the National Academy of Sciences of the United States of America,* 94**,** 9226-9231.

YUAN, L. 1998. Hybrid rice breeding for super high yield. *Denning GL, Mew TW, editors***,** 10-12.

ZHANG, C. J., CHU, H. J., CHEN, G. X., SHI, D. W., ZUO, M., WANG, J., LU, C. G., WANG, P. & CHEN, L. 2007. Photosynthetic and biochemical activities in flag leaves of a newly developed superhigh-yield hybrid rice (*Oryza sativa*) and its parents during the reproductive stage. *Journal of Plant Research,* 120**,** 209-217.

ZHU, A., GREAVES, I. K., LIU, P. C., WU, L., DENNIS, E. S. & PEACOCK, W. J. 2016. Early changes of gene activity in developing seedlings of *Arabidopsis* hybrids relative to parents may contribute to hybrid vigour. *The Plant Journal,* 88**,** 597-607.